MAINTAINING ISLET QUALITY DURING CULTURE

by

Michael James Rappel

Bachelor of Science in Chemical Engineering
University of Minnesota – Minneapolis, 2001

Masters of Science in Chemical Engineering Practice
Massachusetts Institute of Technology, 2003

Submitted to the Department of Chemical Engineering
in Partial Fulfillment of the Requirements for the Degree of
Doctor of Philosophy in Chemical Engineering

at the

Massachusetts Institute of Technology

May 2007
[June 2007]

Author.....
Department of Chemical Engineering
May 21, 2007

Certified by.....
Clark K. Colton
Professor of Chemical Engineering
Thesis Supervisor

Certified by.....
Kenneth A. Smith
Professor of Chemical Engineering
Thesis Supervisor

Accepted by.....
William Deen
Professor of Chemical Engineering
Chairman, Committee for Graduate Students

MAINTAINING ISLET QUALITY DURING CULTURE

by

Michael James Rappel

Submitted to the Department of Chemical Engineering on
May 21, 2007, in Partial Fulfillment of the Requirements for the
Degree of Doctor of Philosophy in Chemical Engineering

Islet transplantation has become a promising treatment for type I diabetes mellitus due to recent success since the development of the Edmonton Protocol. Islet culture prior to transplantation is standard practice in most clinical islet programs. Conventional culture conducted on polystyrene vessels can impose oxygen limitations even at relatively low tissue surface densities. High density islet culture is desirable because it reduces space and handling requirements during culture, but it exacerbates oxygen (O_2) limitations, causing a reduction in islet viability.

The overall objective of this thesis was to maintain islet quality during static culture. As a chemical engineer, I focused on addressing transport limitations present in conventional culture techniques. After demonstrating culture in the absence of O_2 transport limitations resulted in nearly 100% recovery of the original viable tissue placed into culture when the combined non-adherent and adherent tissue were considered, I examined the effect of tissue surface density on the recovery of islet tissue, its viability, and its purity for conventional normoxic culture on a polystyrene dish. With conventional culture, the fractional recovery of viable tissue decreased sharply as viable tissue density increased. To improve islet quality in high density culture, I investigated use of elevated ambient O_2, reduced culture temperature, and culture on an oxygen-permeable silicone rubber membrane. By applying a theoretical O_2 transport model, I investigated how O_2 transport changes for each culture condition and compared predictions to the experimental data to determine whether O_2 is limiting during high density culture using these new techniques. At high tissue surface densities, the fractional recovery of viable tissue was higher with culture on polystyrene in elevated (56%) O_2 or culture at reduced temperature (24°C), and even higher with normoxic culture on a silicone rubber membrane. Theoretical predictions based on O_2 transport were qualitatively similar to experimental results but in general overpredicted the amount of viable tissue recovered. Additional theoretical calculations indicated simplifications made when modeling oxygen along with glucose and pH changes during culture could account for the slight overprediction.

In conclusion, in high density culture, recovery of viable tissue (1) decreases as culture density increases on a polystyrene surface; (2) increases with increasing external O_2; and (3) increases substantially with culture on silicone rubber by removing O_2 limitations. The techniques examined significantly improve tissue oxygenation compared to conventional culture, and allow tissue to be cultured at higher densities without a reduction in viability. These methods can be easily implemented, which would enable clinical centers to reduce space and handling requirements during culture prior to transplantation without the reduction in islet viability that can occur with conventional methods, and thereby maximize the use of limited islet resources.

Thesis Supervisors: Clark K. Colton and Kenneth A. Smith
Title: Professors of Chemical Engineering

Acknowledgements

This thesis was completed only because of the help and support I received from many people. I would like to start by thanking my thesis advisors, Clark K. Colton and Kenneth A. Smith, for their technical guidance and demand for excellence. I thank my committee members William Deen, Leo Otterbein, Klearchos Papas, and Gordon Weir, who have provided invaluable insights and discussion throughout my time here at MIT. Additionally, I thank Susan Bonner-Weir for her insights and assistance in understanding changes islet tissue endures during culture.

I express my deepest gratitude to Anna Pisania and Daryl Powers, who not only provided stimulating discussions, but also made working in the lab enjoyable. I am indebted to them for their help, kindness, and support throughout my time at MIT. I could not have chosen any better lab mates.

I also thank the rest of the Colton Lab for their support throughout the years. I thank Efstathios Avgoustiniatos who provided the base work for this thesis and answered many of my initial questions; Cameron Nienaber from Joslin Diabetes Center for her lessons and patience in teaching me how to perform insulin staining; and Shenghan Yan, a UROP student who worked on the oxygen biosensor system. Shenghan was the ideal UROP student, both hard working and enthusiastic, and was an absolute joy to have in the lab.

I thank the islet isolation core at Joslin Diabetes Center, which includes Vaja Tchipashvili, Gaurav Chandra, James Lei, Abdulkadir Omer, Jack O'Neil, and Vassileios Kostaras, and the ICR for providing the islet tissue used throughout this work, without which none of this would have been possible. I also thank Giner, Inc., particularly Linda Templeman, and the University of Minnesota, particularly Klearchos Papas and Phillip Rozak, for their efforts in our collaborative work on developing and testing a controlled environment container for transportation of islet tissue.

I am particularly thankful to my parents, Don and Elaine Rappel, for their unending love and support throughout my academic education. Without them, I would not be where I am today. I also thank my brothers, Matt and Andy Rappel, who have made it their duty to keep my ego in check. I also thank all my friends I have had the honor of knowing during my years at MIT, who have provided support, laughs, and fun times.

Finally I want to thank my fiancée, Wanda Lau. I cannot begin to list all she has done for me. I am very thankful for her love and support throughout the years we have been together. Even when research was not going well she always found a way to make me smile.

Funding for this research was provided by grants from the NIH and the JDRF Center for Islet Transplantation at Harvard Medical School.

Table of Contents

List of Figures

List of Tables

1 Background, objectives, and overview

1.1 Background

The American Diabetes Association (ADA) defines diabetes as a "disease in which the body does not produce or properly use insulin." Humans need insulin in order for the body to use glucose, the basic fuel for cells. Diabetes is the fifth deadliest disease in the United States, according to the ADA. About 20.8 million people in the U.S. have diabetes; over 6 million of them have yet to be diagnosed. In 2005 1.5 million people over the age of 20 were diagnosed with diabetes or roughly 4,110 people each day. Diabetes can cause problems in virtually any part of the body, leading to nerve damage, amputation, kidney failure, stroke, blindness, and heart disease. In 2002 one out of every 10 dollars spent on health care was used to address diabetes and its complications, with a total estimated cost (direct and indirect medical costs) of $132 billion in the U.S. [1].

The ADA describes three major types of diabetes: type 1 or insulin-dependent diabetes, type 2 or non-insulin-dependent diabetes, and gestational. Type 1 diabetes, which typically develops in children and young adults, occurs when the body does not produce enough insulin, preventing cells from using glucose, and resulting in high blood glucose levels. The decrease in insulin production occurs when the body's immune system destroys insulin-producing cells. An estimated 5-10% of peoples diagnosed with diabetes have type 1 diabetes. Type 2 diabetes, comprising 90-95% of cases, occurs when the body is unable to use insulin it produces, resulting in an increase in blood glucose levels; over time the pancreas loses its ability to produce insulin. Gestational diabetes occurs during pregnancy and typically disappears after birth, though several mothers who have gestational diabetes later develop type 2 diabetes in life [1].

Several approaches are under investigation for treatment of diabetes. Type 2 diabetes can frequently be treated through oral hypoglycemic drugs and a good diet, though a small portion of patients require insulin to control hyperglycemia [2]. Several treatments are also being investigated for Type 1 diabetes. Insulin therapy, which requires daily insulin injections and blood glucose monitoring, is the most common treatment. Though the therapy transforms diabetes into a chronic disease with secondary complications, it also prevents it from becoming rapidly fatal. Implantation of insulin sensors and pumps, artificial pancreas development [3] and stem cells [4; 5] are also considered as possible treatments for diabetes, but are still in the

developmental stages. Whole pancreas transplantation at some centers results in 85% insulin independence one year after transplant with 50% of the patients maintaining good metabolic control five years after. However, whole pancreas transplantation requires major surgery and has significant risks. Islet transplantation is technically a much easier treatment and still offers the possibility of preventing secondary complications. However, until 2000, only 12% of patients were off insulin one year after the transplant [6].

In 2000 the area of islet transplantation took a large leap forward when a group in Edmonton reported insulin independence in seven out of seven patients after islet transplantation [7]. Since the development of the "Edmonton protocol" the success rate of islet transplantation has increased substantially around the world. Sixty-five patients have received islet transplants at the University of Alberta. Of the patients who have completed the procedure (about 12,000 islet equivalents (IE)/kg body weight, where one IE is the tissue volume equivalent to a 150-μm diameter sphere, multiple transplantations usually required) roughly 65% are insulin free one year post transplant, 40% are insulin free two years post-transplant, and 25% are insulin free three years post-transplant. Even patients who return to insulin therapy still show some graft function with 80% of all patients demonstrating transplant function after five years. Though risks are associated with the procedure and the drugs used for immunosuppression, it is possible to achieve insulin independence through islet transplantation for more than five years [8].

The Edmonton protocol made a key modification to the islet transplantation procedure by transplanting a larger islet mass, requiring tissue from multiple donor pancreases [8]. The availability of donor organs limits the number of diabetic patients who can benefit from this procedure. The Edmonton protocol requires about 800,000 IE (islets from two pancreases on average) to achieve insulin independence [8], though islet autotransplantation indicates a minimum of 300,000 IE are necessary to achieve insulin independence in 70% of patients [9]. In addition, insulin secretion was less than expected based on the number of islets transplanted in patients who have undergone the Edmonton protocol. Assuming a non-diabetic pancreas has 1 million islets [10; 11], more than 80% of this mass was transplanted, yet only 19% of the normal acute insulin response to glucose was observed [12]. When stimulated with 50% dextrose intravenously, the area under the insulin versus time curve adjusted for baseline insulin secretion, an indication of islet function, was 36% of control subjects [12], suggesting that most of the islets transplanted were not functioning properly or not viable. Low viability can result from

stresses imposed on the islets prior to and after transplantation. Measures to maintain or increase the amount of viable and functioning tissue transplanted are needed in order to reduce the amount of tissue required to treat diabetic patients.

Several factors affect the quality of the islet tissue starting with the retrieval of the pancreas from the donor. The quality of the original islets in the donor may itself be an important factor. Warm and cold ischemia time of the pancreas prior to islet isolation may result in tissue exposure to hypoxia. Mechanical and enzymatic disruption may decrease islet quality during islet isolation [13-15]. Hypoxia also occurs during most conventional islet culture conditions and may be severe during islet shipment. After transplantation, islets are exposed to more risks, including exposure to hypoxia prior to vascularization and exposure to stress from the immune system. In all cases the quality of the initial islet tissue in the donor pancreas only decreases with time [13]. At this time islets cannot be expanded significantly in culture; as a result, all viable islet tissue is of great importance. Any advances in reducing cell death in islet tissue before transplantation could increase the number of patients who can be treated with available tissue and/or improve the success rate of current islet transplantation procedures.

This thesis focuses on improving islet culture techniques in order to maintain islet quality during culture and shipment prior to transplantation.

1.2 Objectives

The central hypothesis of this project follows: During conventional culture and shipment islet tissue is exposed to oxygen (O_2) transport limitations. Though high density culture is desirable, it will exacerbate O_2 limitations and cause a larger decrease in the amount of viable tissue. When these limitations are removed, the tissue quality after culture and/or shipment will be higher than those using conventional methods. This project investigated this hypothesis through the following objectives:

- Examine islet tissue recovery, purity, and viability after culture in the absence of O_2 limitations.
- Investigate the effect of tissue surface density on the recovery of islet tissue, its purity, and its viability when cultured at 37°C on a polystyrene dish.
- Compare theoretical predictions for viable tissue recovery based on an O_2 transport to experimental results.

- Investigate high density culture techniques that may reduce O_2 limitations by culturing islets at reduced temperature, in elevated O_2, or on an O_2-permeable silicone rubber membrane.
- Through theoretical examination, determine what limitations become important when O_2 limitations are removed specifically considering glucose transport and pH changes.
- By applying lessons learned from the above objectives, develop a transportation device to maintain constant culture conditions during shipment and remove existing O_2 limitations in the current shipment method.

1.3 Overview

Below we briefly note the contents of each subsequent chapter in this thesis.

Chapter 2, written in collaboration with Anna Pisania, covers islet (human, rat, and porcine) and non-islet (human) characterization prior to and following low density culture on polystyrene using techniques developed by our laboratory including islet volume fraction by light microscopy, total amount of tissue by nuclei and DNA counts, viability using O_2 consumption rate (OCR) measurements in a stirred-tank vessel, and membrane integrity by differential staining of nucleic acids before and after cell disruption. Culture at two different temperatures was examined and both adherent and non-adherent tissue was analyzed. This study demonstrated how islet quality changes during culture in the absence of nutrient transport limitations.

Chapter 3 discusses the effect of tissue surface density on the recovery of islet tissue, its viability, and its purity following culture on polystyrene. Using a theoretical model previously developed for O_2 transport during static islet culture [16] we investigated whether O_2 limitations likely cause the reduction in the amount of viable tissue observed during high density islet culture.

Chapter 4 discusses improvements to conventional islet culture techniques, specifically addressing the presence of O_2 limitations. Elevated ambient O_2, reduced culture temperature, and culture on an O_2 -permeable membrane are evaluated as alternative culture techniques with analysis focusing on the recovery of islet tissue and its viability for a range of tissue surface

densities. The theoretical model applied in Chapter 3 was modified to investigate how O_2 transport changes for each new culture technique.

Chapter 5 explores in detail the theoretical O_2 transport models used in chapters 3 and 4. The sensitivity of model predictions to variations in model parameters and the simplifying assumptions made within the model including islet distribution, islet size, slab formation, tissue stacking, and convection are discussed.

Chapter 6 introduces and investigates a transient glucose transport model that predicts concentration profiles during static islet culture to determine if nutrient transport limitations other than O_2 could become limiting. In addition, preliminary experiments are used to elucidate whether islets are exposed to low glucose levels during culture and if so, what affect that has on the recovery of viable tissue.

Chapter 7 lays the groundwork for a theoretical model that predicts transient changes in local pH during static islet culture on either a carbon dioxide (CO_2)-impermeable or CO_2-permeable surface. The model accounts for CO_2, ammonia, and lactate production by the islets, and includes the interaction of H^+ with the bicarbonate buffer. Exploration of the model reveals whether pH could change significantly in the islet tissue from the physiological value of 7.4.

In Chapter 8 the knowledge gained in chapters 3 through 5 was used in collaboration with Giner, Inc., and the University of Minnesota to develop an islet transportation device that actively maintained temperature and O_2 level during shipment, which was tested and compared to the standard method of shipping tissue in a Styrofoam box. After demonstrating the usefulness of this actively controlled system, an inexpensive alternative shipping device is proposed and its feasibility determined through preliminary experiments and theoretical calculations.

1.4 Nomenclature

CO_2	Carbon dioxide
IE	Islet equivalent
O2	Oxygen
OCR	Oxygen consumption rate

2 Characterization of islet and non-islet tissue prior to and following culture

This chapter was written in collaboration with Anna Pisania, who developed and tested many of the tools described here to characterize islet tissue. My contribution involved understanding the changes islet tissue undergoes during low density static culture when no transport limitations are present.

2.1 Introduction

Transplantation of islets of Langerhans is a promising treatment for patients with unstable forms of type 1 diabetes [17-22], but several aspects need improvement to allow widespread application. One need is quantitatively meaningful islet quality assessment tests that can predict the transplantation outcome [21; 23-25]. This is especially important because islet isolation and transplantation success rates vary between centers [26; 27]. The most reliable assay, transplantation under the kidney capsule of nude diabetic mice [28-30], requires a long time and is useful only retrospectively. Currently-employed methods for islet characterization include staining with dithizone (DTZ) for purity assessment and enumeration by visual evaluation under a microscope [31; 32], and staining with fluorescent diacetate/propidium iodide (FDA/PI) for assessment of membrane integrity [33]. These methods are not quantitative and do not correlate with transplantation outcome [34-36].

Recent interest in developing new methods for islet viability assessment has focused on measurements of mitochondrial function, including mitochondrial membrane polarization with dispersed islet cells [37], ATP/ADP concentration ratio with intact islets [38] and oxygen consumption rate (OCR) [39]. The combined use of OCR and DNA measurements in the latter two studies correlated with transplantation outcome with high specificity and selectivity. However, there is a paucity of data in the literature on the OCR of human islet preparations or of any other species.

Islet culture for 36-72 hr prior to transplantation is practiced in most clinical centers [40] to provide time for tissue recovery from the harsh isolation process, possible reduction in immunogenicity [41-46], assessment of purity, membrane integrity, and sterility, recipient matching, patient travel to the islet center, and patient preparation to reach necessary levels of

immunosuppression before transplantation [40; 47; 48]. There is need to better understand islet culture and its effect on purity and viability. Culture conditions, especially temperature, vary between islet centers. Culture at 37°C maintains viability (by membrane integrity) and function better than reduced temperature [47; 49], but also results in increased necrotic death [49-52], which is likely the result of oxygen transport limitations. Culture at 22-24°C results in more islet mantle disintegration and increased apoptosis [53], but also increases the recovery of islet tissue [46; 47; 49; 54]. Currently, only non-adherent tissue is recovered from culture for analysis and subsequent use.

In this study, we examined OCR properties [39] of large numbers of human islet preparations (freshly isolated, precultured, or shipped from various centers), as well as rat and porcine islets. Measurements made upon receipt of islets and after 1 or 2 days of culture included, in addition, total amount of tissue by nuclei counts and DNA content [55], islet volume fraction [55] and β cell number fraction by light microscopy, and quantitative membrane integrity [55]. We also investigated culture temperatures of 37°C and 24°C and examined both adherent and non-adherent tissue recovered from culture.

2.2 Methods

Islet isolation and culture

Rat islets were isolated from male Sprague-Dawley rats by using collagenase digestion/ficoll purification [56-58]. Standard collagenase/protease digestion methods were used for human [7; 15] and porcine [59] isolations. Preparations of rat, and human islets, human non-islet tissue, and porcine islets were provided fresh (4-6 hr after isolation was complete) by the Islet Core at the Joslin Diabetes Center (JDC, Boston, MA). Human islets were also received after culture (1-2 days) from JDC or overnight shipment (sometimes after up to 1 day culture) from other centers contained in culture flasks (T-25 and T-75) or centrifuge tubes in Styrofoam boxes. When first observed, some preparations were in suspension, some in a pellet. Upon receipt, a portion of the preparation was analyzed and the remainder placed into untreated polystyrene culture flasks at 37°C in a humidified environment (5% CO_2), oxygen partial pressure (pO_2) of 142 mmHg, for 34-60 hr during which no medium change occurred. Some cultures were terminated at 18-24 hr for analysis. To test the effect of temperature, some islets were cultured at 24°C and then warmed for 1 hr at 37°C before OCR measurements.

Islets were cultured in supplemented RPMI (11.1 mM D-glucose, 100 U/ml penicillin, 100 μg/ml streptomycin, 2 mM L-glutamine, 1 mM sodium pyruvate (all from Mediatech Inc., Herdon, VA), and 50 μM β-mercaptoethanol (Sigma Aldrich, St. Louis, MO) with 10% fetal bovine serum (FBS, Mediatech Inc.), at low densities (< $8x10^4$ cells/cm^2 or about 50 islet equivalents (IE)/cm^2, where IE is the volume of a sphere with a diameter of 150 μm) in 1.3 mm of medium in tissue culture flasks. After culture the free, non-adherent tissue (which is the only tissue used in current practice) was collected. In selected experiments, adherent human tissue was incubated for 5 min at 37°C in 0.05% trypsin EDTA (Mediatech Inc.), dislodged with fresh medium, and collected. Rat islets and human tissue at 24°C did not adhere significantly. Tissue suspensions were centrifuged for 3 min at 300xg, supernatant removed and the tissue suspended in fresh medium.

Human and porcine islets were also isolated and analyzed at the University of Minnesota (MN) using standard methods [39; 60]. Islets were cultured in CMRL 1066 formulated for islet culture (Mediatech, 99-603), further supplemented with 10% FBS and heparin (10 U/ml). Islets were cultured at 200 IE/cm^2 in 30 ml of medium in tissue culture flasks in an incubator with 5% CO_2 for 18 to 24 hr at 37°C and then 18 to 24 hr at 24°C.

DNA content

At MIT, DNA was measured by fluorospectrophotometry [55] using the CyQUANT Cell Proliferation Assay Kit (Molecular Probes, C-7026 Eugene, OR), and a λ DNA standard (Invitrogen) and 50-250 IE/sample. Fluorescence was read at 480 nm excitation and 520 nm emission wavelengths in a plate reader (Spectra MAX Gemini microplate spectrophotometer, Molecular Devices, Sunnyvale CA). At MN (porcine and human islets), PicoGreen dye was used (Quant-iT PicoGreen dsDNA kit, Molecular Probes, Eugene, OR) [61]. Fluorescence was read at 520 nm excitation and 585 nm emission wavelengths.

Islet enumeration by nuclei counting

Nuclei were prepared by adding equal 100-μl volumes of sample containing 160 or more IE and of lysis solution (0.1 M citric acid (Sigma) and 1% (v/v) Triton X-100 (Sigma)) to a 1.5 ml microtube [55]. The mixture was incubated at room temperature for 5 min with vortex mixing every 1.5 min, and nuclei were liberated by shearing through a needle. Isolated nuclei were diluted with Dulbecco's phosphate buffered saline (D-PBS, Invitrogen, Carlsbad, CA) to a concentration no higher than 5 x 10^5 nuclei/ml, stained with 7-aminoactinomycin D (7-AAD,

Molecular Probes, Eugene, OR), and analyzed using a flow cytometer (Guava Personal Cell Analysis (PCA) system, Guava Technologies, Hayward, CA) to determine the total number of cells with intact nuclei in the sample.

Oxygen consumption rate (OCR)

OCR was measured as previously described [39]. Briefly, suspensions containing about 2500 IE/ml in DMEM containing 4.5 g/l glucose and 0.6 g/l L-glutamine supplemented with 100 U/ml penicillin, 100 μg/ml streptomycin, 10 mM HEPES, and no added serum were sealed in a 200-μl stirred titanium chamber (Micro Oxygen Uptake System, FO/SYSZ- P250, Instech Laboratories, Plymouth Meeting, PA) maintained at 37°C. The time dependent pO_2 within the chamber was recorded with a fluorescence-based oxygen sensor (Ocean Optics, Dunedin, FL), and data at high pO_2 were fit to a straight line. The maximal OCR was evaluated from $OCR=V_{ch}\alpha(\Delta pO_2/\Delta t)$, where V_{ch} is the chamber volume and α = 1.27 nmol/mm·Hg·ml is the Bunsen solubility coefficient for oxygen in medium [16]. OCR measurements were normalized by the measured number of cells (nuclei counting) or DNA content of the sample examined.

Membrane Integrity

7-Aminoactinomycin (7-AAD) sequential staining

Cell membrane integrity was assessed by differential staining with 7-AAD (Molecular Probes, Eugene, OR) [55]. An aliquot of about 300 islets was re-suspended in 100 μl of D-PBS, and 5 μl of 1 mg/ml 7-AAD and incubated for 20 min at 4°C protected from light. After two washes with 1 ml of D-PBS, cells were disrupted by adding equal volume of lysis solution in D-PBS to the islet suspension and sheared as described for islet enumeration. Labeled nuclei were counted immediately in the flow cytometer or stored on ice for less than 15 min before counting. A portion of the islet suspension was further stained with 7-AAD, thereby labeling all of the previously unlabelled nuclei, and the total number of nuclei was counted. The fraction of cells with compromised membranes was estimated as the ratio of the initially stained nuclei (first measurement) to the total number of nuclei (second measurement).

Fluorescein diacetate (FDA)/propidium iodide (PI)

Immediately after human islet isolation was completed, a 250 μl aliquot was taken from the preparation, re-suspended in 5 ml of PBS solution in a 60 mm Petri dish, and 10 μl of 24 mM fluoroscein diacetate (FDA) and 750 μM propidium iodide (PI) was added [62]. The tissue was

examined in a light microscope by focusing through the tissue to visually estimate the volume fraction of cells containing nuclei stained red because of loss of membrane integrity.

Islet volume fraction by morphological analysis

A 0.5 ml aliquot of human islet preparation was processed to produce 1-μm sections stained with toluidine blue and examined by light microscopy [13]. Islet tissue was distinguished from non-islet tissue as previously described [13]. Sections were analyzed at 420X by stereological point counting [63] with a 90-point grid covering adjacent, non-overlapping fields. At point intercepts of the grid with tissue, the nature of the tissue was determined, and the volume fraction of islet tissue, denoted Φ_I, was calculated as previously described [13].

β cell identification by immunocytochemical insulin staining

Tissue samples were washed twice with 1 ml D-PBS, fixed for 1 hr in 10% formalin (Sigma Aldrich), washed twice with 1 ml of D-PBS, and centrifuged at 300xg for 5 min. To the pellet, 500 μl of warm 2% (w/v) agarose was added. The solution was mixed using a vortex mixer for 1 sec, immediately centrifuged at 18000xg for 10 sec, allowed to cool for 2 min, and then 500 μl of 10% formalin was added. After 1-hr incubation at room temperature, formalin was removed, samples were stored in D-PBS until embedded in paraffin, and 5-μm sections were cut. Sections were stained by the unlabeled antibody peroxidase-antiperoxidase (PAP) method [64] using guinea pig anti-bovine insulin (Linco, St. Charles, MO) as primary antibody and goat anti-guinea pig IgG (Cappel, Irvine, CA), as secondary antibody, to link primary antibody to rabbit PAP complex (Jackson ImmunoResearch Laboratories, Inc., West Grove, PA). Use of a heterologous antibody gave specific staining with little background [65]. After applying PAP, slides were stained in 50 ml of a 2 mM 3,3'-diaminobenzidine tetrahydrochloride (DAB, Sigma Aldrich) solution activated with 25 μl of 30% (v/v) hydrogen peroxide (EMD Chemicals Inc, Gibbstown, NJ) for 30-120 sec, then viewed under a microscope. Reaction between hydrogen peroxide, DAB, and PAP formed a dark brown insoluble precipitate [66]. Slides were counterstained with hematoxylin (Sigma Aldrich). β cell volume fraction exclusive of vascular space, denoted $\Phi_{\beta XV}$, was quantified using stereological point counting, as described for morphological analysis, with 200 points or more counted.

This procedure was used with samples after 2 days culture because trypsinization of adherent tissue degraded the structure and produced single cells, which, in turn, made it harder to

morphologically differentiate between cell types and evaluate vascular volume fraction, whereas it was more accurate to distinguish insulin staining. Methods for calculating $\Phi_{\beta XV}$ (day 2) and comparing it with Φ_I (day 0) are described in the Appendix.

Statistics

Measurements were made with three or more replicates and reported as mean ± SD. Statistical significance was determined using a Student t-test for unpaired data for comparing population means, and for paired data when appropriate.

2.3 Results

Nuclei counts, DNA content, membrane integrity by 7-AAD, and OCR were measured with fresh rat, fresh human, and cultured/shipped (data combined) human islets, and fresh human non-islet tissue at MIT; islet and β cell volume fraction were measured with human fresh and cultured/shipped islets. DNA content and OCR were measured with porcine islets at MIT and UMN and with human islets at UMN. Measurements with fresh tissue were performed 4-6 hr after isolation. At MIT, all islet preparations were analyzed on day 0 (day of isolation for all fresh tissue or the day of receipt for cultured/shipped human islets), and a subset on day 1 and 2 of culture. Tissue analyzed in this study was often used for other purposes, and there was usually insufficient tissue for all tests, so that population means did not come from identical preparations. In a series of paired studies, measurements on day 0 and day 2 were made with non-adherent, adherent, and combined (total) tissue samples, enabling measurement of the recovery of the total amount of tissue (DNA and nuclei), the total OCR, and the number of β cells relative to that originally placed in culture. In experiments in which there was insufficient adherent tissue to carry out individual assays, adherent was nonetheless combined with non-adherent tissue for assay of the total.

2.3.1 DNA/cell

Frequency distributions of DNA/cell for day 0 and for non-adherent tissue on day 1 and 2 in culture are shown in Figure 2.1. DNA/content (pg DNA/cell) of rat (6.4 ± 1.6), fresh human islets (6.4 ± 1.1), and human non-islet tissue (5.7 ± 2.3) was similar while that of human cultured/shipped islets (7.9 ± 1.8) was significantly higher ($p<0.01$), thereby suggesting that significant cell death occurred during pre-culture and shipment and that DNA had been released

from dead cells but had not yet degraded. The DNA content of cultured rat islets did not change with time, whereas on day 1 it increased substantially with non-adherent fresh islets ($p<0.01$) and non-islet tissue ($p<0.20$) and decreased with cultured/shipped islets; on day 2, all returned partially towards the day 0 value. Rat islets produced a normal frequency distribution with a coefficient of variation (COV) of 0.25. The COV was 0.14 for fresh human islets and usually about 0.25 for other conditions, all of which were skewed to the right, reflecting the presence of very high DNA/cell in some cultured preparations.

Additional data for the effect of 2-day culture on DNA/cell is tabulated in Table 2.1. At 37°C, day 2, DNA/cell for rat tissue was significantly lower than that of human non-adherent cultured/shipped ($p<0.02$) tissue but not for fresh human tissue. Changes from day 0 to day 2 were not significant for any of the non-adherent islets but was significant for non-adherent human non-islet tissue. At 24°C, DNA/cell of the non-adherent rat islets was substantially higher than at 37°C. The same trend with cultured/shipped human islets was not significant for paired data. The opposite trend was observed for non-adherent fresh human-islets, though only three paired measurements were made, and the mean at 37°C (10.6 ± 1.9) was substantially higher than that for a larger number of preparations (7.2 ± 2.8).

2.3.2 Nuclei and DNA recovery

The fraction of tissue recovered on day 2, as nuclei or DNA, relative to day 0 is summarized in Table 2.1. At 37°C, the fraction recovered for all tissue groups and for the combined subsets within each group, was substantially less than 1.0 based on either nuclei counts ($p<0.01$) or DNA measurements ($p<0.01$ to 0.15). The fractional recovery of nuclei was 0.63 ± 0.14, 0.34 ± 0.15, 0.50 ± 0.17, and 0.40 ± 0.24 respectively, for rat, human fresh, and cultured shipped islets, and non-islet tissue, 0.22 ± 0.10 and 0.30 ± 0.17 for human fresh and cultured/shipped adherent tissue, respectively, and 0.63 ± 0.14, 0.63 ± 0.17, and 0.81 ± 0.20 for rat and human fresh and cultured/shipped total tissue, respectively. When based on DNA, these fractions were slightly lower for rat and cultured/shipped human islets and slightly higher for human fresh islets and non-islet tissue.

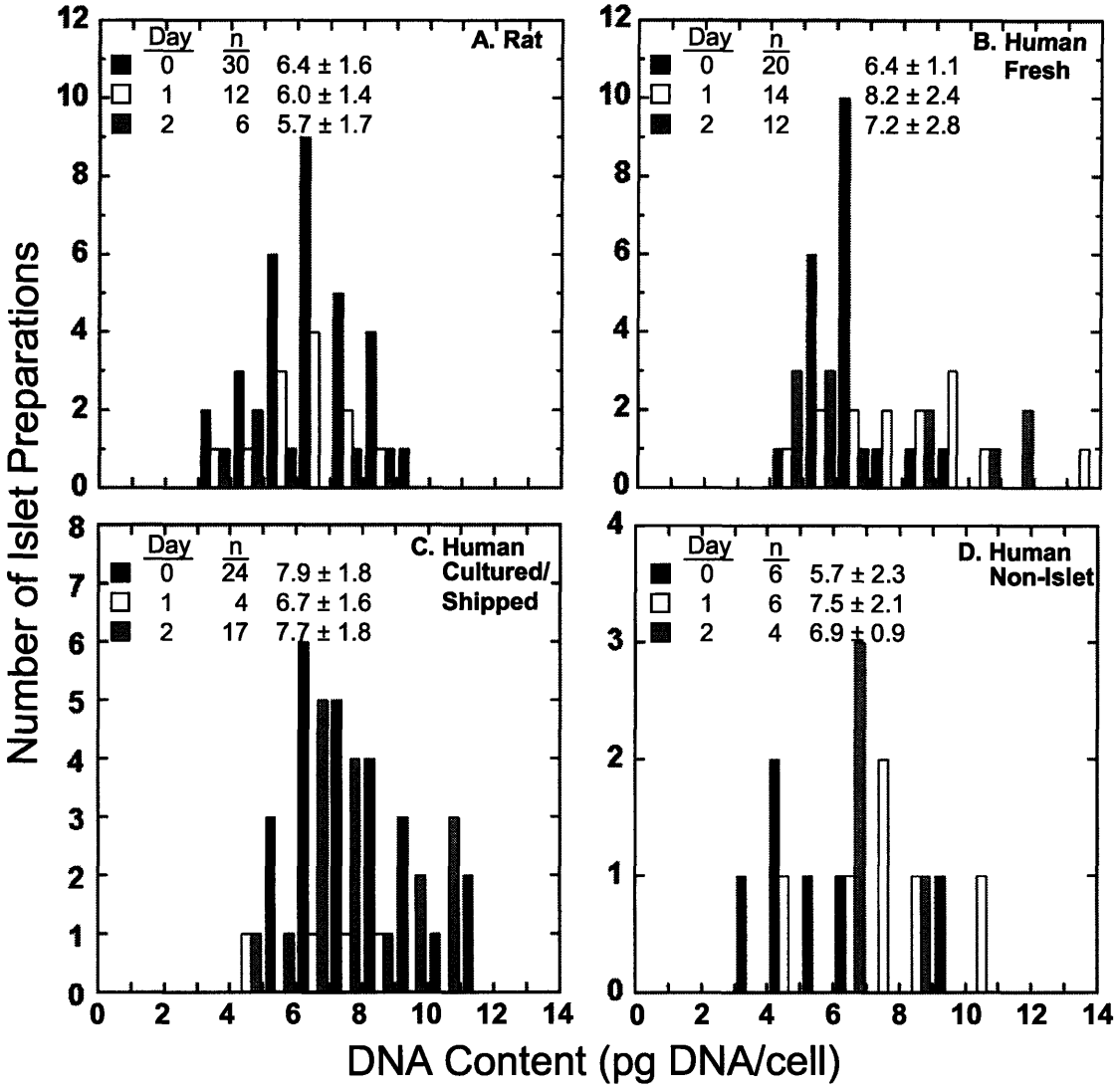

Figure 2.1. Frequency distributions of DNA content for day 0 and for non-adherent tissue on day 1 and 2 in culture for (A) rat, (B) human fresh, and (C) human cultured/shipped islets, and (D) human non-islet tissue.
n is the total number of islet preparations for which measurements were made.

Table 2.1. DNA/cell and the fraction of original tissue recovered (quantified by nuclei and DNA) after 2 days culture.[a]

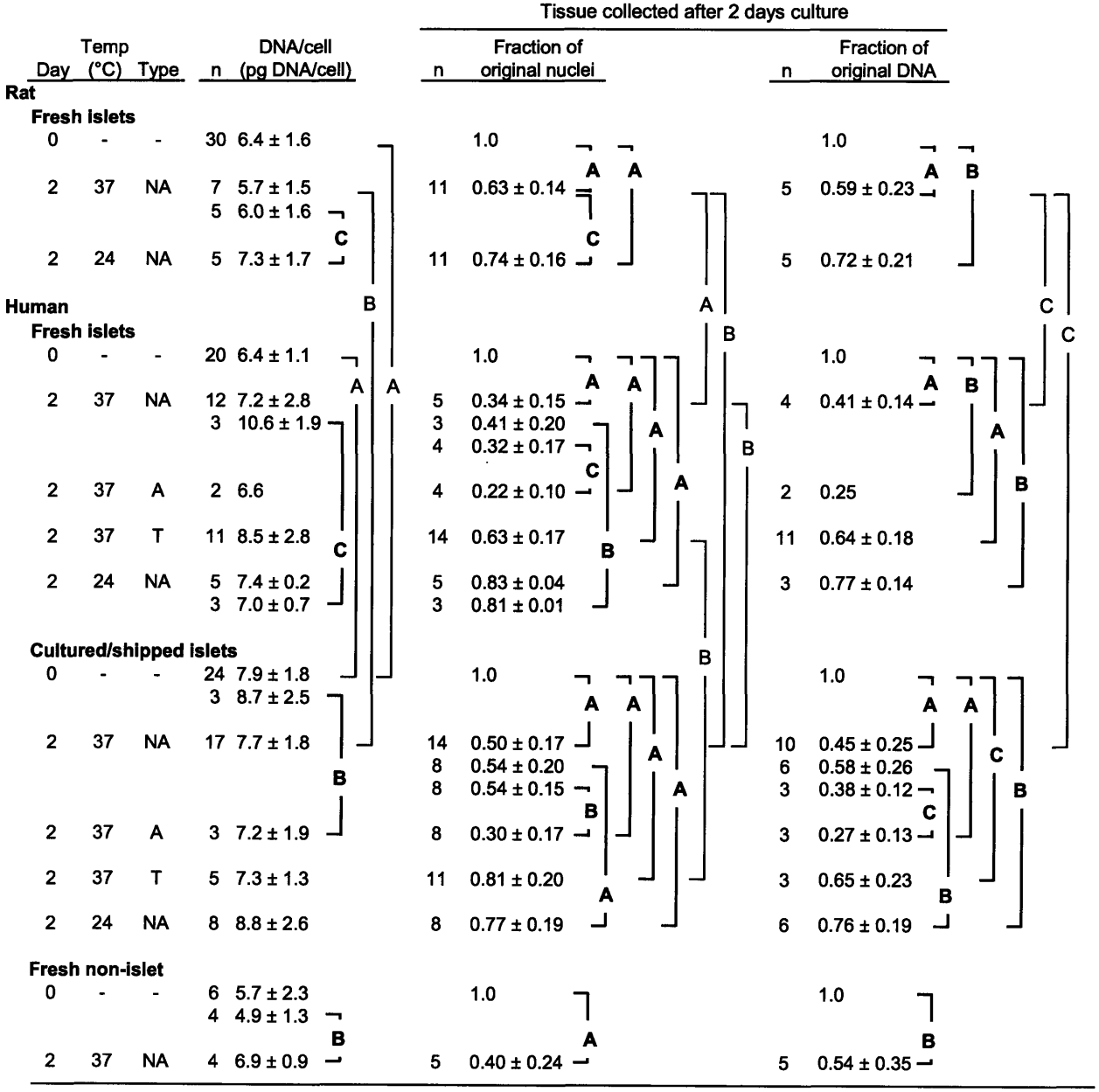

	Temp			DNA/cell	Tissue collected after 2 days culture: Fraction of original nuclei		Fraction of original DNA	
Day	(°C)	Type	n	(pg DNA/cell)	n	original nuclei	n	original DNA
Rat								
Fresh islets								
0	-	-	30	6.4 ± 1.6		1.0		1.0
2	37	NA	7	5.7 ± 1.5	11	0.63 ± 0.14	5	0.59 ± 0.23
			5	6.0 ± 1.6				
2	24	NA	5	7.3 ± 1.7	11	0.74 ± 0.16	5	0.72 ± 0.21
Human								
Fresh islets								
0	-	-	20	6.4 ± 1.1		1.0		1.0
2	37	NA	12	7.2 ± 2.8	5	0.34 ± 0.15	4	0.41 ± 0.14
			3	10.6 ± 1.9	3	0.41 ± 0.20		
					4	0.32 ± 0.17		
2	37	A	2	6.6	4	0.22 ± 0.10	2	0.25
2	37	T	11	8.5 ± 2.8	14	0.63 ± 0.17	11	0.64 ± 0.18
2	24	NA	5	7.4 ± 0.2	5	0.83 ± 0.04	3	0.77 ± 0.14
			3	7.0 ± 0.7	3	0.81 ± 0.01		
Cultured/shipped islets								
0	-	-	24	7.9 ± 1.8		1.0		1.0
			3	8.7 ± 2.5				
2	37	NA	17	7.7 ± 1.8	14	0.50 ± 0.17	10	0.45 ± 0.25
					8	0.54 ± 0.20	6	0.58 ± 0.26
					8	0.54 ± 0.15	3	0.38 ± 0.12
2	37	A	3	7.2 ± 1.9	8	0.30 ± 0.17	3	0.27 ± 0.13
2	37	T	5	7.3 ± 1.3	11	0.81 ± 0.20	3	0.65 ± 0.23
2	24	NA	8	8.8 ± 2.6	8	0.77 ± 0.19	6	0.76 ± 0.19
Fresh non-islet								
0	-	-	6	5.7 ± 2.3		1.0		1.0
			4	4.9 ± 1.3				
2	37	NA	4	6.9 ± 0.9	5	0.40 ± 0.24	5	0.54 ± 0.35

[a]Data are tabulated for day 0 and day 2 non-adherent (NA), adherent (A), and the combined total (T, adherent + non-adherent) tissue within each group and includes overall population means for comparison between groups (e.g. fresh rat versus fresh human) and paired data for comparisons of subsets within each group. Data are reported as mean ± SD for measurements with n different islet preparations. The p values of paired (bold face) and unpaired (not bold face) comparisons (denoted by brackets) are given for $p \leq 0.15$ according to the following notation: A $p \leq 0.01$, B $0.01 < p \leq 0.10$, C $0.10 < p \leq 0.15$. Fractional recoveries for NA and A add up to T only for paired samples.

Fractional recovery of nuclei was higher for rat than non-adherent human fresh ($p<0.01$) and cultured/shipped ($p<0.10$) islets, but total nuclei recovery was not significantly different. The same trends were true with DNA recovery but with higher p values. Human fresh islets had lower recovery than cultured/shipped islets for non-adherent ($p<0.09$) and total ($p<0.02$) tissue. Recoveries of adherent tissue were similar. Significant differences in recoveries of human fresh and cultured/shipped islets were not observed in terms of fraction of original DNA. At 24°C, fractional cell recoveries for rat and non-adherent human fresh and cultured/shipped islets were 0.74 ± 0.16, 0.83 ± 0.04, and 0.77 ± 0.19, respectively, all significantly less than 1.0 but higher than at 37°C. Similar data were obtained with fractional DNA recovery.

2.3.3 OCR/cell and OCR/DNA

Frequency distributions of OCR/cell and OCR/DNA for day 0 and for non-adherent tissue on day 1 and 2 in culture are shown in Figure 2.2 and Figure 2.3, respectively. OCR/cell for rat islets, human fresh and cultured/shipped islets, and human non-islet tissue was 2.7 ± 1.1, 1.5 ± 0.5, 1.6 ± 1.1, and 1.6 ± 0.7 fmol/min cell on day 0, respectively, and 2.6 ± 0.4, 2.6 ± 1.1, 2.3 ± 0.7, and 2.2 ± 0.7 fmol/min cell on day 2. On day 0, none of the distributions were normal. The COV was 0.41 for rat, 0.33 for human fresh, and 0.70 for cultured/shipped islets, and 0.44 for non-islet tissue, all larger than the comparable value of DNA/cell. Furthermore, the ratio of maximum to minimum measured value ranged from about 2.0 to 3.1 for DNA/cell and about 3.5 to 6.4 for OCR/cell. Because the precision in measuring DNA content and OCR was comparable, the wider range of the OCR/cell distributions indicates differences in the viability characteristics of the different preparations. For the frequency distributions of OCR/DNA (Figure 3), trends of the population means between species and days in culture were similar to those shown by the OCR/cell distributions, except that there were larger differences between some mean values and smaller differences between others because of the differences in the DNA/cell between the various types of tissue preparations. Notably, the increase in OCR/DNA from day 0 to day 2 for human fresh non-adherent and total tissue was not significant, whereas it was significant for OCR/cell measurements.

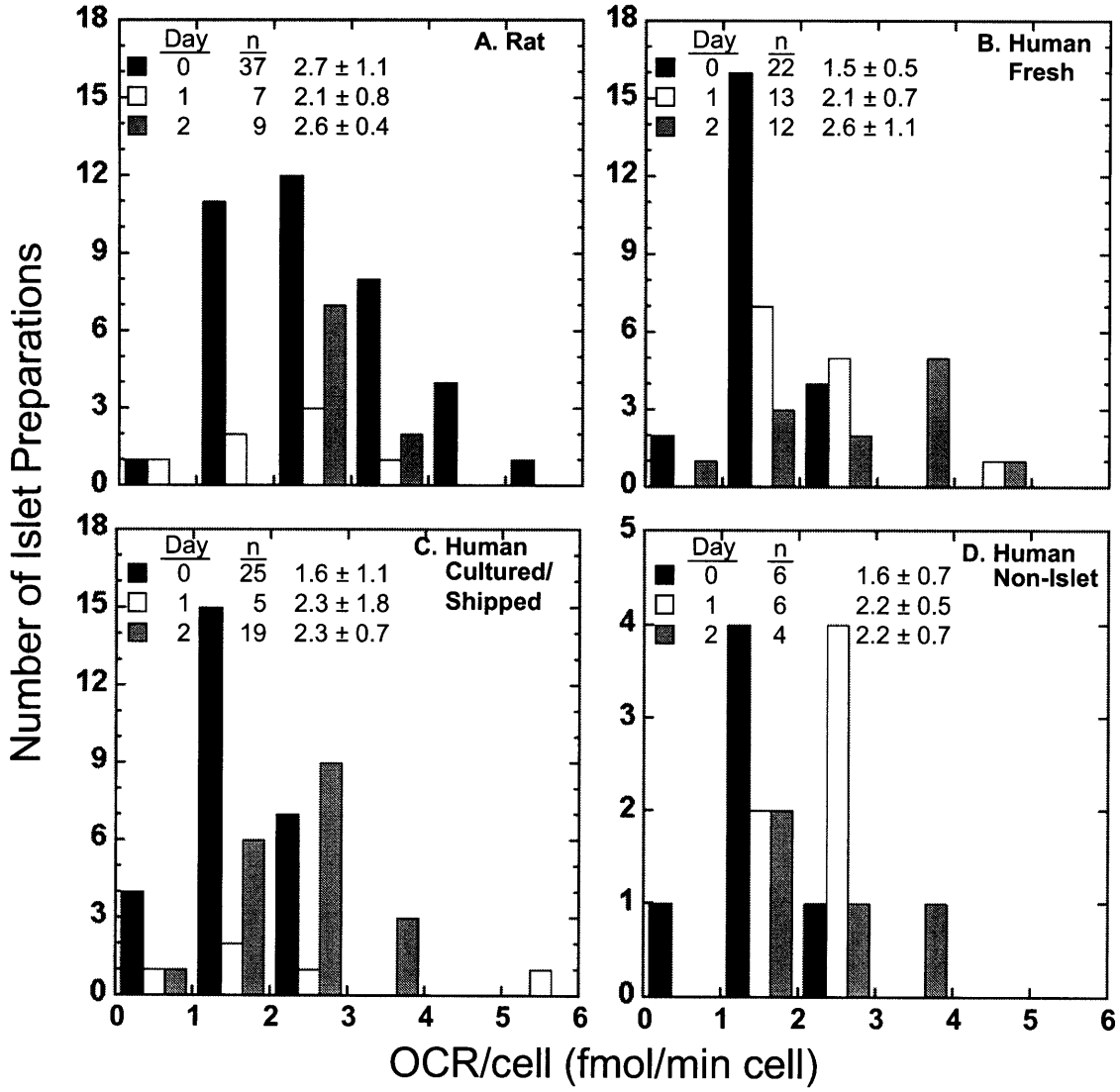

Figure 2.2. Frequency distributions of the OCR/cell for day 0 and for non-adherent tissue on day 1 and 2 in culture for (A) rat, (B) human fresh, (C) human cultured/shipped islets, and (D) human non-islet tissue.
n is the total number of islet preparations for which measurements were made.

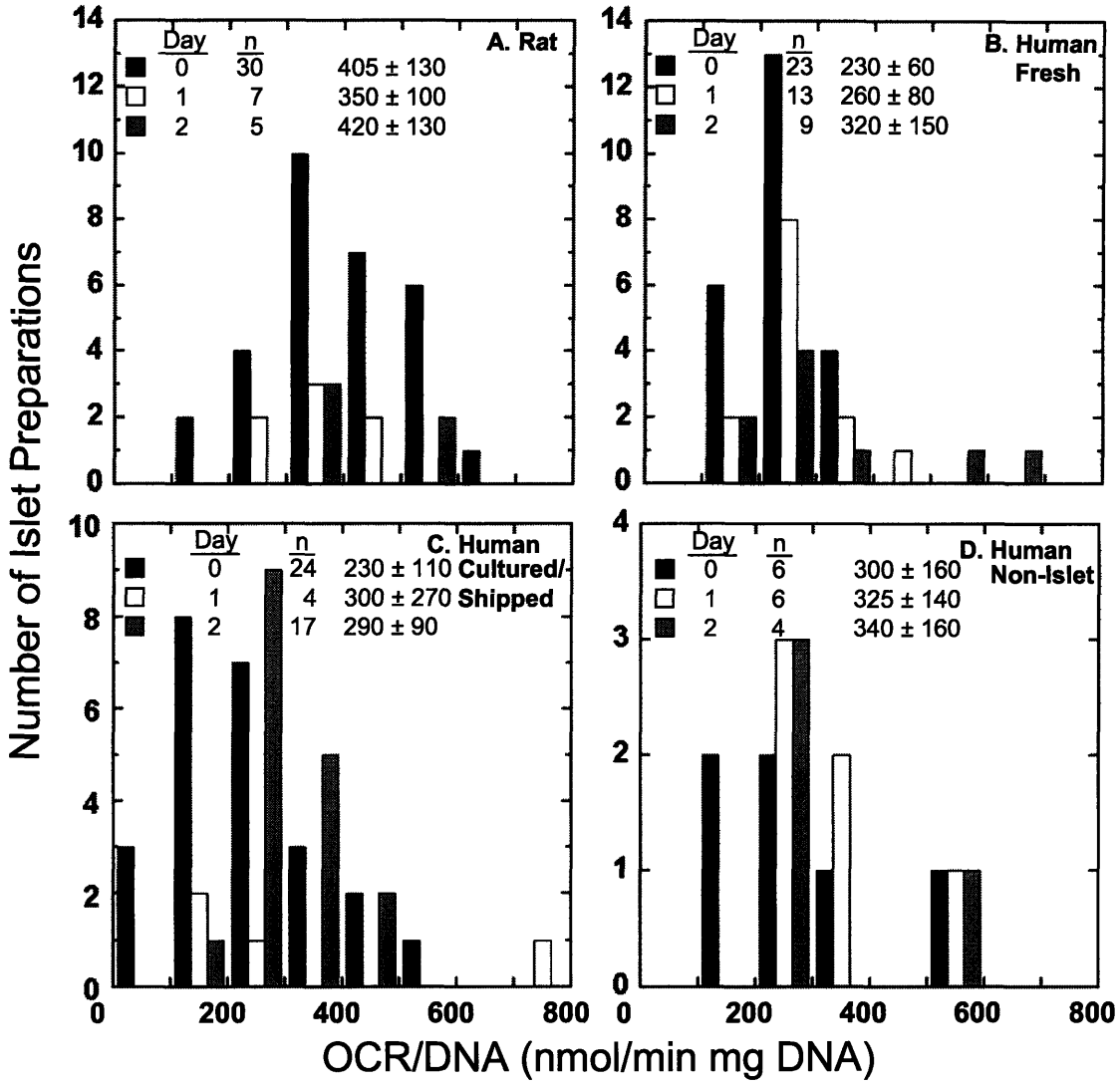

Figure 2.3. Frequency distributions of the OCR/DNA for day 0 and for non-adherent tissue on day 1 and 2 in culture for (A) rat, (B) human fresh, (C) human cultured/shipped islets, and (D) human non-islet tissue.
n is the total number of islet preparations for which measurements were made.

The effect of 2-day culture on OCR/cell and OCR/DNA is tabulated in Table 2.2. The increased OCR/cell with time observed in Figure 2 for non-adherent human tissue was significant in paired t-tests. OCR/cell for all adherent human islets tissue was lower than that of the corresponding non-adherent tissue and was not significantly different than day 0 values. OCR/DNA followed similar trends, but significance in differences did not follow a precise correspondence because of variation in DNA/cell and occasional large COVs. After 2 day 24°C culture, OCR/cell and OCR/DNA of rat non-adherent and human islets were substantially lower

than after 37°C culture. In addition, after 24°C culture OCR/cell of non-adherent tissue was lower for fresh human islets than that of rat and human cultured/shipped islets.

2.3.4 OCR recovery

The fractional recovery of OCR from 2-day, 37°C culture was significantly less than 1.0 for almost all categories (Table 2.2). Fractional recovery of total tissue was 0.65 ± 0.20, 0.75 ± 0.23, and 0.98 ± 0.07 for rat and human fresh and cultured/shipped islets, respectively; that for non-adherent tissue was 0.63 ± 0.06, 0.70 ± 0.27, and 0.46 ± 0.27 for human fresh and cultured/shipped islets and non-islet tissue. Fractional recovery of the adherent component was smallest, about 0.33 for both groups of human islets, but the number of measurements was small, and the data for fresh islets may not be representative. At 24°C, fractional OCR recoveries for non-adherent rat and human fresh islets were 0.63 ± 0.20, and 0.65 ± 0.14, respectively, which are lower than that for non-adherent cultured/shipped islets, 0.83 ± 0.28. All are significantly less than 1.0 but not significantly different from their values at 37°C.

2.3.5 OCR/DNA comparisons between centers

Frequency distributions of the OCR/DNA for islets isolated and analyzed at different centers are shown in Figure 2.4. Fresh human islets at UMN had significantly lower OCR/DNA values (130 ± 30 nmol/min mg DNA) than those isolated at JDC and analyzed at MIT on day 0 ($p<0.01$). These values did not increase significantly with time in culture, and the difference between dates obtained at the two locations was even greater at day 2.

2.3.6 Membrane integrity

Frequency distributions of the fraction of cells with impermeable cell membranes by 7-AAD for day 0 and for non-adherent tissue on day 1 and 2 in culture are shown in Figure 2.5. On day 0, the fraction of cells with impermeable cell membranes averaged 0.85-0.87 for all human tissue and 0.77 for rat islets, and only rat islets had a substantial fraction of preparations below 0.8. The fraction increased with time in culture for rat islets, and did not change for human islets. It also did not change for non-islet tissue (paired t test with $p = 0.2$, and 0.3 for day 1 and 2 respectively), even though the trends of the means in Figure 2.5 are misleading.

Table 2.2. OCR/cell, OCR/DNA, and fraction of original OCR recovered after 2 days culture.[a]

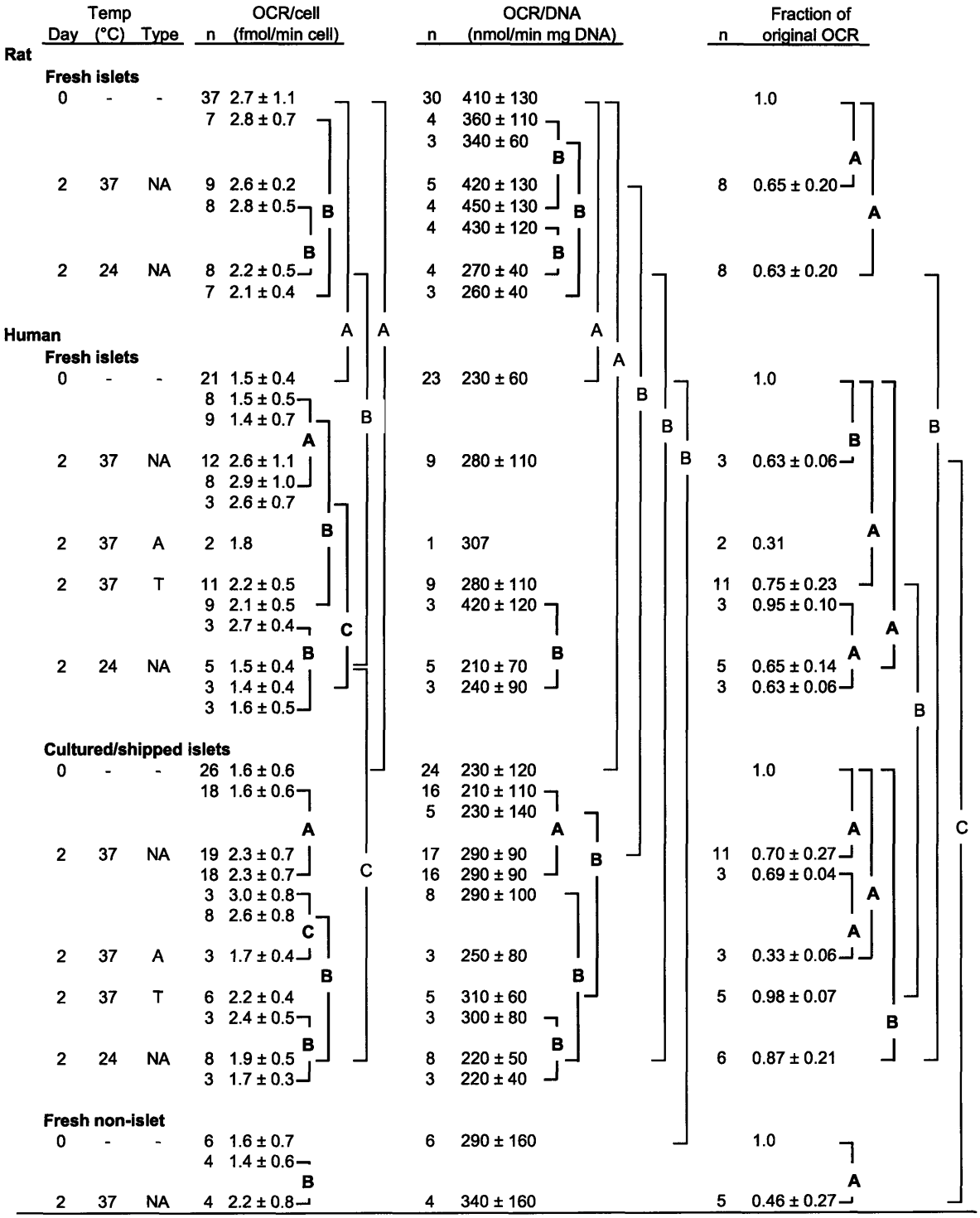

[a]Format is identical to that in Table 1.

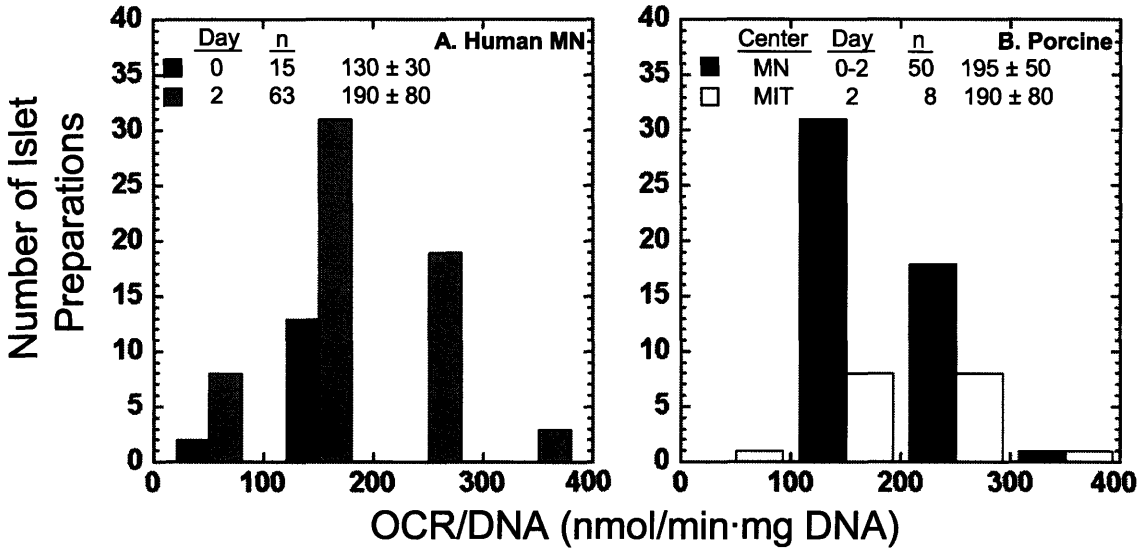

Figure 2.4. Frequency distributions of the OCR/DNA for different centers (MIT, MN) for (A) human, and (B) porcine islets.
Islets were analyzed right after isolation and after 2-day culture at the respective centers. The data for porcine from MN on day 0 and 2 are combined. n is the total number of islet preparations for which measurements were made.

2.3.7 OCR/cell with impermeable cell membranes by 7-AAD

The value of OCR/cell of each preparation was divided by the fraction of cells with impermeable cell membranes by 7-AAD for that preparation. The frequency distributions of this quantity, denoted as $OCR/(cell)_{MI}$, for day 0 and for non-adherent tissue on day 1 and 2 in culture are shown in Figure 2.6. Conversion of OCR/cell data to $OCR/(cell)_{MI}$ had only a small and inconsistent effect on COV for the distribution, and introduced divergences into the value after 2 days in culture.

To further explore the relationships between OCR and membrane integrity measurements, OCR/DNA measurements are plotted versus the fraction of cells with impermeable cell membranes by FDA/PI staining and 7-AAD in Figure 2.7. Whereas OCR/DNA measurements varied from about 150 to 700 nmol/min mg DNA for rat islets, 100 to 350 nmol/min mg DNA for human islets, and 100 to 500 nmol/min mg DNA for porcine islets, values of membrane integrity from FDA/PI staining and 7-AAD sequential staining were always in excess of 70%, except for a few lower values for rat islets.

2.3.8 Purity

The mean islet volume fractions (Φ_I) were 0.64 ± 0.12 (range 0.43 to 0.79) and 0.67 ± 0.09 (range 0.58 to 0.82) for fresh and cultured/shipped human islet preparations on day 0, respectively (Table 2.3). These values fall within the range reported for typical clinical preparations. Φ_I for non-adherent tissue increase on day 2 compared to day 0; the effect was significant only for fresh tissue. The β cell volume fraction exclusive of vascular space ($\Phi_{\beta XV}$) was higher for cultured/shipped islets (0.41 ± 0.03) than for fresh islets (0.33 ± 0.03) on day 0. On day 2, $\Phi_{\beta XV}$ increased for non-adherent tissue and decreased for adherent tissue. The differences were larger for fresh islets. The number fraction β cells (f_β), which was calculated from Φ_I and $\Phi_{\beta XV}$ as outlined in the Appendix, follows a similar trend. Combining f_β and nuclei recovery measurements (Appendix) revealed that the fraction of original β cells recovered from culture (F_β) was significantly higher for non-adherent tissue than adherent tissue, but was less than 1.0 even when the fractions were combined. A loss of about 30% β cells was observed for cultured/shipped tissue while a much larger loss, about 65% was observed for fresh tissue though only two data points were available.

2.4 Discussion

In this paper, we used previously-developed quantitative methods [39; 55] to measure quantity (nuclei counts, DNA content), purity (volume fraction islets and β cells), viability (OCR), and membrane integrity for islet and non-islet preparations of different species (rat, human, and porcine) from different islet isolation centers before and after culture at different temperatures (24°C and 37°C). Measured values were expressed on a per cell basis when appropriate. We also estimated the recovery of total tissue, viable tissue, and β cells after 2-day culture for non-adherent and adherent tissue. This is the first study to report this comprehensive set of quantitative parameters with a large number islet preparations before and after culture.

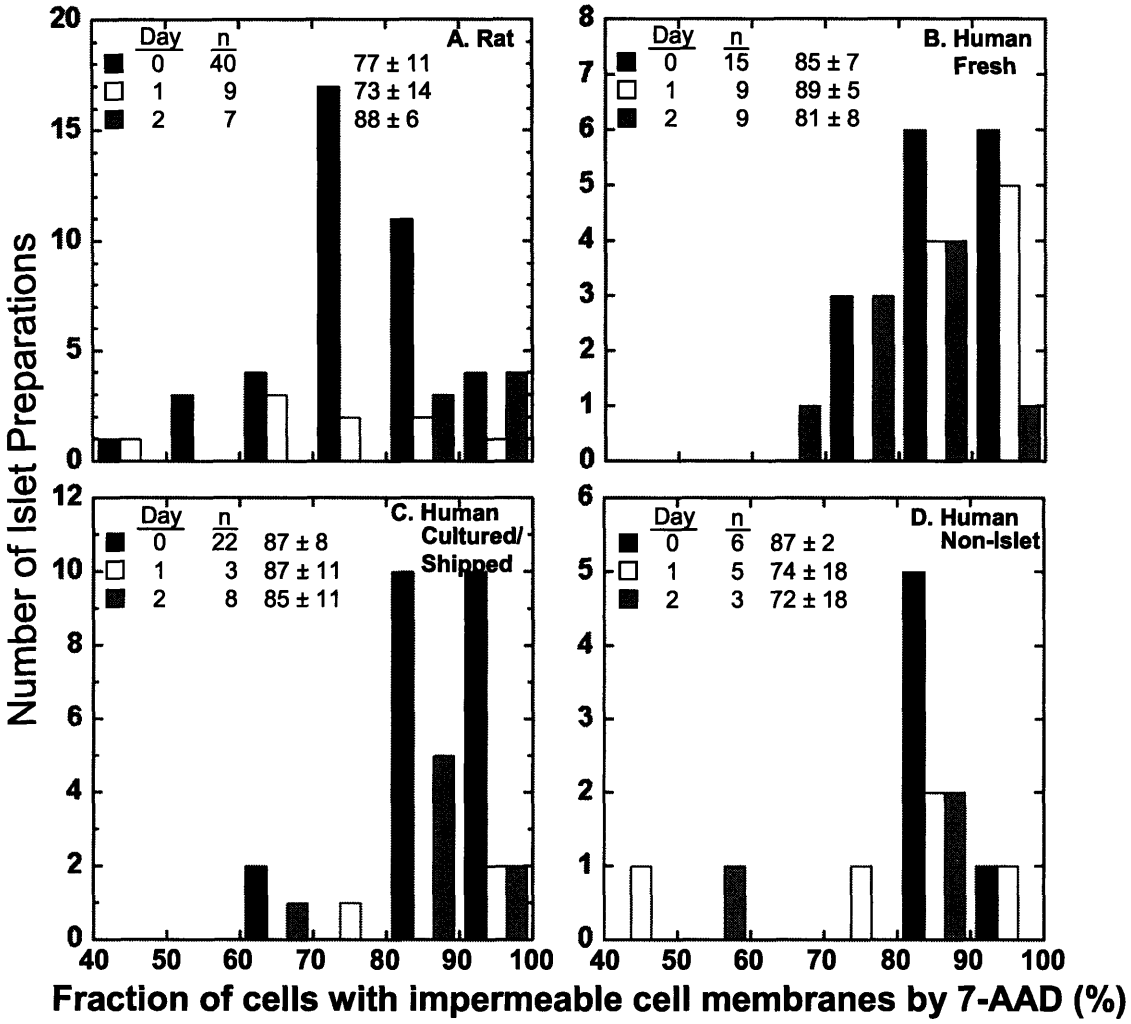

Figure 2.5. Frequency distributions of the fraction of cells with impermeable cell membranes by 7-AAD for day 0 and non-adherent tissue on day 1 and 2 in culture for (A) rat, (B) human fresh, (C) human cultured/shipped islets, and (D) human non-islet tissue.
n is the total number of islet preparations for which measurements were made.

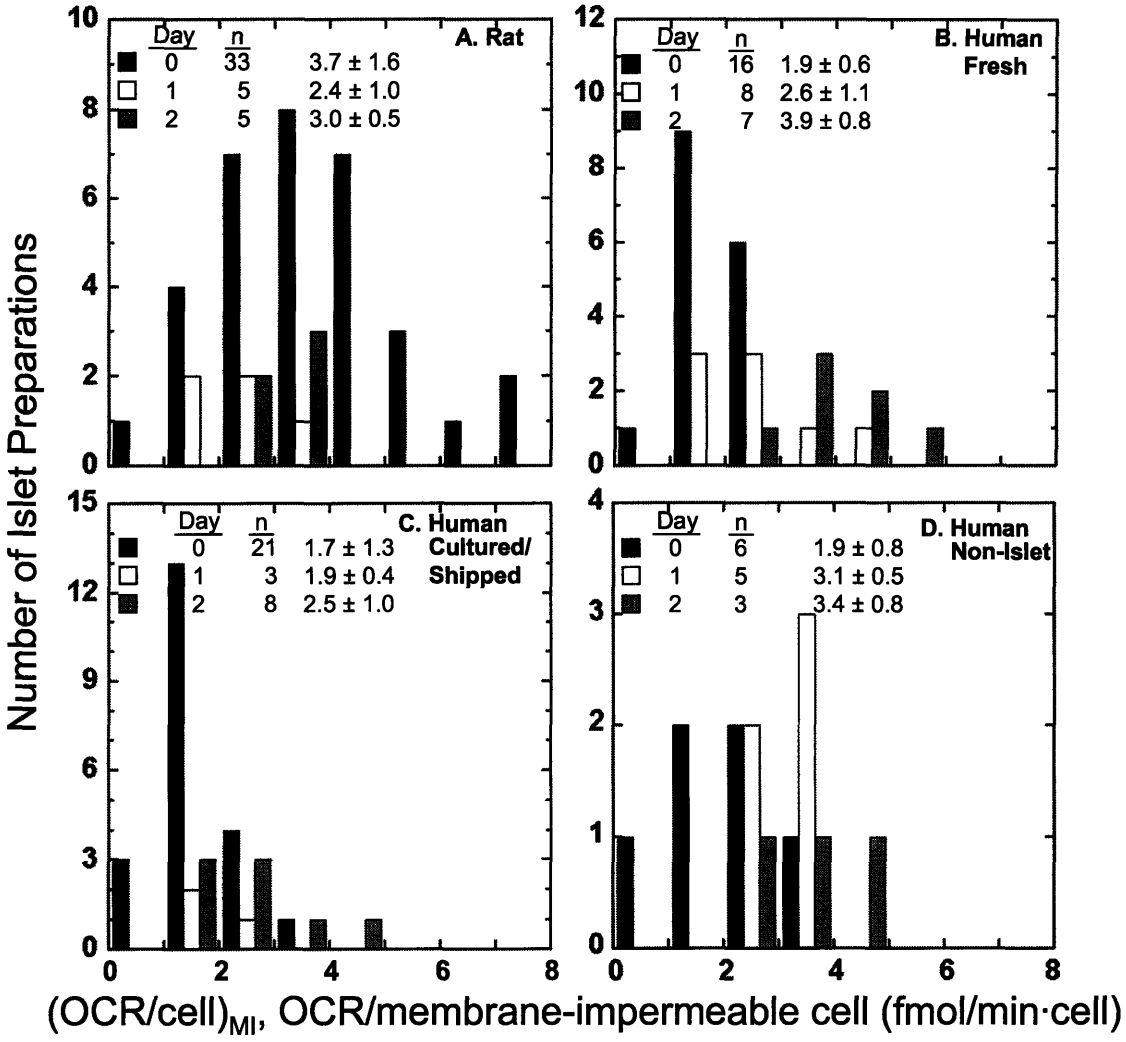

Figure 2.6. Frequency distributions of the OCR/membrane-impermeable cell for day 0 and for non-adherent tissue on day 1 and 2 in culture for (A) rat, (B) human fresh, (C) human cultured/shipped islets, and (D) human non-islet tissue.
n is the total number of islet preparations for which measurements were made.

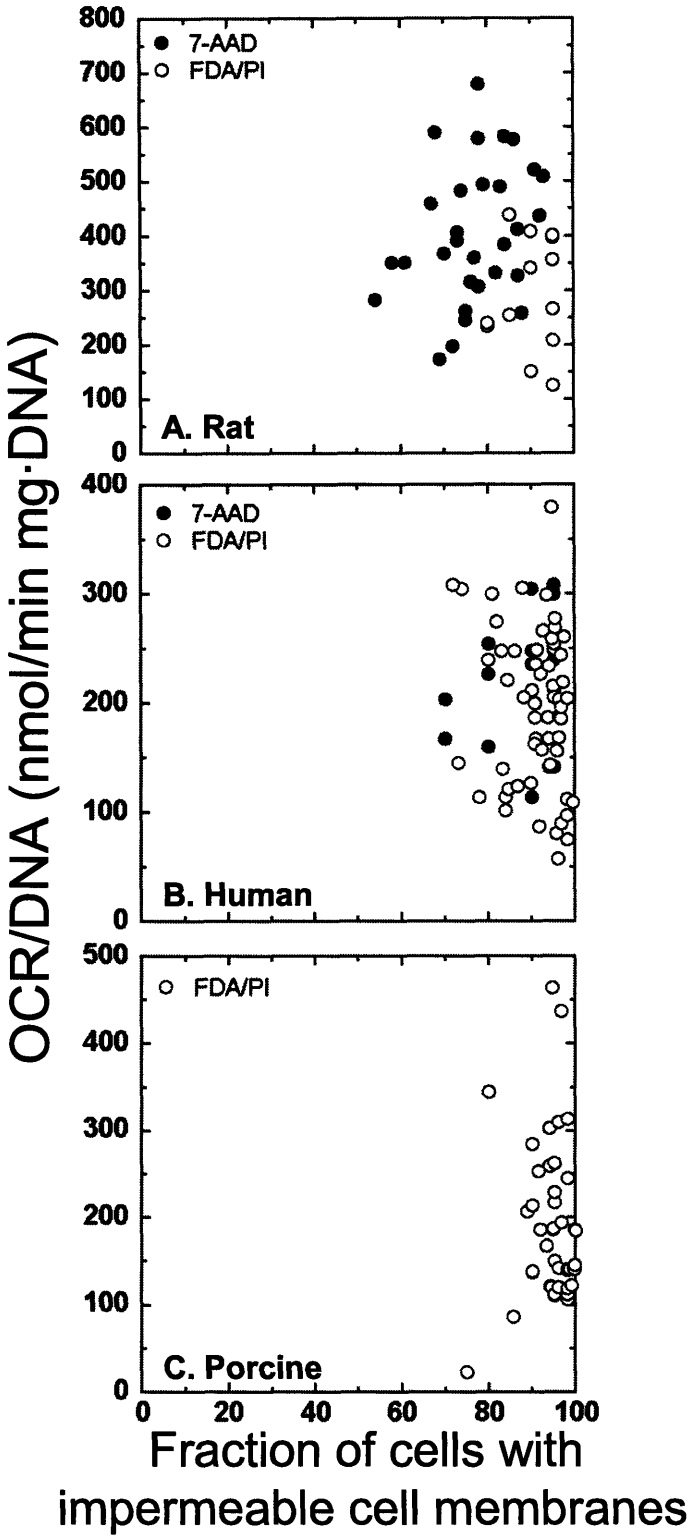

Figure 2.7. OCR/DNA versus fraction of cells with impermeable cell membranes by FDA/PI staining and 7-AAD for (A) rat islets, (B) human fresh islets.

On day 0, fresh islet tissue had DNA values close to 6.5 pg DNA/cell (Table 2.1 and Figure 2.1), which is the value expected for rat [67] and human [68] cells. The higher value for cultured/shipped human islets likely reflects residual, undegraded DNA. With time in culture, DNA/cell did not change for rat islets but increased for fresh human islet and non-islet tissue and decreased for cultured/shipped islets. This behavior is consistent with the notion that the cell death process had proceeded to a greater extent when the cultured/shipped samples were received and that subsequent behavior in culture reflected greater cell death in fresh human islets as a result of stresses imposed during the isolation process.

Losses of tissue during culture, as measured by nuclei counts, were substantial. After culture for 2 days, the non-adherent tissue collected accounted for about 2/3, 1/3, and 1/2 of the rat, human fresh, and human cultured/shipped islet preparation, respectively, placed into culture at day 0. Recovery of non-adherent non-islet tissue was about 40%. The non-adherent fraction of human islet tissue is the part currently used for both research purposes and clinical transplantation. When the adherent tissue (20-30% of the original tissue) is included, the fraction of the original tissue that was actually lost was about 1/3 for rat and fresh human islets and 1/5 for cultured/shipped islets. At 24°C, a substantially larger fraction of the original tissue was recovered as the non-adherent fraction especially for fresh human islets (0.83), consistent with previous reports for human [47] and porcine islets [49]. Thus, from the same original preparation, the amount of tissue recovered after 2 days at 24°C was more than double that at 37°C. Culture at 24°C did not result in significant adherence and thus could explain the higher tissue recovery. In addition, since the combined tissue recovery was also lower at 37°C than non-adherent tissue recovery at 24°C, it is likely that there are slower rates of DNA and nuclei degradation at reduced temperature.

Trends with DNA measurements were similar but not as sharp and often with lower p values. Nonetheless, measurements with both methods are desirable because DNA/cell estimates provide a measure of the extent of recent cell death.

Table 2.3. Human islet and β cell purity measurements and fraction of β cells recovered after culture for 2 days at 37°C.[a]

Day	Type	n	Islet volume fraction Φ_I	n	β cell volume fraction exclusive of vascular space $\Phi_{\beta XV}$	n	Number fraction β cells f_β	n	Fraction of original β cells F_β	n	Fraction of original nuclei
Fresh											
0	-	18	0.64 ± 0.12								
		4	0.67 ± 0.12								
		2	0.50 ± 0.04	2	0.33 ± 0.03	2	0.31 ± 0.03	2	1.0	2	1.0
2	NA	4	0.75 ± 0.07	2	0.48 ± 0.01	2	0.45 ± 0.01	2	0.30 ± 0.13	2	0.20 ± 0.09
2	A			2	0.10 ± 0.06	2	0.08 ± 0.11	2	0.04 ± 0.01	2	0.13 ± 0.02
2	T							2	0.34 ± 0.13	2	0.33 ± 0.07
Cultured/shipped											
0	-	9	0.67 ± 0.09								
		5	0.61 ± 0.04	5	0.41 ± 0.03	5	0.39 ± 0.03	5	1.0	5	1.0
2	NA	4	0.70 ± 0.15	5	0.44 ± 0.09	5	0.41 ± 0.09	5	0.60 ± 0.14	5	0.58 ± 0.09
2	A			5	0.17 ± 0.08	5	0.14 ± 0.07	5	0.09 ± 0.03	5	0.33 ± 0.22
2	T							5	0.69 ± 0.14	5	0.92 ± 0.18

[a]Format is identical to that in Table 1. Φ_I, $\Phi_{\beta XV}$, and the fraction of original nuclei were measured; f_β and F_β were calculated as described in Appendix.

OCR/cell and OCR/DNA of human tissue (islet and non-islet) was lower than that of rat on day 0 likely because of the harsher isolation procedure. After 2-day culture at MIT in 37°C rat and human OCR/cell values of non-adherent islet and non-islet tissue were similar indicating that tissue respiration in stable, undamaged tissue is similar for different cell types and for rat and human tissue. However, porcine islets, both from MIT and MN, had a lower OCR/DNA than rat and human islets (MIT), suggesting there could be intrinsic differences in respiration between certain species. The OCR/cell values we obtained are within the range of values reported in the literature for intact islets of different species measured by different methods, 2-3.5 fmol/min cell (data converted to similar units for comparison purposes) [69-75]. One study reports lower values (0.3-0.5 fmol/min cell) but the measurements were made with a system of unreliable accuracy [13].

Human islets from MN had a lower OCR/DNA than those analyzed at MIT that could be explained by differences in the isolation and/or culture procedure for which temperature and density can have large effects. The effect of temperature is supported by the lower OCR/cell and OCR/DNA measurements obtained on day 2 at 24°C compared to 37°C for rat, human fresh, and cultured/shipped islets. Decreases in membrane integrity and cellular function (stimulation index) have been observed following reduced temperature culture [47; 49]. The lower OCR/cell following 24°C culture could also be an indication that the respiration of the tissue has not acclimated to 37°C or that the reduced culture temperature has permanently changed cellular machinery resulting in cells that require less oxygen as previously suggested [51] bringing up questions about changes in cellular function. Brandhorst et al concluded that 37°C culture of porcine islets resulted in superior insulin content, secretion, and dynamic response to glucose as compared to culture at 22°C [49], which is consistent with results for human islets [47] suggesting that 37°C culture maintains islet function better than reduced culture temperatures.

OCR recovery of non-adherent human non-islet tissue was lower than that of non-adherent fresh human islets. When accounting for both non-adherent and adherent tissue the total OCR recovery of cultured/shipped tissue was about 1 indicating no loss in viable tissue, while fresh tissue resulted in an average 25% decrease in viable tissue during culture, probably because tissue had not completed the cell death process initiated during isolation. OCR recovery for rat islets was less than 1 either because of loss of viable tissue during culture for similar reasons as

fresh human islet tissue or because adherent tissue was not analyzed, though based on visual observations very little tissue adhered.

The fraction of cells with impermeable cell membranes by 7-AAD for fresh rat islets was lower than that for human tissue. A possible explanation could be that human non-islet cells are less susceptible to damage on their membrane integrity than islet cells. The fraction of cells with intact membranes spans a narrower range than respective OCR/DNA measurements for rat, human, and porcine islets (Figure 2.7). This behavior is consistent with our findings that OCR, a mitochondrial function assay, is an earlier indicator of cell death than membrane integrity tests [55].

If the fraction of membrane-impermeable cells in islets 4 hr after isolation or receipt actually represented the fraction of viable cells, the OCR/viable cell or OCR/DNA for viable cells can be calculated. Because the spread of the distributions (Figure 2.6) was wider than those of the OCR/cell and the fraction of cells with impermeable cell membranes by 7-AAD, it is suggested that the normalization of OCR with 7-AAD does not result in a unique value for OCR of viable cell. If islet and non-islet tissue 4 hr after isolation are still recovering from damage incurred during the isolation process, then the fraction of cells that are viable (as assessed, for example, by a mitochondrial function assay such as OCR) is likely to be much smaller than that inferred from membrane integrity measurements, as has been observed [55], because permeabilization of the cell membrane occurs relatively late in cell death processes [76].

The islet volume fraction of the non-adherent fresh human islets increased in culture because non-islet tissue preferentially adhered to the flask, consistent with a lower β cell volume fraction exclusive of vascular space. In cultured/shipped tissue about 30% of the original β cells were lost in culture though they were likely dead prior to culture since the OCR recovery was almost 1. This could also be attributed to β cell dedifferentiation that would cause loss of insulin expression [77].

Our study provides the basis for a complete understanding of islet and non-islet tissue behavior in culture, at different temperatures, in terms of purity, quantity, viability, and β cell fraction. Other methods on islet characterization have intrinsic shortcomings that render them inappropriate and unreliable for islet assessment prior to transplantation. In order to obtain the β cell viability index that Ichii et al. [37] introduced, islets needed to be dissociated, which has been shown to result in samples not representative of the original islet [78]. The study of

ATP/ADP ratio by Goto et al. [38] is hindered by the extreme sensitivity of the assay to changes in environmental conditions and therefore it can be quite difficult to use the assay to get an accurate prediction, especially with islets that are large aggregates, and cells in the outer and inner regions may experience very different microenvironments depending on the assay conditions [79]. Finally, even though Guarino et al. [75; 80] used oxygen consumption rate measurements as an islet assessment method, the system they chose to use, BD OBS, is offset by difficulties in obtaining accurate and meaningful OCR estimates. Reported OCR values measured with the OBS do not agree with measurements made with other methods and therefore render the assay questionable.

2.5 Nomenclature

7-AAD	7-aminoactinomycin D
A	Adherent tissue
α	Solubility of oxygen in medium
COV	Coefficient of variation
DAB	2 mM 3,3'-diaminobenzidine tetrahydrochloride
D-PBS	Dulbecco's phosphate buffered saline
DTZ	Dithizone
f_β	Number fraction of β cells among all cells
F_β	Fraction of original β cells collected from culture
FBS	Fetal bovine serum
FDA	Fluorescent diacetate
IE	Islet equivalent
JDC	Joslin Diabetes Center
MIT	Massachusetts Institute of Technology
MN	University of Minnesota
NA	Non-adherent tissue
OBS	Oxygen biosensor system
OCR	Oxygen consumption rate
$OCR/(cell)_{MI}$	OCR per viable cell

PAP	Peroxidase-antiperoxidase
PI	Propidium iodide
pO_2	Oxygen partial pressure
t	Time
T	Total (non-adherent + adherent) tissue
V_{ch}	Volume of OCR chamber
$\Phi_{\beta XV}$	Volume fraction of β cells exclusive of islet vascular spaces
Φ_I	Volume fraction of islets

3 The effect of surface density on tissue quality during static islet culture on untreated polystyrene

3.1 Introduction

Following the initial report of success [7] islet transplantation has become a promising option for treating type 1 diabetes though many complications remain [8; 12; 21; 81-83]. After islet tissue is isolated from a donor pancreas by mechanical and enzymatic treatment [13-15], it may transplanted directly or cultured [14; 40]. Islet culture prior to transplantation is desirable for many reasons and is standard practice in most clinical centers [40]. Culture provides time for islet tissue to recover from the harsh isolation process while tissue quality is assessed for purity, viability, and sterility and for recipient matching, patient travel to the islet center, and patient preparation such that necessary levels of immunosuppression are attained before transplantation [40; 47; 48]. Additionally the immunogenicity of islet tissue may be reduced through culture [41-46], thus lowering the body's immune response upon transplantation. Culture could also provide the time necessary to apply treatments currently under investigation (e.g. gene manipulation or chemical treatment such as carbon monoxide, Appendix 10.2) that may reduce cell death prior to and following transplantation [84-90].

A need to better understand islet culture exists. Culture conditions, including islet density, temperature, and duration vary between islet centers. There is little published information to determine the effect of these variables on the recovery of islet tissue, its viability, and its purity. A large amount of literature discusses media formulations and additives [40; 48], but little is available about the effect of islet density on islet quality [40]. Islet surface density and size are thought to be related to necrotic death [91] because experiments with low islet surface densities result in higher recoveries and higher stimulation indices compared to culture with high islet surface densities [47]. This decrease in islet tissue quality with increasing density may result from insufficient oxygen (O_2) transport to the core of the islet and is consistent with observations that indicate higher necrotic death in islets at 37°C compared to lower temperatures where metabolic rates are reduced [49; 50; 52].

Oxygen transport is crucial for maintaining islet viability and function [92]. Because isolated islets lose their blood supply and blood vessels collapse during static culture [93-95], O_2 is supplied to the interior only by diffusion resulting in the formation of O_2 gradients in and

around each islet. If islets are too large or too close together, O_2 is depleted before it reaches the center of the islet, thereby causing the core to become severely hypoxic and leading to the development of dead tissue by necrosis and/or apoptosis [16; 49; 92; 96]. A theoretical model describing this phenomena with islets cultured on an O_2-impermeable surface has been developed [16].

Oxygen supply limitations will not cause deleterious effects at very low tissue surface densities [16]. However, the large surface area required to culture the islets obtained from a single isolation in the absence of O_2 limitations is impractical. As a result, the density of human islet tissue typically employed, 200-400 islet equivalents (IE)/cm^2 (K. Papas and A. Omer, personal communications), is thought to balance possible reduction in islet quality after culture against practical limitations, even though this density may be an order of magnitude higher than the surface density at which O_2 diffusion limitations begin [16]. Because little data is available for the effect of islet density on islet quality, the extent to which islet quality is affected by current practice is unknown.

In a previous study (Chapter 2), in which human islet tissue was cultured on untreated polystyrene vessels at low tissue surface density, we observed effects on recovery of islet tissue, its viability, and its purity. In this study, we explored whether culture at high density resulted in additional changes in these characteristics. In addition, we employed a theoretical O_2 transport model to investigate whether O_2 supply limitations can explain the reduction in the amount of viable tissue observed during high density islet culture. The results of this study demonstrate that tissue surface density has a significant impact on the recovery of islet tissue, its viability, and its purity. The decrease in the amount of viable tissue observed following high density culture is qualitatively similar to that predicted by an O_2 transport model, indicating that O_2 limitations are likely the primary cause of the decrease.

3.2 Methods

Islet isolation and culture

Standard collagenase/protease digestion methods were used for human [7; 15] isolations. Preparations human islets were provided fresh (4-6 hr after isolation was complete) by the Islet Core at the Joslin Diabetes Center (JDC, Boston, MA). Human islets were also received after culture (1-2 days) from JDC or overnight shipment (sometimes after up to 1 day culture) from

other centers contained in culture flasks (T-25 and T-75) or centrifuge tubes in Styrofoam boxes. When first observed, some preparations were in suspension, some in a pellet. Upon receipt, a portion of the preparation was analyzed and the remainder placed into untreated polystyrene culture flasks at 37°C in a humidified environment (5% CO_2), oxygen partial pressure (pO_2) of 142 mmHg, for 34-60 hr during which no medium change occurred.

Islets were cultured in supplemented RPMI (11.1 mM D-glucose, 100 U/ml penicillin, 100 μg/ml streptomycin, 2 mM L-glutamine, 1 mM sodium pyruvate (all from Mediatech Inc., Herdon, VA), and 50 μM β-mercaptoethanol (Sigma Aldrich, St. Louis, MO) with 10% fetal bovine serum (FBS, Mediatech Inc.), in 3 mm of medium in untreated polystyrene tissue culture flasks. After culture the free, non-adherent tissue (which is the only tissue used in current practice) was collected. At densities $<50 \times 10^4$ cells/cm^2, adherent human tissue was incubated for 5 min at 37°C in 0.05% trypsin EDTA (Mediatech Inc.), dislodged with fresh medium, and collected. Tissue suspensions were centrifuged for 3 min at 300xg, supernatant removed and the tissue suspended in fresh medium. At high densities ($>50 \times 10^4$ cells/cm^2), trypsinization was not required because adherent tissue was an insignificant fraction of the total.

DNA content

At MIT, DNA was measured by fluorospectrophotometry [55] using the CyQUANT Cell Proliferation Assay Kit (Molecular Probes, C-7026 Eugene, OR), and a λ DNA standard (Invitrogen) and 50-250 IE/sample. Fluorescence was read at 480 nm excitation and 520 nm emission wavelengths in a plate reader (Spectra MAX Gemini microplate spectrophotometer, Molecular Devices, Sunnyvale CA).

Islet enumeration by nuclei counting

Nuclei were prepared by adding equal 100-μl volumes of sample containing 160 or more IE and of lysis solution (0.1 M citric acid (Sigma) and 1% (v/v) Triton X-100 (Sigma)) to a 1.5 ml microtube [55]. The mixture was incubated at room temperature for 5 min with vortex mixing every 1.5 min, and nuclei were liberated by shearing through a needle. Isolated nuclei were diluted with Dulbecco's phosphate buffered saline (D-PBS, Invitrogen, Carlsbad, CA) to a concentration no higher than 5×10^5 nuclei/ml, stained with 7-aminoactinomycin D (7-AAD, Molecular Probes, Eugene, OR), and analyzed using a flow cytometer (Guava Personal Cell Analysis (PCA) system, Guava Technologies, Hayward, CA) to determine the total number of cells with intact nuclei in the sample.

Oxygen consumption rate (OCR)

OCR was measured as previously described [39]. Briefly, suspensions containing about 2500 IE/ml in DMEM containing 4.5 g/l glucose and 0.6 g/l L-glutamine supplemented with 100 U/ml penicillin, 100 µg/ml streptomycin, 10 mM HEPES, and no added serum were sealed in a 200-µl stirred titanium chamber (Micro Oxygen Uptake System, FO/SYSZ- P250, Instech Laboratories, Plymouth Meeting, PA) maintained at 37°C. The time dependent pO_2 within the chamber was recorded with a fluorescence-based oxygen sensor (Ocean Optics, Dunedin, FL), and data at high pO_2 were fit to a straight line. The maximal OCR was evaluated from $OCR=V_{ch}\alpha(\Delta pO_2/\Delta t)$, where V_{ch} is the chamber volume and α = 1.27 nmol/mm·Hg·ml is the Bunsen solubility coefficient for oxygen in medium [16]. OCR measurements were normalized by the measured number of cells (nuclei counting) or DNA content of the sample examined.

Membrane Integrity

7-Aminoactinomycin (7-AAD) sequential staining

Cell membrane integrity was assessed by differential staining with 7-AAD (Molecular Probes, Eugene, OR) [55]. An aliquot of about 300 islets was re-suspended in 100 µl of D-PBS, and 5 µl of 1 mg/ml 7-AAD and incubated for 20 min at 4°C protected from light. After two washes with 1 ml of D-PBS, cells were disrupted by adding equal volume of lysis solution in D-PBS to the islet suspension and sheared[16] as described for islet enumeration. Labeled nuclei were counted immediately in the flow cytometer or stored on ice for less than 15 min before counting. A portion of the islet suspension was further stained with 7-AAD, thereby labeling all of the previously unlabelled nuclei, and the total number of nuclei was counted. The fraction of cells with compromised membranes was estimated as the ratio of the initially stained nuclei (first measurement) to the total number of nuclei (second measurement).

Islet volume fraction by morphological analysis

A 0.5 ml aliquot of human islet preparation was processed to produce 1-µm sections stained with toluidine blue and examined by light microscopy [13]. Islet tissue was distinguished from non-islet tissue as previously described [13]. Sections were analyzed at 420X by stereological point counting [63] with a 90-point grid covering adjacent, non-overlapping fields. At point intercepts of the grid with tissue, the nature of the tissue was determined, and the volume fraction of islet tissue, denoted Φ_I, was calculated as previously described [13].

β cell identification by immunocytochemical insulin staining

Tissue samples were washed twice with 1 ml D-PBS, fixed for 1 hr in 10% formalin (Sigma Aldrich), washed twice with 1 ml of D-PBS, and centrifuged at 300xg for 5 min. To the pellet, 500 μl of warm 2% (w/v) agarose was added. The solution was mixed using a vortex mixer for 1 sec, immediately centrifuged at 18000xg for 10 sec, allowed to cool for 2 min, and then 500 μl of 10% formalin was added. After 1-hr incubation at room temperature, formalin was removed, samples were stored in D-PBS until embedded in paraffin, and 5-μm sections were cut. Sections were stained by the unlabeled antibody peroxidase-antiperoxidase (PAP) method [64] using guinea pig anti-bovine insulin (Linco, St. Charles, MO) as primary antibody and goat anti-guinea pig IgG (Cappel, Irvine, CA), as secondary antibody, to link primary antibody to rabbit PAP complex (Jackson ImmunoResearch Laboratories, Inc., West Grove, PA). Use of a heterologous antibody gave specific staining with little background [65]. After applying PAP, slides were stained in 50 ml of a 2 mM 3,3'-diaminobenzidine tetrahydrochloride (DAB, Sigma Aldrich) solution activated with 25 μl of 30% (v/v) hydrogen peroxide (EMD Chemicals Inc, Gibbstown, NJ) for 30-120 sec, then viewed under a microscope. Reaction between hydrogen peroxide, DAB, and PAP formed a dark brown insoluble precipitate [66]. Slides were counterstained with hematoxylin (Sigma Aldrich). β cell volume fraction exclusive of vascular space, denoted $\Phi_{\beta XV}$, was quantified using stereological point counting, as described for morphological analysis, with 200 points or more counted.

This procedure was used with samples after 2 days culture because trypsinization of adherent tissue degraded the structure and produced single cells, which, in turn, made it harder to morphologically differentiate between cell types and evaluate vascular volume fraction, whereas it was more accurate to distinguish insulin staining. Methods for calculating $\Phi_{\beta XV}$ (day 2) and comparing it with Φ_I (day 0) are described in the Appendix.

Statistics

Measurements were made with three or more replicates and reported as mean ± SD. Statistical significance was determined using a Student t-test for unpaired data for comparing population means, and for paired data when appropriate.

3.3 Theoretical oxygen transport model

The species conservation equation for O_2 in the absence of convection [16; 97] is given by

$$\frac{\partial C}{\partial t} = D\nabla^2 C + R \qquad \textbf{3.1}$$

where C is the concentration of O_2, D is the diffusivity of O_2, and R is the production rate of O_2. For convenience, the concentration terms in Equation 3.1 are replaced with O_2 partial pressure (p) using

$$C = \alpha p \qquad \textbf{3.2}$$

where α is the solubility of O_2. We assume that solubility is constant in each phase so that at steady state Equation 3.1 becomes

$$0 = D\alpha\nabla^2 p + R \qquad \textbf{3.3}$$

O_2 consumption within the islet is assumed to follow Michaelis-Menten kinetics [16] for which the reaction rate is expressed as

$$R = -\frac{V_{max} p}{K_m + p} \qquad \textbf{3.4}$$

where V_{max} is the maximum reaction velocity, and the Michaelis constant K_m is the value of p at which the reaction rate is $V_{max}/2$. O_2 consumption occurs only above a critical value, p_{crit}. Below p_{crit}, the tissue dies and no longer consumes O_2. The species conservation equations in medium (m) and in the islet tissue (i) become, respectively,

$$(D\alpha)_m \nabla^2 p = 0 \qquad \textbf{3.5}$$

$$0 = (D\alpha)_i \nabla^2 p - \frac{V_{max} p}{K_m + p} \qquad \textbf{3.6}$$

To model islet culture on an O_2 -impermeable dish, all the tissue (islet and non-islet) was assumed to be in the form of spheres with uniform diameter (d) that were arranged in a square

array with center-to-center distance w in a stagnant medium of height h (Figure 3.1). Because of symmetry within the system, Equation 3.1 was solved within a unit cell containing only an eighth of an islet (dashed lines in Figure 3.1). The boundary conditions for this model [16] include continuity of p across the gas-liquid interface,

at $z = h$, $$p_{gas} = p_m \quad \textbf{3.7}$$

no O_2 flux across the O_2 -impermeable surface,

at $z = 0$, $$\frac{\partial p}{\partial z} = 0 \quad \textbf{3.8}$$

continuity of O_2 flux and partial pressure across the medium-islet interface,

at $r = R_{islet}$, $$n \bullet \left[(-D\alpha\nabla p)_i - (-D\alpha\nabla p)_m\right] = 0 \quad \textbf{3.9}$$

$$p_i = p_m \quad \textbf{3.10}$$

and symmetry across each side of the unit cell including both medium and islet domains as well as at $r = 0$,

$$n \bullet (-D\alpha\nabla p) = 0 \quad \textbf{3.11}$$

Table 3.1 contains the values for the parameters used in the simulations. [98]

In order to accurately predict oxygen profiles during culture all tissue, islet and non-islet need to be considered. Traditionally islet density is reported as IE/cm^2, which underestimates tissue quantity by ignoring the exocrine tissue that can be a significant fraction of the overall preparation volume. This density is related to the density in the simulations through

$$\Gamma = \frac{\rho}{\Phi_I} \quad \textbf{3.12}$$

where Φ_I is the islet volume fraction of the islet preparation, ρ is the islet surface density in IE/cm^2, and Γ is the sphere surface density in "IE"/cm^2 used in our model. In this case "IE" does not refer specifically to islet tissue, but rather a quantity of total tissue volume. This conversion

adds the assumption that the exocrine tissue is present as 150-μm diameter spheres. In this study tissue was quantified using nuclei counts, which relate to the model density through

$$\Gamma = \frac{\chi}{n_{IE}} \qquad \textbf{3.13}$$

where χ is the cell surface density (cells/cm^2) and n_{IE} is the number of cells in an IE (1560 cells/IE, [13]). Again we assume that exocrine tissue is similar to islet tissue in that a volume of tissue equal to a 150-μm diameter sphere contains the same number of cells as an IE. Total tissue surface density can be converted to an OCR surface density, which is the total OCR of the tissue divided by the area of culture, using

$$\lambda = \chi V_{max} \frac{V_{IE}}{n_{IE}} = \Gamma V_{max} V_{IE} \qquad \textbf{3.14}$$

where λ is the OCR density with units of flux and V_{IE} is the volume of an IE.

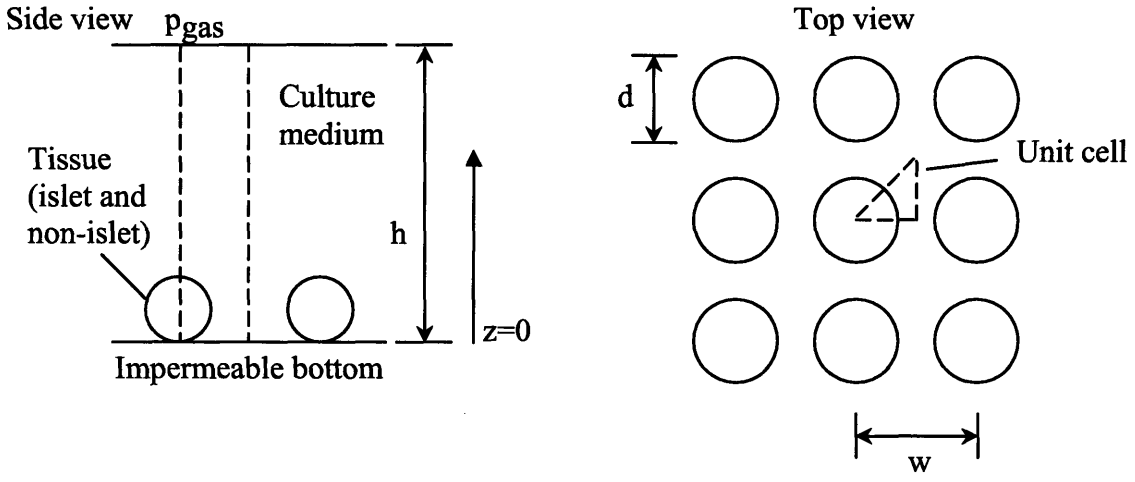

Figure 3.1. Geometry assumed for analysis of high density islet culture on an impermeable surface.
Dashed lines denote unit cell in which Equation 3.1 was solved.

The model was solved with the finite element method using the commercially available software COMSOL Multiphysics (COMCOL Inc., Burlington, MA) in conjunction with Matlab (Mathworks, Natick, MA). We required the mesh to contain more than 1000 nodes and set a convergence criterion such that the change in successive solution vectors for concentration

estimated by the iterative solver in the finite element software (i.e. the difference between the current and previous concentration vectors) was less than 10^{-2} [99]. This corresponded to an average error in the fraction of non-viable tissue of < 0.01 (maximum error was 0.04) based on a variety of simulations run multiple times using different mesh and convergence criteria.

3.4 Results

3.4.1 Predictions of theoretical mode

The theoretical model was used to estimate O_2 partial pressure profiles in and around islets in culture. As illustrated in Figure 3.2, the partial pressure at the sphere surface decreases as tissue surface density increases. If this is too low, not enough O_2 will reach the center, and cores of dead tissue will develop. These cores increase in size as the tissue density increases, thereby decreasing the amount of viable tissue that can be collected from culture.

Figure 3.3 explores this phenomenon in greater detail. As the initial tissue surface density increases, the minimum value of p decreases until it reaches p_{crit} at which the tissue dies and a necrotic core begins to develop. Using the calculated partial pressure field in the islet, the viable tissue volume (V_V) was calculated by integrating the volume of tissue with $p > p_{crit}$. The volume fraction of the viable tissue remaining after culture was calculated from

$$F_V = \frac{V_V}{\frac{4}{3}\pi R_{islet}^3} \qquad \textbf{3.15}$$

Once p reaches p_{crit}, the volume fraction of non-viable tissue ($1-F_V$) increases as initial tissue surface density increases.

Table 3.1 Values for the parameters used in islet culture simulations and the source from which they were obtained.

Parameter	Symbol	Value	Units	Source
Michaelis constant	K_m	0.44	mmHg	[98]
O_2 diffusivity in medium	D_m	2.78×10^{-5}	cm^2/s	[16]
O_2 diffusivity in tissue	D_i	1.22×10^{-5}	cm^2/s	[16]
O_2 solubility in medium	α_m	1.27×10^{-9}	mol/cm^3 mmHg	[16]
O_2 solubility in tissue	α_i	1.02×10^{-9}	mol/cm^3 mmHg	[16]
Minimum p for viability	p_{crit}	0.1	mmHg	[16]
Maximal O_2 consumption rate	V_{max}	9-38.5	nmol/s cm^3	Experimentally measured (Chapter 2)
Media height	h	3	mm	Based on medium volume and well area
Islet radius	R_{islet}	75	μm	Based on definition of IE
External p	p_{gas}	142	mmHg	Partial pressure of O_2 in humidified incubator at 37°C with 95% air/5% CO_2

The minimum oxygen partial pressure for viability (p_{crit}), defined as the value below which a cell will not survive, is assumed to be 0.1 mmHg [16].

$$V_{max} = \frac{OCR}{n_c}\frac{n_{IE}}{V_{IE}}$$

where OCR is the value measured in a sample containing n_c cells determined from nuclei counting, n_{IE} = 1560 is the number of cells in an IE [13], and $V_{IE} = 1.77 \times 10^{-6}$ cm^3 it the volume of an IE (a sphere having a diameter of 150 μm).

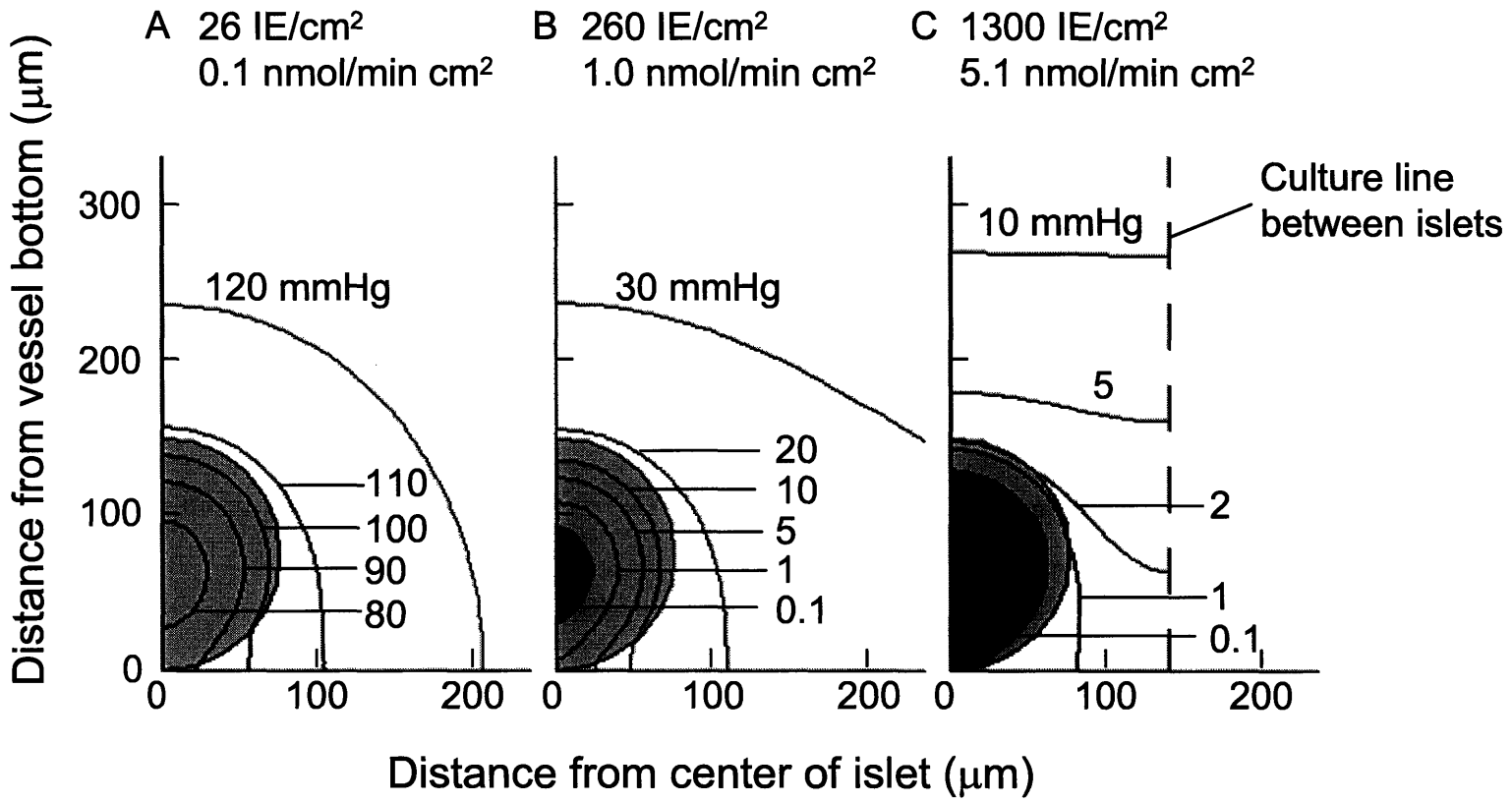

Figure 3.2. Predicted contours of constant partial pressure in and around islets in culture.
Data obtained using different tissue surface densities: (A) 0.1 nmol/min cm^2 (26 IE/cm^2), (B) 1 nmol/min cm^2 (260 IE/cm^2), and (C) 5 nmol/min cm^2 (1300 IE/cm^2). The cross section of half of an islet is illustrated for each density. The gray regions represent viable islet tissue and the black regions represent dead cores. Surface volume and OCR density were related by using V_{max} = 36.8 nmol/s cm^3 (2.5 fmol/min cell, Chapter 2).

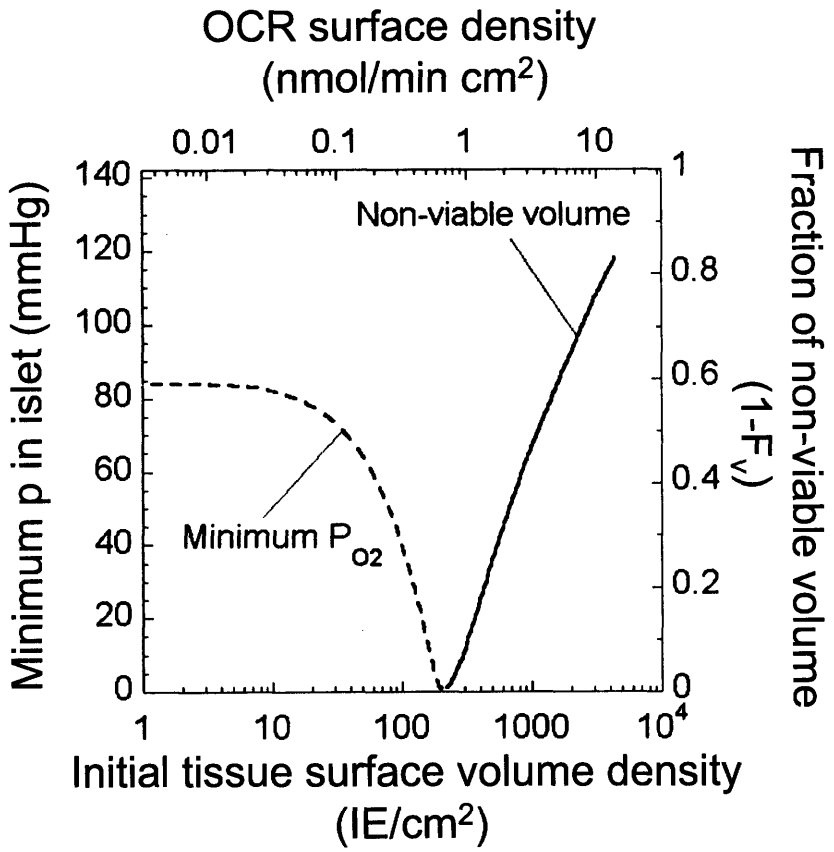

Figure 3.3. Theoretical prediction for minimum islet p (dashed line) and non-viable tissue volume (solid line) as a function of islet surface density and OCR density. Surface volume and OCR density were related by using V_{max} = 36.8 nmol/s cm^3 (2.5 fmol/min cell, Chapter 2).

3.4.2 Visual observations

Tissue morphology changed during high density culture form discrete cell clusters with defined boundaries distributed throughout the dish to a mixture of larger less defined clusters with a less uniform distribution surrounded by a significant number of single cells (Figure 3.4). Portions of the dish become completely covered by tissue while other areas were nearly void of tissue. Islets in low density culture kept their well defined boundaries and do not clump.

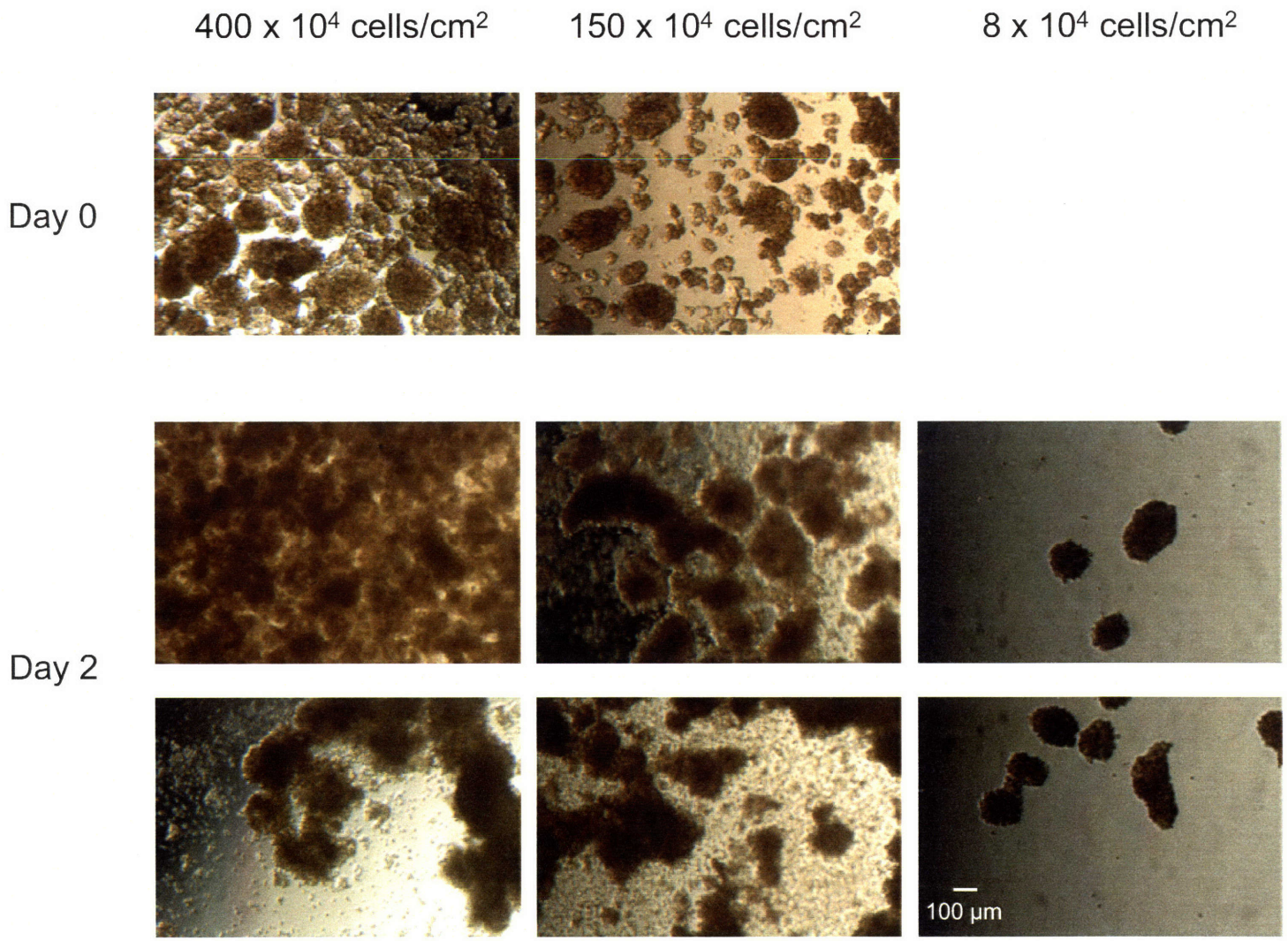

Figure 3.4. Light microscopy pictures of human islets.
Pictures taken on day 0 and after 39 hr culture at densities of 400, 150, and 8 x 10^4 cells/cm^2 on untreated polystyrene at 37°C. The scale bar represents 100 µm. Magnification is the same in all panels.

3.4.3 Effect of surface density on tissue recovery.

Following culture only non-adherent tissue is collected and transplanted in most, if not all, clinical islet programs and islet research studies. Previously we showed that low-density (< 8 x 10^5 cells/cm^2) human islet culture for 34-60 hours in a fully humidified environment at 37°C (142 mmHg O_2) on untreated polystyrene resulted in significant tissue adherence (Chapter 2). In this study we collected both adherent and non-adherent tissue. As the initial tissue surface density increased, the fraction of original cells (measured by nuclei counting) collected from culture as adherent tissue decreased while that of non-adherent tissue increased (Figure 3.5). At all except the lowest tissue surface densities, the sum of the non-adherent + adherent cells collected was equal to that of the initial tissue placed into culture for all the cultured/shipped preparations. The data in Figure 3.5A were also plotted as tissue surface density of collected adherent tissue versus the initial tissue surface density in Figure 3.6. As the initial surface density of cultured/shipped islets increased the adherent surface density increased, and began to level off at high initial surface densities. In both Figure 3.5A and Figure 3.6, there is insufficient data for fresh islets to determine if they behave similarly to cultured/shipped islets.

In culture experiments carried out at densities > 50 x 10^4 cell/cm^2 trypsinization was not conducted because the fraction of the total tissue that was adherent was usually less than 10%. This was always confirmed by visual inspection under the microscope. The fraction of original tissue collected as non-adherent tissue in terms of nuclei and DNA is plotted versus initial tissue surface density in Figure 3.7A and B, respectively, for densities > 50 x 10^4 nuclei/cm^2. The fractions recovered averaged 0.80 ± 0.21, and the DNA content averaged 7.8 ± 1.6 pg DNA/cell (Figure 3.7C). No consistent trend was observed for fresh or cultured/shipped tissue with initial tissue surface density, but fresh tissue tended to have a lower average nuclei recovery (0.69 ± 0.13) and higher DNA recovery (0.90 ± 0.16) than cultured/shipped tissue (0.91 ± 0.16 and 0.64 ± 0.20, respectively, $p < 0.01$ in both cases for unpaired t-test).

The volume fraction of insulin positive cells excluding vascular space ($\Phi_{\beta XV}$) in tissue collected from culture is shown as a function of tissue surface density in Figure 3.8A for non-adherent tissue and Figure 3.8B for adherent tissue. $\Phi_{\beta XV}$ was always substantially higher for non-adherent tissue (0.47 ± 0.01 for fresh, 0.39 ± 0.09 for cultured/shipped) than for adherent tissue (0.15 ± 0.10 for fresh, 0.21 ± 0.07 for cultured/shipped). The $\Phi_{\beta XV}$ of the tissue upon

receipt at MIT prior to experimentation (day 0) was 0.32 ± 0.03 for fresh and 0.41 ± 0.03 for cultured/shipped human islet tissue, which was higher than that for adherent tissue ($p < 0.01$ for both fresh and culture/shipped human islets), similar to that for cultured/shipped non-adherent tissue ($p > 0.64$), and lower than that for the fresh human islet non-adherent tissue ($p < 0.01$) collected from culture.

By combining the data for tissue recovery with that for $\Phi_{\beta XV}$ the number fraction of original β cells remaining after culture F_β was determined (Appendix 10.1). As indicated in Figure 3.9, the non-adherent tissue collected from culture contained more insulin positive cells than the adherent tissue, for which the fraction recovered was less than 15% for all densities and preparations considered except at very low density.

3.4.4 Membrane integrity and oxygen consumption rate

Membrane integrity measurements were made using sequential nuclei staining with 7AAD. OCR measurements were made with the same samples and normalized by number of cells (from nuclei counting) or mass of DNA in the sample. Membrane integrity decreased as the initial tissue surface density increased, but data were widely scattered (Figure 3.10A). OCR/cell (Figure 3.10B) and OCR/DNA (Figure 3.10C) decreased sharper and to a much greater extent than the fraction of cells with intact membranes, and the scatter between measurements from different experiments was relatively small.

Figure 3.11 shows the fraction of the original OCR collected after culture as a function of the initial tissue surface density (Figure 3.11A) and initial OCR density (Figure 3.11B). The fraction of OCR recovered was 0.98 ± 0.07 and 0.75 ± 0.23 at low density ($< 8 \times 10^4$ cells/cm^2) for fresh and cultured/shipped islets, respectively (Chapter 2). The fraction decreased as the initial density increased and dropped to about 0.1 at the highest densities studied. By plotting the data versus OCR surface density the data collapsed into a tighter cluster with less scatter compared to the same data plotted versus tissue surface density.

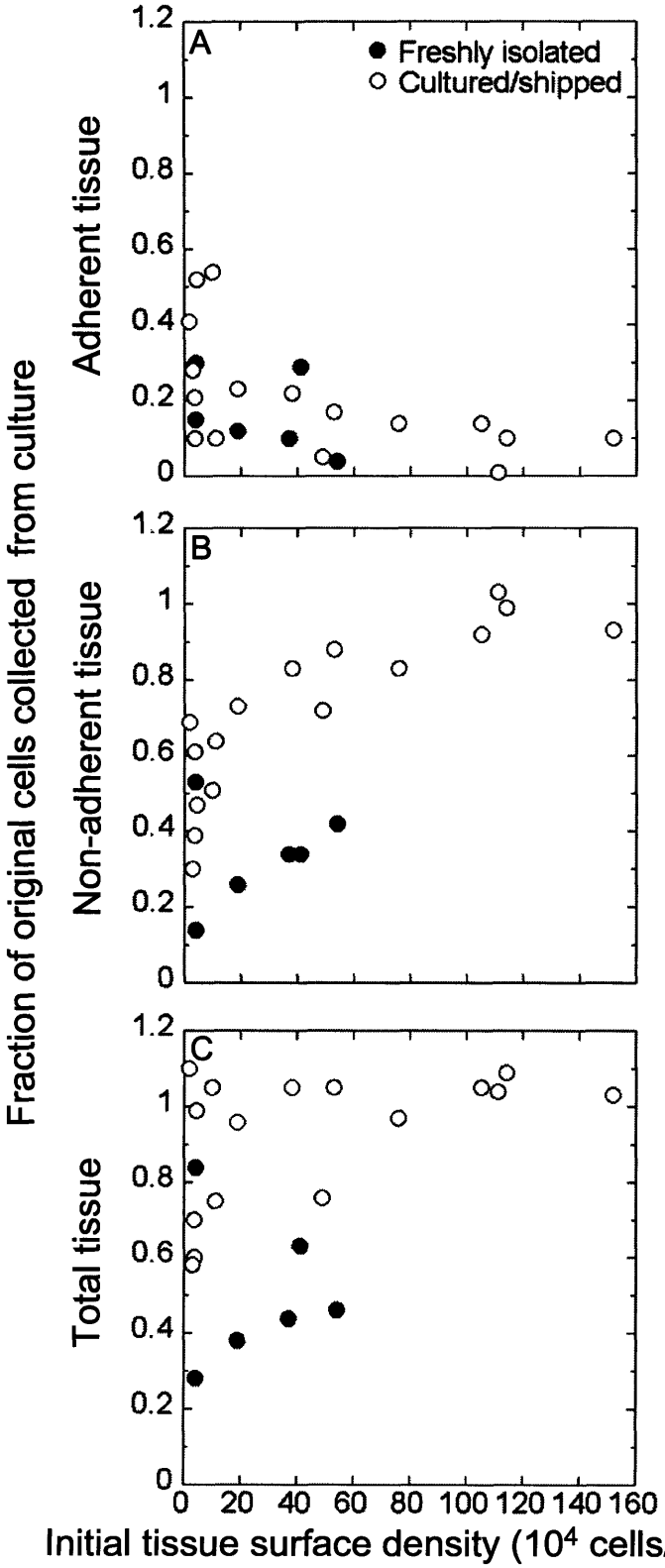

Figure 3.5. The fraction of original tissue collected from culture as (A) adherent, (B) non-adherent, and (C) total tissue as a function of the initial tissue surface density.

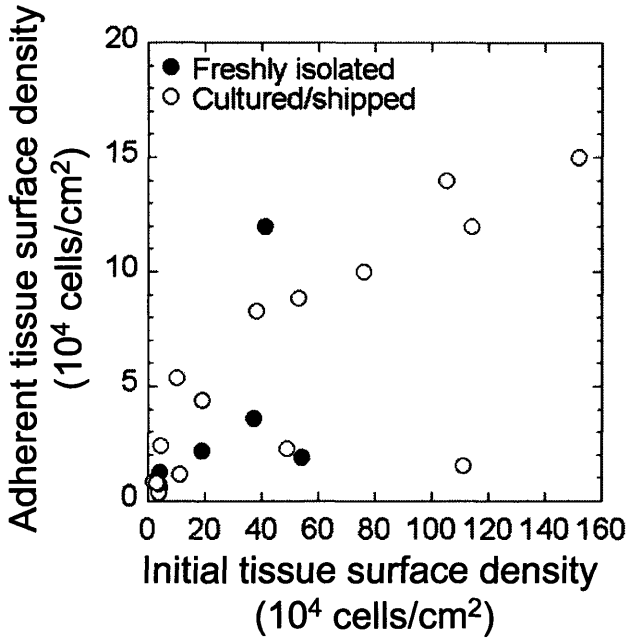

Figure 3.6. Data from Figure 3.5A are plotted in terms if the actual surface density of adherent tissue collected from culture versus the initial tissue surface density.

The OCR density after culture, defined as the total OCR of the tissue remaining divided by the surface area of culture, which has units of O_2 flux, is plotted as a function of the initial OCR density in Figure 3.12. The OCR density increases before leveling off at roughly 1.5 nmol/min cm^2 at an initial OCR density of roughly 4 nmol/min cm^2. The O_2 flux for one-dimensional Fickian diffusion is calculated by

$$N = \frac{D\alpha}{h}\left(p_{gas} - p_{surf}\right) \qquad \textbf{3.16}$$

where N is the O_2 flux and p_{surf} is the partial pressure at the top of the islet. Using the values in Table 3.1 the maximum O_2 flux to the tissue, which occurs when p_{surf} is zero, is 1.0 nmol/min cm^2.

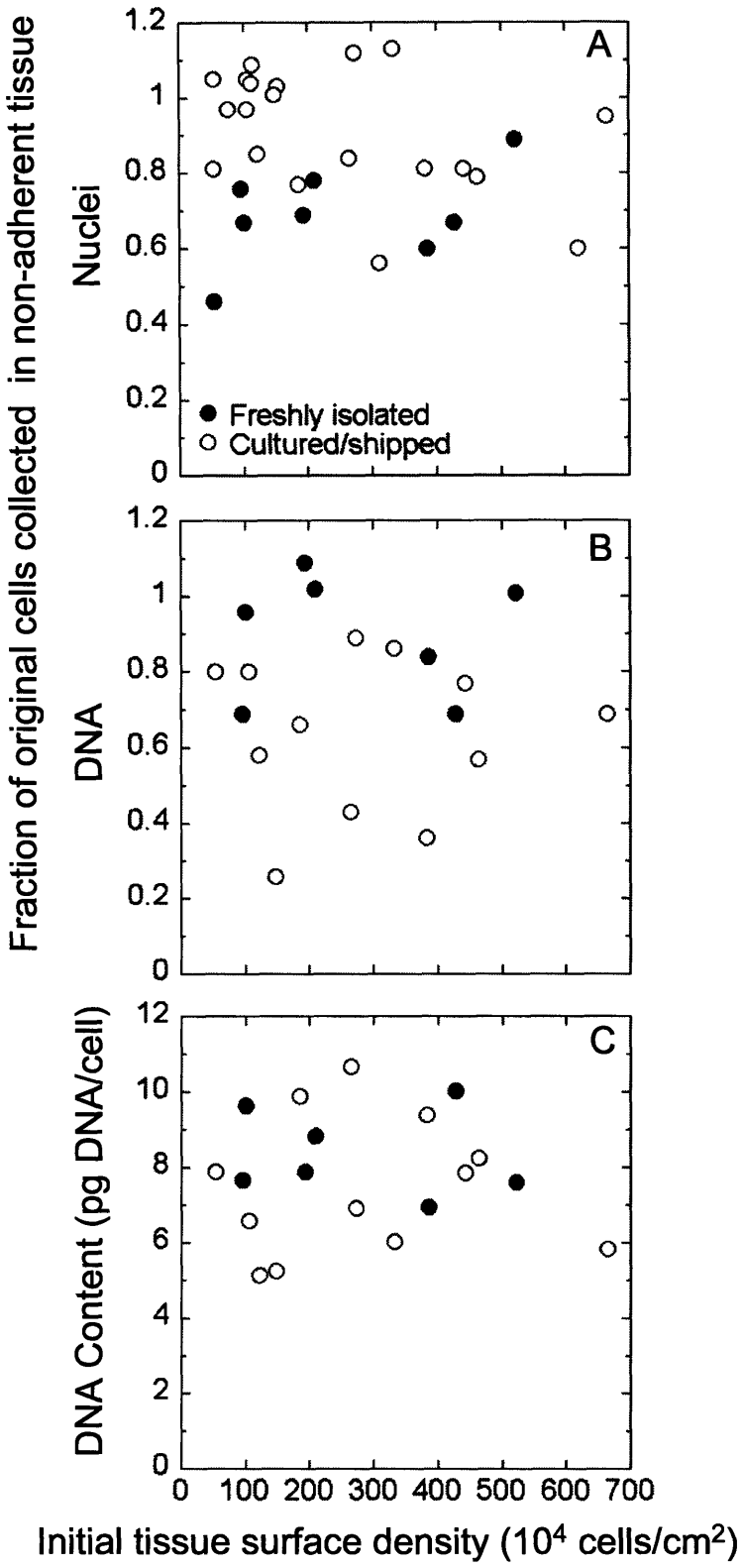

Figure 3.7. The fraction of original cells collected as non-adherent tissue, plotted as (A) nuclei and (B) DNA, and (C) the DNA content per cell of tissue.

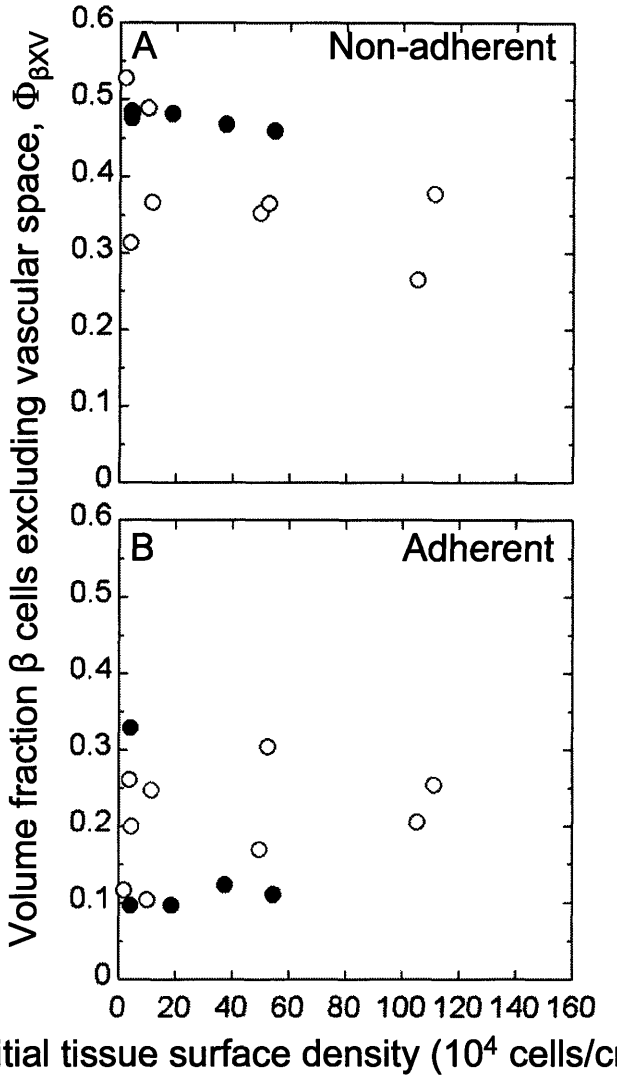

Figure 3.8. The volume fraction of insulin positive tissue excluding vascular space for adherent (A) and non-adherent (B) tissue collected from culture.

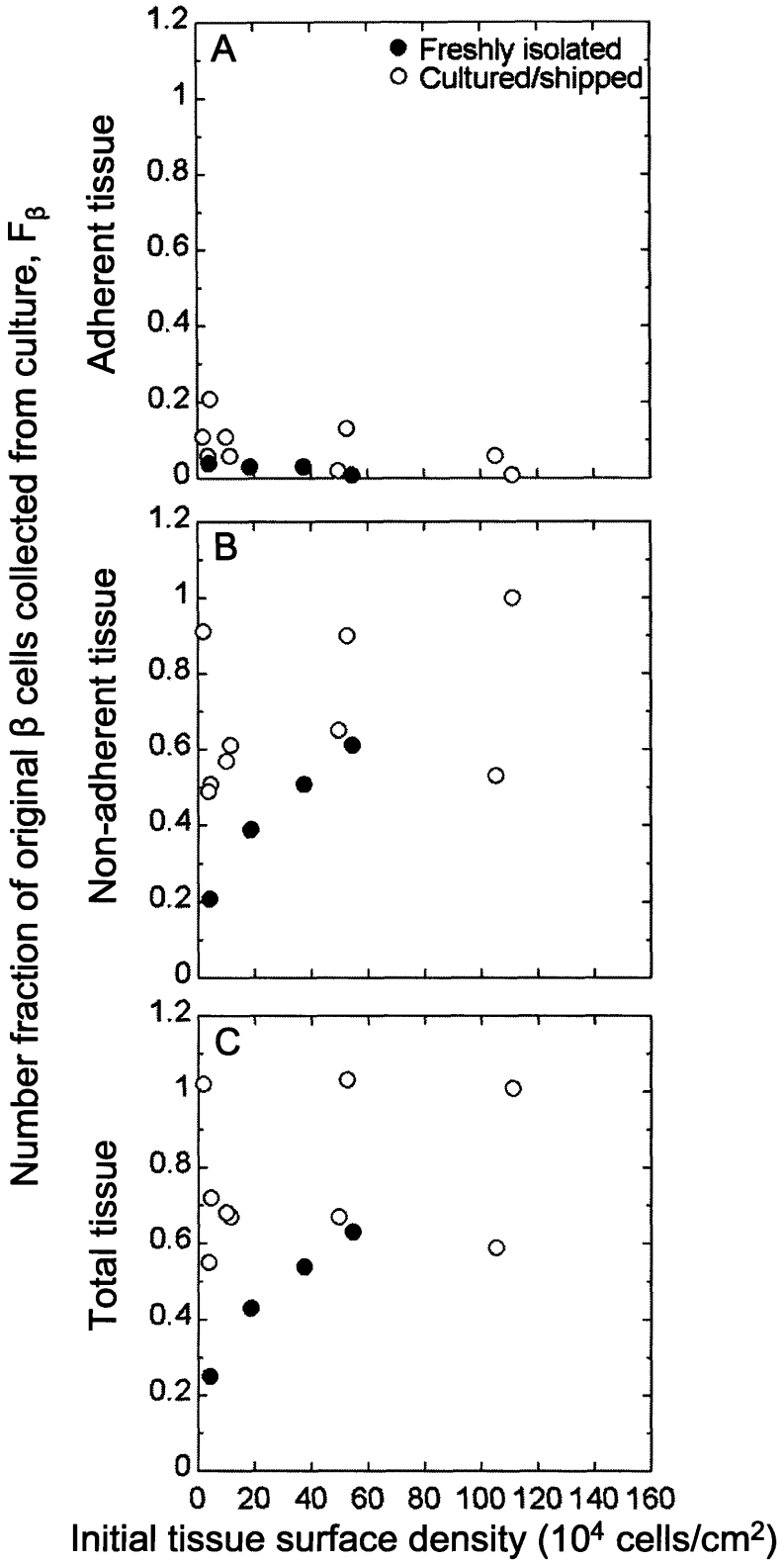

Figure 3.9. Fraction of original insulin positive cells for adherent (A), non-adherent (B), and total tissue (C) collected from culture as a function of the initial tissue surface density.

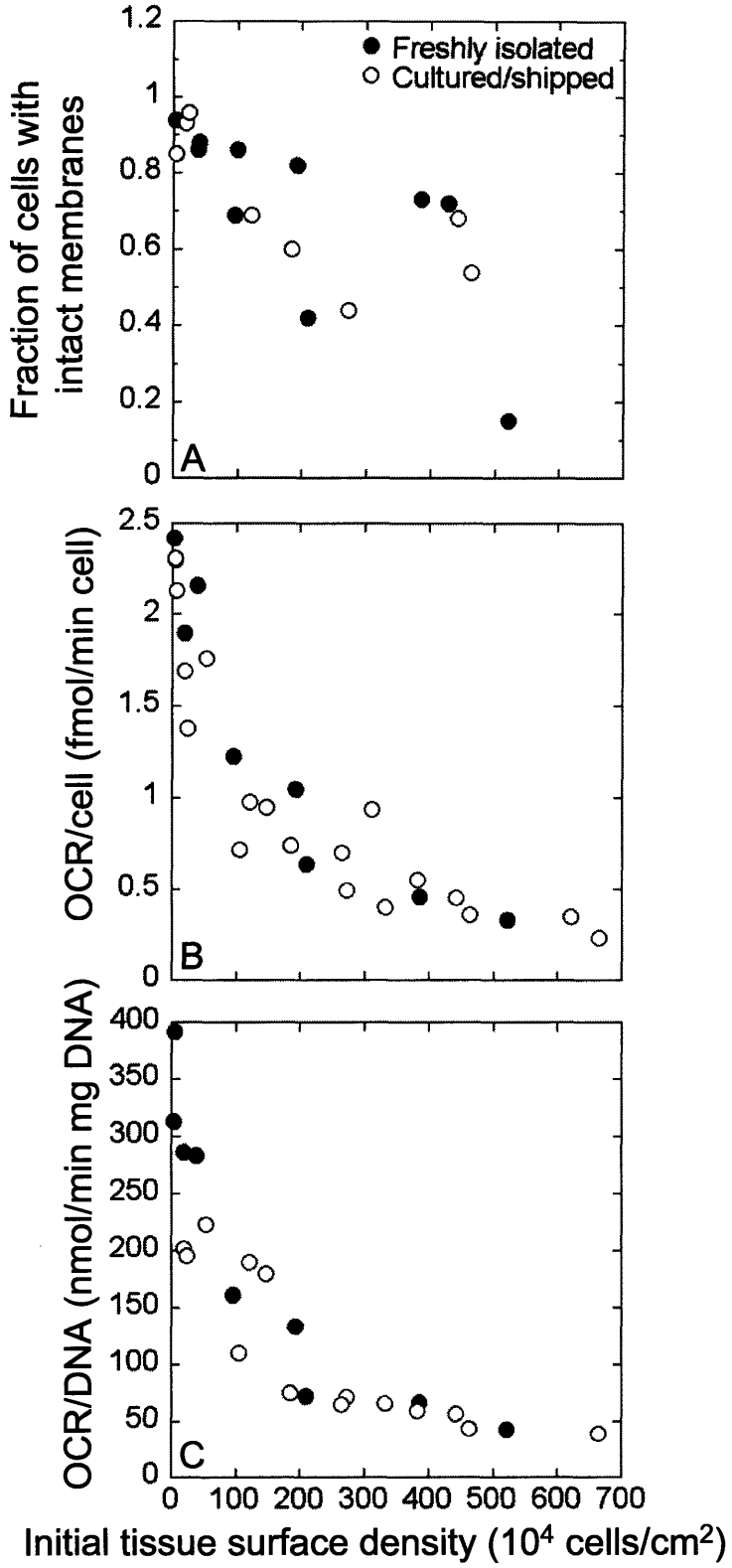

Figure 3.10. (A) Fraction of cells with intact membranes as measured by 7AAD sequential staining, (B) OCR/cell, and (C) OCR/DNA after culture versus initial tissue surface density.

3.4.5 Prediction of oxygen transport theory compared to experimental data

The experimental data from Figure 3.11 were compared to theoretical predictions of the O_2 transport model and are plotted versus initial tissue surface density (Figure 3.13A) and initial OCR surface density (Figure 3.13B). The theoretical model indicates that the fraction of original viable tissue recovered after culture, F_V is a function of both initial tissue surface density and V_{max} (Figure 3.13A). The two theoretical curves in Figure 3.13 represent the lowest and highest V_{max} for the islet preparations used in this study. At large V_{max}, the model predicts that F_V decreases sharply with even small increases in tissue surface density. Because V_{max} of the tissue used in this study varied significantly between islet preparations, a separate plot would be required to compare prediction with data for each preparation. The same theoretical predictions from Figure 3.13A are plotted in Figure 3.13B with tissue surface density replaced by initial OCR surface density. When plotted on these coordinates, all theoretical predictions collapse to a small band of curves for all values of V_{max}, thereby permitting comparison of results from different experiments on one figure. A similar collapse is seen with the experimental data resulting in a tighter cluster with less scatter as noted above. The experimental data follow the same trend as theory predicts, but consistently give a lower F_V than predicted.

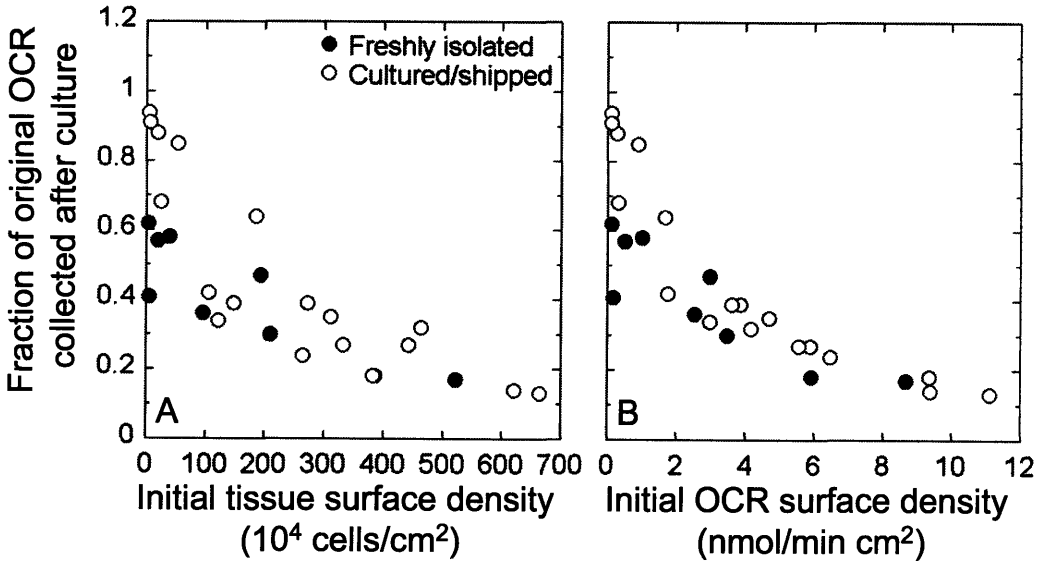

Figure 3.11. The fraction of original OCR remaining as a function of (A) initial tissue surface density and (B) initial OCR density following culture.

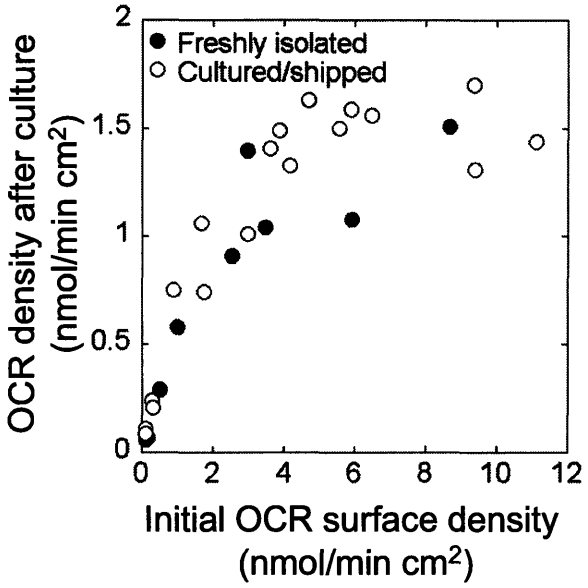

Figure 3.12. The OCR density of all tissue remaining after culture as a function of the initial OCR surface density.

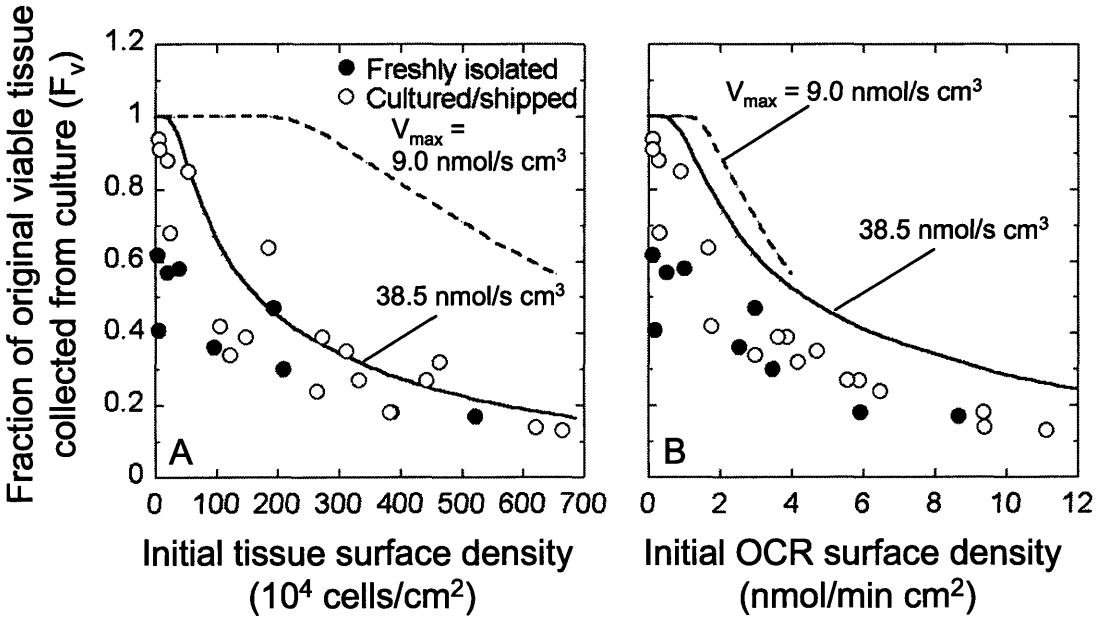

Figure 3.13. Experimental results and theoretical predictions for the fraction of original viable tissue recovered from culture versus (A) tissue surface density and (B) OCR density. In order to plot the theoretical predictions and experimental results versus initial tissue surface density, we assumed that there are 1560 nuclei/IE [13].

3.5 Discussion

There is little published information on the effect of surface density on the recovery of islet tissue and its viability and purity after culture. In this study, we studied culture of human islet tissue on untreated polystyrene vessels for two days and investigated the effect of tissue surface density on recovery of islet tissue and its viability and purity. Through the use of a theoretical O_2 transport model, we also explored the notion that the reduction in the amount of viable tissue observed during high density islet culture resulted from O_2 limitations.

At low densities ($< 8 \times 10^4$ cells/cm^2), a fraction of the tissue adheres during culture on untreated polystyrene (Chapter 2). We observed that as initial tissue surface density increased the amount of adherent tissue increased, the fraction that was adherent decreased, and the fraction non-adherent increased (Figure 3.5). At all except the lowest tissue surface densities, all of the tissue was recovered in the two fractions after 2-day culture from cultured/shipped islet preparations but not from fresh tissue. This difference may reflect damage to tissue during isolation, resulting in cells that have begun the death process and are destined to die but have intact nuclei when culture of fresh tissue is initiated. In contrast, these damaged cells and their nuclei have already disappeared when the cultured/shipped tissue is placed into culture. The occasional recovery of more than 100% of initial tissue is likely due to experimental error. Pancreatic tissue growth is unlikely because it occurs at low rates and is observed only after longer culture periods [77; 100].

There are at least three possible explanations for the decrease in the fraction of adherent tissue with increasing tissue surface density: (1) As tissue covers the culture surface there is less area for remaining tissue to attach, and the density of adherent tissue begins to level off at high initial tissue surface densities (Figure 3.6). (2) Healthy tissue may adhere to a greater extent. Some cells detach from a surface early in the cell death process when exposed to specific stresses [101; 102]. This hypothesis is consistent with the largest adherent fraction occurring at low density (Chapter 2), for which O_2 limitations are minimized. (3) Tissue may adhere to other tissue instead of the vessel surface, leading to clumping that was observed in the highest-density cultures (Figure 3.4).

Cultured/shipped tissue had higher nuclei recoveries than fresh tissue (Figure 3.7), whereas DNA recoveries were higher for fresh tissue. As noted previously, fresh tissue has more recently entered the cell death process following the harsh isolation procedure than

cultured/shipped tissue, which has proceeded further through the cell death process. During culture of fresh tissue, nuclei of damaged cells degrade and liberate DNA, which degrades at a slower rate. At the start of our culture experiments, cultured/shipped tissue had already largely completed these steps. Therefore, our data reflects a greater loss of nuclei from cells already committed to the cell death process in fresh tissue at the start of culture and the presence of a higher amount of DNA released from dead nuclei but not yet degraded by DNAase in the recovered fresh tissue as compared to the data for cultured/shipped tissue.

As observed with low density culture (Chapter 2), the volume fraction of β cells exclusive of vascular space ($\Phi_{\beta XV}$) of the non-adherent tissue was higher than that of the adherent tissue (Figure 3.8), indicating that non-β cells, and thus non-islet tissue, preferentially adhered to the culture vessel. Combination of $\Phi_{\beta XV}$ measurements with tissue recovery data revealed that the number fraction of original β cells collected as adherent tissue was always less than 0.25 at low density (Figure 3.9) and less than 0.15 otherwise, indicating that the current clinical practice of collecting only non-adherent tissue usually results in collecting most of the insulin positive tissue. In most cultures (10 of 13 in Figure 3.9C) the combined tissue lost at least 25% of the original β cells. This loss occurred even under low density conditions when no loss in viable tissue was observed (Chapter 2), indicating that the β cells lost were already dead at the beginning of culture or dedifferentiated during culture [77]. During high density culture, the amount of viable tissue decreased, suggesting that the reduction in the number fraction of original β cells could also have resulted from stresses during culture.

Initial tissue surface density had a large impact on tissue viability. A consistent decrease in membrane integrity was observed as the initial tissue surface density increased (Figure 3.10A). A much larger and more consistent decline was observed in OCR/cell and OCR/DNA (Figure 3.10B and C) because loss of membrane integrity occurs late in the cell death process whereas a decrease in OCR reflects mitochondrial dysfunction, which is an earlier indicator of commitment to the cell death process [13]. This viability decrease is consistent with the higher glucose stimulation indices measured after low surface density compared to high surface density culture [47].

The fraction of original OCR remaining after culture, which represented the fraction of original viable tissue F_V, decreased drastically as initial tissue surface density (Figure 3.11A) and initial OCR surface density (Figure 3.11B) increased. The drop was especially sharp in the range

of 0-10^6 cells/cm^2 and 0-2 nmol/min cm^2, respectively. The data were scattered when plotted versus tissue surface density but collapsed together when plotted versus OCR surface density, especially at high density. This behavior is consistent with the O_2 transport model. The initial OCR surface density takes into account variation in V_{max} between islet preparations, which ranged from 9.0 to 36.8 nmol/s cm^3 in this study. This difference in V_{max} is not taken into account when plotting versus tissue surface density, whereas OCR density combines the independent effects of tissue surface density and V_{max}. Furthermore, the OCR density represents the oxygen flux averaged over the surface, which becomes an increasingly good estimate of the actual flux at very high tissue densities wherein the tissue layer takes on the characteristics of a slab rather than discrete spheres.

The OCR surface density of respiring tissue following high density culture leveled off at 1.5 nmol/min cm^2 (Figure 3.12), a value higher than the maximum O_2 flux of 1.0 nmol/min cm^2 for one-dimensional Fickian diffusion through 3 mm medium, which was calculated using the parameters in Table 3.1. OCR density of recovered tissue is based on measurements made with tissue that is fully oxygenated. During high density culture, tissue is not fully oxygenated, and a substantial fraction of viable tissue is exposed to very low values of p on the order magnitude of the Michaelis constant K_m at which the OCR is reduced according to Equation 3.4. Thus, OCR measurements of recovered tissue, which are made under reoxygenated conditions to assess fractional viability, cannot be used to estimate the actual OCR density under culture conditions because they lead to a higher OCR density than is actually present in culture at very high density.

Fraction viability predicted by theory followed the same trend as the experimental data (Figure 3.13), suggesting that O_2 limitations caused at least part of the decrease in viable tissue during culture. However, model predictions consistently overpredicted the fraction viable by about 10-20%. The difference between theoretical predictions and experimental measurements could be due to inaccuracies in the parameter values selected or assumptions made in the theoretical model (Chapter 5). In developing the model we assumed there are 150-μm diameter spheres (the average for human islets) of islet and non-islet tissue, arranged in a square array. Human islet preparations are a mixture of islets and exocrine tissue, and the OCR/cell for each type is about the same (Chapter 2). However, the two types can vary significantly in shape, size, and spatial distribution, and occasionally very large clumps of non-islet tissue were observed. In

addition, tissue cultured at high density tended to clump even more (Figure 3.4), which exacerbated local O_2 limitations. Differences between theoretical predictions and experimental data may also have been linked to the lack of medium change during culture. At high density, nutrients (i.e. glucose) are depleted and waste (i.e. lactate and ammonia) is produced faster than at low density, and the concentrations of these species at the cell surface are further influenced by diffusional limitations. Investigation into the effect of glucose and waste diffusional limitations are described elsewhere (Chapter 6 and 7). Products produced by islet tissue may also have toxic effects especially at high surface densities. NO, which can be produced by islet tissue, can damage pancreatic β-cells leading to cell death [103; 104]. Further, cell death by necrosis results in leakage of cell contents [105] which could also expose the tissue to damaging toxins.

Current practice of collecting only non-adherent tissue is supported by our results, which indicate that impure tissue is removed with little loss of β cells in the adherent fraction. Sequential culture on fresh polystyrene surfaces may further purify tissue, as suggested by our results with precultured and shipped tissue. Using estimates of 1560 cells/IE and about 50% islet cells in an average human islet preparation [55], 200 and 400 IE/cm^2 correspond to 0.625 and 12.5 x 10^6 cells/cm^2, respectively. Our data indicate that culture at these densities in 3 mm medium, which is typical of clinical preparations, results in F_V values that vary from 0.4 to 0.9 depending on damage prior to culture, which is prevalent in fresh tissue (Chapter 2), and on limitations imposed by culture, which at a high V_{max} will decrease F_V by 20%. Rather than culturing for 2 days at 37°C, some islet centers culture one day at 37°C followed by one day at about 25°C, during which OCR, and therefore O_2 diffusion limitations are reduced. We suggest that, because the time constant for diffusion through the culture medium at 37°C is about an hour (even less inside an islet) steady state O_2 gradients prevail within the system at 37°C, exposing tissue to hypoxia for more than 20 hours in high density culture and cause irreversible damage. Thus even though O_2 limitations are reduced at 25°C, the damage is already done during 37°C culture on the first day and similar results to those presented here should be observed. The empirical data and theoretical predictions presented here can serve as a guide to choosing a safe culture density based on measurements of nuclei counts and OCR measurements with the freshly isolated tissue preparation, which can usually be completed in less than an hour [39; 55].

3.6 Nomenclature

7-AAD	7-aminoactinomycin D
C	Concentration of O_2
d	Diameter of islet
D	Diffusivity of O_2
DAB	2 mM 3,3'-diaminobenzidine tetrahydrochloride
D-PBS	Dulbecco's phosphate buffered saline
F_β	Number fraction of original β cells collected from culture
FBS	Fetal bovine serum
F_V	The fraction of original viable tissue after culture
h	Medium depth
IE	Islet equivalent
JDC	Joslin Diabetes Center
K_m	Michaelis constant, the p at which the reaction rate is $V_{max}/2$
MIT	Massachusetts Institute of Technology
N	O_2 flux
n_{IE}	Number of cells in an islet equivalent volume
O_2	Oxygen
OCR	O_2 consumption rate
p	O_2 partial pressure
PAP	Peroxidase-antiperoxidase
p_{crit}	The p below which a cell dies and no longer consumes O_2
p_{gas}	Ambient partial pressure of O_2
pO_2	O_2 partial pressure
p_{surf}	p at the surface of the islet
r	Radial direction
R	Production rate of O_2
R_{islet}	Radius of islet
t	Time

V_{ch}	Volume of OCR chamber
V_{IE}	Volume of an islet equivalent (1.77×10^6 μm^3)
V_{max}	Maximum reaction velocity
V_V	Viable tissue volume
w	Center-to-center distance between islets
z	Vertical axis
α	Solubility of O_2 in medium
$\Phi_{\beta XV}$	Volume fraction of β cells exclusive of islet vascular spaces
Φ_I	Volume fraction of islets
Γ	Sphere surface density in "IE"/cm^2 where "IE" refers to total tissue volume.
ρ	Islet surface density in IE/cm^2
χ	Cell surface density (cells/cm^2)
λ	OCR density with units of flux

Subscripts for D, α, p, C

m	Medium
i	Islet tissue

4 Reducing oxygen limitations during static islet culture

4.1 Introduction

Since its initial report of success [7] transplantation of pancreatic islets has become a promising option for treating type 1 diabetes. After islet tissue is isolated from a donor pancreas by mechanical and enzymatic treatment [13; 14], it may transplanted directly or cultured [14; 40]. Islet culture prior to transplantation is standard practice in most clinical centers [40]. During culture in standard polystyrene culture vessels, at very low islet tissue surface densities, islets are usually free of oxygen (O_2) transport limitations (Chapter 2 and 3 and [16]), but it is impractical to culture islet tissue at these densities because of large space requirements. At islet densities of 200-400 islet equivalents (IE)/cm^2 typically employed in clinical applications [106; 107], there are significant O_2 limitations that lead to a loss in viability (Chapter 3, [16]). It is desirable to culture at even higher densities without sacrificing viable tissue.

Improvements in culture techniques have been explored, but only a few address O_2 limitations present in conventional culture. Lower medium depths decreased the O_2 diffusion distance to the islet, thereby increasing islet oxygenation [48; 49; 108] and improving islet stimulation index [47]. However, at high surface densities, culture in low medium depths may result in nutrient (e.g. glucose) depletion from the medium (Chapter 6). Culture at the interface of culture medium and an oxygenated perfluorocarbon (PFC), which acts as an O_2 reservoir because of its high O_2 solubility, caused islets to have more DNA fragmentation and a lower stimulation index compared to islets cultured without the PFC [109]. However, very low surface densities (15 IE/cm^2) were used, for which O_2 limitations are not present, and further study further study is needed to determine whether PFC could be beneficial for high density culture. Structural integrity and islet function are better preserved with rotational culture systems compared to static cultures [110; 111] and have been used extensively with single cell suspensions [108; 112-114], but questions remain about islet clumping and scale up for large quantities of tissue.

In this paper we investigate three static culture techniques that focus on decreasing O_2 supply limitations in high density culture, including culture at reduced temperatures, in elevated O_2 environments, and on silicone rubber membranes that have high oxygen permeability. Decreasing culture temperature reduces cellular O_2 consumption rate (OCR) [115] thereby

reducing the magnitude of oxygen diffusion gradients in the islets and culture medium. Among studies examining reduced temperature islet culture, several report lower necrotic death [50; 52] and higher recoveries [49] compared to culture at 37°C, which is consistent with the notion of reduced O_2 transport limitations at reduced temperature. However, 37°C culture results in better function and/or higher viability than culture at reduced temperatures [49]. The interplay between islet surface density and temperature may be the cause of these conflicting reports.

Increasing ambient O_2 in the incubator, which is easily achieved using a premixed gas cylinder, increases the maximum O_2 flux to the tissue, thereby improving tissue oxygenation. However, at high O_2 levels, O_2 toxicity may damage the tissue. The O_2 partial pressure (pO_2) at which O_2 becomes toxic to islet tissue is unknown.

Culture on a thin, O_2 -permeable membrane bottom greatly increases O_2 transfer to the tissue. The estimated pO_2 drop during culture at 400 IE/cm^2 across 3 mm medium is > 140 mmHg while that across a 500-μm silicone rubber membrane is < 10 mmHg. An initial investigation indicated that a small foot-print vessel with an O_2 -permeable silicone rubber bottom can be used to culture islet tissue at high density [60].

In this study we investigated islet culture at elevated pO_2, reduced temperature, and on a silicone rubber membrane and compared the results to conventional culture in terms of the recovery of islet tissue and its viability for a range of surface densities. In addition, we utilized a theoretical O_2 transport model to investigate how O_2 transport changes for each system. The results of this study demonstrate that at high tissue surface densities the recovery of viable tissue is higher following culture in elevated O_2, at reduced temperature, or on a silicone rubber membrane compared to conventional culture in polystyrene vessels because O_2 limitations are reduced.

4.2 Methods

Islet Isolation and Culture

Standard collagenase/protease digestion methods were used for human [7; 15] isolations. Preparations of human islets were provided fresh (4-6 hr after isolation was complete) by the Islet Core at the Joslin Diabetes Center (JDC, Boston, MA). Human islets were also received after culture (1-2 days) from JDC or overnight shipment (sometimes after up to 1 day culture) from other centers contained in culture flasks (T-25 and T-75) or centrifuge tubes in Styrofoam

boxes. When first observed, some preparations were in suspension, some in a pellet. Upon receipt, a portion of the preparation was analyzed and the remainder placed into untreated polystyrene culture flasks at 37°C in a humidified environment (5% CO_2), oxygen partial pressure (pO_2) of 142 mmHg, for 34-60 hr during which no medium change occurred.

Islets were cultured in supplemented RPMI (11.1 mM D-glucose, 100 U/ml penicillin, 100 μg/ml streptomycin, 2 mM L-glutamine, 1 mM sodium pyruvate (all from Mediatech Inc., Herdon, VA), and 50 μM β-mercaptoethanol (Sigma Aldrich, St. Louis, MO) with 10% FBS (Mediatech Inc.), at low densities (< $8x10^4$ cells/cm^2 or about 50 islet equivalents (IE)/cm^2, where IE is the volume of a sphere with a diameter of 150 μm) in 1.3 mm of medium in tissue culture flasks. After culture the free, non-adherent tissue (which is the only tissue used in current practice) was collected. In selected experiments, adherent human tissue was incubated for 5 min at 37°C in 0.05% trypsin EDTA (Mediatech Inc.), dislodged with fresh medium, and collected.

Elevated O_2 islet culture

Culture at elevated ambient pO_2 was the same as conventional culture except that the culture vessels were kept in a separate 5 L chamber in a 37°C incubator with a dish of water to provide a fully humidified environment during the experiment. Through the chamber a gas mixture of 60% O_2, 5% CO_2, and balance N_2 (p = 428 mmHg when fully humidified) was purged for 15 min at 3 L/min, before reducing to a very small flow rate in order to keep the gas composition constant throughout the experiment.

Reduced temperature islet culture

Culture at reduced temperature was conducted at 24°C in 5 L chambers through which a gas mixture of 20.9% O_2, 5% CO_2, and balance N_2 flowed (at 24°C $pO_2 \approx 154$ mmHg). A flow rate of 3 L/min was used to purge the chamber for 15 min, after which the flow rate was reduced to a very small flow rate. After 34-60 hr culture at 24°C, islets were cultured for an additional hour at 37°C to allow tissue metabolic rates to acclimate to 37°C before analysis.

Islet culture on silicone rubber membranes

Culture on silicone rubber membranes was conducted using custom made epoxy blocks containing wells with a membrane at the bottom that was either 100 or 500-μm thick (Wilson Wolf Manufacturing Inc., New Brighton, MN). Culture medium, environment, duration and analysis were conducted as with conventional culture. Cultures conducted on silicone rubber

membranes used a medium depth of 22 mm in order to avoid nutrient depletion from the medium. Because islet tissue surface densities greater than 80 x 10^4 cells/cm^2 were tested, no trypsinization was required.

Cell culture

βTC3 cells (passages 40-50) were cultured in DMEM supplemented with 10% FBS, 100 U/ml penicillin, and 100 μg/ml streptomycin (Mediatech Inc., Herdon, VA). Cells were cultured in T-flasks placed in 5 L chambers. Using gas cylinders, O_2 partial pressure was controlled at 20, 40, 60, 80, and 95% O_2, with 5% CO_2 in all mixtures. The chambers were purged for 15 min at 3 L/min before reducing the flow rate.

DNA Content

At MIT, DNA was measured by fluorospectrophotometry [55] using the CyQUANT Cell Proliferation Assay Kit (Molecular Probes, C-7026 Eugene, OR), and a λ DNA standard (Invitrogen) and 50-250 IE/sample. Fluorescence was read at 480 nm excitation and 520 nm emission wavelengths in a plate reader (Spectra MAX Gemini microplate spectrophotometer, Molecular Devices, Sunnyvale CA). At UMN (porcine and human islets), PicoGreen dye was used (Quant-iT PicoGreen dsDNA kit, Molecular Probes, Eugene, OR) [39]. Fluorescence was read at 520 nm excitation and 585 nm emission wavelengths.

Islet Enumeration by Nuclei Counting

Nuclei were prepared by adding equal 100-μl volumes of sample containing 160 or more IE and of lysis solution (0.1 M citric acid (Sigma) and 1% (v/v) Triton X-100 (Sigma)) to a 1.5 ml microtube [55]. The mixture was incubated at room temperature for 5 min with vortex mixing every 1.5 min, and nuclei were liberated by shearing through a needle. Isolated nuclei were diluted with Dulbecco's phosphate buffered saline (D-PBS, Invitrogen, Carlsbad, CA) to a concentration no higher than 5 x 10^5 nuclei/ml, stained with 7-aminoactinomycin D (7-AAD, Molecular Probes, Eugene, OR), and analyzed using a flow cytometer (Guava Personal Cell Analysis (PCA) system, Guava Technologies, Hayward, CA) to determine the total number of cells with intact nuclei in the sample.

Oxygen Consumption Rate (OCR)

OCR was measured as previously described [39]. Briefly, suspensions containing about 2500 IE/ml in DMEM containing 4.5 g/l glucose and 0.6 g/l L-glutamine supplemented with

100 U/ml penicillin, 100 μg/ml streptomycin, 10 mM HEPES, and no added serum were sealed in a 200-μl stirred titanium chamber (Micro Oxygen Uptake System, FO/SYSZ- P250, Instech Laboratories, Plymouth Meeting, PA) maintained at 37°C. The time dependent pO_2 within the chamber was recorded with a fluorescence-based oxygen sensor (Ocean Optics, Dunedin, FL), and data at high pO_2 were fit to a straight line. The maximal OCR was evaluated from $OCR=V_{ch}\alpha(\Delta pO_2/\Delta t)$, where V_{ch} is the chamber volume and α = 1.27 nmol/mm·Hg·ml is the Bunsen solubility coefficient for oxygen in medium [16]. OCR measurements were normalized by the measured number of cells (nuclei counting) or DNA content of the sample examined.

Membrane Integrity

7-Aminoactinomycin (7-AAD) Sequential Staining

Cell membrane integrity was assessed by differential staining with 7-AAD (Molecular Probes, Eugene, OR) [55]. An aliquot of about 300 islets was re-suspended in 100 μl of D-PBS, and 5 μl of 1 mg/ml 7-AAD and incubated for 20 min at 4°C protected from light. After two washes with 1 ml of D-PBS, cells were disrupted by adding equal volume of lysis solution in D-PBS to the islet suspension and sheared as described for islet enumeration. Labeled nuclei were counted immediately in the flow cytometer or stored on ice for less than 15 min before counting. A portion of the islet suspension was further stained with 7-AAD, thereby labeling all of the previously unlabelled nuclei, and the total number of nuclei was counted. The fraction of cells with compromised membranes was estimated as the ratio of the initially stained nuclei (first measurement) to the total number of nuclei (second measurement).

Sytox Orange/LDS 751

Cell suspensions were stained with a solution (in D-PBS) containing 0.8 μM LDS 751 (Molecular Probes), a membrane permeable dye and 0.2 μM Sytox Orange (Molecular Probes), a membrane impermeable dye. LDS 751 was dissolved in dimethyl sulfoxide (DMSO). Samples with a cell concentration no higher than $5x10^5$ cells/ml were incubated for 5 min at room temperature and analyzed in a flow cytometer (Guava PCA) using the Guava Viacount software. The fraction of cells with compromised membranes was the ratio of the number of cells stained with Sytox Orange over the number of cells stained with LDS 751.

Statistics

Measurements were made with three or more replicates and reported as mean ± SD. Statistical significance was determined using a Student t-test for unpaired data for comparing population means, and for paired data when appropriate.

4.3 Theoretical model

4.3.1 Culture on oxygen-impermeable surfaces

The steady state theoretical O_2 transport model for culture on an O_2-impermeable dish was described previously (Chapter 3), and only parameter values needed to be changed in this study. For elevated O_2 concentration, the ambient partial pressure of O_2 (p_{gas}) was set to 428 mmHg, which was obtained using a premixed gas cylinder of 60% O_2 at 37°C. At 24°C with normoxic conditions, p_{gas} was 154 mmHg. Reduced culture temperature affected several parameters. The O_2 diffusivities and solubilities at 37°C and 24°C are given in Table 4.1. V_{max} was assumed to follow an Arrhenius expression such that it decreased exponentially with inverse temperature as illustrated for a variety of cell lines [115]. The values for the parameters in the expression were determined experimentally and are given later.

4.3.2 Culture on silicone rubber

The diffusion-reaction equation applied to steady state conventional culture (Chapter 3) was modified for culture on silicone rubber. O_2 consumption within the islet is assumed to follow Michaelis-Menten kinetics [16] for which the reaction rate is expressed as

$$R = -\frac{V_{max} p}{K_m + p} \qquad \textbf{4.1}$$

where p is the partial pressure of O_2, V_{max} is the maximum reaction velocity, and the Michaelis constant K_m is the partial pressure at which the reaction rate is $V_{max}/2$. This O_2 consumption reaction only occurs above a critical value, p_{crit}. Below p_{crit}, the tissue dies and no longer consumes O_2. The species conservation equation in medium (m), islet tissue (i), and silicone rubber (Si) become, respectively,

$$(D\alpha)_m \nabla^2 p = 0 \qquad \textbf{4.2}$$

$$(D\alpha)_i \nabla^2 p - \frac{V_{max} p}{K_m + p} = 0 \qquad \textbf{4.3}$$

$$(D\alpha)_{Si} \nabla^2 p = 0 \qquad \textbf{4.4}$$

where α is the solubility of O_2 and D is the diffusivity of O_2.

All the tissue (islet and non-islet) was assumed to be in the form of spheres with uniform diameter (d) that were arranged in a square array with center-to-center distance w in a stagnant medium of height h (Figure 4.1) on an O_2 -permeable surface of thickness δ. Because of symmetry within the system, Equations 4.2-4.4 were solved within a unit cell containing only an eighth of an islet (dashed lines in Figure 4.1). The boundary conditions for this model include continuity of pO_2 across the gas-liquid and gas-silicone rubber interfaces

at $z = h$, $$p_{gas} = p_m \qquad \textbf{4.5}$$

at $z = -\delta$, $$p_{gas} = p_{Si} \qquad \textbf{4.6}$$

continuity of the O_2 flux and pO_2 across the liquid-islet interface,

$$n \bullet ((-D\alpha \nabla p)_i - (-D\alpha \nabla p)_m) = 0 \qquad \textbf{4.7}$$

$$p_i = p_m \qquad \textbf{4.8}$$

the membrane-islet interface,

at $r = 0, z=0$, $$n \bullet ((-D\alpha \nabla p)_i - (-D\alpha \nabla p)_{Si}) = 0 \qquad \textbf{4.9}$$

$$p_i = p_{Si} \qquad \textbf{4.10}$$

and across the membrane-liquid interface,

$$n \bullet ((-D\alpha \nabla p)_{Si} - (-D\alpha \nabla p)_m) = 0 \qquad \textbf{4.11}$$

$$p_{Si} = p_m \quad \textbf{4.12}$$

and symmetry across each side of the unit cell including medium, islet, and silicone rubber domains (indicated by dashed lines in Figure 4.1)

$$n \bullet (-D\alpha \nabla p) = 0 \quad \textbf{4.13}$$

The O_2 solubility in silicone rubber is 1.21 x 10^{-8} mol/mmHg cm^3 [116], the O_2 diffusivity in silicone rubber is 2.17 x 10^{-5} cm^2/s [116] and the thickness of the silicone membrane was either 100 or 500 μm. As with conventional culture V_{max} = 36.8 nmol/s cm^3 (about 2.5 fmol/min cell from Chapter 2 and 1560 cells/IE [13]). Though 2.5 fmol/min cell is higher than the OCR of fresh human islet tissue determined in Chapter 2, it is only used when determining theoretical predictions plotted versus OCR density, which was shown only weakly dependent on V_{max} (Chapter 3).

As illustrated previously (Chapter 3) in order to accurately predict oxygen profiles during culture all tissue, islet and non-islet need to be considered. Islet density reported as IE/cm^2 is related to the density in the simulations through

$$\Gamma = \frac{\rho}{\Phi_I} \quad \textbf{4.14}$$

where Φ_I is the islet volume fraction of the islet preparation, ρ is the islet surface density in IE/cm^2, and Γ is the sphere surface density in "IE"/cm^2 used in our model. In this case "IE" does not refer specifically to islet tissue, but rather a quantity of total tissue volume. This conversion adds the assumption that the exocrine tissue is present as 150-μm diameter spheres. In this study tissue was quantified using nuclei counts, which relate to the model density through

$$\Gamma = \frac{\chi}{n_{IE}} \quad \textbf{4.15}$$

where χ is the cell surface density (cells/cm^2) and n_{IE} is the number of cells in an IE (1560 cells/IE, [13]). Again exocrine tissue is assumed to be similar to islet tissue such that a volume of tissue equal to a 150-μm diameter sphere contains the same number of cells as an IE.

Table 4.1. Oxygen diffusivities and solubilities at 37°C and 24°C in culture medium and tissue used in the theoretical O_2 transport model.

Property	Phase	Temperature °C	Value	Units	Reference
Oxygen diffusivity, D_m	Medium	37	2.78×10^{-5}	cm^2/s	[16]
		24	2.20×10^{-5}	cm^2/s	Wilke - Chang equation [117]
Oxygen diffusivity, D_i	Tissue	37	1.22×10^{-5}	cm^2/s	[16]
		24	9.65×10^{-6}	cm^2/s	*
Oxygen solubility, α_m	Medium	37	1.27×10^{-9}	mol/cm^3 mmHg	[16]
		24	1.71×10^{-9}	mol/cm^3 mmHg	Value for water [118]
Oxygen solubility, α_i	Tissue	37	1.02×10^{-9}	mol/cm^3 mmHg	[16]
		24	1.31×10^{-9}	mol/cm^3 mmHg	*

***The O_2 diffusivity in tissue at 24°C was estimated by multiplying the O_2 diffusivity in tissue at 37°C by the ratio of the diffusivities in medium at 24°C and 37°C. A similar calculation was conducted for O_2 solubility in tissue.**

Total tissue surface density can be converted to an OCR surface density, which is the total OCR of the tissue divided by the area of culture, using

$$\lambda = \chi V_{max} \frac{V_{IE}}{n_{IE}} = \Gamma V_{max} V_{IE} \qquad \textbf{4.16}$$

where λ is the OCR density with units of flux and V_{IE} is the volume of an IE.

The model was solved with the finite element method using commercially available software (COMSOL Multiphysics, COMSOL Inc., Burlington, MA) in conjunction with Matlab (Mathworks, Natick, MA), as described previously (Chapter 3).

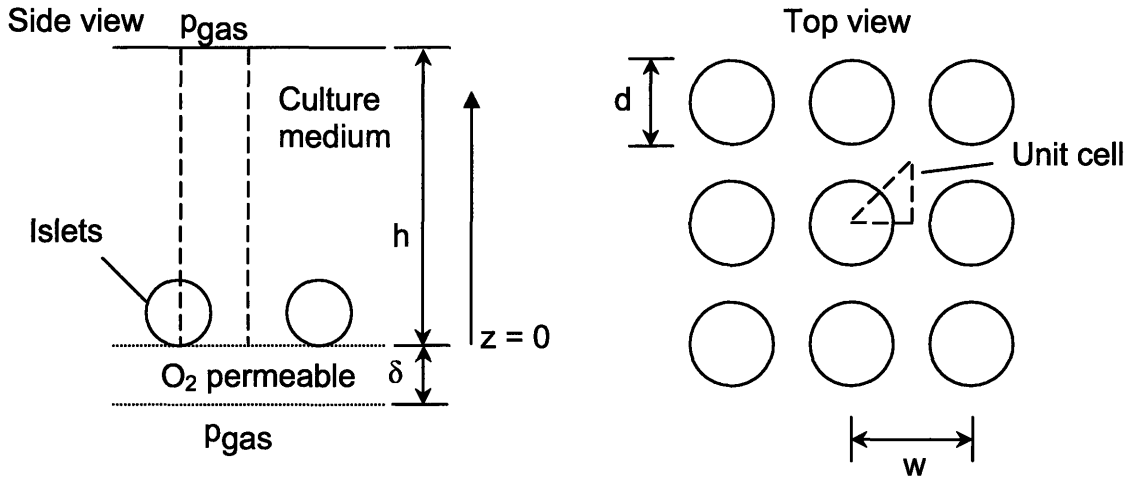

Figure 4.1. Geometry assumed for simulations of islet culture on an O_2-permeable surface. Dashed lines denote unit cell.

4.4 Results

Data from cultures carried out with elevated pO_2, at reduced temperature, and on silicone rubber membranes were compared to data from parallel cultures on polystyrene at 37°C and 142 mmHg in terms of the fraction of original cells collected from culture as measured by nuclei counting (Figure 4.3), tissue viability as quantified by OCR/cell (Figure 4.4), and the fraction of original viable tissue collected from culture F_V, as measured by OCR (Figure 4.5), all after culture for 2 days. In addition, membrane integrity measurements were also made for reduced culture temperature experiments. The islet preparations used in this study varied in initial quality with an average OCR/cell of 1.6 ± 0.5 with a range of 0.6 to 2.5 fmol/min cell.

4.4.1 Culture at elevated ambient oxygen partial pressure

The fraction of original cells recovered after culture did not change consistently with initial tissue surface density (Figure 4.3A) and averaged 0.84 ± 0.17 and 0.82 ± 0.16 at pO_2 of 142 and 428 mmHg, respectively. OCR/cell and the fraction of the original OCR recovered after culture dropped sharply with increasing tissue density at 142 mmHg, slightly less so at 428 mmHg. Using estimates of 1560 cells/IE and about 50% islet cells in an average human islet preparation [55], 200 and 400 IE/cm^2 correspond to 0.625 and 12.5 x 10^6 cells/cm^2, respectively. The data in Figure 4.5A indicate a corresponding loss of about 10 to 50% of the original OCR from islet preparations cultured for 2 days at 37°C with these densities.

At very low culture density F_V was significantly lower at 428 (about 0.6) than at 142 mmHg O_2 (about 1.0). Furthermore, low density culture at 570 mmHg O_2 for 48 hr resulted in even lower F_V (0.22 ± 0.06 from 570 mmHg culture versus 0.69 ± 0.05 from 142 mmHg for a paired experiment). It is likely these decreases in F_V are caused by O_2 toxicity. To further explore this phenomenon, we cultured βTC3 cells at varying pO_2 over a 4-day period. Membrane integrity measurements are plotted versus time in culture in Figure 4.6. These data indicate O_2 has a toxic effect on these cells that is both dose and time dependent, and it is likely also toxic to islets.

4.4.2 Culture at reduced temperature

Measurements of rat islet OCR decreased exponentially with inverse temperature (Figure 4.2), resulting in an average activation energy from three experiments of 53 ± 4 kJ/mol, which is smaller than previously reported values for cell lines (79-93 kJ/mol) [115]. Assuming human islet tissue has a similar activation energy and the OCR at 37°C for human islet tissue is 2.5 fmol/min cell (Chapter 2) the following equation for V_{max} as a function of temperature is obtained.

$$V_{max} = V_O \cdot \exp\left[-E / R_{gas} T\right] \qquad \textbf{4.17}$$

where V_O is 1.86 x 10^3 mol/min cm^3 (adjusted to volume basis assuming 1560 nuclei/IE [13]), E is 53 kJ/mol, and R_{gas} is the gas constant (0.008314 kJ/mol K). This Arrhenius function will be used for V_{max} when comparing experimental and theoretical results.

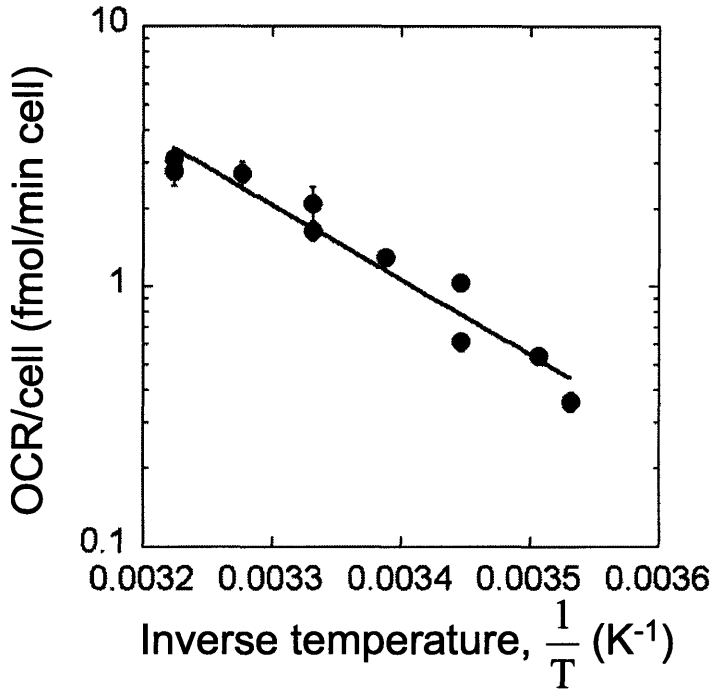

Figure 4.2. OCR as a function of inverse temperature from three rat islet preparations. Error bars are ± standard deviation for triplicate measurements.

The fractional recoveries of human islet tissue averaged 0.76 ± 0.10 and 0.83 ± 0.13 at 37 and 24°C, respectively, and there was no effect of tissue surface density (Figure 4.3B). The decrease in OCR/cell and fractional OCR recovery (Figure 4.4B and Figure 4.5B) with increasing surface density was less severe at 24°C, although the data is limited and scattered. At very low density, the values of these parameters were lower at 24 than at 37°C. Culture at 12°C at very low density gave similar OCR/cell and fractional OCR recoveries as those from 24°C culture (data not shown). Membrane integrity measurements (Figure 4.7) made in conjunction with this series of experiments demonstrated negligible change with tissue density at 24°C. There was a decrease at 37°C that was much less sharp than OCR/cell measurements.

4.4.3 Silicone rubber culture

Culture on a 500-μm silicone rubber membrane (with h = 22 mm) resulted in a fractional cell recovery of 0.80 ± 0.12 (Figure 4.3C), which was significantly lower than that for culture at the same medium depth on polystyrene, 0.93 ± 0.06 ($p<0.01$). OCR/cell and fractional recovery of OCR were substantially higher at all culture densities on a silicone rubber membrane

compared to polystyrene culture at the same medium depth (Figure 4.4C and Figure 4.5C) as well as at the smaller depth, 3mm (Figure 4.5A and B). In addition, fractional OCR recovery was not affected when the silicone rubber membrane thickness was decreased from 500 to 100-μm.

4.4.4 Comparison with prediction of oxygen transport model

As mentioned previously, the partial pressure field in the islet calculated by the theoretical model was used to determine the viable tissue volume (V_V) by integrating the volume of tissue with $pO_2 > p_{crit}$. The volume fraction of the viable tissue remaining after culture was calculated from

$$F_V = \frac{V_V}{\frac{4}{3}\pi R_{islet}^3} \qquad \textbf{4.18}$$

The experimental data Figure 4.5 are compared to the predictions of the theoretical O_2 transport model in Figure 4.8, in which fractional OCR recovery is plotted versus initial OCR density, so that in this way, all theoretical predictions collapse to a closely clustered curve for all values of V_{max}, thereby permitting comparison of results from different experiments with one predicted curve (Chapter 3). OCR density was determined for each experiment through

$$\lambda = \chi V_{max} \frac{V_{IE}}{n_{IE}} \qquad \textbf{4.19}$$

where λ is the OCR density with units of flux, χ is the cell surface density (cells/cm^2) based on nuclei counts prior to culture, n_{IE} is the number of cells in an IE (1560 cells/IE, [13]), and V_{IE} is the volume of an IE. V_{max} was determined for each isolation prior to culture.

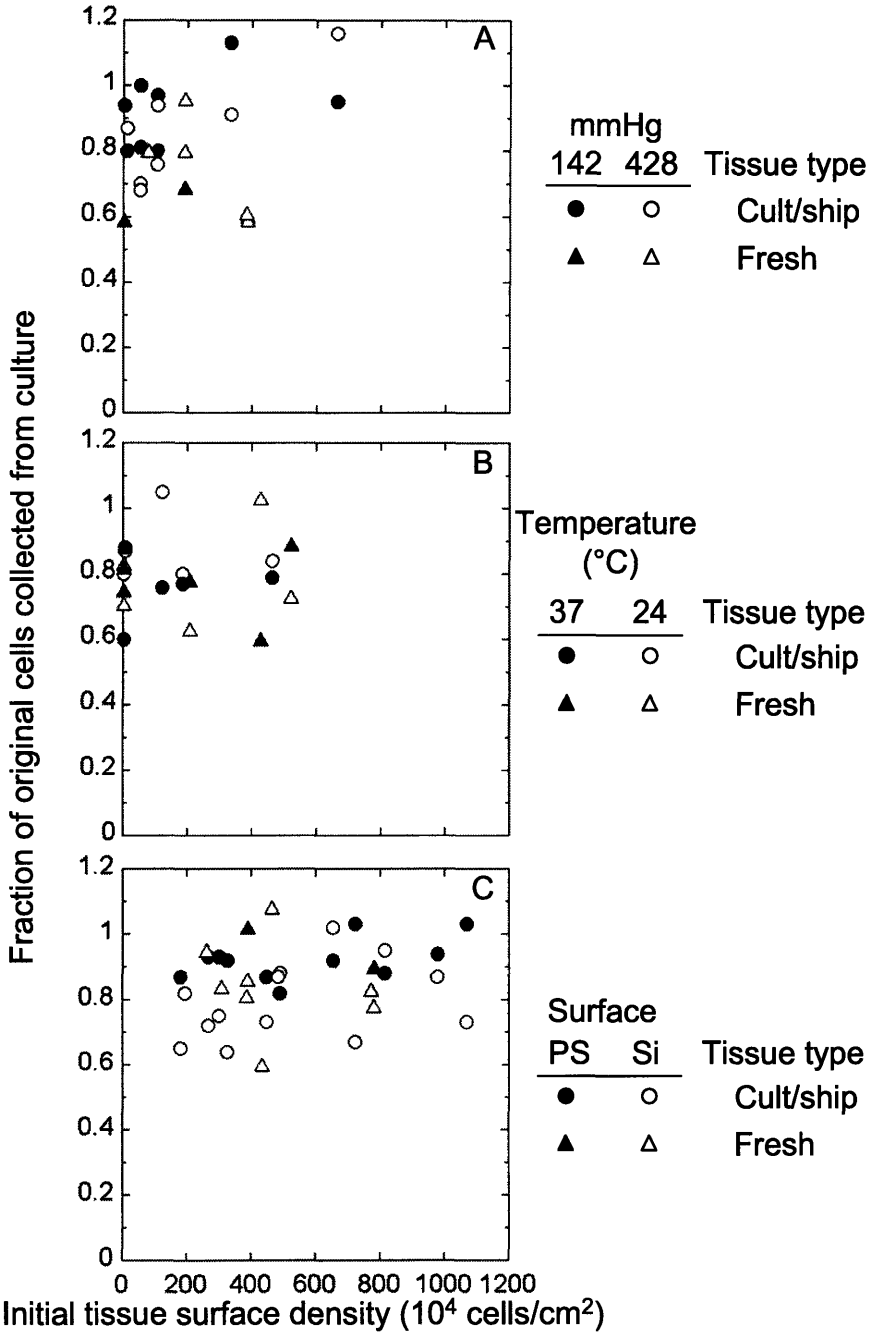

Figure 4.3. The total fraction of original cells recovered after culture with various culture techniques as a function of the initial tissue density.
Culture performed (A) on polystyrene at 37°C, 428 mmHg with h = 3 mm, (B) on polystyrene at 24°C, 154 mmHg with h = 3mm, and (C) on a 500-μm silicone rubber membrane (Si) at 37°C, 142 mmHg with h = 22 mm. Parallel cultures of islets from the same preparations on polystyrene (PS) at 142 mmHg, 37°C, and the same medium height are included when available.

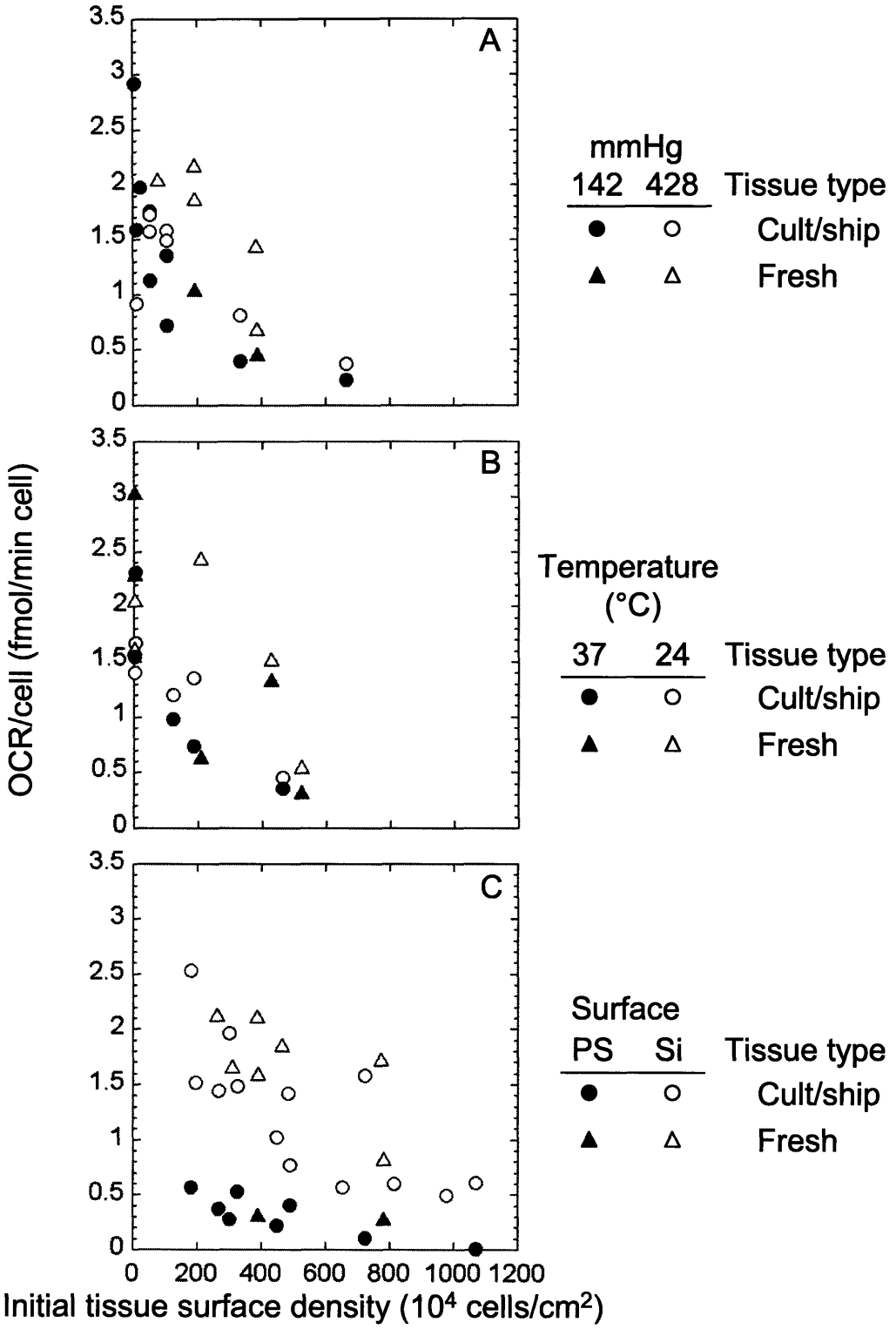

Figure 4.4. OCR/cell following culture as a function of the initial tissue density for different culture techniques
Culture performed in similar format as Figure 4.1.

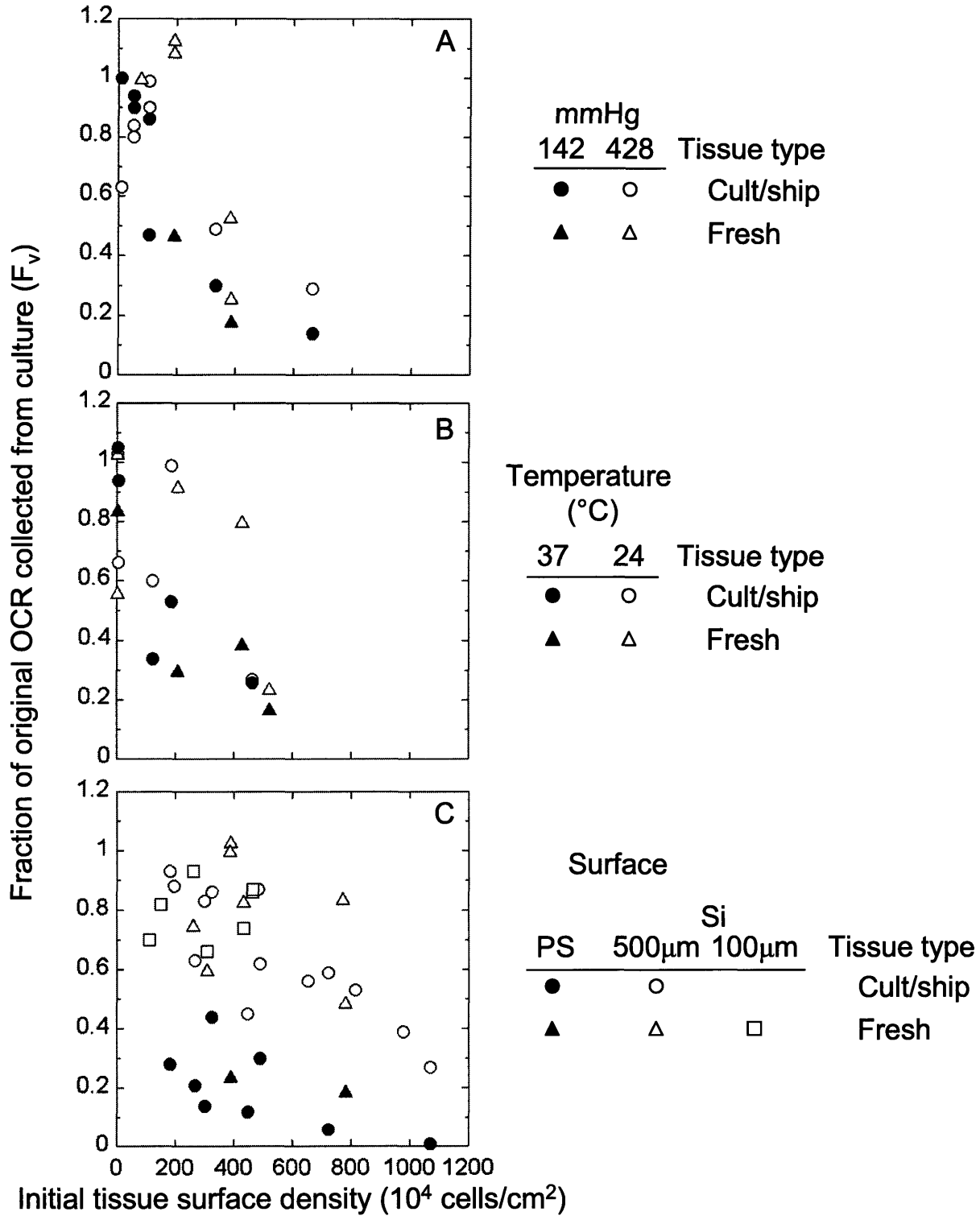

Figure 4.5. Fraction of original OCR recovered from culture as a function of surface density for different culture techniques.
Culture performed in similar format as Figure 4.1.

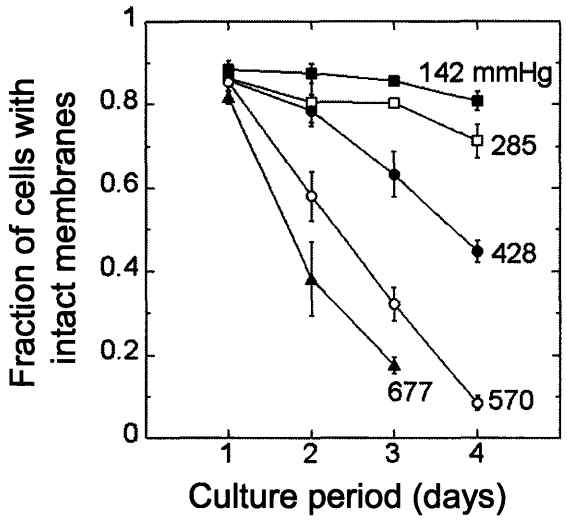

Figure 4.6. The fraction of βTC3 cells with intact cell membranes exposed to varying O_2 concentrations over 4 days of culture.
Membrane integrity determined by Sytox Orange/LDS 751 staining. Error bars are ± standard deviation for measurements from 3-5 independent experiments.

The theoretical model predictions indicate that the fractional recovery of OCR should be improved by each of the three oxygen delivery enhancement approaches investigated. For both increased incubator pO_2 and reduced culture temperature, F_V is predicted to be 1.0 up to some point and then decreases as initial OCR surface density increases. For cultures on silicone rubber membranes, F_V is predicted to be 1.0 over the entire range of tissue density. For both increased pO_2 and reduced culture temperature, the model predictions are substantially higher than experimental data at all but the lowest densities. The same is true for culture on silicone rubber. However, the model underpredicts the experimental data for culture on polystyrene for the case of a large medium depth.

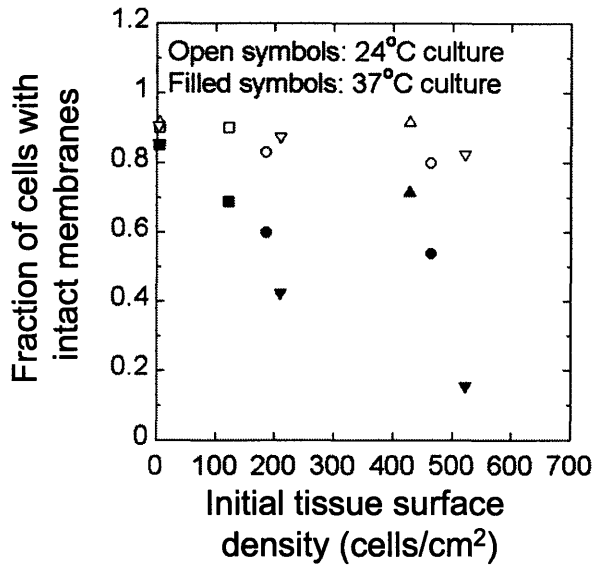

Figure 4.7. The fraction of tissue with intact cell membranes as a function of tissue surface density for culture at varying temperatures.
Culture performed on polystyrene in 3 mm medium at 37°C, 142 mmHg (open symbols) or 24°C, 154 mmHg (filled symbols). The differently shaped symbols represent different islet isolations.

4.5 Discussion

In this study we examined how tissue recovery and viability of islet preparations changed as a function of tissue surface density after culture for 2 days using three techniques designed to reduce O_2 supply limitations present during conventional static culture including culture under (1) elevated pO_2, (2) at reduced temperature, and (3) on a silicone rubber membrane. For each technique, parallel cultures were carried out using conventional culture (pO_2 of 142 mmHg, 37°C, untreated polystyrene surface). By applying a theoretical model of O_2 consumption and diffusion, we also explored how O_2 profiles change in each system, and we used the model to predict the recovery of viable tissue relative to viable tissue placed into culture. We hypothesized that improved oxygenation would increase the fraction of viable tissue remaining following high density culture.

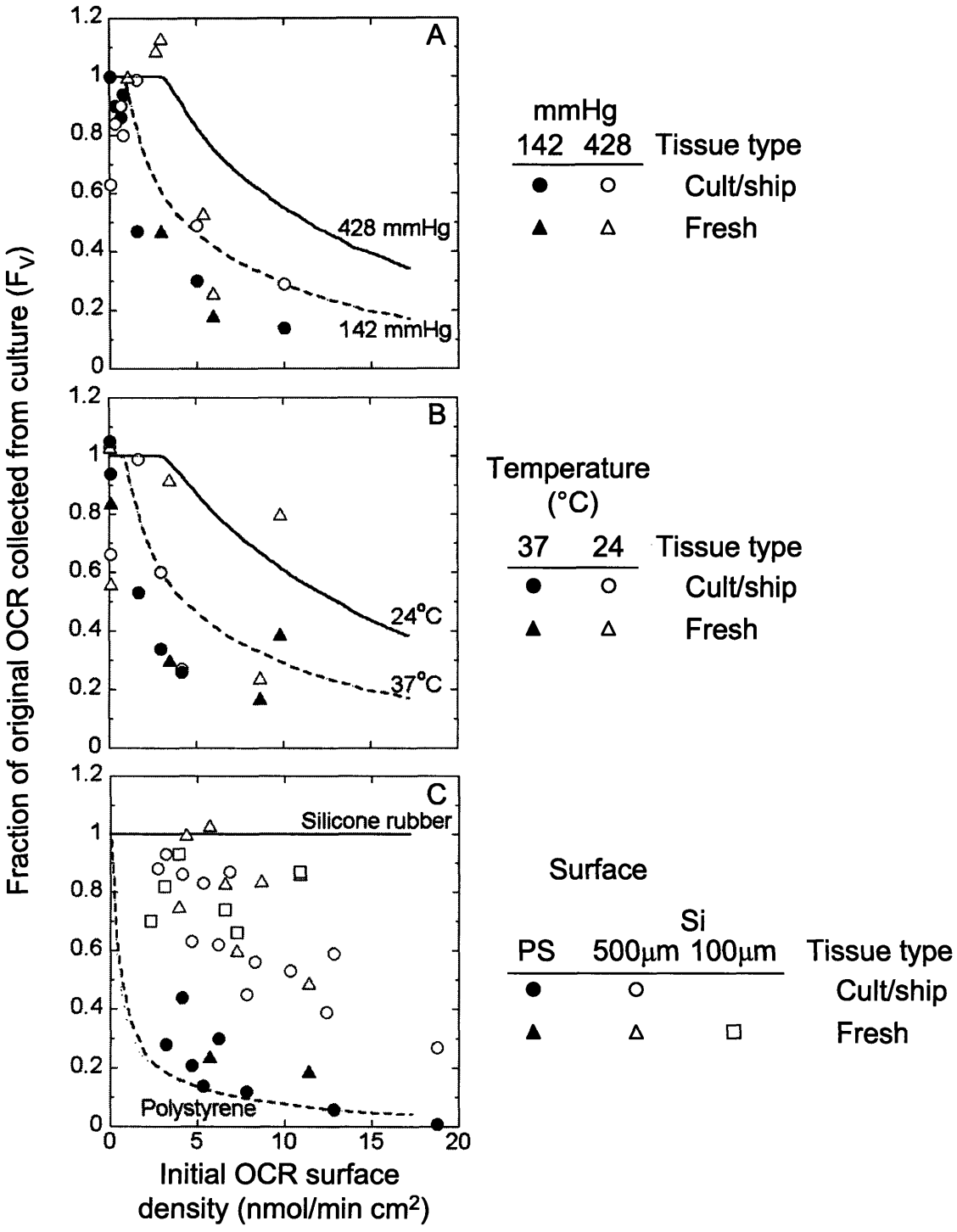

Figure 4.8. Experimental results and theoretical predictions for the fraction of original viable tissue collected following culture for various culture techniques.
Culture performed in similar format as Figure 4.1. The solid and dashed lines are predictions of the theoretical model, which was evaluated with V_{max} = 2.5 fmol/min cell = 36.8 nmol/s cm^3.

The fraction of original cells recovered after culture, as measured by nuclei counting, did not change with increasing islet tissue surface density in any of the experiments (Figure 4.3). It was not influenced by increased pO_2 or decreased culture temperature but there was a small consistent decrease in cell recovery when cultured on silicone rubber as compared to conventional culture.

With increasing tissue density, culture at 428 mmHg led to higher OCR/cell (Figure 4.4) and fractional recovery of OCR (Figure 4.5) as compared to conventional culture. Because the only difference between the culture conditions was pO_2, the higher recovery of viable tissue at elevated pO_2 is consistent with the notion that O_2 supply limitations play an important role in the decrease of F_V at high culture densities during conventional culture (Chapter 3).

Culture at very low density at 24°C resulted in lower OCR/cell and F_V than culture at 37°C. A similar trend was observed in a previous study (Chapter 2), which suggests that there is a mechanism for loss of viability at 24°C that is independent of oxygen supply limitations. Lower viability at 22°C compared to 37°C was also reported for islets cultured at 3 IE/cm^2 with 2 mm medium depth [49]. At tissue surface densities greater than about 10^6 cells/cm^2, culture at 24°C resulted in higher OCR/cell and fractional OCR recovery than at 37°C (Figure 4.4B and Figure 4.5B), which is consistent with previous reports indicating higher necrotic death [50; 52] or lower recoveries [49] with 37°C culture than at reduce temperatures. The data at 24°C was highly scattered. One possible reason could be changes in cellular respiration continue to occur as the tissue acclimates to 37°C during the 1 hr incubation at 37°C prior to analysis. This short period may not be sufficient to allow all metabolic processes to reach a new steady state at 37°C.

Culture on silicone rubber membranes had the largest impact on tissue characteristics. OCR/cell (Figure 4.4C) and fractional OCR recovery (Figure 4.5C) were significantly higher than for culture on polystyrene. For example, F_V for culture on polystyrene at densities up to about 6 x 10^6 cells/cm^2, corresponding to about 10 nmol/min cm^2 (Figure 4.8C) averaged 0.25 whereas culture on a 500-μm silicone rubber membrane averaged 0.81. Decreasing membrane thickness to 100-μm had no significant effect on F_V indicating that the 500-μm membrane had effectively removed all of the oxygen supply limitations.

The sharp decrease with increasing tissue density in fractional OCR recovery for cells undergoing conventional culture, and to a lesser degree for cells cultured on silicone rubber and the other culture manipulations are indicative of large fractions of the cells having entered the

cell death process. By contrast, the recovery of nuclei did not change with increasing tissue density. Thus, exposure of islets to anoxia in this study caused cells to enter the cell death process, but after 2 days it had not progressed to the point where nuclei were fragmented. Membrane integrity was also independent of tissue density at 24°C and decreased with increasing tissue density at 37°C, but not nearly as much as OCR/cell. Thus, at 37°C the extent of cell membrane dysfunction lagged the reduction of OCR at 37°C, which is consistent with prior studies [55] and the cells did not reach this stage at all at 24°C.

The theoretical model correctly predicted no loss of OCR at low tissue density, which was consistent with experimental data, and the predictions were qualitatively correct in predicting a decrease with moderate to high tissue density and a greater recovery of OCR with techniques to reduce oxygen supply limitations. However, in every case the theory overestimated F_V when compared to experimental data except for culture in 22 mm medium on polystyrene for which it underestimated F_V. The disparity was large for culture on silicone rubber at very high density for which the theory predicted there should be adequate oxygen supply. The discrepancies between theoretical predictions and experimental measurements for conventional culture have been discussed previously (Chapter 3), some of the same explanations hold for the culture techniques investigated here, including (1) inaccuracies in the model assumptions or parameter values, (2) diffusional limitations of nutrients (i.e. glucose) linked to the lack of medium change during culture, and (3) products produced by islet tissue (i.e. lactate, ammonia, nitric oxide) that could have toxic effects especially at high surface densities.

Among the possible inaccuracies in the assumptions for the model is the possibility that representation of islets as arranged in the orderly pattern of Figure 4.1 is unrealistic, e.g., islets may clump together locally to form a sheet-like structure or multi-layer structures. Development of models to investigate these various possibilities is described elsewhere (Chapter 5). For culture on silicone rubber, the first explanation is unlikely because there is excess oxygen supply capability as evidenced by no change in experimental data when membrane thickness was reduced from 500 to 100 μm. Application of the theoretical model to culture at 24°C is not straight forward because $F_V < 1$ for culture at very low density, indicating that even when no transport limitations are present not all of the viable tissue can be recovered (Chapter 2). The underestimation of F_V for culture in 22 mm medium on polystyrene can be explained by (1) removal of additional diffusion limitations present at low medium depths and (2) changes in

gene expression. Islet β cells normally have a low level of lactate dehydrogenase (LDH) expression [119] but up-regulate LDH when exposed to a hypoxic environment for 24 hr (G. Weir, personal communication), which allows them to produce energy by glycolysis in the absence of O_2. If tissue in the islet preparation can up-regulate LDH fast enough, a larger fraction would be able to survive than predicted by the theoretical model.

The techniques examined improve tissue oxygenation compared to conventional culture, thereby allowing tissue to be cultured at higher densities without a reduction in viability. Theoretical and experimental results indicate that during conventional culture (142 mmHg O_2, 37°C, 3 mm) at OCR densities greater than 0.9 nmol/min cm^2 O_2 limitations occur causing a reduction in viability. Culture on polystyrene in 428 mmHg O_2 (37°C, 3 mm) supplies sufficient O_2 until 3 nmol/min cm^2, a 3-fold increase in density over conventional culture, but O_2 toxicity needs to be considered. A similar enhancement is obtained from culture on polystyrene at 24°C in 154 mmHg O_2 (h = 3 mm). However, reduced temperature culture may "precondition" tissue by changing the cellular machinery [51], thus bringing up questions about changes in tissue function. Brandhorst et al [49] concluded that 37°C culture of porcine islets resulted in superior insulin content, secretion, and dynamic response to glucose as compared to culture at 22°C which suggest that 37°C is better than reduced culture temperature in maintaining islet function. Though reduced temperature culture may be an improvement to conventional culture at high densities, it may not be the best choice. Culture on a 500-μm silicone rubber membrane removes all O_2 limitations for densities less than 15 nmol/min cm^2 though decreases in F_V are observed experimentally at densities greater than 5 nmol/min cm^2 due to O_2-independent mechanisms. To put this in perspective consider a preparation containing 400,000 IE that has an islet volume fraction of 50% (i.e. a total tissue volume equivalent to 800,000 IE) and a total tissue OCR of 1.9 μmol/min (accounting for both islet and non-islet tissue, 1560 cells/IE [13], 1.5 fmol/min cell Chapter 2). Using conventional culture with 3 mm medium, a culture area of about 2100 cm^2 (14 T-150 flasks) would be required to provide sufficient O_2 to prevent a decrease fractional OCR recovery while culture in 428 mmHg O_2 or at 24°C (154 mmHg O_2) would reduce this area to 700 cm^2 (5 T-150 flasks) and culture on a 500-μm silicone rubber membrane would require only 420 cm^2 (3 T-150 flask). This reduction in culture area would save space and time while providing sufficient O_2 to the tissue.

4.6 Nomenclature

7-AAD	7-aminoactinomycin D
C	Concentration of O_2
D	Diffusivity of O_2
d	Diameter of islet
D-PBS	Dulbecco's phosphate buffered saline
E	Activation energy
FBS	Fetal bovine serum
$F_{n,a}$	The fraction of original cells collected as adherent tissue after culture
$F_{n,na}$	The fraction of original cells collected as non-adherent tissue after culture
$F_{n,a}$	The fraction of original cells collected as the combined total (adherent + non-adherent) tissue after culture
F_V	The fraction of original viable tissue after culture
h	Medium depth
IE	Islet equivalent
K_m	Michaelis constant, the pO_2 at which the reaction rate is $V_{max}/2$
LDH	Lactate dehydrogenase
n_{IE}	Number of cells in an IE
O_2	Oxygen
OCR	O_2 consumption rate
p	O_2 partial pressure
p_{crit}	The pO_2 below which a cell dies and no longer consumes O_2
PDMS	Polydimethylsiloxane
p_{gas}	Ambient partial pressure of O_2
R	Production rate of O_2
R_{gas}	Gas constant
R_{islet}	Radius of islet
T	Total (non-adherent + adherent) tissue
t t	Time

V_{ch}	Volume of OCR chamber
V_{IE}	Volume of an IE
V_{max}	Maximum reaction velocity
V_{NV}	Non-viable tissue volume
V_o	Constant in Arrhenius equation
V_V	Viable tissue volume
w	Center-to-center distance between islets
α	Solubility of O_2 in medium
δ	Thickness of silicone rubber membrane
Φ_I	Islet volume fraction of the islet preparation,
Γ	Sphere surface density
λ	OCR density with units of flux
ρ	Islet surface density in IE/cm^2
χ	Cell surface density (cells/cm^2)

Subscripts for D, α, p, C

m	Medium
i	Islet tissue
Si	Silicone rubber

5 Oxygen transport during islet culture: A closer look

5.1 Introduction

Tissue surface density has a large impact on the fraction of original viable tissue (F_V) collected from static culture on polystyrene and on silicone rubber membranes (Chapter 3 and 4). As tissue surface density increases during culture on polystyrene, F_V decreases due, at least in part, to oxygen (O_2) limitations (Chapter 3 and 4). However, though the empirical decrease in F_V was qualitatively similar to theoretical predictions based on O_2 transport, there were consistent quantitative discrepancies, which may result from inaccuracies in the theoretical O_2 transport model.

The discrepancies could result from applying inaccurate parameter values to the theoretical O_2 transport model. Parameter values taken from literature can vary widely between studies resulting in significant uncertainty. If the parameter value chosen was inaccurate, it would introduce error into the prediction.

Discrepancies between empirical data and the theoretical predictions could also result from inaccurate assumptions made by the model. The model assumes that all tissue (islet and non-islet) is in 150-μm diameter spheres arranged in a square array. In reality the mixture of islet and exocrine tissue varies in shape, size, and spatial distribution, each of which alter predicted O_2 profiles during culture.

In this chapter we describe a sensitivity analysis conducted to determine which model parameters, in particular K_m, p_{crit}, D_i, α_i, D_m, α_m, D_{Si}, and α_{Si}, have a large effect on theoretical predictions for culture on polystyrene and silicone rubber membranes. The confidence in the values chosen through comparisons with other reported values is discussed. We also examine the assumptions made within the model to determine the extent to which they may impact theoretical predictions specifically addressing islet surface density distribution, size, slab formation, tissue stacking, and convection.

5.2 Theoretical model

The theoretical models used to simulate islet culture on an O_2-impermeable dish and on an O_2-permeable dish have been presented in detail previously (Chapter 3 and 4). Both models

apply the diffusion-reaction equation to simulate O_2 transport for spheres of uniform size arranged in a square array in a medium of known depth on either an O_2-impermeable surface (Chapter 3) or an O_2-permeable surface of known thickness (Chapter 4). Oxygen consumption within the tissue was assumed to follow Michaelis-Menten kinetics.

The base case model used in these comparisons assumes culture at 37°C in a fully humidified environment with 95% air / 5% CO_2 (142 mmHg O_2) and a tissue V_{max} of 53.3 nmol/s cm^3. This V_{max} is intended to indicate a worst-case scenario and corresponds to 3.6 fmol/min cell, which is at the upper end of OCR/cell distributions (Chapter 2) and is higher than the V_{max} used previously (Chapter 3 and 4). Since F_V versus initial OCR density is only slightly dependent on V_{max} (Chapter 3), the change does not have a large effect on the overall trend. The base case parameter values estimated from literature are given in Table 5.1. The base case predictions for culture on polystyrene in 3 mm and 22 mm and for culture in 22 mm medium on a 500-μm silicone rubber membrane are illustrated in Figure 5.1. Recall that the experimental F_V was lower than predicted for culture in 3 mm medium on polystyrene (Chapter 3) and for culture in 22 mm medium on a 500-μm silicone rubber membrane (Chapter 4) while it was higher than predicted for culture in 22 mm medium on polystyrene (Chapter 4).

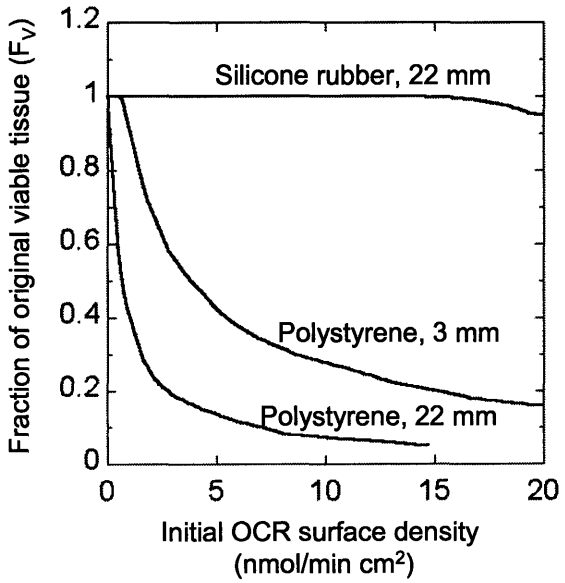

Figure 5.1. The base case O_2 transport model predictions for culture in 3 mm and 22 mm on polystyrene and in 22 mm medium on a 500-μm silicone rubber membrane.

Table 5.1. Base case parameter values used in simulations for O_2 transport during static islet culture.

Parameter	Symbol	Value	Units	Reference
Michaelis constant	K_m	0.44	mmHg	[98]
O_2 diffusivity in medium	D_m	2.78×10^{-5}	cm^2/s	[16]
O_2 diffusivity in tissue	D_i	1.22×10^{-5}	cm^2/s	[16]
O_2 diffusivity in silicone rubber	D_{Si}	2.17×10^{-5}	cm^2/s	[116]
O_2 solubility in medium	α_m	1.27×10^{-9}	mol/cm^3 mmHg	[16]
O_2 solubility in tissue	α_i	1.02×10^{-9}	mol/cm^3 mmHg	[16]
O_2 solubility in silicone rubber	α_{Si}	1.21×10^{-9}	mol/cm^3 mmHg	[116]
Maximal O_2 consumption rate	V_{max}	53.3	nmol/s cm^3	Experimentally measured
Minimum pO_2 for viability	p_{crit}	0.1	mmHg	[16]
Media height	h	3 or 22	mm	Based on medium volume and well area
Membrane thickness	δ	500	μm	Based on equipment
External p	p_{gas}	142	mmHg	Partial pressure of O_2 in humidified incubator at 37°C with 95% air/5% CO_2
Islet radius	R_{islet}	75	μm	Based on definition of IE

5.3 Inaccuracies in parameter values

This section explores the sensitivity of theoretical predictions based on O_2 transport to changes in model parameters (K_m, p_{crit}, D_i, α_i, D_m, α_m, D_{Si}, and α_{Si}) providing insight into whether parameter inaccuracies may account for the discrepancies observed between the theoretical predictions and empirical data.

The Michaelis constant K_m, which is the partial pressure of O_2, p, at which the O_2 consumption rate is $V_{max}/2$, was 0.7 μM (0.44 mmHg) for the base case [98], which is consistent with O_2 consumption measurements in hepatocytes [120; 121]. However, data for O_2 consumption of cardiomyocytes at 5 μM concentrations suggests K_m = 3.05 μM (about 3 mmHg) [122]. Models for O_2 delivery to muscle tissue and energy metabolism in multicellular spheroids have used values ranging from 1 to 4.5 mmHg [123; 124]. Variation between species, tissue type, and temperature could contribute to reported K_m values ranging from 0.25-4.5 mmHg [16; 73; 98; 120-126]. Increasing K_m from 0.44 to 1 mmHg shifts F_V upward while decreasing K_m shifts F_V downward (Figure 5.2). If the actual K_m is higher than the base case as suggested by the range available in literature, then the predicted F_V for culture on polystyrene shifts away from experimental data at low medium depths and towards experimental data at large medium depths. Little change would occur in F_V for culture on a silicone rubber membrane since the tissue is at a higher pO_2 than tissue at the corresponding density on polystyrene.

D and α are always present together in the steady state model equations (Chapter 3 and 4) so changes $D\alpha$, the permeability of O_2, will be considered. First, consider O_2 permeability in islet tissue $(D\alpha)_i$. Oxygen diffusivities for several different tissues range from 0.46-2.41 x 10^{-5} cm^2/s [16; 73; 123; 124; 127-135] while solubility has been reported from 0.94-1.53 x 10^{-9} mol/cm^3 mmHg [16; 73; 124; 129; 131; 132; 134-136] and O_2 permeability from 1.24-3.69 x 10^{-14} mol/cm mmHg s [16; 127-129; 131; 135; 137; 138]. Using the extremes of these reported values a range of 0.43 – 3.69 x 10^{-14} mol/cm mmHg s was determined for the permeability of O_2 in tissue. The base case value (1.24 x 10^{-14} mol/cm mmHg s [16]) was in the middle of this range. A 50% increase or decrease in $(D\alpha)_i$ does not result in a large change in

F_V (Figure 5.3); as such, it is not likely that an inaccuracy in $(D\alpha)_i$ would cause large inaccuracies in F_V for cultures on polystyrene or silicone rubber.

The base case value for O_2 permeability in medium, $(D\alpha)_m$, is 3.53 x 10^{-14} mol/cm mmHg s [16]. The diffusivity of O_2 in 37°C aqueous solutions reported in literature ranges from 2.4-3.43 x 10^{-5} cm^2/s [127; 133; 136; 139; 140] while the solubility ranges from 1.11-1.46 x 10^{-9} mol/cm^3 mmHg [16; 73; 118; 125; 130; 140]. These values result in a fairly narrow permeability range of 2.66-5.01 x 10^{-14} mol/cm mmHg s within which the base case value lies. A decrease in $(D\alpha)_m$ results in a significant downward shift in F_V while an increase results in an upward shift (Figure 5.4). Thus $(D\alpha)_m$ lower than the base case value shifts theory closer to experimental F_V for polystyrene culture at low medium depth, but away from experimental data at large medium depths. $(D\alpha)_m$ has little to no effect on F_V for culture on silicone rubber since the majority of the O_2 supplied to the tissue is through the O_2-permeable membrane (data not shown).

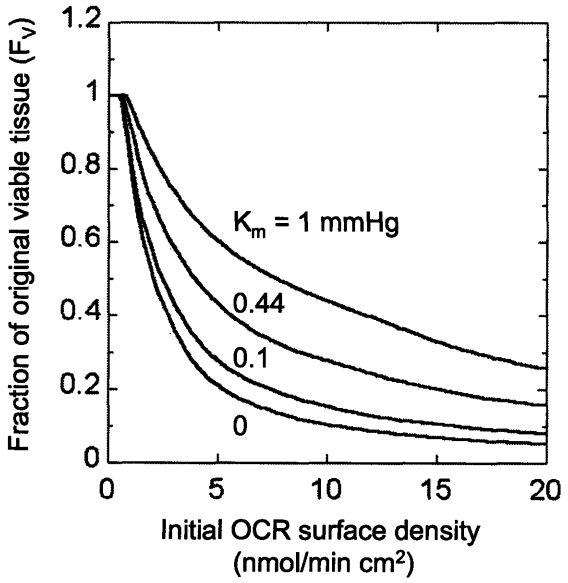

Figure 5.2. Theoretical predictions for the fraction of original viable tissue after culture as a function of initial OCR surface density and K_m.
Predictions assume islet culture in 3 mm medium on an O_2-impermeable dish for values of K_m ranging from 0-1 mmHg.

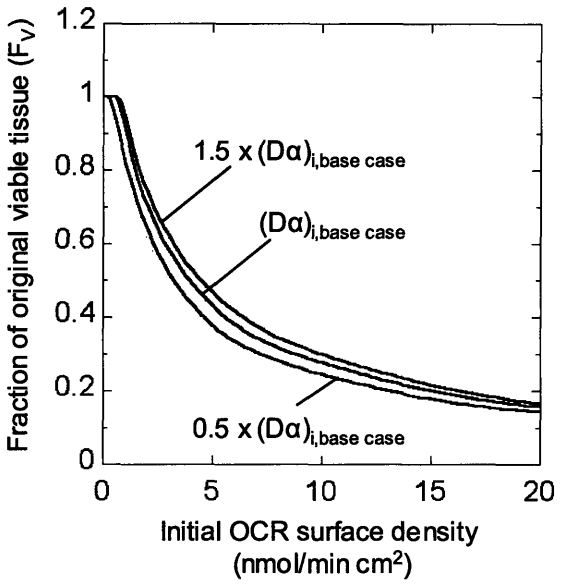

Figure 5.3. Theoretical predictions for the fraction of viable tissue after culture as a function of initial OCR surface density for different values of $(D\alpha)_i$.
Predictions assume islet culture in 3 mm medium on an O_2-impermeable dish.

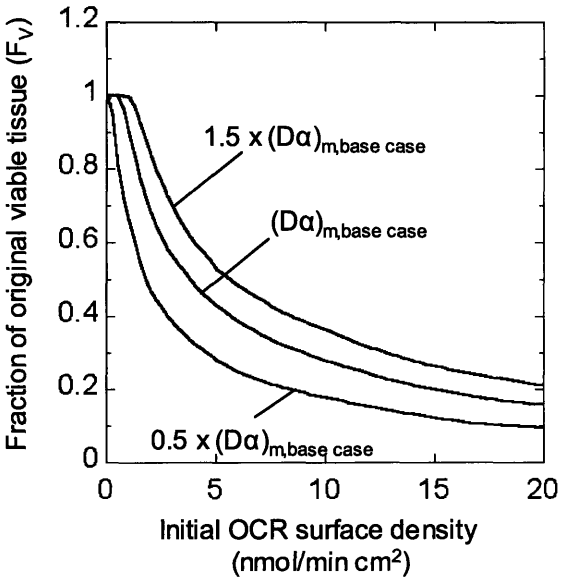

Figure 5.4. Theoretical predictions for the fraction of viable tissue after culture as a function of initial OCR surface density for different values of $(D\alpha)_m$.
Predictions assume islet culture in 3 mm medium on an O_2-impermeable dish.

Data for p_{crit}, the partial pressure of O_2 at which a cell dies, is scarce in comparison to the other parameters used in the model. Avgoustiniatos discussed the use of p_{crit} and its estimation based on data in literature and concluded that 0.1-0.3 mmHg is the best estimate though he notes that other factors including nutrients present and tissue type may play a role in determining p_{crit} [16]. p_{crit} is unlikely to be higher than 1 mmHg since similar pO_2 are observed in vivo [16]. The base case value was 0.1 mmHg. As p_{crit} increases F_V decreases because a higher pO_2 is required for cell survival. Thus if 0.1 mmHg is low (i.e. $p_{crit} > 0.1$ mmHg), F_V shifts downward toward empirical data for culture on polystyrene at low medium depths, but make predictions worse for large medium depths (Figure 5.5). For culture on a silicone rubber membrane F_V decreases from 0.96 to 0.95 at an initial OCR density of 20 nmol/min cm^2 as p_{crit} increases from 0.1 to 0.5 mmHg indicating a very small impact.

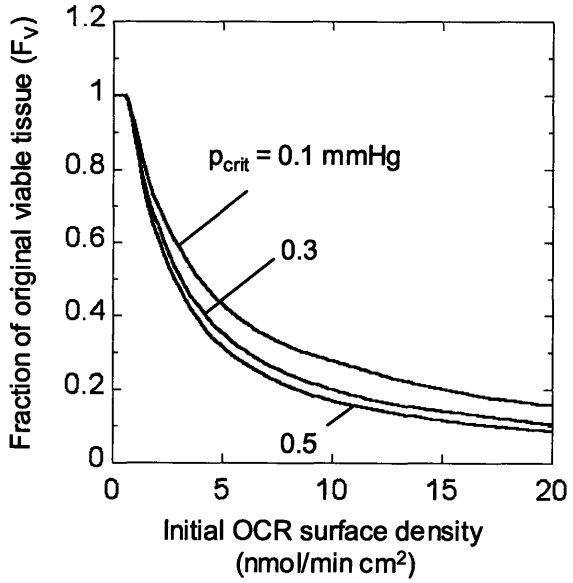

Figure 5.5. Theoretical predictions for the fraction of viable tissue after culture as a function of initial OCR surface density for different values of p_{crit}.
Prediction assumes islet culture in 3 mm medium on an O_2-impermeable dish.

The final parameter taken from literature, O_2 permeability in silicone rubber $(D\alpha)_{Si}$, only affects simulations for culture on an O_2-permeable membrane. The permeability of O_2 in silicone rubber varies widely depending on the exact formulation with values ranging from 0.49 – 41.6 x 10^{-14} mol/cm mmHg s at 35°C [141]. The membranes used in our experiments were polydimethylsiloxane (PDMS) for which a value of 26.3 x 10^{-14} mol/cm mmHg s [116] was used. Unfortunately not all articles investigating silicone rubber membranes note the exact formulation of the silicone rubber tested. The diffusivity of O_2 in silicone rubber ranges from about 1.1 – 2.22 x 10^{-5} cm^2/s [116; 140; 142; 143] for temperatures 35-37°C. However, the Polymer Data Handbook reports a diffusivity of 16 x 10^{-5} cm^2/s for O_2 in PDMS at 25°C [144], which would increase when adjusting to 37°C. Oxygen solubility in silicone rubber ranges from 1.1-20 x 10^{-9} mol/cm^3 mmHg [116; 140; 142; 143]. The resulting range for $(D\alpha)_{Si}$ is 0.49-320 x 10^{-14} mol/cm mmHg s for silicone rubbers of various formulations. Limiting data to studies specifically using PDMS at 35-37°C reduces the range to 2.4-37 x 10^{-14} mol/cm mmHg s [141; 143-145] within which the base case value lies (near high end of range).

As $(D\alpha)_{Si}$ decreases the predicted F_V decreases (Figure 5.6). Therefore if the base case value is high, as suggested by the range of values obtained from literature, then the theoretical predictions will become closer to the experimental data.

5.4 Inaccurate model assumptions

To efficiently simulate islet culture, we made several assumptions that simplified the model. All tissue, islet and non-islet, was arranged in a square array of uniform 150-μm diameter spheres in stagnant medium. Unfortunately this hardly represents reality. Human islets prior to culture (day 0) have a wide spatial and size distribution (Figure 5.7A and D) and at high densities may result in tissue stacking. To complicate things further, during high density culture, the islet distribution and morphology change, resulting in the formation of tissue slabs (Figure 5.7B, C, E, and F) rather than the individual islets that are obtained from low density cultures (Figure 5.7G and H). The model also assumes convection does not occur. In this section we explore the extent to which these phenomena could affect the theoretical prediction of F_V.

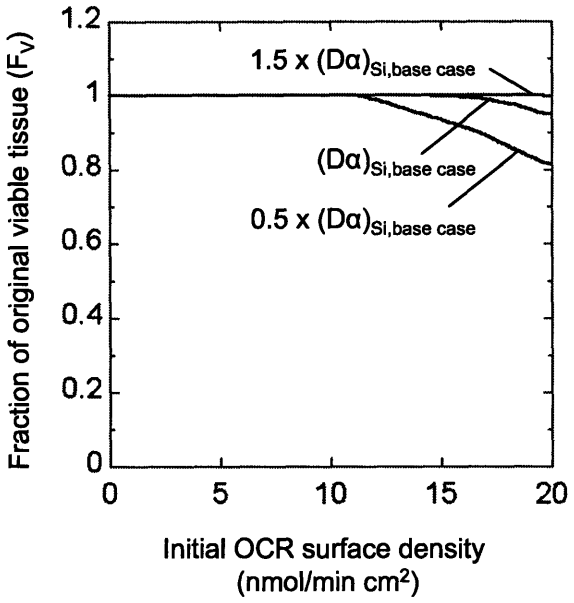

Figure 5.6. Theoretical predictions for the fraction of viable tissue after culture as a function of initial OCR surface density for different values of $(D\alpha)_{Si}$. Predictions for culture on a 500-μm silicone rubber membrane in 22 mm medium.

5.4.1 OCR density distribution

To explore the impact of a non-uniform OCR surface density we assume that the OCR surface density distribution follows a normal distribution, which can be written as

$$P(x) = \frac{1}{\sigma\sqrt{2\pi}} \exp\left(-\frac{(x-\mu)^2}{2\sigma^2}\right) \qquad \textbf{5.1}$$

where P(x) is the probability that the tissue is at the local OCR density x, μ is the average OCR density, and σ is the standard deviation of the OCR density. By applying this normal distribution function we assume that each islet at a given density is independent and identically distributed (i.e. the Central Limit Theorem holds). Though this assumption is not completely valid, the fact that we ignore the interaction between islets at different OCR densities is likely minor compared to the error in the assumed density distribution. As such, the adjustments to the prediction should not be considered an accurate representation for islets in culture, but rather an indication of how F_V would shift.

In order to apply the normal density distribution to the prediction the expected value of $F_{V,adj}$ is calculated using

$$F_{V,adj}(\mu) = \frac{\sum_{x} P(x) \cdot \Delta x \cdot F_V(x)}{\sum_{x} P(x) \cdot \Delta x} \qquad \textbf{5.2}$$

where Δx is the width between our discrete bins (0.1 nmol/min cm^2), $F_V(x)$ is the prediction of the model using a uniform OCR density, and $F_{V,adj}(\mu)$ is the new prediction for density μ that has been adjusted to account for the normal distribution. The predicted F_V as a function of uniform initial OCR surface density was broken into three functions: a linear function with a slope of zero at $F_V = 1$ for densities 0-0.6 mol/min cm^2, a quadratic function from 0.6-5.1 nmol/min cm^2, and a second quadratic function from 5.1-25 nmol/min cm^2 (Figure 5.8, a maximum OCR density of 25 nmol/min cm^2 was assumed for monolayer culture). The piecewise function for F_V and the normal distribution function in Equation 5.1 were used in Equation 5.2 to calculate $F_{V,adj}$.

Adjusting for a normal OCR density distribution did not have a large effect on F_V (Figure 5.9) for culture on polystyrene in 3 mm medium. When adjusting for the normal distribution F_V decreases at low densities and increases at high densities as the distribution widens (Figure 5.9B and A respectively). Though this adjustment makes our simulations more realistic, it does not have a large impact on the prediction for any of the culture techniques studied.

5.4.2 Islet size

Tissue size varies widely from small cell clusters to large islets more than 250 μm in diameter (Figure 5.7). If we increase uniform islet size in the O_2 transport model (> 150-μm diameter), F_V decreases substantially indicating that the size of the tissue clumps has a large impact on the O_2 limitations imposed by static culture (Figure 5.10A). For culture on silicone rubber a similar trend is observed (Figure 5.10B) though the decrease in F_V is not substantial enough to bring the predictions close to the empirical results.

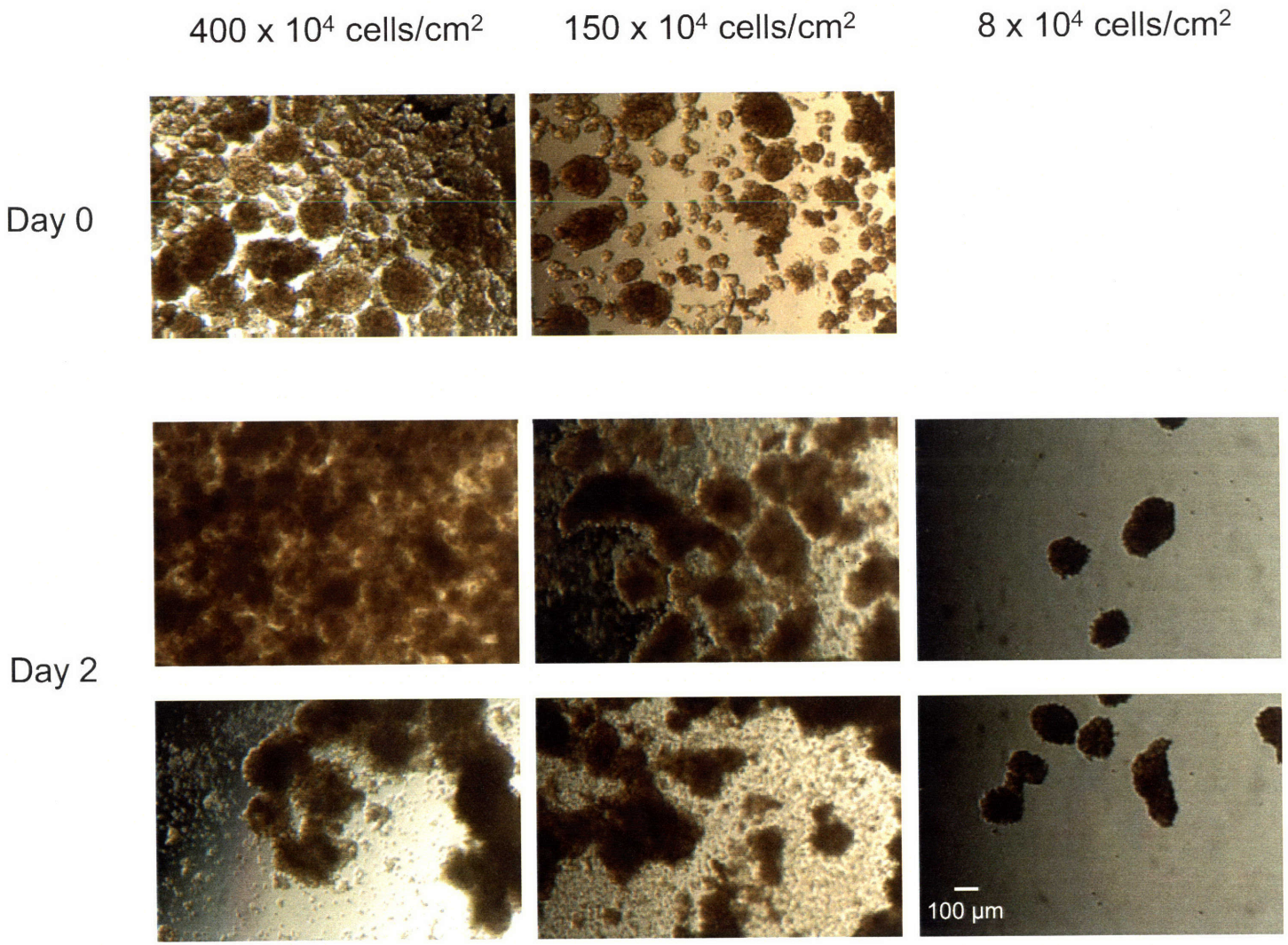

Figure 5.7. Light microscopy pictures of human islets.
Pictures taken on day 0 and after 39 hr culture at densities of 400, 150, and 8 x 10^4 cells/cm^2 on untreated polystyrene at 37°C. The scale bar represents 100 µm. Magnification is the same in all panels.

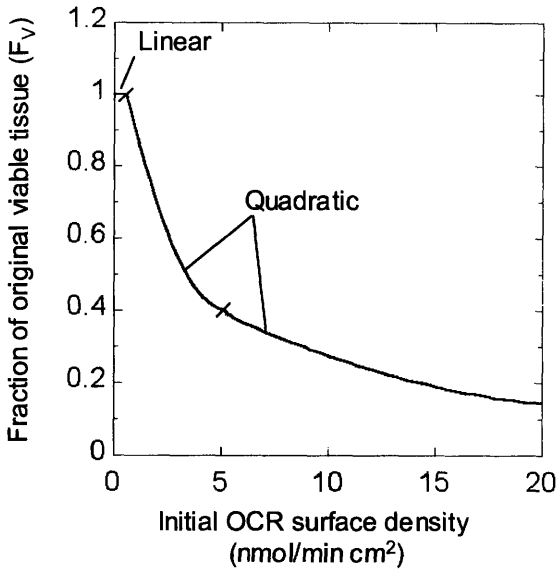

Figure 5.8. Piecewise function for theoretical predictions of F_V as a function of initial OCR surface density for a uniform density distribution (base case).
The three functions include a linear function with a slope of zero at $F_V = 1$ for densities 0-0.6 mol/min cm^2, a quadratic function from 0.6-5.1 nmol/min cm^2, and a second quadratic function from 5.1-25 nmol/min cm^2.

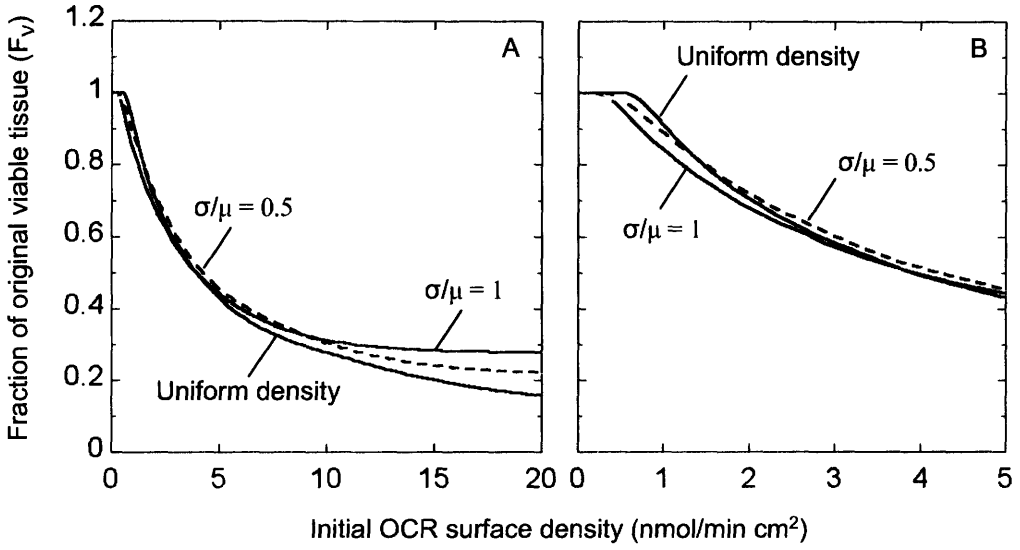

Figure 5.9. Theoretical predictions using a uniform or a normally distributed OCR density. Data for $\sigma/\mu = 0.5$ and 1 for culture on polystyrene in 3 mm medium for initial OCR surface densities (A) 0 to 20 and (B) 0 to 5 nmol/min cm^2.

Human islet size distributions vary widely between isolations where some preparations have an average islet diameter significantly > 150 μm and some significantly < 150 μm (A. Omer, personal communication). As a result no single distribution can reflect the variation in islet size for all islet preparations. To investigate the effects of size distribution on F_V we will use the normal distribution function in Equation 5.1 where x is the local islet radius, P(x) is the probability that the tissue has the radius x, μ is the average islet radius, and σ is the standard deviation of the islet size distribution. Again, built within the assumption of a normal distribution is that each islet size is independent and identically distributed such that the Central Limit Theorem holds. In other words, an islet of a particular size does not depend on the size of its closest neighbors. For example, the prediction for an islet with a 75-μm radius at a particular OCR density should not depend on whether the islets around it have a radius of 25 or 125 μm. As a result F_V for mixtures with different islet sizes should equal the volume weighted average of F_V obtained using uniform sphere sizes if this independence holds.

To investigate whether islets of different size are independent of each other a model using spheres of two different sizes was developed. The equations used within the model were the same as previous (Chapter 3 and 4), but the model geometry changed. The geometry included spherical tissue clusters of two different sizes set in a square array (Figure 5.11A). F_V for a mixture of islets with radii of 75 and 125-μm and for each individual islet size in the mixture are shown in Figure 5.11B. The overall F_V obtained using the model with two different islet sizes was nearly identical to the volume weighted average F_V obtained using predictions with spheres of uniform size (Figure 5.11C) indicating very little interaction between islets at the same OCR density. Since the predictions for a given islet size at a given OCR density are approximately independent of the surrounding tissue an adjusted F_V can be calculated using a normal islet size distribution.

For simplicity mixtures of spheres with radii of 25, 50, 75, 100, 125, and 150-μm will be considered. The expected value of $F_{V,adj}$ is calculated using Equation 5.3.

$$F_{V,adj}(\mu) = \frac{\sum_x P(x) \cdot \Delta x \cdot w_x \cdot F_V(x)}{\sum_x P(x) \cdot \Delta x \cdot w_x} \qquad \textbf{5.3}$$

where Δx is the width between the discrete bins (25 μm), $F_V(x)$ is the prediction using uniform sphere size x, w_x is equal to the volume of a sphere with radius x, and $F_{V,adj}(\mu)$ is the new prediction for the average islet radius μ adjusted to account for the size distribution. F_V as a function of OCR surface density was broken into two to four separate linear or quadratic functions for each uniform islet size. These piecewise functions and the normal size distribution function were used in Equation 5.3 to calculate $F_{V,adj}$.

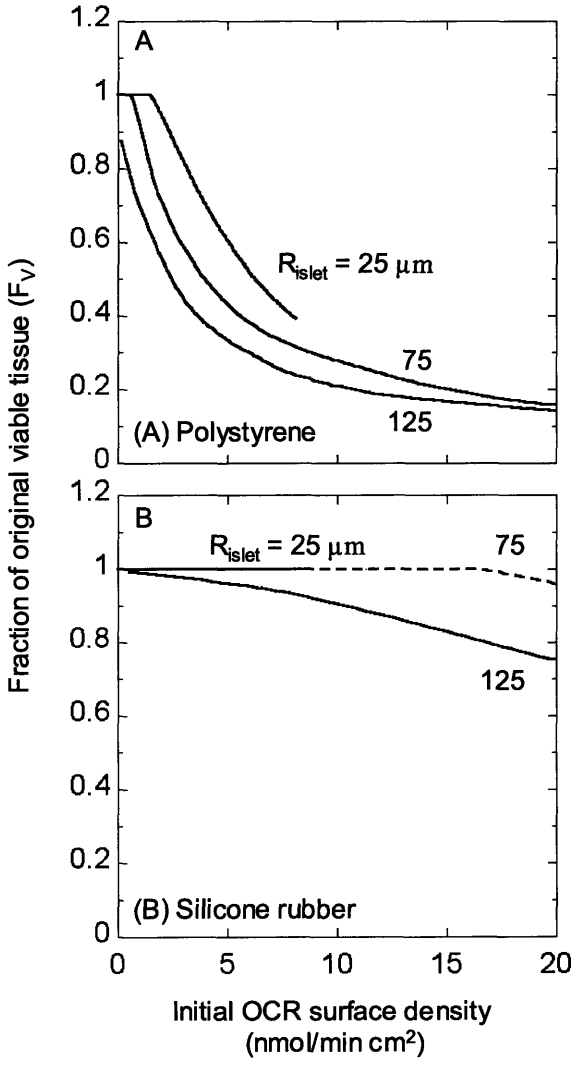

Figure 5.10. Theoretical predictions for islets with uniform radii of 25, 75, and 125 μm on (A) a polystyrene dish in 3 mm medium or (B) a 500-μm silicone rubber membrane in 22 mm medium.

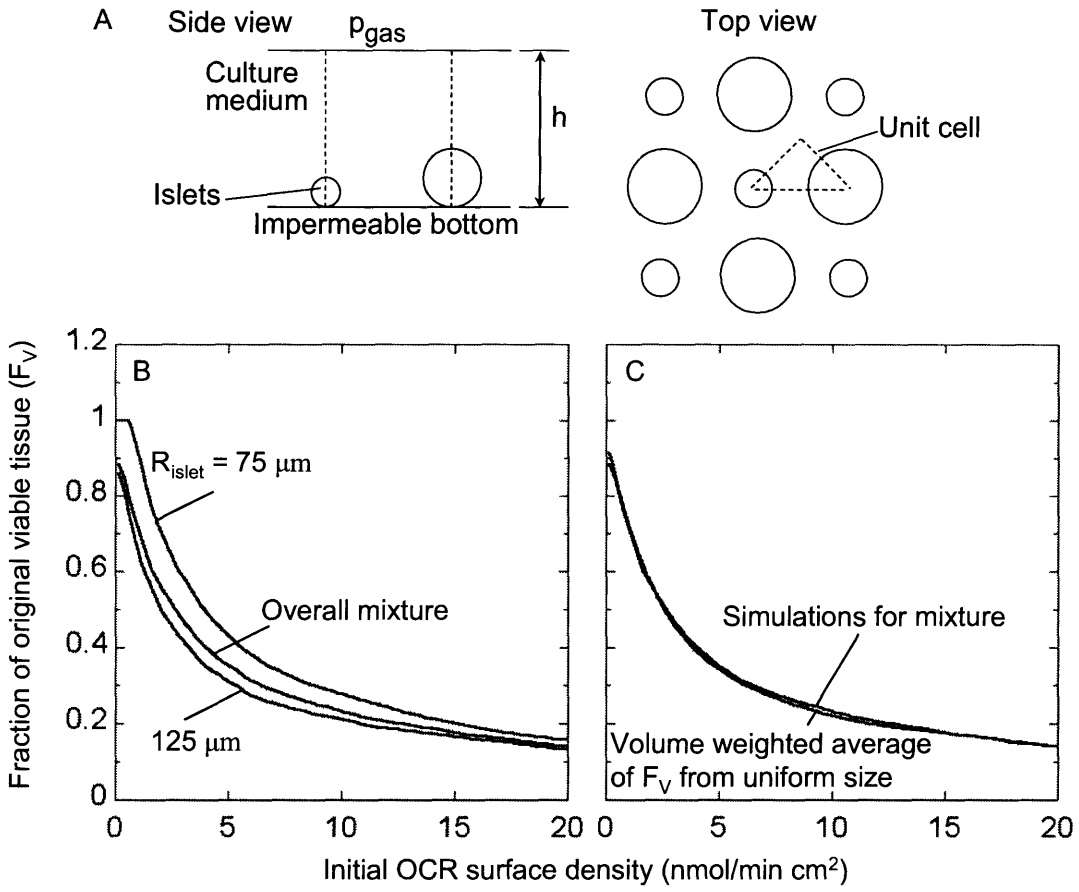

Figure 5.11. Model geometry and predictions assuming a mixture of islet sizes. (A) Geometry used to model islets of two different sizes. The dashed lines indicate the portion actually modeled. (B) Theoretical predictions for a 50:50 mixture of spheres with radii of 75 and 125 μm. F_V from the simulation of the mixture is given for each islet size within the mixture and the overall combined tissue. (C) Comparison between overall model predictions for a 50:50 mixture of spheres with radii of 75 and 125 μm to that of the volume weighted average F_V from uniform islet size predictions.

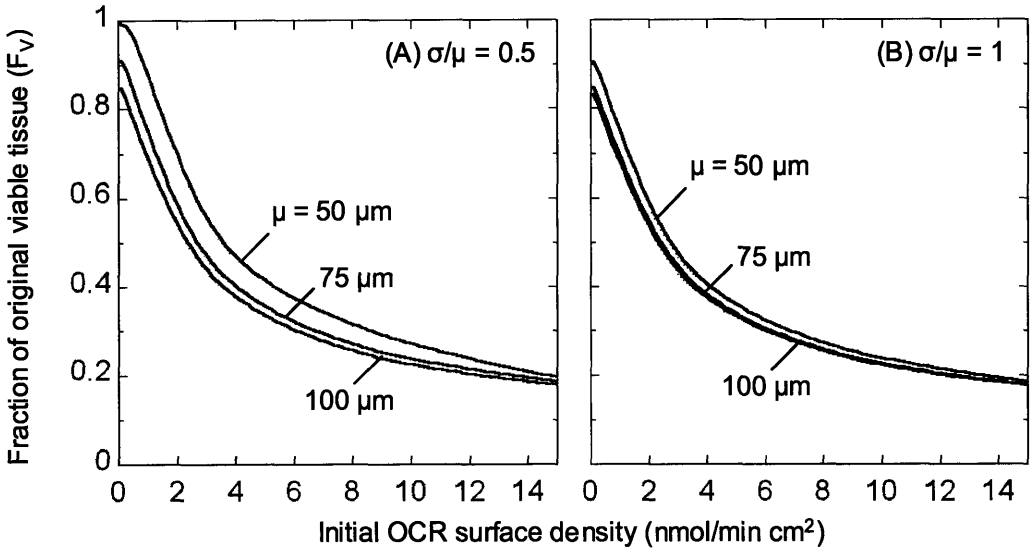

Figure 5.12. Theoretical predictions for F_V assuming a normal islet size distribution. Prediction for culture in 3 mm medium on a polystyrene dish. The average islet size μ varied from 50 – 100 μm. Results are shown for both σ/μ equal to (A) 0.5 and (B) 1.

Theoretical predictions taking into account a normal islet size distribution with μ equal to 50, 75, and 100 μm and σ/μ equal to 0.5 and 1 for culture in 3 mm medium on polystyrene are given in Figure 5.12. As μ and σ/μ increase, F_V decreases indicating that not only the average size, but also distribution width can cause departure from predictions using uniform islet size. Further, a distribution with μ = 75 μm results in lower F_V than predictions with a uniform islet radius of 75 μm indicating that just by accounting for a size distribution predictions shift downward (Figure 5.10A and Figure 5.12).

5.4.3 Tissue slab

Tissue clumped during high density culture resulting in slab-like regions (Figure 5.7). A model using the same theoretical equations discussed previously (Chapter 3 and 4) was developed to model one-dimensional O_2 transport using the geometry illustrated in Figure 5.13A. Slab formation causes severe limitations resulting in large drops in F_V during culture on polystyrene and for large slab thicknesses on silicone rubber membranes (Figure 5.13B). These predictions act as a lower bound on F_V indicating a worst-case scenario. All data for culture on polystyrene (3 and 22 mm medium) are above this worst-case prediction. However, a 150-μm

thick slab of tissue on a silicone rubber membrane should result in only a 0.03 decrease in F_V, which is not below empirical data (Chapter 4).

5.4.4 Islet stacking

A theoretical model using equations described previously (Chapter 3 and 4) was developed using the geometry indicated in Figure 5.14A to determine the extent to which islet stacking affects F_V. Stacking causes a large decrease in F_V for culture on a 500-μm silicone rubber membrane each time a new layer is added (Figure 5.14B). The impact for culture on polystyrene is less significant because the majority of the tissue is already dead with monolayer coverage. In a similar manner as that for slab formation, these predictions can be used as a lower bound on F_V. For culture on polystyrene (3 and 22 mm medium) islet stacking of just 2 layers is below all empirical data (Chapter 3 and 4) (data not shown for 22 mm medium depth). Culture on a 500-μm silicone rubber membrane in 22 mm medium results in F_V of roughly 0.50 for a bilayer of islets (Figure 5.14B) above which nearly all of the experimental data falls (Chapter 4). Further, only a fraction of the tissue will be stacked with the remainder in some monolayer distribution resulting in some combination of the two predictions that decreases with increasing density, which is consistent with the empirical trends observed for culture on polystyrene and silicone rubber (Chapter 3 and 4).

5.4.5 Convection

Convection complicates the theoretical model significantly since there is much uncertainty in the exact form and extent of the convective transport. As such we did not explore convection using a theoretical model, but instead tried to bound the effect experimentally. We investigated a oxygen biosensor system (OBS) developed for the measurement of OCR of tissue in static culture [146] (see Appendix 10.3 for details). The OBS utilizes an O_2 sensitive fluorophor embedded in silicone rubber upon which cells or tissue is placed. As the tissue consumes O_2, the O_2 partial pressure at the bottom of the plate decreases and is detected by the sensor. While investigating this technique we showed that gelled culture medium containing 0.9% agarose resulted in an average 15% increase in the apparent OCR/cell determined by the system as compared to the same with liquid medium (Appendix 10.3). This increase in apparent OCR/cell occurred because convection was removed from the system with gelled medium,

thereby decreasing the O_2 flux to the tissue approximately 15% (1-1/1.15) or < 0.1 nmol/min cm^2 and decreasing the O_2 partial pressure at the bottom of the dish (lower O_2 partial pressure at bottom means higher apparent OCR/cell).

Equating this flux (0.1 nmol/min cm^2) to the consumption rate of tissue indicates that an additional tissue volume equivalent to 18 IE/cm^2 could be provided with sufficient O_2 (assumes zero-order kinetics, 150-μm diameter islets, ignores transport limitations). At low densities this additional viable tissue could have a significant effect on F_V whereas at high densities it is not likely to have a large effect. For example, at a density of 200 IE/cm^2 where F_V from the base case is roughly 0.9 (20 IE/cm^2 not viable, 180 IE/cm^2 viable), the additional flux shifts F_V to about 0.99 (20-18 = 2 IE/cm^2 not viable, 180+18 = 198 viable).

However, at a density of 2000 IE/cm^2, where F_V is roughly 0.25 (1500 IE/cm^2 not viable, 500 IE/cm^2 viable) in the base case, the additional flux would shift F_V less than 0.01 (1500-18 = 1488 IE/cm^2 not viable, 500+18 = 518 viable, F_V = 0.259). In addition, the convective effect observed in the OBS study is likely a gross overestimation of convection present during culture because the convection imposed by transferring dishes from the incubator to a plate reader and within the plate reader is likely dominant compared to vibrations from the incubator (Appendix 10.3). Still, the data allow us to limit the extent to which convection could increase F_V.

5.5 Discussion

In this study we explored the sensitivity of theoretical predictions based on a simplified O_2 transport model discussed in Chapters 3 and 4 to changes in the model parameters and assumptions for culture at low and high medium depths on polystyrene and at large medium depths on silicone rubber. This sensitivity analysis provides insight into why theoretical predictions only have qualitative agreement, and not quantitative agreement, with empirical data. Additionally, a better understanding of how each parameter and assumption affect the theoretical prediction could lead to improved methods for islet culture.

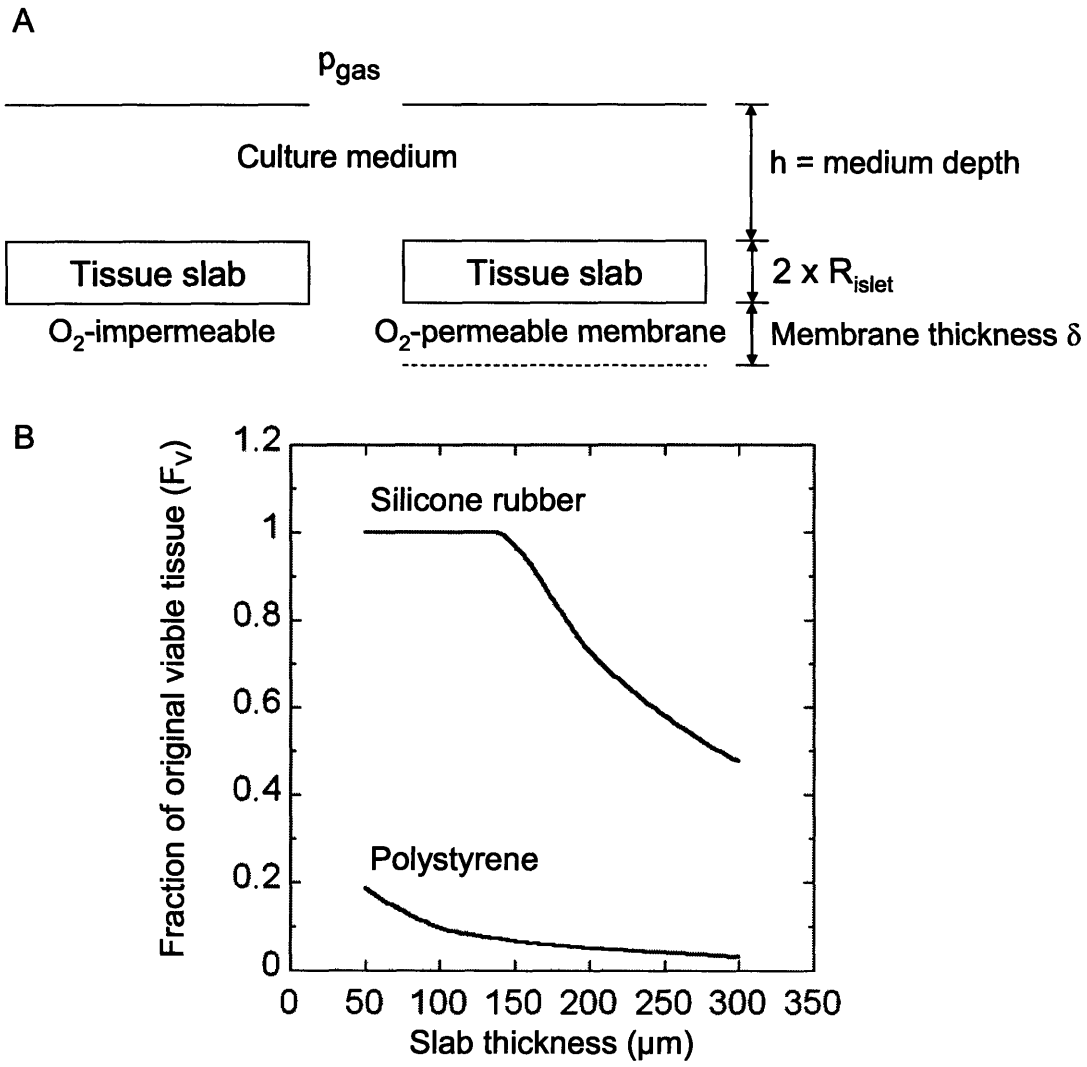

Figure 5.13. Model geometry and predictions assuming a slab of tissue.
(A) Geometry used to simulate O_2 transport in a slab of tissue with varying thickness.
(B) Theoretical prediction for F_V as a function of tissue slab thickness for culture on polystyrene in 3 mm medium and for culture on a 500-μm silicone rubber membrane in 22 mm medium.

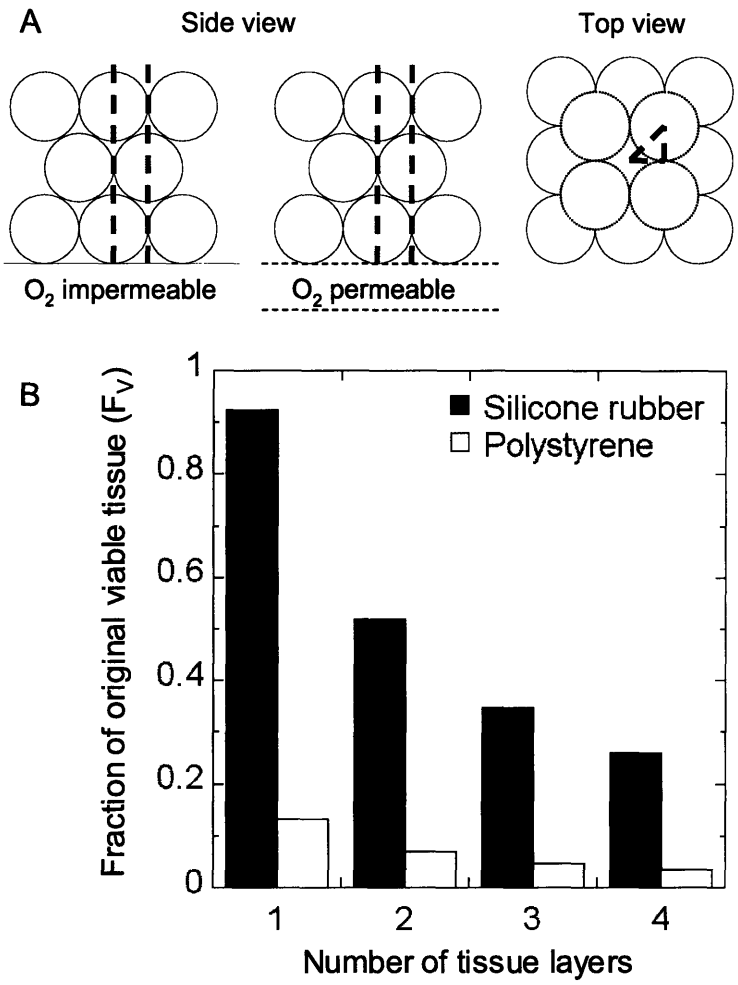

Figure 5.14. Model geometry and predictions assuming stacked islets.
(A) Geometry used to simulate O_2 transport in stacked spheres of tissue. (B) Theoretical prediction for F_V as a function of the number of sphere layers for culture on polystyrene in 3 mm medium and for culture on a 500-μm silicone rubber membrane in 22 mm medium.

Theoretical predictions for the simplified O_2 transport model overestimated the empirical F_V for culture on polystyrene in 3 mm medium (Chapter 3). Since decreases in F_V during 3 mm culture on polystyrene have been shown to be at least partially due to O_2 limitations (Chapter 4), it is reasonable to conclude that inaccuracies in the O_2 transport model parameters and/or assumptions could account for the discrepancies observed between theoretical predictions and experimental measurements. The theoretical predictions shift closer to empirical data if K_m or $(D\alpha)_m$ are lower than in the base case model, however this is unlikely based on values reported in literature. Inaccuracies in $(D\alpha)_i$ and adjusting for a normal OCR density distribution (rather than a uniform density) do not have any significant effect on the prediction and convection

would only cause a further departure from the empirical data. Theoretical F_V shifts toward empirical data if adjusting the model for larger islet size, slab formation, or tissue stacking, which have been observed during culture, or if p_{crit} is > 0.1 mmHg, which is possible based on the discussion of Avgoustiniatos [16], indicating four inaccuracies that could explain the discrepancies between theory and experiments.

For culture on polystyrene in 22 mm medium theoretical predictions based on the simplified model underestimated empirical F_V (Chapter 4). As a result an upward shift in F_V is toward empirical data, which is the opposite of 3 mm culture on polystyrene. Thus an underestimation of K_m or $(D\alpha)_m$ by the base case, which is likely when considering the values available in literature, or an overestimation of p_{crit}, which is not likely based on literature, results in a shift toward empirical data. As with culture on polystyrene in 3 mm medium inaccuracies in $(D\alpha)_i$ and adjusting for an OCR density distribution have little effect on the prediction. Though large islets, slab formation, and tissue stacking have been observed during culture, accounting for them would shift the prediction downward away from empirical data whereas accounting for convection now shifts the predictions closer to the experimental data. Thus inaccuracies in K_m and $(D\alpha)_m$ or ignoring convection could explain why theoretical predictions using the simplified model underestimated experimental F_V for culture on polystyrene in 22 mm medium.

Since O_2 has been shown to be limiting in 3 mm medium on polystyrene (Chapter 4), it is also very likely limiting in 22 mm medium. However, any adjustments made to the theoretical model that would bring the prediction for culture on polystyrene in 22 mm medium closer to empirical data would result in larger discrepancies during culture in 3 mm medium and vice versa. This suggests that inaccuracies in the O_2 transport model are not the only cause of the discrepancies between theory and experiments. Islet β cells normally have a low level of lactate dehydrogenase (LDH) expression [119], but up-regulate LDH when exposed to a hypoxic environment for 24 hr (G. Weir, personal communication), which allows them to produce energy by glycolysis in the absence of O_2. If tissue in the islet preparation can up-regulate LDH fast enough, a larger fraction would be able to survive than predicted by the theoretical model. Thus the discrepancies observed at large medium depths on polystyrene are likely to result from this change in cellular machinery and not inaccuracies in the basic O_2 transport model.

Most inaccuracies in the O_2 transport model did not affect predictions for culture on a 500-μm silicone rubber membrane (h = 22 mm) to the same extent as culture on polystyrene. Inaccuracies in $(D\alpha)_m$ become irrelevant because the majority of O_2 is transported to the tissue through the membrane. K_m and p_{crit} are of less importance since the pO_2 within the tissue is significantly higher than tissue on polystyrene thereby diminishing the effect of Michaelis-Menten kinetics. As with culture on polystyrene, variations in $(D\alpha)_i$ and accounting for a normal density distribution have little impact on the prediction while accounting for convection would only cause farther departure from empirical data. In addition, though islet size variation and slab formation have been observed, accounting for these phenomena individually does not result in a large enough shift in F_V to explain the discrepancies between experiments and theory.

On the other hand, if $(D\alpha)_{Si}$ is overestimated in the base case, which is suggested by the range in values obtained from literature, then the predicted F_V shifts toward experimental data. Additionally, tissue stacking in a bilayer can drop F_V to 0.50, above which nearly all of the experimental data for silicone rubber falls (Chapter 4). Thus inaccuracies in $(D\alpha)_{Si}$ and the presence of tissue stacking are both reasonable explanations for the discrepancies observed between theoretical and experimental data. However, despite this, they are unlikely the cause of the discrepancies. As mentioned previously, the empirical decrease in F_V observed following culture on a 500-μm silicone rubber membrane is unlikely to result due to O_2 limitations since empirical measurements from cultures on membranes of different thickness were not significantly different (Chapter 4). Thus O_2 is not limiting and inaccuracies in the O_2 transport model cannot explain why there is a departure from theory.

In summary this chapter has illustrated that inaccuracy in model assumptions and/or parameters does have a significant impact on the theoretical predictions of our simplified O_2 transport model, which could explain some of the discrepancies observed between theory and experiments for culture on polystyrene at either low medium depths or high medium depths, but not both. Though the inaccuracies also provide valuable insight for culture on silicone rubber, they are not likely the cause of the departure from experimental F_V.

5.6 Nomenclature

D	Diffusivity of O_2
F_V	The fraction of original viable tissue after culture
$F_{V,adj}$	F_V adjust to account for non-idealities
h	Medium depth
IE	Islet equivalent
K_m	Michaelis constant, the pO_2 at which the reaction rate is $V_{max}/2$
LDH	Lactate dehydrogenase
O_2	Oxygen
OCR	O_2 consumption rate
p	O_2 partial pressure
p_{crit}	The pO_2 below which a cell dies and no longer consumes O_2
p_{gas}	Ambient partial pressure of O_2
P(x)	Probability of getting result x
R_{islet}	Radius of islet
V_{max}	Maximum reaction velocity
w_x	Volume of a sphere with radius x
x	Variable of interest
α	Solubility of O_2 in medium
δ	Thickness of silicone rubber membrane
σ	Standard deviation the values of x
μ	Average value for all x
Δx	Width between discrete bins

Subscripts for D, α, p, C

i	Islet tissue
m	Medium
Si	Silicone rubber

6 Glucose transport during islet culture

6.1 Introduction

The fraction of original viable tissue collected from static culture (F_V) decreases as tissue surface density increases on polystyrene and on silicone rubber membranes (Chapter 3 and 4). For culture on polystyrene this dependence was due at least in part to oxygen (O_2) limitations (Chapter 3 and 4). For culture on a silicone rubber membrane, theoretical predictions based on O_2 transport and empirical data using membranes of different thickness determined O_2 was not limiting during culture (Chapter 4). The decrease in F_V on silicone rubber membranes may result from nutrient transport limitations other than O_2. Nutrient depletion may have occurred since medium was not changed during 34-60 hr culture. Culture in a low medium depth, such with culture on polystyrene in elevated O_2, will deplete the bulk nutrient supply faster than culture with a large medium depth. However, even when a large medium depth is used, diffusional limitations may prevent nutrients from reaching the tissue at a sufficient rate thereby causing a nutrient shortage even though the bulk concentration is not depleted.

β cell survival during culture has been shown to be dependent on the glucose concentration of the culture medium [147-150]. Specifically, rat β-cell survival increases with glucose concentration in a dose-dependent manner up to 10 mM glucose through a reduction in β-cell apoptosis [147; 149]. Further, culture in zero glucose results in nearly a 50% reduction in rat islet ATP concentration within just two hours [151]. Prolonged exposure to zero glucose is thus unlikely to allow sufficient production of ATP to maintain cell function or viability.

A transient model that predicts glucose concentration profiles during culture was developed to investigate whether glucose transport limitations could occur during high density culture. In this study we explore the theoretical glucose transport model and with preliminary experimental data discuss the likelihood of whether glucose transport could cause decreases in islet viability during high density culture.

6.2 *Methods*

Islet isolation and culture

Standard collagenase/protease digestion methods were used for human [7; 15] isolations. Preparations of human islets were provided fresh (4-6 hr after isolation was complete) by the Islet Core at the Joslin Diabetes Center (JDC, Boston, MA). Human islets were also received after culture (1-2 days) from JDC or overnight shipment (sometimes after up to 1 day culture) from other centers contained in culture flasks (T-25 and T-75) or centrifuge tubes in Styrofoam boxes. When first observed, some preparations were in suspension, some in a pellet. Upon receipt, a portion of the preparation was analyzed and the remainder placed into untreated polystyrene culture flasks at 37°C in a humidified environment (5% CO_2), oxygen partial pressure (pO_2) of 142 mmHg, for 34-60 hr during which no medium change occurred. Some cultures were terminated at 18-24 hr for analysis. To test the effect of temperature, some islets were cultured at 24°C, then warmed for 1 hr at 37°C before OCR measurements.

Islets were cultured in supplemented RPMI (11.1 mM D-glucose, 100 U/ml penicillin, 100 μg/ml streptomycin, 2 mM L-glutamine, 1 mM sodium pyruvate (all from Mediatech Inc., Herdon, VA), and 50 μM β-mercaptoethanol (Sigma Aldrich, St. Louis, MO) with 10% fetal bovine serum (FBS, Mediatech Inc.), at low densities (< $8x10^4$ cells/cm^2 or about 50 islet equivalents (IE)/cm^2, where IE is the volume of a sphere with a diameter of 150 μm) in 1.3 mm of medium in untreated polystyrene culture flasks. For some experiments parallel cultures in 0 mM glucose RPMI were conducted. After culture the free, non-adherent tissue (which is the only tissue used in current practice) was collected. In selected experiments, adherent human tissue was incubated for 5 min at 37°C in 0.05% trypsin EDTA (Mediatech Inc.), dislodged with fresh medium, and collected.

Islet enumeration by nuclei counting

Nuclei were prepared by adding equal 100-μl volumes of sample containing 160 or more IE and of lysis solution (0.1 M citric acid (Sigma) and 1% (v/v) Triton X-100 (Sigma)) to a 1.5 ml microtube [55]. The mixture was incubated at room temperature for 5 min with vortex mixing every 1.5 min, and nuclei were liberated by shearing through a needle. Isolated nuclei were diluted with Dulbecco's phosphate buffered saline (D-PBS, Invitrogen, Carlsbad, CA) to a concentration no higher than 5 x 10^5 nuclei/ml, stained with 7-aminoactinomycin D (7-AAD,

Molecular Probes, Eugene, OR), and analyzed using a flow cytometer (Guava Personal Cell Analysis (PCA) system, Guava Technologies, Hayward, CA) to determine the total number of cells with intact nuclei in the sample.

Oxygen consumption rate (OCR)

OCR was measured as previously described [39]. Briefly, suspensions containing about 2500 IE/ml in DMEM containing 4.5 g/l glucose and 0.6 g/l L-glutamine supplemented with 100 U/ml penicillin, 100 μg/ml streptomycin, 10 mM HEPES, and no added serum were sealed in a 200-μl stirred titanium chamber (Micro Oxygen Uptake System, FO/SYSZ- P250, Instech Laboratories, Plymouth Meeting, PA) maintained at 37°C. The time dependent pO_2 within the chamber was recorded with a fluorescence-based oxygen sensor (Ocean Optics, Dunedin, FL), and data at high pO_2 were fit to a straight line. The maximal OCR was evaluated from $OCR=V_{ch}\alpha(\Delta pO_2/\Delta t)$, where V_{ch} is the chamber volume and α = 1.27 nmol/mm·Hg·ml is the Bunsen solubility coefficient for oxygen in medium [16]. OCR measurements were normalized by the measured number of cells (nuclei counting) or DNA content of the sample examined.

Membrane Integrity

Statistics

Measurements were made with three or more replicates and reported as mean ± SD. Statistical significance was determined using a Student t-test for unpaired data for comparing population means, and for paired data when appropriate.

Glucose quantification

Samples were taken of the original culture medium and spent medium following culture and analyzed for glucose content using the Glucose Assay Kit (GAGO20, Sigma Aldrich, St. Louis, MO). Triplicate samples diluted to concentrations between 20-100 μg/ml were placed in a 96-well plate along with samples for a six-point standard curve ranging in concentration from 0-100 μg/ml. The Glucose Assay Reagent was added to each well. After 25 min at 37°C 12N sulfuric acid was added to each well. The absorbance was measured at 544 nm on a plate reader.

6.3 *Theoretical glucose transport model*

The species conservation equation for glucose in the absence of convection [16; 97] is given by

$$\frac{\partial C}{\partial t} = D\nabla^2 C + R \qquad \textbf{6.1}$$

where C is the concentration of glucose, D is the diffusivity of glucose, and R is the production rate of glucose.

Glucose consumption within the islet is assumed to follow Michaelis-Menten kinetics [16] for which the reaction rate is expressed as

$$R = -\frac{V_{max} C}{K_m + C} \qquad \textbf{6.2}$$

where V_{max} is the maximum reaction velocity, and the Michaelis constant K_m is the C at which the reaction rate is $V_{max}/2$. The species conservation equation in medium (m) and in the islet tissue (i) become, respectively,

$$\frac{\partial C}{\partial t} = D_m \nabla^2 C \qquad \textbf{6.3}$$

$$\frac{\partial C}{\partial t} = D_i \nabla^2 C - \frac{V_{max} C}{K_m + C} \qquad \textbf{6.4}$$

To model islet culture in a dish, we assumed all the tissue (islet and non-islet) was in the form of spheres with uniform diameter (d) that were arranged in a square array with center-to-center distance w in a stagnant medium of height h (Figure 6.1). Because of symmetry within the system, Equation 6.1 was solved within a unit cell containing only an eighth of an islet (dashed lines in Figure 6.1). The initial and boundary conditions for this model [16] include uniform glucose concentration throughout system,

at t = 0, $$C_{t=0} = C_{initial} \qquad \textbf{6.5}$$

zero flux at the air-liquid interface and at the bottom of dish,

at z = 0 and z = h,
$$\frac{\partial C}{\partial z} = 0 \qquad \textbf{6.6}$$

continuity of glucose flux and concentration across the liquid-islet,

$$\mathbf{n} \bullet ((-D\nabla C)_i - (-D\nabla C)_m) = 0 \qquad \textbf{6.7}$$

$$C_m = C_i \qquad \textbf{6.8}$$

and symmetry across each side of the unit cell including both medium and islet domains

$$\mathbf{n} \bullet (-D\nabla C) = 0 \qquad \textbf{6.9}$$

The governing equations were non-dimensionalized using the non-dimensional variables

$$\eta = \frac{C}{C_{initial}} \qquad \textbf{6.10}$$

$$X = \frac{x}{R_{islet}}, \; Y = \frac{y}{R_{islet}}, \; Z = \frac{z}{R_{islet}} \qquad \textbf{6.11}$$

$$\tau = \frac{t(D)_i}{R_{islet}^2} \qquad \textbf{6.12}$$

Substituting these variables into 6.4 and 6.5 results in

$$\frac{\partial \eta}{\partial \tau} = \frac{D_m}{D_i} \nabla^2 \eta \qquad \textbf{6.13}$$

$$\frac{\partial \eta}{\partial \tau} = \nabla^2 \eta - \frac{V_{max} R_{islet}^2}{D_i C_{initial}} \left(\frac{\eta}{\frac{K_m}{C_{initial}} + \eta} \right) \qquad \textbf{6.14}$$

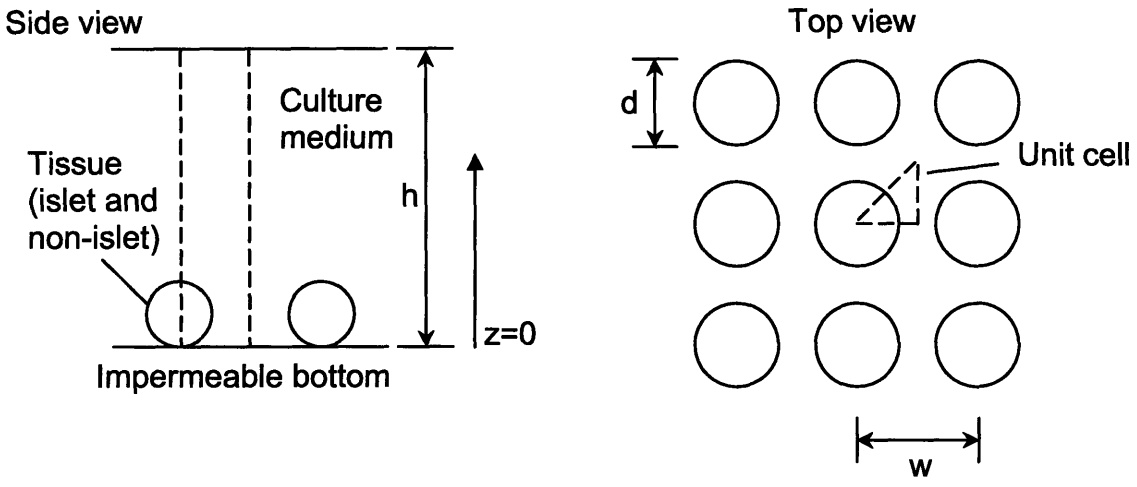

Figure 6.1. Islet geometry assumed for modeling glucose transport during islet culture on either a polystyrene dish or a silicone rubber membrane.

The initial condition becomes

at $\tau = 0$, $$\eta_{\tau=0} = 1 \qquad \textbf{6.15}$$

The boundary conditions become

at $Z = 0$ and $Z = H$ (where $H = h/R_{islet}$), $$\frac{\partial \eta}{\partial Z} = 0 \qquad \textbf{6.16}$$

$$\mathbf{n} \bullet \left(\left(-\frac{D_i}{D_m} \nabla \eta \right)_i - (-\nabla \eta)_m \right) = 0 \qquad \textbf{6.17}$$

$$\eta_m = \eta_i \qquad \textbf{6.18}$$

$$\mathbf{n} \bullet (-D \nabla C) = 0 \qquad \textbf{6.19}$$

There are three key non-dimensional groups that determine glucose concentration profiles during static islet culture. The first is the Damkohler number (Da), which is a measure of the rate of reaction relative to the rate of diffusion, defined in this case as

$$Da = \frac{V_{max} R_{islet}^2}{C_{initial} D_i} \qquad \textbf{6.20}$$

The other non-dimensional parameters are D_m/D_i, a relative diffusivity, and $K_m/C_{initial}$, the non-dimensional Michaelis constant. Though this model was described for glucose transport, it could be applied to any nutrient in the medium that is consumed by the islet tissue and not replenished continuously.

Table 6.1 contains the values for glucose consumption rates at high glucose concentrations (>15mM) available in literature. V_{max} was also determined experimentally as discussed below. Table 6.2 contains data for all other parameters used in the model. The estimate for glucose diffusivity in islet tissue is similar to that for diffusivities in human cell spheroids of 2.3-5.5 x 10^{-7} cm^2/s [152].

The model was solved with the finite element method using the commercially available software COMSOL Multiphysics (COMCOL Inc., Burlington, MA) in conjunction with Matlab (Mathworks, Natick, MA). We required the mesh to contain more than 2500 nodes and set an absolute tolerance for glucose concentration in the time dependent solver of 10^{-4} [99].

6.4 Glucose consumption rate measurement

Glucose consumption rate (GCR) was determined by measuring the glucose concentration of culture medium before and after culture, which was converted to a decrease in total glucose and normalized using nuclei counts after culture. The GCR was 4.07 ± 1.90 x 10^{-5} μg/cell hr (n = 12) or 5.55 ± 2.59 x 10^{-8} mol/s cm^3 (assuming 1560 cells/IE [13]) and the distribution is given in Figure 6.2. Adjusting the measured GCR for a K_m of 8 mM (and an average glucose concentration) resulting in an empirical V_{max} of about 1.0 x 10^{-7} mol/s cm^3.

Table 6.1. Literature values for glucose consumption by islet tissue.

Species	Literature value	Original units	Converted value	Adjusted for K_m	Converted units	Reference
Mouse islets	0.48 ± 0.14	pmol/min nL islet	8.0×10^{-9}	12×10^{-9}	mol/s cm^3	[153]
Mouse islets	2626 ± 159	pmol/h ug DNA	4.19×10^{-9}	5.9×10^{-9}	mol/s cm^3	[154]
Rat islets	2612 ± 146	pmol/h ug DNA	4.17×10^{-9}	5.8×10^{-9}	mol/s cm^3	[154]
Rat islets	102 ± 24	umol/h per g dry weight	4.9×10^{-9}	7.2×10^{-9}	mol/s cm^3	[155]
Rat islets	1.53 ± 0.13	pmol/ng DNA h	2.4×10^{-9}	3.5×10^{-9}	mol/s cm^3	[156]
Hamster islets	115.9 ± 2.93	pmol/islet 2 hr	9.1×10^{-9}	13×10^{-9}	mol/s cm^3	[157]

V_{max} values were determined at high glucose concentrations (>15 mM) to minimize the effect of K_m on the measured rate. Glucokinase acts as the limiting enzyme in glucose phosphorylation regulating the rate of glycolysis and it has a K_m between 5-11 mM (we will use 8 mM for the base case) [153; 158; 159]. The original units were converted to common units (mol/s cm^3) using 1560 cells/IE [13], 1.77×10^{-6} cm^3/IE (volume of a sphere with 150-μm diameter), 6.5 pg DNA/cell [68], and 33.2 ng DNA/μg dry weight [155]. The converted GCR were adjusted to account for the K_m of glucokinase using 6.2 and assuming an average glucose concentration.

Table 6.2. Values for the parameters used in islet culture simulations and the source from which they were obtained.

Parameter	Symbol	Value	Units	Reference
Diffusivity of glucose in medium	D_m	6.7×10^{-6}	cm^2/s	[118]
Diffusivity of glucose in tissue	D_i	3.8×10^{-7}	cm^2/s	[153]
Michaelis constant	K_m	5 - 11	MM	[153; 158; 159]
Maximal glucose consumption rate	V_{max}	$5.8\text{-}13 \times 10^{-9}$	$mol/s\ cm^3$	Table 6.1 [153-155]
Islet radius	R_{islet}	75	Um	Based on definition of IE
Medium depth	h	3 or 22	Mm	Based on medium volume and culture area
Initial concentration of glucose	$C_{initial}$	10	MM	Based on medium composition

The estimate for glucose diffusivity in islet tissue is similar to that for human cell spheroids of $2.3\text{-}5.5 \times 10^{-7}$ cm^2/s [152].

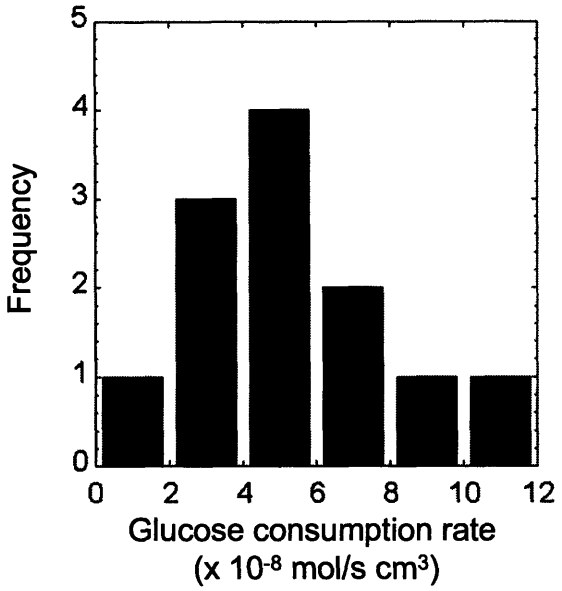

Figure 6.2. The distribution of GCR measurements from human islet preparations.

6.5 Predictions of theoretical models

Transient glucose profiles in the islet and medium change drastically during high density culture (4440 IE/cm^2, approximately a monolayer coverage, Figure 6.3). Bulk glucose is depleted from culture in 3 mm medium independent of which Da, and thus which GCR (for empirical GCR, Da =1.48 and for literature GCR, Da = 0.14), is accurate. If Da = 1.48, glucose is depleted to < 0.5 mM in < 10 hr (Figure 6.3C) whereas Da = 0.14 requires 45-50 hr to reduce the bulk concentration to a similar level (Figure 6.3A). Bulk glucose is not depleted during 60 hr culture in 22 mm medium independent of the Da (Figure 6.3B and D). However, despite a reasonable bulk glucose concentration (average > 3 mM, concentration at the top > 6 mM), glucose limitations (< 0.5 mM) may occur if diffusion to the tissue is limiting as indicated in Figure 6.3D.

The minimum concentration of glucose in the islet after 60 hr of culture varies with tissue surface density (Figure 6.4). Culture in 3 mm medium results in glucose concentrations below 1 mM in the islet at densities between 200 and 300 IE/cm^2 assuming Da = 1.48. At same Da culture in 22 mm medium keeps the glucose concentration in the islet above 1 mM until a density of about 1700 IE/cm^2 is reached. At lower Da, these limitations only occur at higher surface densities if at all.

Since glucose transport never reaches steady state the duration of culture also has an impact on the concentration within the tissue. The non-dimensional glucose concentration at the top of the islet, which also corresponds to the maximum glucose concentration in the islet, as a function of time and tissue surface density is illustrated in Figure 6.5. Culture in 3 mm medium assuming a low Da results in exposure to very low glucose concentrations only at high densities and long culture times (Figure 6.5A) and 22 mm medium provides sufficient glucose for the duration of culture even at high density (Figure 6.5B). For high Da glucose concentration decreases much faster resulting in exposure to low glucose at lower densities and earlier times (Figure 6.5C and D).

As indicated in Figure 6.3, Figure 6.4, and Figure 6.5, Da has a significant impact on the glucose concentration in the tissue during culture. Figure 6.6 explores how the maximum concentration in islets at 4440 IE/cm^2 changes as a function of time and Da. Da as low as 0.1 could cause exposure to glucose concentrations < 0.5 mM at long culture times in 3 mm medium while large Da result in exposure to < 0.5 mM in < 10 hr (Figure 6.6A). Culture in 22 mm medium increases glucose concentration, but exposure to < 1 mM results if Da > 1.0 (Figure 6.6B). As Da increases, the time to reach a low glucose concentration in the tissue decreases.

A second non-dimensional parameter that had an impact on the predicted glucose profiles during islet culture is D_m/D_i, which for the previous simulations was about 18. The glucose concentration in the islet is dependent on D_m/D_i for low Da (Figure 6.7A and B). However, 60 hr culture in 3 mm medium results in exposure to glucose concentrations < 1 mM regardless of the D_m/D_i. Culture in 22 mm medium prevents these low concentrations from occurring unless D_m/D_i is extremely low. The increased consumption at high Da results in exposure to low glucose concentrations regardless of D_m/D_i and medium depth (Figure 6.7C, and D) though the larger medium depth (22 mm) does delay the decrease in glucose.

The final dimensionless parameter is $K_m/C_{initial}$, which was 0.8 for earlier simulations. $K_m/C_{initial}$ has a significant effect on the maximum glucose concentration in the islet when low Da is assumed (Figure 6.8A and B). Concentrations of < 1 mM occur after 60 hr culture in 3 mm medium when $K_m/C_{initial}$ < 1.6 (Figure 6.8A), but does not reach 1 mM with $K_m/C_{initial}$ as low as 0.1 for culture in 22 mm medium (Figure 6.8B). High Da result in concentrations < 1 mM for all $K_m/C_{initial}$ considered after 60 hr independent of medium depth (Figure 6.8C and D).

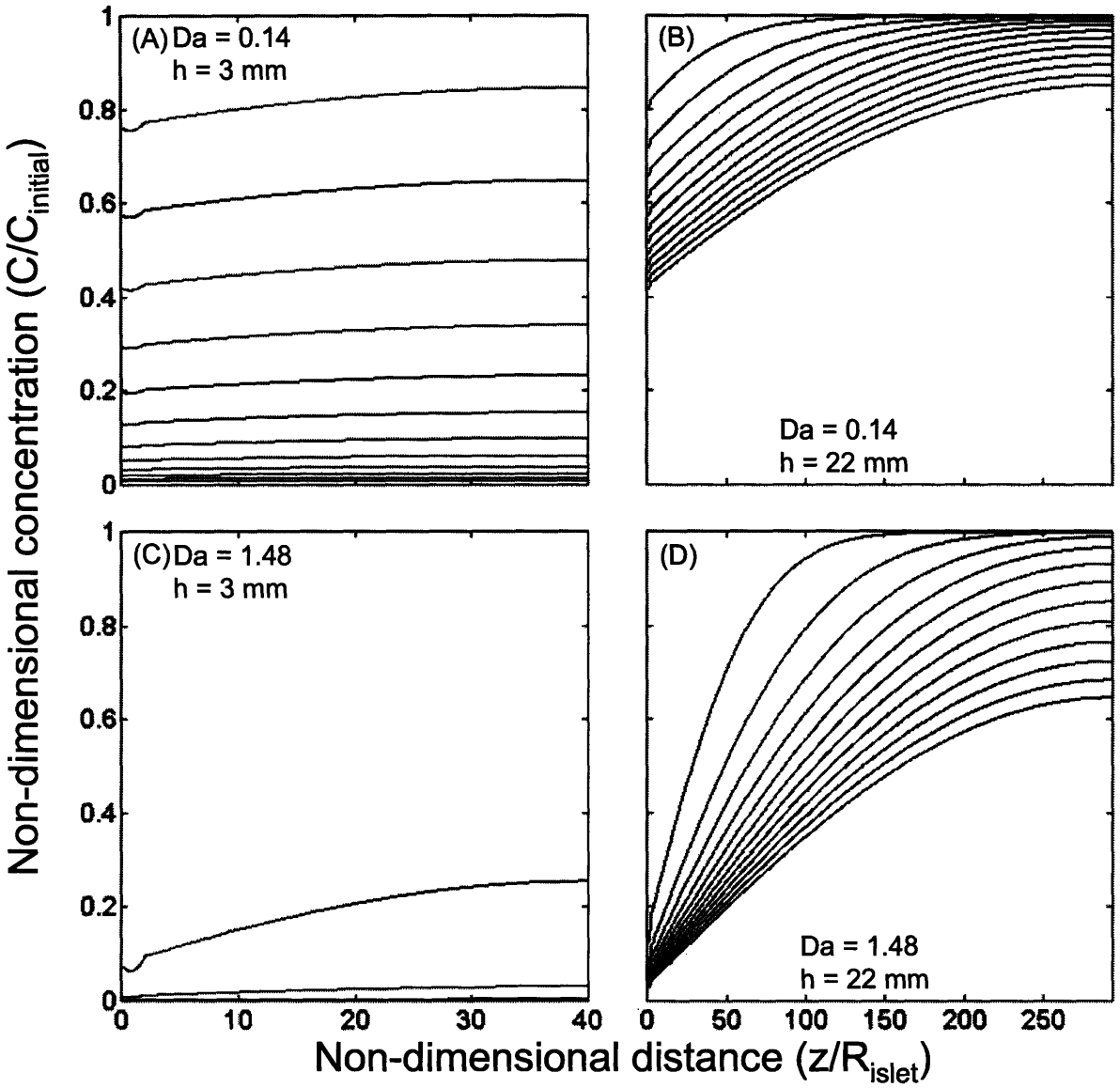

Figure 6.3. Transient glucose profiles as a function of position during islet culture. Predictions for islets cultured at 4440 IE/cm^2 in 3 (A and C) or 22 mm medium (B and D) assuming Da = 0.14 (A and B) or Da = 1.48 (C and D). The non-dimensional distance (z/R_{islet}) is from the bottom of the plate where $z/R_{islet} = 0$ through the center of the islet to the top of the islet where $z/R_{islet} = 2$ to the top of the culture medium where $z/R_{islet} = 40$ for 3 mm medium and $z/R_{islet} = 293$ for 22 mm medium. The time between each profile is 5 hours with the initial condition $C/C_{initial} = 1$ everywhere within the system.

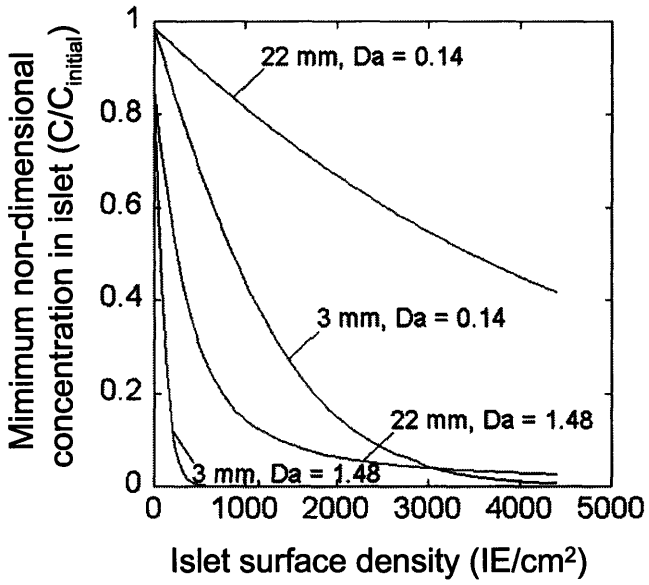

Figure 6.4. The minimum glucose concentration in the islet as a function of islet surface density for tissue cultured for 60 hr.

6.6 Experimental results

At low density, islet tissue cultured in medium containing 0 mM glucose had a significantly lower F_V than tissue cultured in 10 mM glucose (Figure 6.9). F_V of the tissue in 0 mM glucose was 0.56 ± 0.12 (n = 3 experiments), 0.40 less than that at 10 mM glucose (0.95 ± 0.05) indicating a substantial, but not a complete loss of viable tissue.

Supernatant samples analyzed for glucose content indicated that culture on polystyrene in 3 mm medium at densities > 150 x 10^4 cells/cm^2 (about 1000 IE/cm^2) resulted in glucose depletion from the bulk medium to concentrations < 0.6 mM whereas densities < 78 x 10^4 cells/cm^2 (about 500 IE/cm^2) contained > 3 mM glucose. In a single experiment tissue cultured on polystyrene in 3 mm medium at about 400 x 10^4 cells/cm^2 (2500 IE/cm^2) resulted in glucose depletion to bulk concentration < 0.5 mM within 9 h from culture initiation. Culture on silicone rubber in 22 mm medium also resulted in glucose depletion to a bulk concentration < 0.5 mM at densities > 240 x 10^4 cells/cm^2 (1500 IE/cm^2). Depletion may also occur at lower densities or earlier times on silicone rubber, but data is currently unavailable.

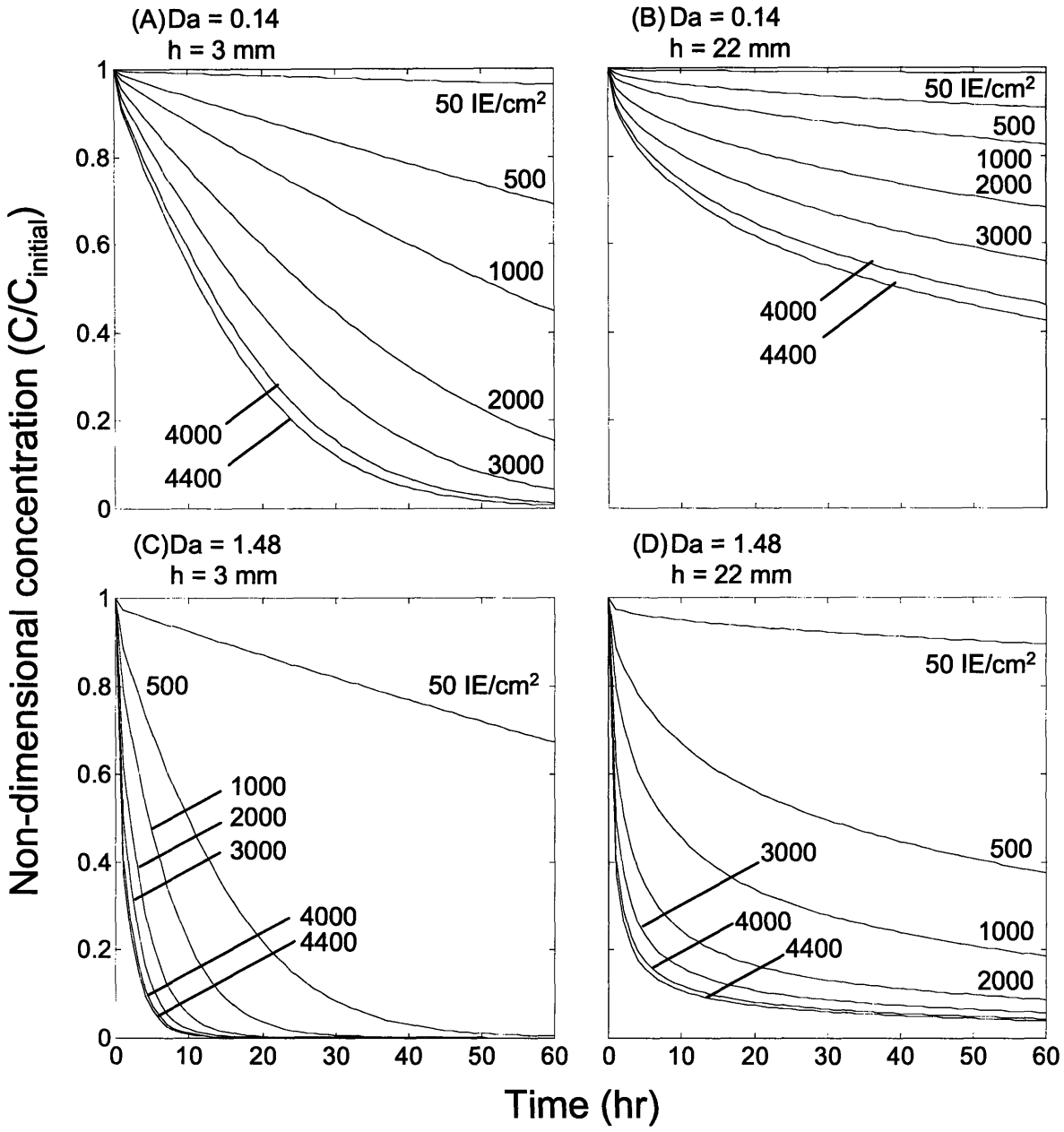

Figure 6.5. The maximum non-dimensional glucose concentration in the islet as a function of time and islet surface density
Predictions for culture in 3 (A and C) or 22 (B and D) mm medium assuming Da = 0.14 (A and B) or Da = 1.48 (C and D).

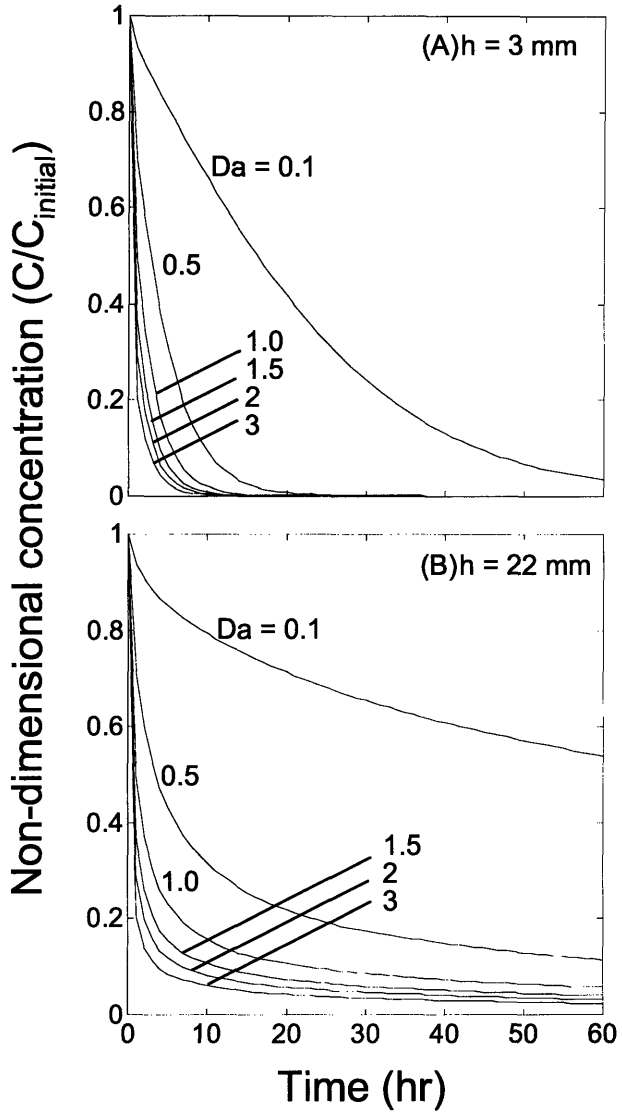

Figure 6.6. The maximum non-dimensional glucose concentration in the islet as a function of time and Da.
Predictions for culture in 3 (A) or 22 (B) mm medium at an islet surface density of 4440 IE/cm^2.

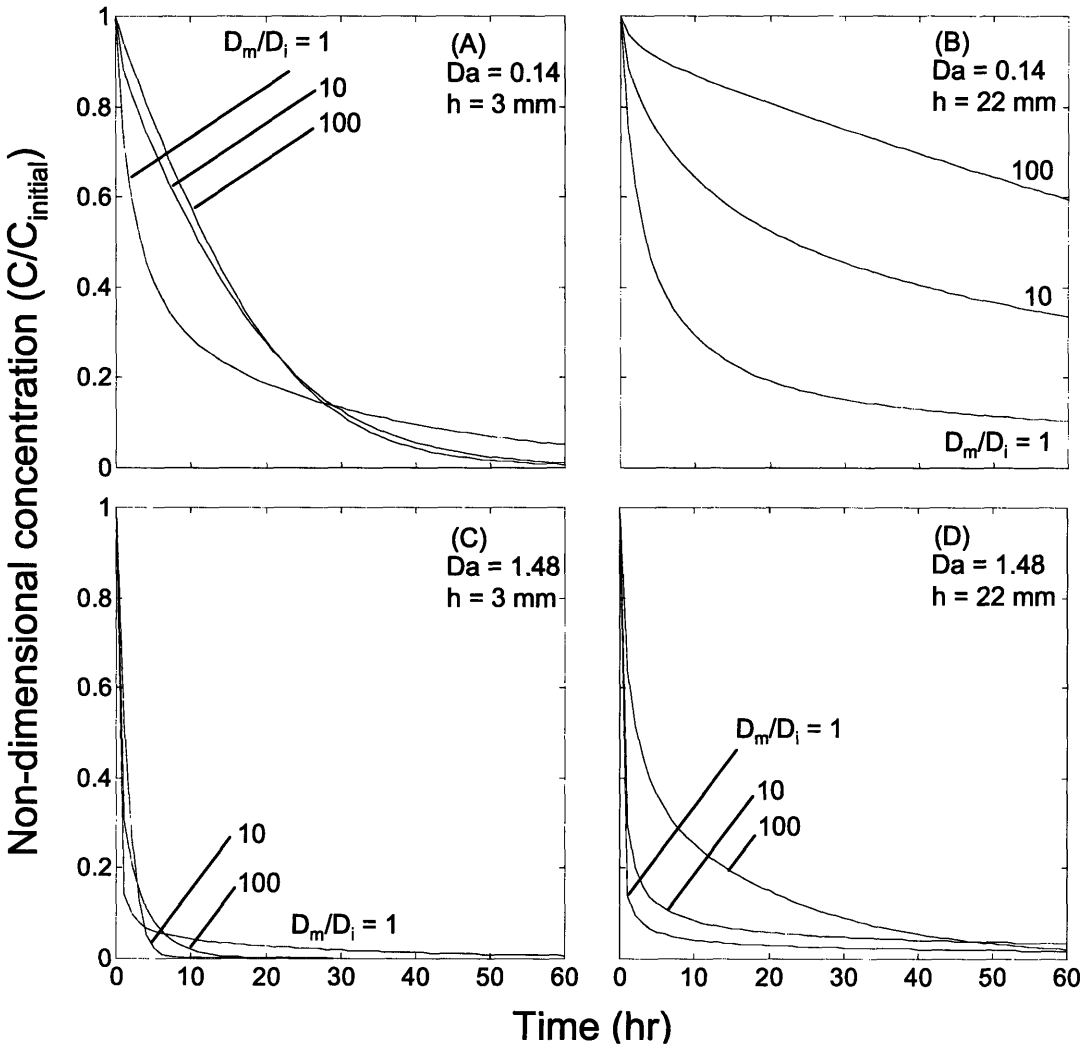

Figure 6.7. The maximum non-dimensional glucose concentration in the islet as a function of time and D_m/D_i.

Predictions for culture in 3 (A and C) or 22 (B and D) mm medium assuming Da = 0.14 (A and B) or Da = 1.48 (C and D) at an islet surface density of 4440 IE/cm^2.

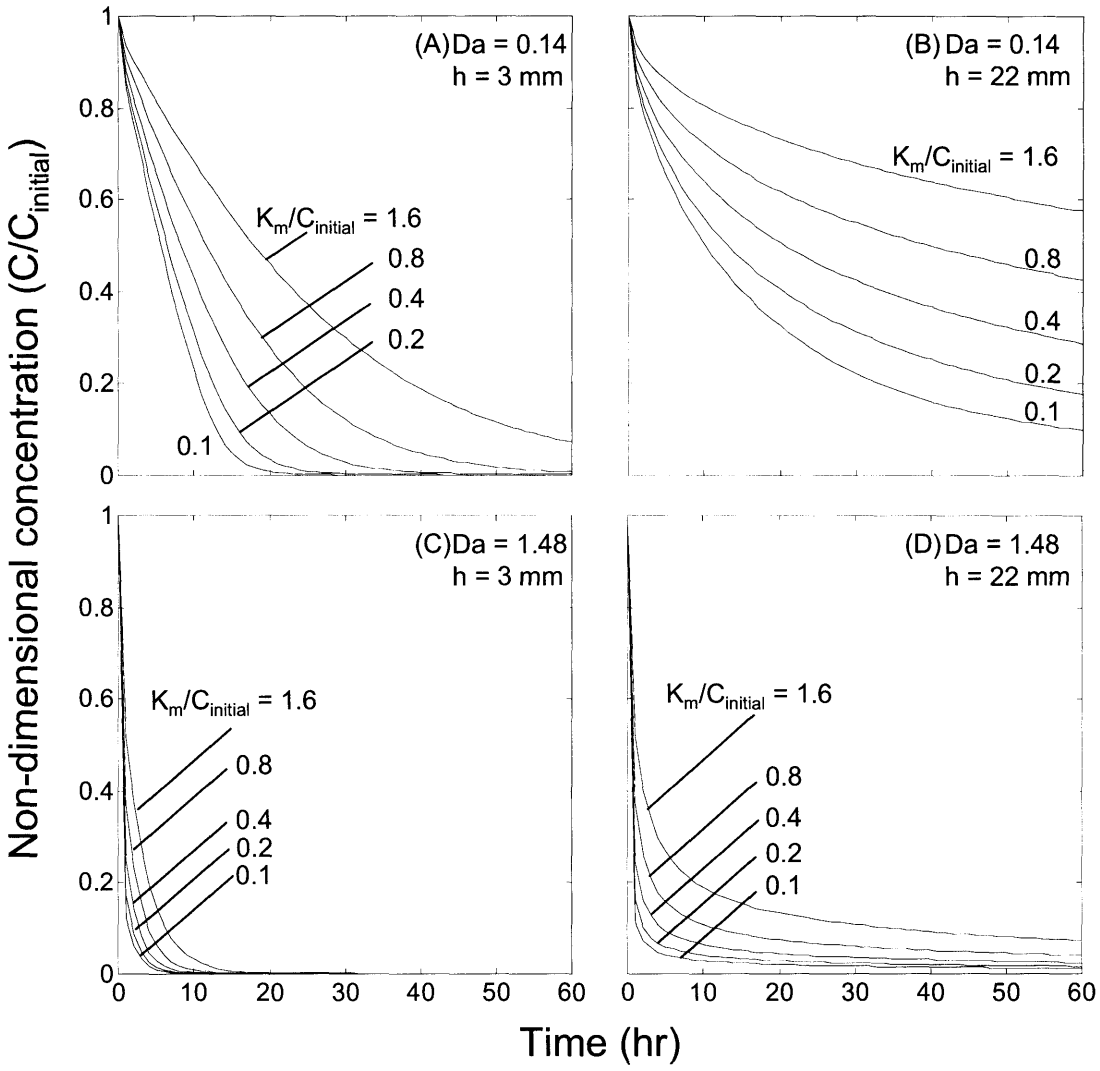

Figure 6.8. The maximum non-dimensional glucose concentration in the islet as a function of time and $K_m/C_{initial}$.
Predictions for culture in 3 (A and C) or 22 (B and D) mm medium assuming Da = 0.14 (A and B) or Da = 1.48 (C and D) at an islet surface density of 4440 IE/cm^2.

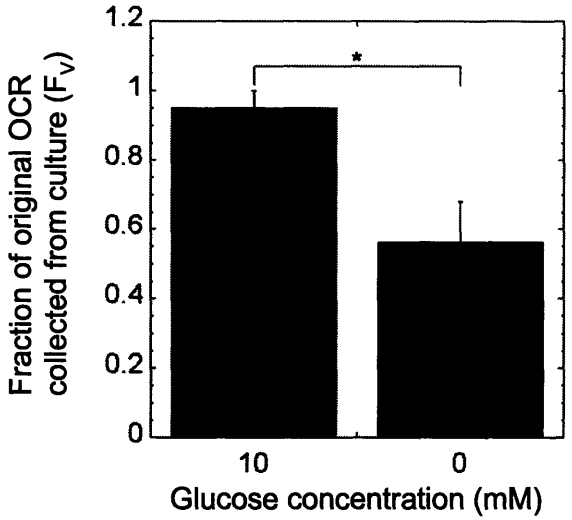

Figure 6.9. The fraction of original OCR collected from culture for human islets cultured in 3 mm of 0 or 10 mM glucose medium at < 8 x 10^4 cells/cm^2.
The error bars represent the standard deviation for 3 independent experiments. * indicates statistical significance ($p < 0.05$) for a paired two-tailed t-test.

6.7 Discussion

Data from literature indicates that β cell survival during culture is dependent on the glucose concentration of the culture medium [147-150]. When islet tissue is cultured at high density on silicone rubber a decrease in the fractional recovery of viable tissue is observed even though oxygen limitations are removed (Chapter 4). This decrease may be due to glucose transport limitations that become dominating at high densities. Additionally, though 5 mM glucose was determined to be optimal for human islet culture [160], the glucose concentration in tissue during culture is not only a function of initial glucose concentration, but also surface density, tissue GCR, and duration of culture. Therefore a better understanding of the interaction between these variables could elucidate how medium composition or culture technique could be modified for optimal culture.

In this study we developed and explored a transient glucose transport model to determine if tissue was exposed to low glucose concentration during high density islet culture. In addition we conducted preliminary experiments to determine if bulk glucose is depleted during high density culture and whether culture in zero glucose leads to a decreased viability.

Three non-dimensional parameters are present in the theoretical model including Da, D_m/D_i, and $K_m/C_{initial}$ which if inaccurate could introduce error into the predictions. Da > 0.1 and > 1, which are close to 0.14-1.48, the range of Da obtained assuming the literature GCR and our empirical GCR, result in exposure to < 1 mM glucose for culture in 3 and 22 mm medium, respectively (Figure 6.6). The ratios of D_m/D_i (Figure 6.7) and $K_m/C_{initial}$ (Figure 6.8) do not have as large of an effect on the maximum glucose concentration in the tissue at high Da because the consumption of the tissue is dominating. At low Da, when consumption is not dominating, D_m/D_i and $K_m/C_{initial}$ can have a significant impact for culture in large medium depths (Figure 6.7B and Figure 6.8B). Thus Da also determines how sensitive the model is to both D_m/D_i and $K_m/C_{initial}$ further indicating its importance. The parameter within Da that has the most variation based on all available data is V_{max} (GCR).

GCR measurements made with human islets were an order of magnitude higher than previously reported values for islet tissue (1×10^{-7} vs 9.4×10^{-9} mol/s cm^3) [153-157]. However, previously reported values were for rodent islet tissue. Human islet preparations are not only a different species, but also contain exocrine tissue (non-islet tissue in the pancreas) that is normally not present in rodent islet preparations. Non-islet tissue may have a higher GCR than islet tissue thereby increasing the overall GCR suggesting a correlation with preparation purity. However, no correlation was observed between islet volume fraction measurements prior to culture and GCR (data not shown), and too few measurements post culture were available to determine whether a correlation existed. Variation in GCR could also result from tissue preparations of differing quality that in previous studies varied over fourfold (Chapter 3). However, if nuclei from dead cells were present after culture, our measurement would underestimate the GCR of the viable tissue suggesting an even higher GCR. More experiments are needed with human islet preparations to confirm the experimental GCR.

The glucose model revealed that glucose concentration in the islet is strongly dependent on tissue surface density, tissue GCR, and the duration of culture. Bulk glucose concentration can be depleted in 3 mm medium over the course of 60 hr, and depending on the tissue density and GCR could be depleted as early as 10 hr (Figure 6.3 and Figure 6.4), which is consistent with experimental measurements indicating near zero glucose at densities > 150×10^4 cells/cm^2 after 34-60 hr and after just 9 hr of culture at 400×10^4 cells/cm^2 on polystyrene in 3 mm

medium. Culture in 22 mm medium theoretically prevents glucose depletion from the bulk medium (Figure 6.3), but at high Da resulted in islet exposure to < 0.5 mM glucose within 5-10 hr due to the slow diffusion of glucose to the islet surface (Figure 6.3 and Figure 6.5). However, experimental measurements for culture on silicone rubber in 22 mm medium indicated that glucose was depleted from the bulk medium to a concentration < 0.5 mM after 34-60 hr at densities > 240 x 10^4 cells/cm^2. The reason for this discrepancy in unknown but suggests the model overpredicts glucose concentration such that limitations would occur faster than predicted.

Most islet centers culture the "high purity" fraction of tissue from the isolation in approximately 3 mm medium at a density of 200-400 IE/cm^2 (K. Papas, A. Omer, personal communications), which is an underestimation of total tissue volume since non-islet tissue is ignored. The "high purity" fraction could be as low as 70% islet tissue by volume (A. Omer, personal communication) corresponding to a total tissue volume equivalent to 570 "IE"/cm^2, where "IE" in this case is based on total tissue, not only islet tissue. It should be emphasized that the theoretical model accounts for the total tissue surface density because all viable tissue consumes glucose. Thus all references to IE in all the figures indicate a total tissue volume, not islet volume specifically. The minimum concentration in the islet drops below 1 mM after 60 hr culture at 300 IE/cm^2 (Figure 6.4) and within 30 hr at 500 IE/cm^2 (Figure 6.5C) in 3 mm medium (assuming our empirical GCR) indicating that even in conventional methods, exposure to low glucose concentrations may occur unless medium is change every 30 hr.

The glucose concentration in the islet drops below 1 mM after 60 hr at densities above 1700 IE/cm^2 (approximately an OCR surface density of 6.6 nmol/min cm^2 assuming 1560 cells/IE [13] and 2.5 fmol/min cell, Chapter 2) for culture in 22 mm medium (Figure 6.4, assumes our empirical GCR). This may explain decreases in the fractional recovery of viable tissue observed for culture on a silicone rubber membrane in 22 mm medium at OCR densities > 5 nmol/min cm^2 that are independent of O_2 transport (Chapter 4).

Though exposure to low glucose concentration is likely, the question remains whether a reduced glucose level will cause tissue death. Rat β cell survival during culture increases with glucose concentration in a dose-dependent manner up to 10 mM [147-150]. Though 5.5 mM glucose CMRL 1066 was shown resulted in better GSIS than 10 mM glucose RPMI [40; 160] for human islets, it is reasonable to expect that concentrations below 5.5 mM may result in a similar dose-dependent cell death. In addition, even if 5.5 mM glucose is optimal for human islets, the

concentration in the tissue will vary with culture surface density, tissue viability, and culture duration. Unfortunately a critical glucose concentration below which a cell dies is unknown making it difficult to predict viability decreases using our theoretical model. A further complication is that islet tissue may be able to survive for a period of time in the absence of glucose which upon addition of glucose may function normally as observed for the glucose sensitivity of islets [40; 72]. Tissue cultured in 0 mM glucose resulted in a fractional recovery of viable tissue 40% lower than that of tissue cultured in 10 mM glucose (Figure 6.9) indicating a significant, but not complete loss in viability thereby suggesting that a portion of the tissue was able to survive for 34-60 hr without glucose. The tissue likely survived using other nutrients such as amino acids or free fatty acids within the medium to generate ATP. Alternatively the reduced glucose level could signal tissue to reduce its ATP demand and as such decrease requirements of ATP generation.

In summary, the glucose model and preliminary experimental data indicates that islet tissue is exposed to low glucose levels during high density culture. Though further experimentation is needed to determine the rate of death for human islet tissue as a function of glucose concentration, these results suggest that glucose transport limitations present in both polystyrene and silicone rubber cultures likely result in tissue death.

6.8 Nomenclature

7-AAD	7-aminoactinomycin D
C	Concentration of glucose
$C_{initial}$	Initial glucose concentration
D	Diffusivity of glucose
d	Diameter of islet
Da	Damkohler number
D-PBS	Dulbecco's phosphate buffered saline
FBS	Fetal bovine serum
F_V	The fraction of original viable tissue after culture
GCR	Glucose production rate
h	Medium depth
H	Non-dimensional medium depth, h/R_{islet}

IE	Islet equivalent
JDC	Joslin Diabetes Center
K_m	Michaelis constant, the C at which the reaction rate is $V_{max}/2$
LDH	Lactate dehydrogenase
O_2	Oxygen
OCR	Oxygen consumption rate
pO_2	Oxygen partial pressure
R	Production rate of glucose.
R_{islet}	Radius of islet
t	Time
V_{ch}	Volume of OCR chamber
V_{max}	Maximum reaction velocity
w	Center-to-center distance between islets
x	Axis in Cartesian coordinates
X	Non-dimensional axis in Cartesian coordinates, x/R_{islet}
y	Axis in Cartesian coordinates
Y	Non-dimensional axis in Cartesian coordinates, y/R_{islet}
z	Vertical axis in Cartesian coordinates
Z	Non-dimensional vertical axis in Cartesian coordinates, z/R_{islet}
α	Solubility of O_2 in medium
τ	Non-dimensional time
η	Non-dimensional concentration

Subscripts for D, p, C

m	Medium
i	Islet tissue

7 Changes in pH during static islet culture

7.1 Introduction

An alternative limitation to that of oxygen (Chapters 3-5) and glucose (Chapter 6) that may be present during high density islet culture is the accumulation of waste and/or changes in pH. The rate at which tissue produces waste, the depth of the medium, the rate at which waste is transported away from the tissue, and the duration of culture all play important roles in whether a significant pH shift could occur during culture.

The pH within cells changes as a function of the external pH [161]. Shifts in pH can affect many cellular processes including protein secretion and metabolic rates [162-164]. Islet cells in particular are considered to have an "elevated sensitivity" to variations in pH [165]. In βTC3 cells, a murine insulinoma cell line, exposure to pH of 6.4 for 4 hr decreased total ATP content compared to cells at pH 7.1 [164]. Insulin secretion rate of rat islets followed a bell shape curve with reductions on either side of pH 7.1-7.4 when in a bicarbonate buffered medium while the ATP/ADP ratio progressively declined as external pH increased from 6.5-7.7 [163]. These studies indicate significant changes to cellular rates which may cause decreases in tissue viability over time. At pH 8.0 porcine islet viability decreases significantly within 3 days while pH 7.0 results in a higher proportion of dead single cells after 3 weeks of culture compared to culture in pH 7.3 medium [166].

A transient model that simulates changes in local pH during islet culture was developed to investigate the extent to which pH could change during high density culture. Here we introduce and explore this theoretical model to determined the likelihood of whether pH changes significantly.

7.2 Methods

Islet isolation and culture

Standard collagenase/protease digestion methods were used for human [7; 15] isolations. Preparations of human islets were provided fresh (4-6 hr after isolation was complete) by the Islet Core at the Joslin Diabetes Center (JDC, Boston, MA). Human islets were also received after culture (1-2 days) from JDC or overnight shipment (sometimes after up to 1 day culture) from other centers contained in culture flasks (T-25 and T-75) or centrifuge tubes in Styrofoam

boxes. When first observed, some preparations were in suspension, some in a pellet. Upon receipt, a portion of the preparation was analyzed and the remainder placed into untreated polystyrene culture flasks at 37°C in a humidified environment (5% CO_2), oxygen partial pressure (pO_2) of 142 mmHg, for 34-60 hr during which no medium change occurred. Some cultures were terminated at 18-24 hr for analysis. To test the effect of temperature, some islets were cultured at 24°C, then warmed for 1 hr at 37°C before OCR measurements.

Islets were cultured in supplemented RPMI (11.1 mM D-glucose, 100 U/ml penicillin, 100 μg/ml streptomycin, 2 mM L-glutamine, 1 mM sodium pyruvate (all from Mediatech Inc., Herdon, VA), and 50 μM β-mercaptoethanol (Sigma Aldrich, St. Louis, MO) with 10% fetal bovine serum (FBS, Mediatech Inc.), at low densities (< $8x10^4$ cells/cm^2 or about 50 islet equivalents (IE)/cm^2, where IE is the volume of a sphere with a diameter of 150 μm) in 1.3 mm of medium in untreated polystyrene culture flasks. For some experiments parallel cultures in 0 mM glucose RPMI were conducted. After culture the free, non-adherent tissue (which is the only tissue used in current practice) was collected. In selected experiments, adherent human tissue was incubated for 5 min at 37°C in 0.05% trypsin EDTA (Mediatech Inc.), dislodged with fresh medium, and collected.

Islet enumeration by nuclei counting

Nuclei were prepared by adding equal 100-μl volumes of sample containing 160 or more IE and of lysis solution (0.1 M citric acid (Sigma) and 1% (v/v) Triton X-100 (Sigma)) to a 1.5 ml microtube [55]. The mixture was incubated at room temperature for 5 min with vortex mixing every 1.5 min, and nuclei were liberated by shearing through a needle. Isolated nuclei were diluted with Dulbecco's phosphate buffered saline (D-PBS, Invitrogen, Carlsbad, CA) to a concentration no higher than 5 x 10^5 nuclei/ml, stained with 7-aminoactinomycin D (7-AAD, Molecular Probes, Eugene, OR), and analyzed using a flow cytometer (Guava Personal Cell Analysis (PCA) system, Guava Technologies, Hayward, CA) to determine the total number of cells with intact nuclei in the sample.

Ammonia quantification

Samples were taken of the original culture medium and spent medium following culture and analyzed for ammonia content using the Ammonia Assay Kit (Product Code AA0100 Sigma Aldrich, St. Louis, MO). Triplicate samples diluted to concentrations between 30-100 μg/ml were placed in a 96-well plate along with samples for a six-point standard curve ranging in

concentration from 0-150 μg/ml. The Ammonia Assay Reagent was added to each well. After shaking the plate for 5 min 10X L-Glutamate Dehydrogenase Solution was added to each well. The plate was mixed on a shaker for 5 min before adding 3-(4,5-dimethylthiazol-2-yl)-5-(3-carboxymethoxyphenyl)-2-(4-sulfophenyl)-2H- tetrazolium (MTS) solution. After briefly mixing the plate was read on the plate reader with an absorbance of 492 nm on a plate reader.

Lactate quantification

Samples were taken of the original culture medium and spent medium following culture and analyzed for lactate content by modifying the protocol for the Glucose Assay Kit (GAGO20, Sigma Aldrich, St. Louis, MO). Triplicate samples diluted to concentrations between 0.1-0.5 mM were placed in a 96-well plate along with samples for a six-point standard curve ranging in concentration from 0-0.5 mM. The Lactate Assay Reagent, a mixture of Lactate Oxidase (12.5 units/ml), Lactate Peroxidase (2.5 Purpurogallin units/ml), and o-Dianisidine (0.1 mg/ml) in deionized water, was added to each well. After 25 min at 37°C 12N sulfuric acid was added to each well. The absorbance was measured at 544 nm on a plate reader.

7.3 Theoretical pH model

This transient model predicts the local pH in and around islets in static culture. The species accounted for include hydrogen ions (H^+), carbon dioxide (CO_2), bicarbonate ions (HCO_3^-), lactic acid (HL), and ammonia (NH_3).

In order to make this problem more feasible the following assumptions are made:

- Bicarbonate is the only important buffer in the system. Phosphate buffers are also present, but at a lower concentration (over four times more bicarbonate buffer than phosphate buffer). The conversion from CO_2 and water (H_2O) to HCO_3^- and H^+ follows

$$H_2O + CO_2 \underset{k_{-1}}{\overset{k_f}{\rightleftharpoons}} H_2CO_3 \overset{K}{\rightleftharpoons} HCO_3^- + H^+ \qquad \textbf{7.1}$$

  where k_f is the first-order hydration reaction rate constant, k_{-1} is the first-order dehydration reaction rate constant, and K is the ionization constant for carbonic acid. According to Garg and Maren [167] at near neutral pH the concentration of H_2CO_3 is

very small because the dissociation of it to H^+ and HCO_3^- is very fast allowing 7.1 to be simplified to

$$H_2O + CO_2 \underset{k_r}{\overset{k_f}{\rightleftharpoons}} HCO_3^- + H^+ \qquad \textbf{7.2}$$

where k_f is still a first-order dehydration reaction rate constant and k_r is a second-order reverse reaction rate constant. This simplified conversion will be used in our model using values determined by Garg and Maren [167].

- All lactic acid produced by the tissue is immediately dissociated into ions through the following equation.

$$HL \Rightarrow H^+ + Lac^- \qquad \textbf{7.3}$$

where Lac^- is a lactate ion. Since the pKa of lactic acid is 3.86 [118], this should be a reasonable assumption unless the pH drops significantly from neutral pH.

- All ammonia produced by the tissue immediately combines with a hydrogen ion through the following equation.

$$NH_3 + H^+ \Rightarrow NH_4^+ \qquad \textbf{7.4}$$

where NH_3 is ammonia and NH_4^+ is the ammonium ion. Since the pKa of ammonia is 9.25 [118] this will hold true unless the pH increases significantly above neutral pH.

- An effective diffusivity is used for each species in the tissue (in other words we do not distinguish between intercellular and intracellular diffusion within the tissue).
- There is no significant partition of any species between the medium and islet tissue except for CO_2, which will partition based on its solubility in each domain.
- Electrostatic effects can be ignored (i.e. transport due to charge is negligible, preliminary calculations support this assumption).
- Water is in equilibrium with its ions.
- The species conservation equation in the absence of convection is given by [16; 97]

$$\frac{\partial C_j}{\partial t} - D_j \nabla^2 C_j = R_j \qquad \textbf{7.5}$$

where C_j is the concentration of species "j", D_j is the diffusivity of species "j", and R_j is the production rate of species "j".

To model islet culture all the tissue (islet and non-islet) was assumed to be in the form of spheres with uniform diameter (d) that were arranged in a square array with center-to-center distance w in a stagnant medium of height h on either a CO_2-impermeable or CO_2-permeable membrane of known thickness (Figure 7.1). Because of symmetry within the system, Equation 7.5 was solved within a unit cell containing only an eighth of an islet (dashed lines in Figure 7.1).

Here we present the model equations for islets on a CO_2-impermeable surface. The boundary conditions for CO_2 in this model include constant external partial pressure of CO_2 (pCO_2,gas) across the gas-medium (m) interface,

at z = h, $$pCO_2,gas = pCO_2,m \quad \textbf{7.6}$$

no CO_2 flux through the impermeable dish,

at z=0, $$\frac{\partial C_{CO_2}}{\partial z} = 0 \quad \textbf{7.7}$$

continuity of pCO_2 and CO_2 flux across the medium-islet (i) interface,

$$\mathbf{n} \bullet ((-D_{CO_2} \nabla C_{CO_2})_i - (-D_{CO_2} \nabla C_{CO_2})_m) = 0 \quad \textbf{7.8}$$

$$pCO_2,i = pCO_2,m \quad \textbf{7.9}$$

and symmetry across each side of the unit cell including both medium and islet domains

$$\mathbf{n} \bullet (-D_{CO_2} \nabla C_{CO_2}) = 0 \quad \textbf{7.10}$$

CO_2 is produced by the tissue at a rate V_{max,CO_2}. Substituting in the production rate of the tissue and the interaction with the bicarbonate and hydrogen ions (7.2) a separate equation for each domain is obtained, one that describes CO_2 transport in the medium (m) and one that describes CO_2 transport in the islet (i).

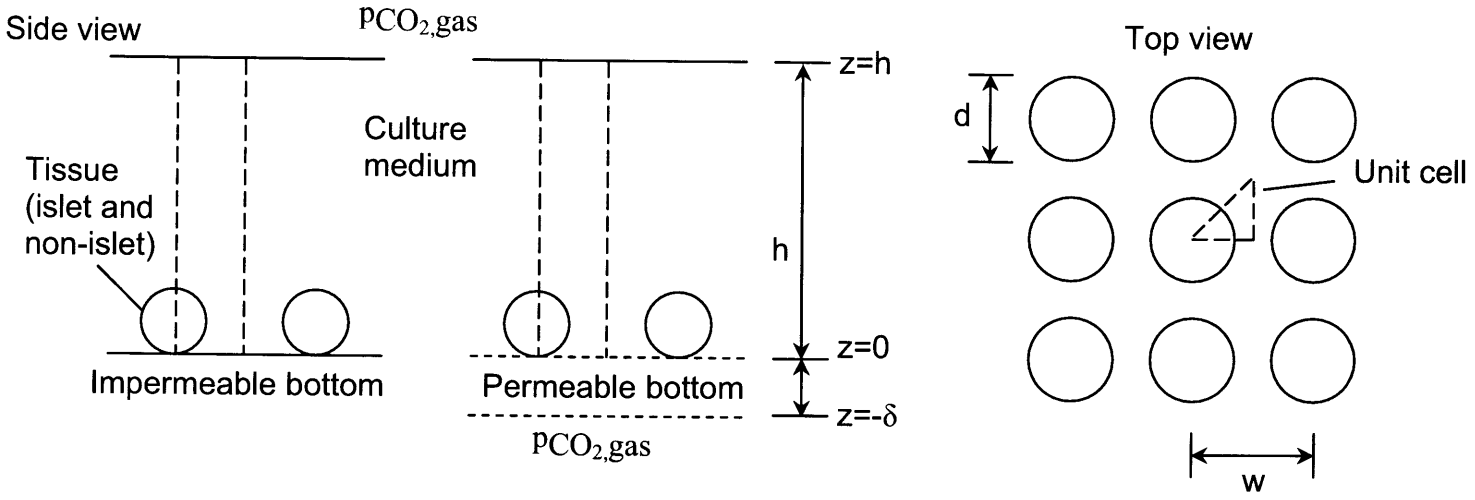

Figure 7.1. Islet geometry assumed for modeling pH changes for islet tissue on either a polystyrene dish or a 500-μm silicone rubber membrane.

$$\frac{\partial C_{CO_2}}{\partial t} - D_{CO_2,i}\nabla^2 C_{CO_2} = V_{max,CO_2} - k_f C_{CO_2} + k_r C_{H^+} C_{HCO_3^-} \quad \textbf{7.11}$$

$$\frac{\partial C_{CO_2}}{\partial t} - D_{CO_2,m}\nabla^2 C_{CO_2} = -k_f C_{CO_2} + k_r C_{H^+} C_{HCO_3^-} \quad \textbf{7.12}$$

For the hydrogen ion, lactate ion, ammonium ion, and bicarbonate ion the boundary conditions include no flux through the bottom of the culture vessel or through the air-liquid surface,

at z=0 and z=h, $$\frac{\partial C_j}{\partial z} = 0 \quad \textbf{7.13}$$

continuity of flux across the liquid-islet interface,

$$\mathbf{n} \bullet ((-D_j \nabla C_j)_i - (-D_j \nabla C_j)_m) = 0 \quad \textbf{7.14}$$

and symmetry across each side of the unit cell including both medium and islet domains

$$\mathbf{n} \bullet (-D_j \nabla C_j) = 0 \quad \textbf{7.15}$$

Ammonia and lactic acid production are known constant rates within the islet. Separate equations were used for each domain, one that describes transport in the medium (m) and one that describes transport in tissue (i) for each solute.

$$\frac{\partial C_{Lac^-}}{\partial t} - D_{Lac^-,i}\nabla^2 C_{Lac^-} = R_{Lac^-} \quad \textbf{7.16}$$

$$\frac{\partial C_{Lac^-}}{\partial \tau} - D_{Lac^-,m}\nabla^2 C_{Lac^-} = 0 \quad \textbf{7.17}$$

$$\frac{\partial C_{NH_4^+}}{\partial t} - D_{NH_4^+,i}\nabla^2 C_{NH_4^+} = R_{NH_4^+} \quad \textbf{7.18}$$

$$\frac{\partial C_{NH_4^+}}{\partial t} - D_{NH_4^+,m}\nabla^2 C_{NH_4^+} = 0 \quad \textbf{7.19}$$

$$\frac{\partial C_{HCO_3^-}}{\partial t} - D_{HCO_3^-,i}\nabla^2 C_{HCO_3^-} = \left(k_f C_{CO_2} - k_r C_{H^+} C_{HCO_3^-}\right) \quad \textbf{7.20}$$

$$\frac{\partial C_{HCO_3^-}}{\partial t} - D_{HCO_3^-,m}\nabla^2 C_{HCO_3^-} = \left(k_f C_{CO_2} - k_r C_{H^+} C_{HCO_3^-}\right) \quad \textbf{7.21}$$

$$\frac{\partial C_{H^+}}{\partial t} - D_{H^+,i}\nabla^2 C_{H^+} = \left(R_{Lac^-} - R_{NH_4^+} + k_f C_{CO_2} - k_r C_{H^+} C_{HCO_3^-}\right) \quad \textbf{7.22}$$

$$\frac{\partial C_{H^+}}{\partial t} - D_{H^+,m}\nabla^2 C_{H^+} = \left(k_f \eta_{CO_2} - k_r C_{H^+} C_{HCO_3^-}\right) \quad \textbf{7.23}$$

The equations of the transient model were non-dimensionalized. The non-dimensional variables used are

$$\eta_i = \frac{C_i}{C_{CO_2,m,t=0}} \quad \textbf{7.24}$$

$$X = \frac{x}{R_{islet}},\ Y = \frac{y}{R_{islet}},\ Z = \frac{z}{R_{islet}} \quad \textbf{7.25}$$

$$\tau = \frac{D_{CO_2,m}t}{R_{islet}^2} \quad \textbf{7.26}$$

Using these non-dimensional variables the governing equations can be rewritten in non-dimensional form.

$$\frac{\partial \eta_{CO_2}}{\partial \tau} - \frac{D_{CO_2,i}}{D_{CO_2,m}}\left(\nabla^2 \eta_{CO_2}\right) = \frac{R_{islet}^2}{D_{CO_2,m}}\left(\frac{V_{max,CO_2}}{C_{CO_2,m,t=0}} - k_f \eta_{CO_2} + k_r C_{CO_2,m,t=0} \eta_{H^+} \eta_{HCO_3^-}\right) \quad \textbf{7.27}$$

$$\frac{\partial \eta_{CO_2}}{\partial \tau} - \left(\nabla^2 \eta_{CO_2}\right) = \frac{R_{islet}^2}{D_{CO_2,m}}\left(-k_f \eta_{CO_2} + k_r C_{CO_2,m,t=0} \eta_{H^+} \eta_{HCO_3^-}\right) \quad \textbf{7.28}$$

$$\frac{\partial \eta_{Lac^-}}{\partial \tau} - \frac{D_{Lac^-,i}}{D_{CO_2,m}} \nabla^2 \eta_{Lac^-} = \frac{R_{islet}^2}{D_{CO_2,m} C_{CO_2,m,t=0}} R_{Lac^-} \quad \textbf{7.29}$$

$$\frac{\partial \eta_{Lac^-}}{\partial \tau} - \frac{D_{Lac,m}}{D_{CO_2,m}} \nabla^2 \eta_{Lac^-} = 0 \quad \textbf{7.30}$$

$$\frac{\partial \eta_{NH_4^+}}{\partial \tau} - \frac{D_{NH_4^+,i}}{D_{CO_2,m}} \nabla^2 \eta_{NH_4^+} = \frac{R_{islet}^2}{D_{CO_2,m} C_{CO_2,m,t=0}} R_{NH_4^+} \quad \textbf{7.31}$$

$$\frac{\partial \eta_{NH_4^+}}{\partial \tau} - \frac{D_{NH_4^+,m}}{D_{CO_2,m}} \nabla^2 \eta_{NH_4^+} = 0 \quad \textbf{7.32}$$

$$\frac{\partial \eta_{HCO_3^-}}{\partial \tau} - \frac{D_{HCO_3^-,i}}{D_{CO_2,m}} \nabla^2 \eta_{HCO_3^-} = \frac{R_{islet}^2}{D_{CO_2,m}} \left(k_f \eta_{CO_2} - k_r C_{CO_2,m,t=0} \eta_{H^+} \eta_{HCO_3^-} \right) \quad \textbf{7.33}$$

$$\frac{\partial \eta_{HCO_3^-}}{\partial \tau} - \frac{D_{HCO_3^-,m}}{D_{CO_2,m}} \nabla^2 \eta_{HCO_3^-} = \frac{R_{islet}^2}{D_{CO_2,m}} \left(k_f \eta_{CO_2} - k_r C_{CO_2,m,t=0} \eta_{H^+} \eta_{HCO_3^-} \right) \quad \textbf{7.34}$$

$$\frac{\partial \eta_{H^+}}{\partial \tau} - \frac{D_{H^+,i}}{D_{CO_2,m}} \nabla^2 \eta_{H^+} = \frac{R_{islet}^2}{D_{CO_2,m}} \left(\frac{R_{Lac^-} - R_{NH_4^+}}{C_{CO_2,m,t=0}} + k_f \eta_{CO_2} - k_r C_{CO_2,m,t=0} \eta_{H^+} \eta_{HCO_3^-} \right) \quad \textbf{7.35}$$

$$\frac{\partial \eta_{H^+}}{\partial \tau} - \nabla \cdot \frac{D_{H^+,m}}{D_{CO_2,m}} \nabla^2 \eta_{H^+} = \frac{R_{islet}^2}{D_{CO_2,m}} \left(k_f \eta_{CO_2} - k_r C_{CO_2,m,t=0} \eta_{H^+} \eta_{HCO_3^-} \right) \quad \textbf{7.36}$$

The non-dimensional boundary conditions for CO_2 in this model include constant external p_{CO_2} across the gas-medium interface,

at z=H where $H = h/R_{islet}$, $\eta_{CO_2} = 1$ **7.37**

no CO_2 flux through the impermeable dish,

at z=0,
$$\frac{\partial \eta CO_2}{\partial Z} = 0 \tag{7.38}$$

continuity of p_{CO_2} and CO_2 flux across the medium-islet interface,

$$\mathbf{n} \bullet \left(\left(-\frac{D_{CO_2,i}}{D_{CO_2,m}} \nabla \eta CO_2 \right)_i - (-\nabla \eta CO_2)_m \right) = 0 \tag{7.39}$$

$$\eta CO_2,i = \frac{\alpha CO_2,i}{\alpha CO_2,m} \eta CO_2,m \tag{7.40}$$

where $\alpha CO_2,i$ is the solubility of CO_2 in islet tissue and $\alpha CO_2,m$ is the solubility of CO_2 in medium, and symmetry across each side of the unit cell including both medium and islet domains

$$\mathbf{n} \bullet (-\nabla \eta CO_2) = 0 \tag{7.41}$$

For transport of the hydrogen ion, lactate ion, ammonium ion, and bicarbonate ion the boundary conditions include no flux through the bottom of the culture vessel or through the air-liquid surface,

at z=0 and z=H,
$$\frac{\partial \eta_j}{\partial Z} = 0 \tag{7.42}$$

continuity of flux across the liquid-islet interface,

$$\mathbf{n} \bullet \left(\left(-\frac{D_{j,i}}{D_{j,m}} \nabla \eta_j \right)_i - (-\nabla \eta_j)_m \right) = 0 \tag{7.43}$$

and symmetry across each side of the unit cell including both medium and islet domains

$$\mathbf{n} \bullet (-\nabla \eta_j) = 0 \tag{7.44}$$

When modeling islet culture on a CO_2-permeable membrane an additional conservation equation (with no reaction term) is required for transport of carbon dioxide in the silicone rubber.

The boundary condition in Equation 7.7 is replaced by continuity equations similar to those in Equation 7.8 and 7.9 except it is evaluated at the interface of the medium and silicone rubber. In addition, CO_2 at a constant external pO_2 is in equilibrium with the bottom of the silicone rubber membrane surface and symmetry conditions like those in Equation 7.11 are applied to the sides of the unit cell. All equations and boundary conditions for other species remain the same. Non-dimensionalization of these equations was performed in a similar manner as that above.

Hydrogen ion profiles, and thus pH profiles, in the theoretical model are governed by four key Damkohler numbers (Da) including

$$Da_{CO_2} = \frac{V_{max,CO_2} \cdot R_{islet}^2}{D_{CO_2,m} \cdot C_{CO_2,m,t=0}} \quad \textbf{7.45}$$

$$Da_{k_f} = \frac{k_f \cdot R_{islet}^2}{D_{CO_2,m}} \quad \textbf{7.46}$$

$$Da_{k_r} = \frac{k_r \cdot C_{CO_2,m,t=0} \cdot R_{islet}^2}{D_{CO_2,m}} \quad \textbf{7.47}$$

$$Da_{Lac-Am} = \frac{\left(R_{Lac^-} - R_{NH_4^+}\right) \cdot R_{islet}^2}{D_{CO_2,m} \cdot C_{CO_2,m,t=0}} \quad \textbf{7.48}$$

Though non-dimensional diffusivities are also present, the uncertainty in their values and their corresponding impact is likely minor compared to the uncertainty in the Da values. As such, the theoretical analysis focuses on changes in pH profiles due to changes in Da_{CO_2}, Da_{k_f}, Da_{k_r}, and Da_{Lac-Am}.

The model was solved with the finite element method using the commercially available software COMSOL Multiphysics (COMCOL Inc., Burlington, MA) in conjunction with Matlab (Mathworks, Natick, MA). We required the mesh to contain more than 1000 nodes and set an absolute tolerance for each concentration of 10^{-6} [99].

The diffusion coefficients and cellular production rates obtained from literature are listed in Table 7.1 and Table 7.2, respectively. The average of the production rates for ammonia and lactate in literature were used as the base case from literature. Experimental measurements were also conducted to determine the lactate and ammonia production rates of human islet tissue and will be discussed later. The remaining parameter values are given in Table 7.3 along with how/where the values were obtained.

Table 7.1. Diffusivities of each species used in the model in tissue and in culture medium.

Species	Domain	Diffusivity (cm^2/s)	Reference
CO_2	Tissue	1.0×10^{-5}	[138]
	Medium	2.55×10^{-5}	[117; 118]
	Silicone rubber	2.9×10^{-5}	[141]
Lac^-	Tissue	5.3×10^{-6}	[168]
	Medium	1.1×10^{-5}	[169]
NH_4^+	Tissue	2×10^{-6}	[170]
	Medium	2.7×10^{-5}	[117]
HCO_3^-	Tissue	8.6×10^{-7}	[171]
	Medium	1.19×10^{-5}	[171; 172]
H^+	Tissue	6×10^{-6}	[171]
	Medium	11.2×10^{-5}	[171; 172]

Diffusion coefficients reported at temperatures other than 37°C were adjusted to 37°C assuming $D\mu/T$ = constant [117], where μ is the viscosity of the solvent (water) at the specified temperature T.

Table 7.2. Cellular production rates for CO_2, ammonia, and lactate.

Chemical species	Islet type	Original value	Original units	mol/s cm3	Reference
CO_2	Human	-	-	3.68×10^{-8}	Chapter 2
NH_4^+	Rat	80 - 220	nmol/2h 1000 islets	$6.3 - 17.3 \times 10^{-9}$	[151]
Lac^-	Mouse	3629 ± 357	pmol/h ug DNA	5.78×10^{-9}	[154]
	Rat	3576 ± 153	pmol/h ug DNA	5.70×10^{-9}	[154]
	Rat	78 ± 37	umol/h g dry weight	3.74×10^{-9}	[155]

Assumptions include (1) 10.14 ng DNA per IE based on 1560 cells per IE [13] and 6.5 pg DNA/cell [68], (2) an IE is the volume of tissue equivalent to a 150-micron sphere, (3) there are 33.2 ng DNA/ug dry weight (average of 3 values referenced in [155]), (4) production of CO_2 was assumed to be equal to the OCR of the tissue based on stoichiometric relationships for the Krebs cycle. The average OCR, and thus CO_2 production rate, is about 2.5 fmol/min cell (Chapter 2).

Table 7.3. Parameter values used in pH model for high density islet culture.

Parameter	Value	Units	Reference
k_f	0.145	s^{-1}	[167]
k_r	17.2×10^4	L/mol s	[167]
External partial pressure of CO_2	38	mmHg	5% CO_2 in incubator
Initial pH of medium	7.4		Experimentally determined
Initial ammonium ion concentration	0	mol/L	Medium composition
Initial lactate ion concentration	0	mol/L	Medium composition
CO_2 solubility in tissue	3.21×10^{-5}	M/torr	[138]
CO_2 solubility in medium	3.18×10^{-5}	M/torr	[125; 172]
CO_2 solubility in silicone rubber	7.7×10^{-5}	M/torr	[173]

CO_2 solubility in tissue is obtained by dividing CO_2 permeability data in a variety of tissues by the diffusion coefficient 1.19×10^{-5} cm^2/s [138]. CO_2 solubility in water was used as an approximation for the CO_2 solubility in the medium [125; 172].

7.4 Ammonia and lactate production rate measurements

The change in lactate and ammonia concentration determined using the original and spent medium was converted to an increase in total lactate and ammonia which was normalized using nuclei counts after culture to obtain the production rates. The lactate production rate (LPR) was determined to be $5.3 \pm 1.6 \times 10^{-8}$ mol/s cm^3 (n = 11, data ranged from $2.5 - 7.8 \times 10^{-8}$ mol/s cm^3) assuming 1560 cells/IE [55] while the ammonia production rate (APR) was $5.0 \pm 2.6 \times 10^{-8}$ mol/s cm^3 (n = 6, data ranged from $1.6 - 6.9 \times 10^{-8}$ mol/s cm^3). These values will be used for the base case from empirical data.

7.5 Predictions of theoretical model

Since values of lactate and ammonia production determined experimentally were significantly different than those reported in literature, two sets of base case parameters will be modeled as indicated in Table 7.4.

Culture on polystyrene at 4400 IE/cm^2 results in large changes in pH throughout the medium (Figure 7.2A-D) whereas culture on silicone rubber maintains pH between 7.2 and 7.5 for more than 60 hr (Figure 7.2E and F). Due to CO_2 production, which causes the bicarbonate reaction (7.2) to shift toward the presence of H^+ in solution, there is a substantial decrease in pH

within 5 hr of initiating culture on polystyrene resulting in exposure to pH < 7 in the islet tissue, which is where the pH changes the most. This shift is almost completely removed by culture on a silicone rubber membrane because the CO_2 can escape through the membrane preventing the bicarbonate reaction from shifting to more acidic conditions. Assuming data from literature is accurate culture on polystyrene in 3 mm medium recovers from the initial shift in pH over time (Figure 7.2A), however, the empirical data indicates that pH would continue to decrease (Figure 7.2B). Bulk pH of the system is much higher than what the islet is exposed to, especially for large medium depths on polystyrene.

The data in Figure 7.2 assume culture is conducted at 4400 IE/cm^2, nearly a monolayer of islets, and is meant to provide a worst case scenario. At lower densities the shift in pH is less substantial (Figure 7.3). In almost all cases the pH at the top of the islet at any given time is closest to physiologic pH of 7.4 at lower densities compared to higher surface densities independent of which base case is assumed (exception is Figure 7.3E, silicone rubber with 22 mm medium). Based on the predictions in Figure 7.3, large pH changes at the islet surface only occur for culture on polystyrene and at densities > 1000 IE/cm^2 in 3 mm medium, but in 22 mm medium could occur at densities < 500 IE/cm^2. Though this is specifically for the top of the islet, the pH change within the islet is relatively small (Figure 7.2A and B).

Table 7.4. Damkohler numbers based on data in literature and empirical measurements used in the base case simulations.

Base case	Damkohler number	Value
Literature	Da_{CO_2}	0.067
	Da_{k_f}	0.32
	Da_{k_r}	460
	Da_{Lac-Am}	-0.012
Experimental	Da_{CO_2}	0.067
	Da_{k_f}	0.32
	Da_{k_r}	460
	Da_{Lac-Am}	0.0055

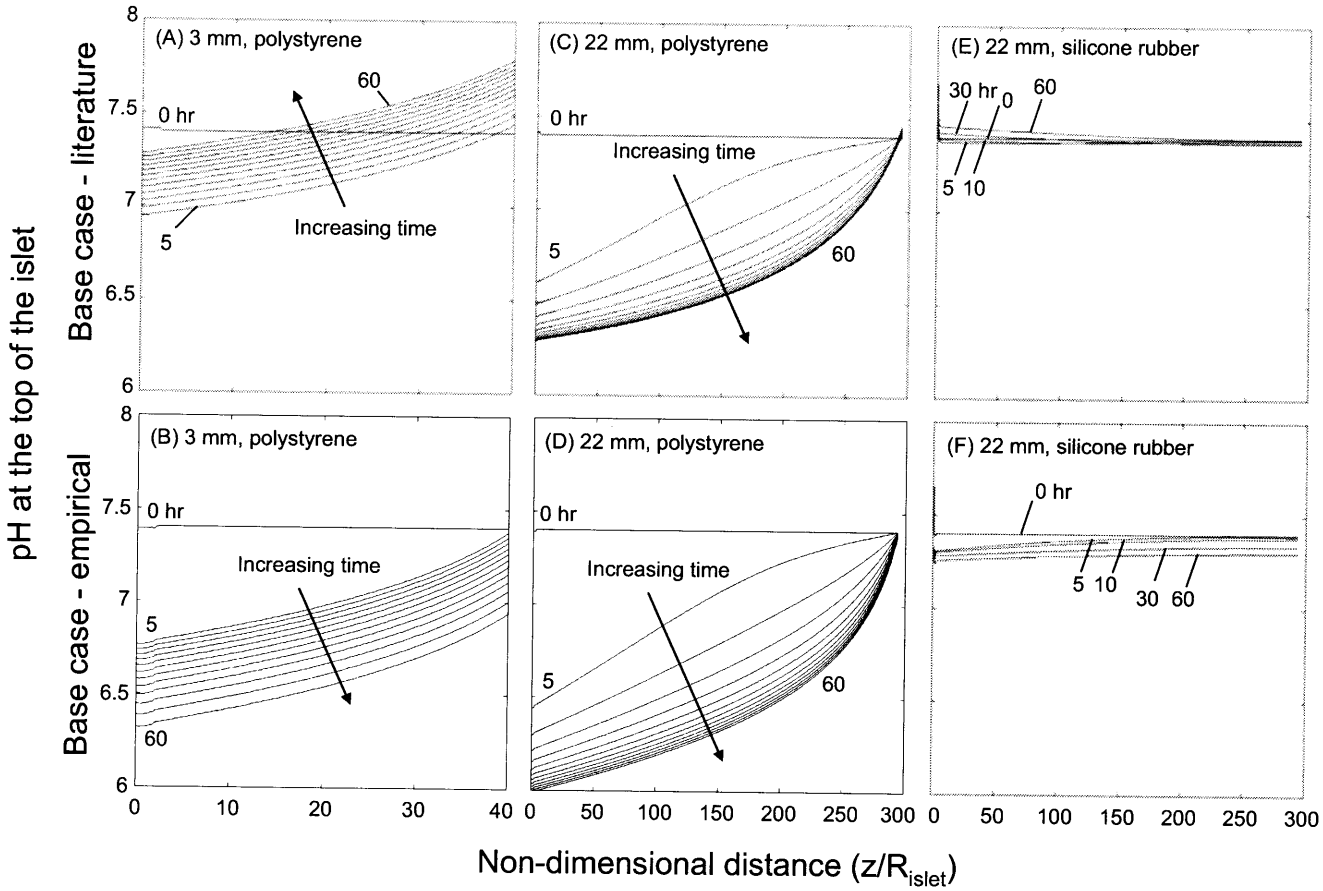

Figure 7.2. Transient pH profiles for islets as a function of position.
Predictions for culture at 4400 IE/cm^2 in 3 (A and B) or 22 mm medium (C and D) on polystyrene or on a 500-μm thick silicone rubber membrane in 22 mm medium (E and F). Plots are given using parameters from literature (A, C, and E) and using experimentally determined parameters (B, D, and F). The non-dimensional distance (z/R_{islet}) is from the bottom of the plate where $z/R_{islet} = 0$ through the center of the islet to the top of the islet where $z/R_{islet} = 2$ to the top of the culture medium where $z/R_{islet} = 40$ for 3 mm medium and $z/R_{islet} = 293$ for 22 mm medium. The time between each profile in A-D is 5 hours.

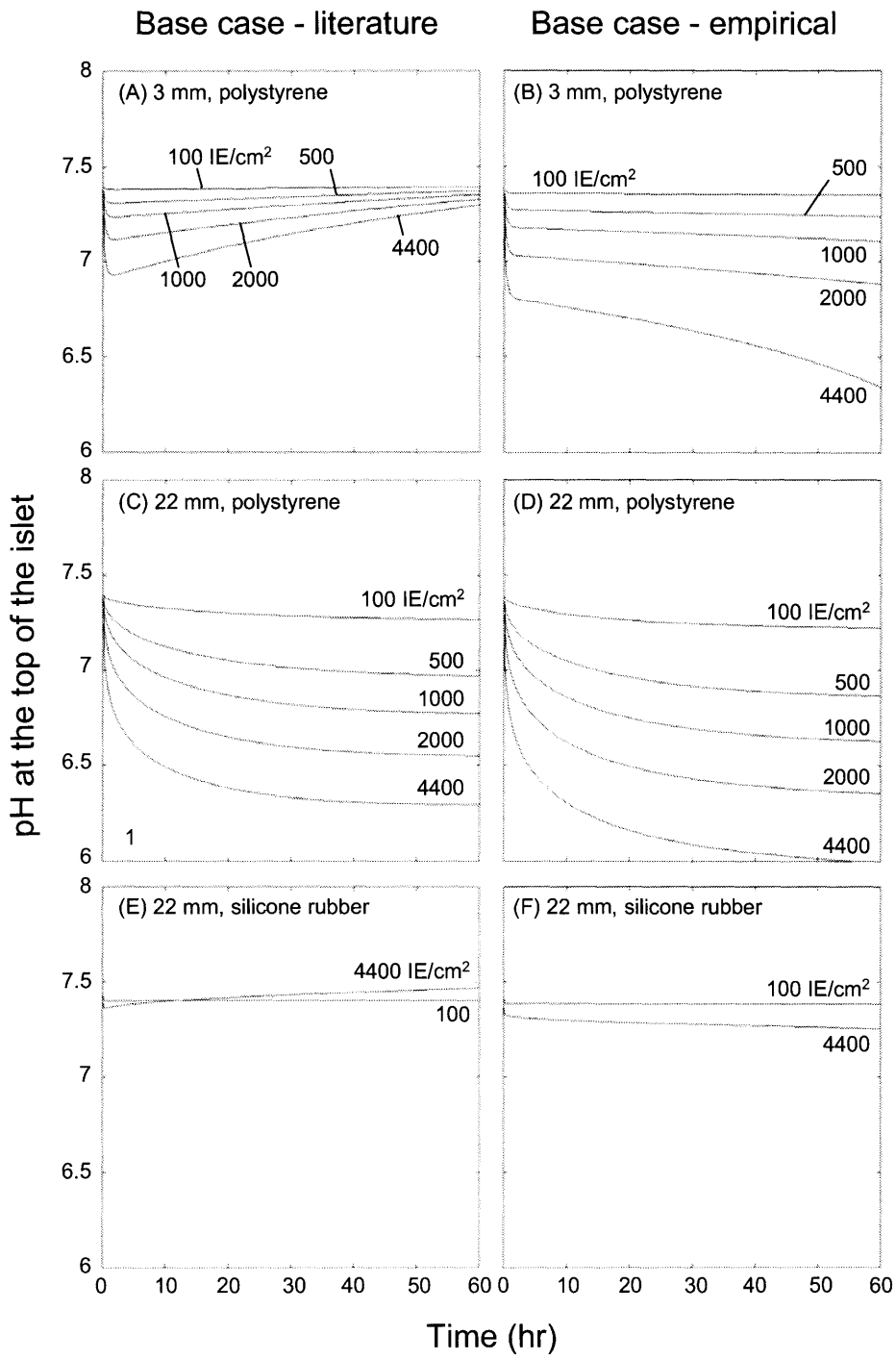

Figure 7.3. The pH at the top of the islet as a function of time and islet density. Predictions for culture on polystyrene in 3 (A and B) or 22 (C and D) mm medium or on a 500-μm thick silicone rubber membrane in 22 mm medium (E and F). Plots are given using parameters from literature (A, C, and E) and using experimentally determined parameters (B, D, and F).

Da can have a large impact on the pH profiles. Assuming the empirical base case, the magnitude of the initial drop in pH increases and the long term pH value decreases as Da_{CO_2} is increased from 0.001 to 10 (Figure 7.4B, D, and F). Therefore the more CO_2 produced by the tissue (i.e. the healthier the tissue), the larger the initial downward shift in pH. For the base case assuming literature data for lactate and ammonia production is accurate, a similar trend is obtained (Figure 7.4A and C), but pH slowly increases after the initial drop. For culture on polystyrene the pH after 60 hr changes from < 7.4 to > 7.4 at Da_{CO_2} between 0. 1 and 0.01. Culture on silicone rubber results in a much smaller shift in pH compared to that on polystyrene and changes very little with time after an initial transient period (Figure 7.4E and F) as observed above.

The effect of Da_{k_f} and Da_{k_r} on the pH at the islet surface are shown in Figure 7.5 and Figure 7.6, respectively. The higher the Da_{k_f} or the lower the Da_{k_r}, the lower the pH is during culture. This trend is consistent across all culture conditions and independent of which base case values are used. Further, the shape of the profile for each individual case does not changed significantly with Da_{k_f} or Da_{k_r}, it just shifts up or down.

$Da_{Lac-Am} > 0$, when lactate production exceeds ammonia production indicating a net production of H^+, causes pH to continually decrease with time. $Da_{Lac-Am} < 0$, a net removal of H^+, decreases the extent of which pH drops in the initial transient period after which it continually increases pH. At $Da_{Lac-Am} > 0.1$ a drastic decreases in the pH for all cultures was observed. When Da_{Lac-Am} is between -0.01 and 0.001 (i.e. lactate and ammonia production are similar) no large shifts in pH are observed after the initial transient period that results from CO_2 production (Figure 7.7). However, even within this range for Da_{Lac-Am} the pH during culture can be significantly below 7.4 for culture on polystyrene.

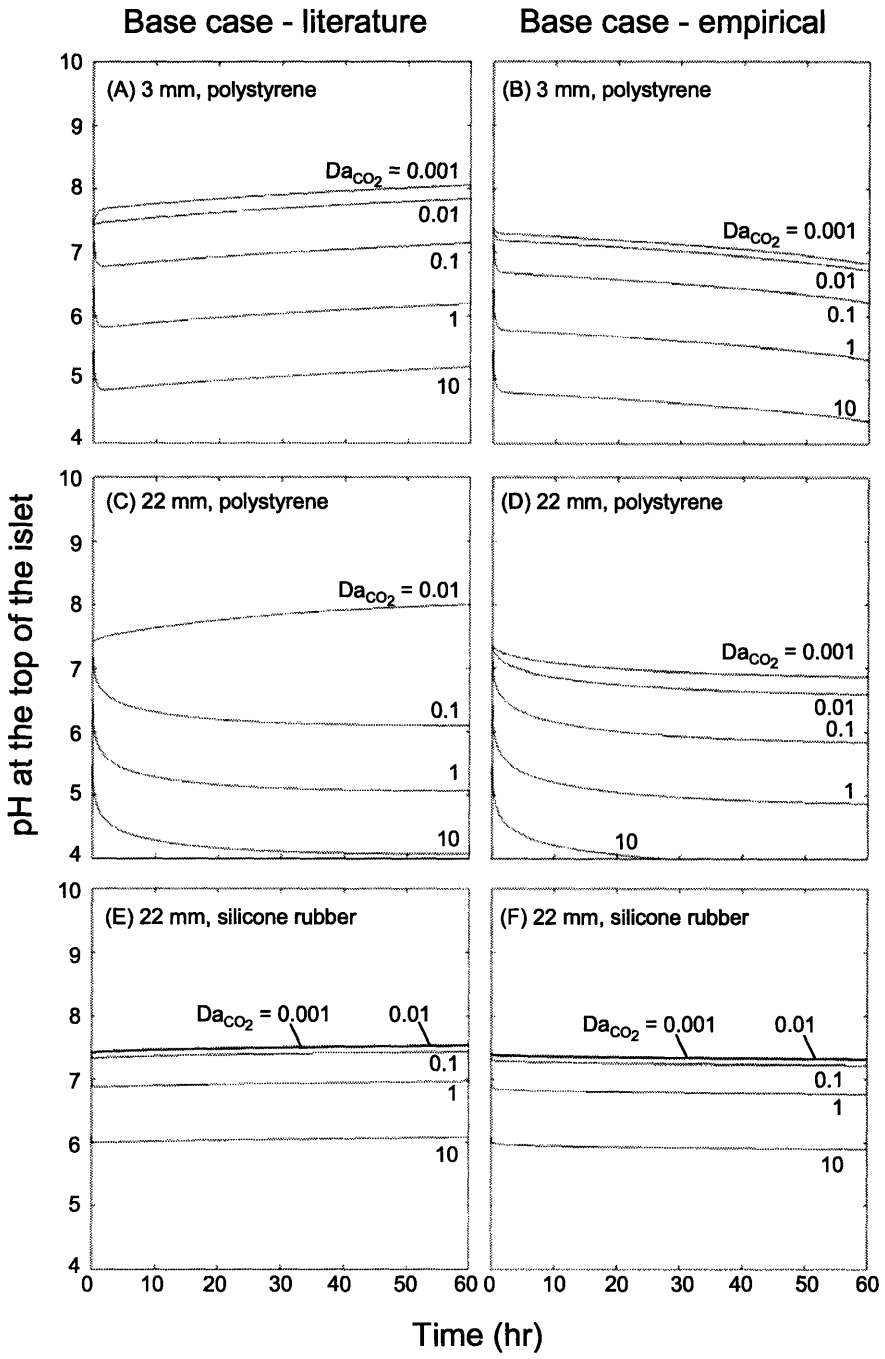

Figure 7.4. The pH at the top of the islet as a function of time and Da_{CO_2}.
Predictions for culture on polystyrene in 3 (A and B) or 22 (C and D) mm medium or on a 500-μm thick silicone rubber membrane in 22 mm medium (E and F) at an islet surface density of 4400 IE/cm^2. Plots are given using parameters from literature (A, C, and E) and using experimentally determined parameters (B, D, and F).

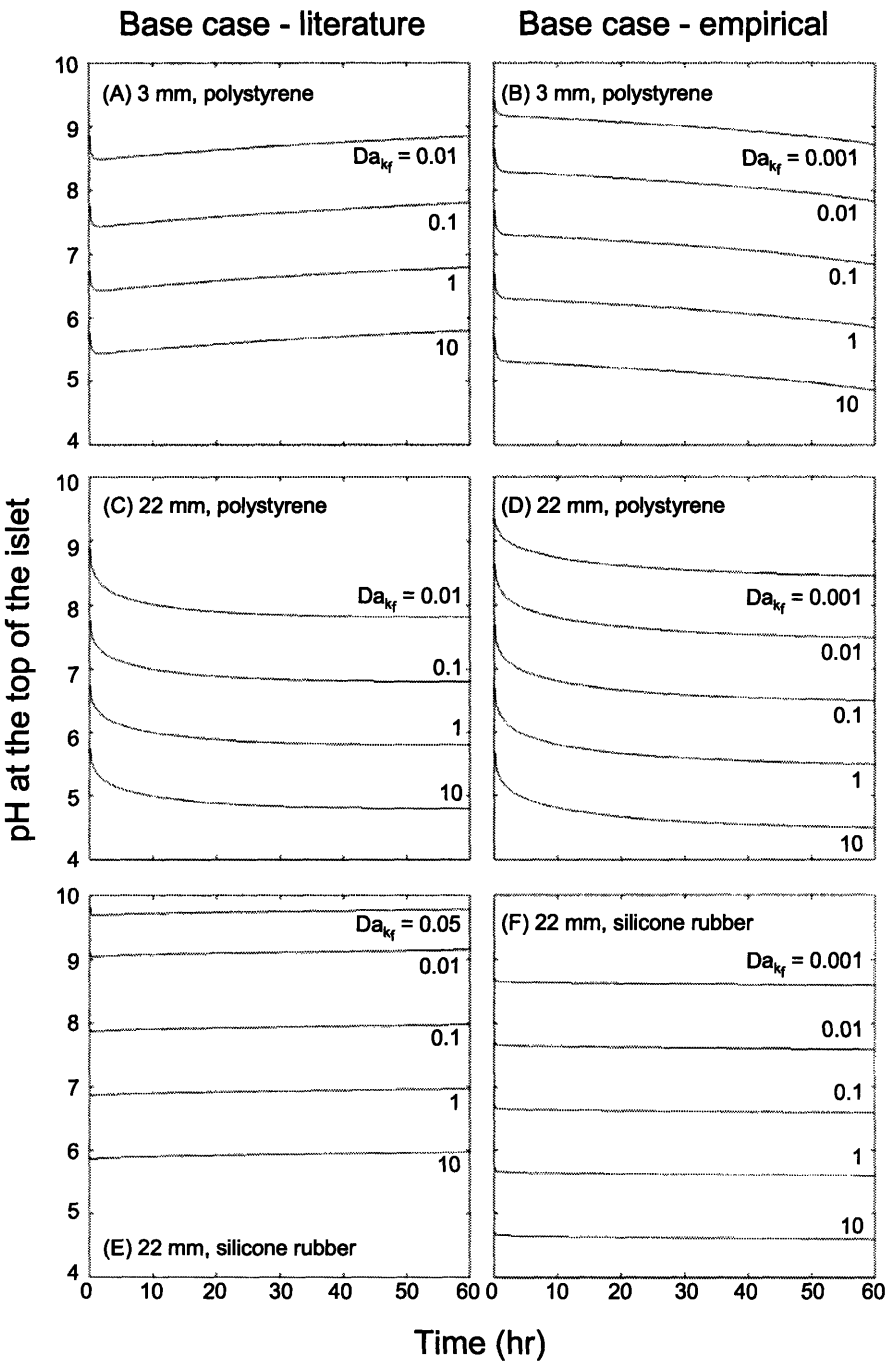

Figure 7.5. The pH at the top of the islet as a function of time and Da_{kf}.
Predictions for culture on polystyrene in 3 (A and B) or 22 (C and D) mm medium or on a 500-μm thick silicone rubber membrane in 22 mm medium (E and F) at an islet surface density of 4400 IE/cm^2. Plots are given using parameters from literature (A, C, and E) and using experimentally determined parameters (B, D, and F).

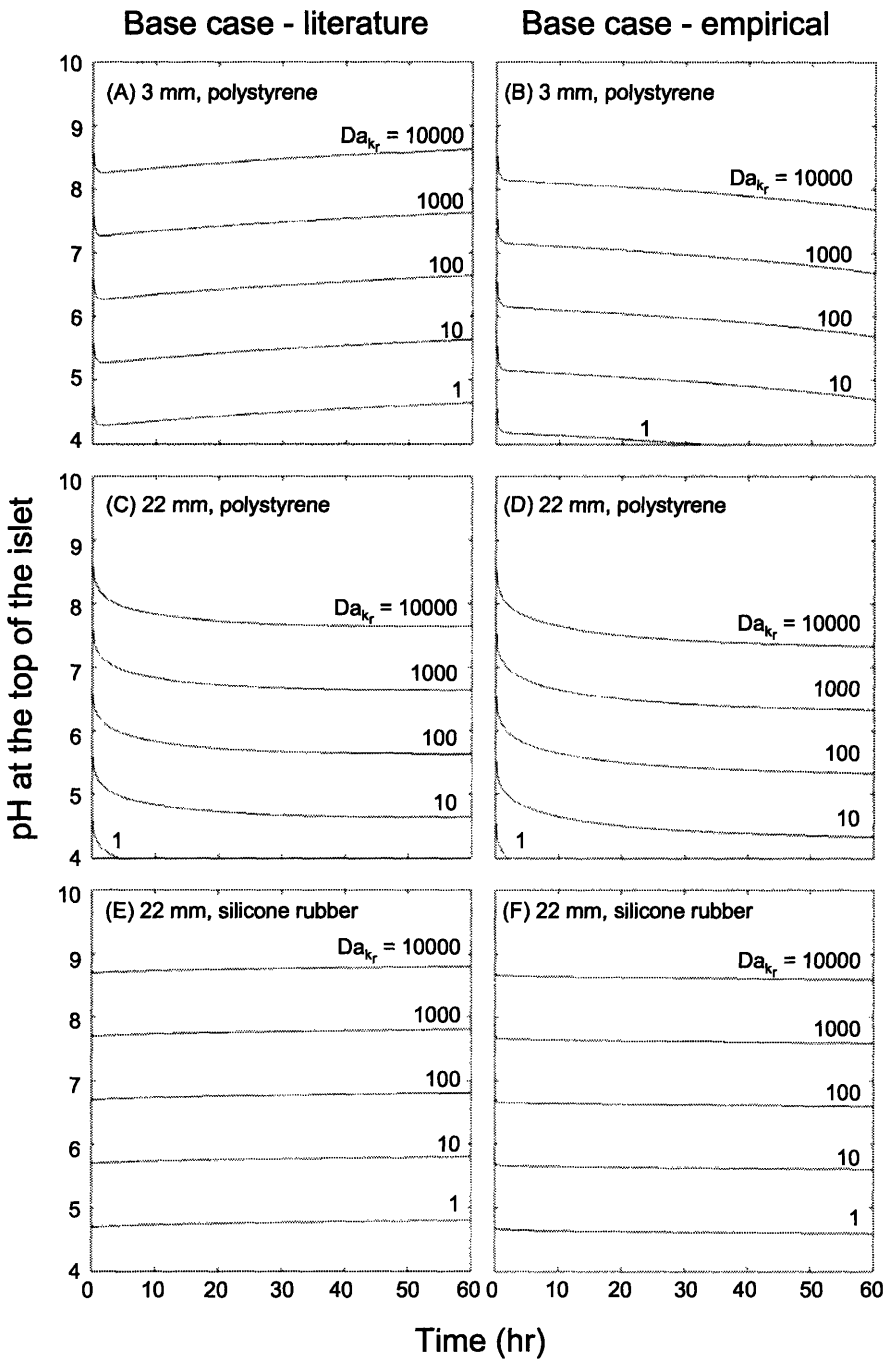

Figure 7.6. The pH at the top of the islet as a function of time and Da_{Kr}.
Predictions for culture on polystyrene in 3 (A and B) or 22 (C and D) mm medium or on a 500-μm thick silicone rubber membrane in 22 mm medium (E and F) at an islet surface density of 4400 IE/cm^2. Plots are given using parameters from literature (A, C, and E) and using experimentally determined parameters (B, D, and F).

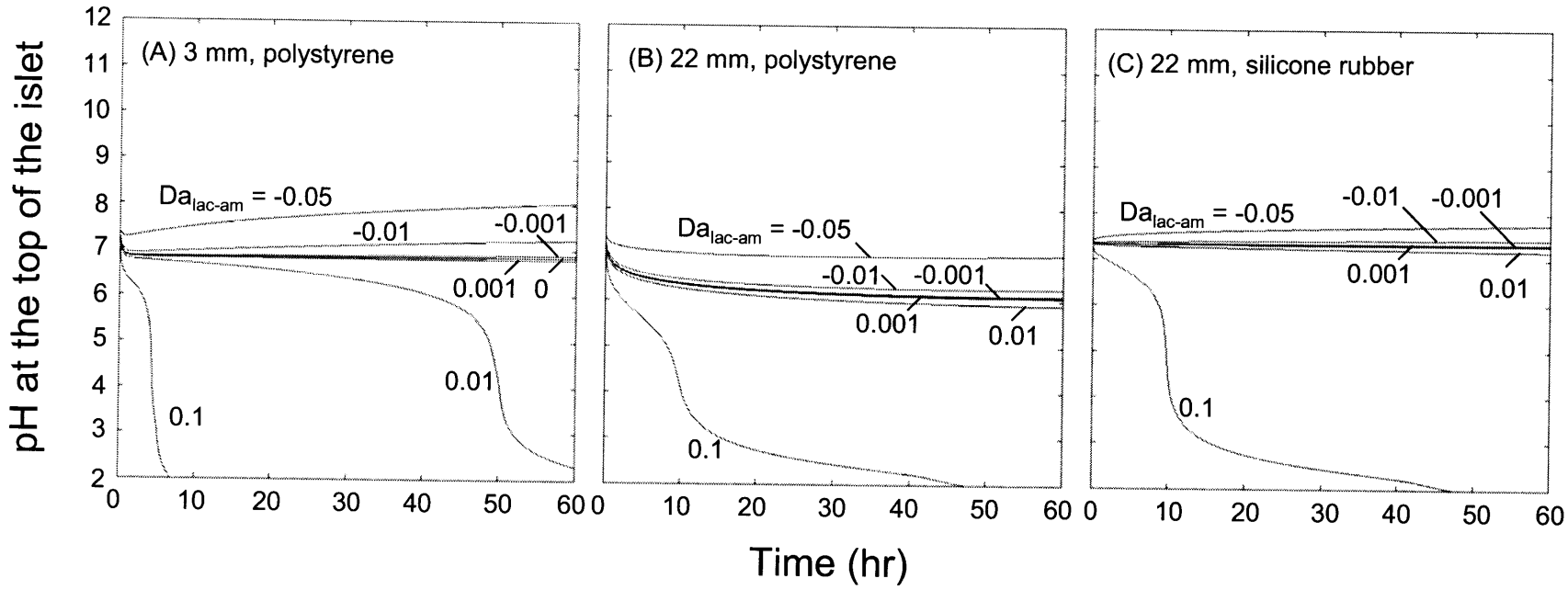

Figure 7.7. The pH at the top of the islet as a function of time and $Da_{Lac\text{-}Am}$.
Predictions for culture on polystyrene in 3 (A) or 22 (B) mm medium or on a 500-μm thick silicone rubber membrane in 22 mm medium (C) at an islet surface density of 4400 IE/cm^2. $Da_{Lac\text{-}Am} < -0.1$ caused problems within the theoretical model because negative H+ concentrations were observed. This problem could be avoided by modifying the code, but significantly more time and computation memory would be required.

7.6 Discussion

Significant changes in cellular processes occur with changes in pH [162-164]. Islet tissue has an "elevated sensitivity" to variations in pH [165], which can affect insulin secretion rates and ATP/ADP [163] and reduce viability [166]. A better understanding of how pH changes for various static culture techniques could reveal how medium composition or culture technique could be modified for optimal culture. In this study we developed and explored a theoretical model that predicts changes in local pH during islet culture to determine the extent to which pH could change during high density culture. The model took into account hydrogen ions, carbon dioxide, bicarbonate ions, lactate, and ammonia.

The pH profiles for polystyrene culture are strongly dependent on tissue surface density and the duration of culture. The pH at the islet surface changes significantly within 5 hours of culture whereas that at the surface of the medium and in the bulk does not shift to the same extent until much later (Figure 7.2) suggesting that monitoring surface or bulk pH gives an inaccurate representation of the pH in the tissue. Though pH shifts are significant during high density culture, they are greatly reduced at lower densities (Figure 7.3).

The four non-dimensional Damkohler numbers present in the model have a large impact on how pH changes during culture. Da_{k_f} and Da_{k_r} shift pH profiles up or down, but do not change the shape of the profile (Figure 7.5 and Figure 7.6). Changing Da_{k_f} and Da_{k_r} essentially changes the pKa of the bicarbonate buffer and the equilibrium of the bicarbonate reaction 7.2, but not the kinetics of the system. Da_{CO_2} has a large impact on the pH profiles especially within the first few hours of culture (Figure 7.4). The presence of CO_2 shifts the bicarbonate reaction 7.2 toward the presence of H^+ in solution lowering pH indicating that healthier tissue will cause a larger shift in pH. Unlike Da_{CO_2} (CO_2 production), Da_{Lac-Am} (lactate and ammonia production), which using the extremes of all available data could range from 0.15 to -0.15, cause pH to change continuously over the entire culture period (Figure 7.7). Thus an accurate CO_2 production rate is critical for predicting local pH throughout culture while accurate APR and LPR are most important at longer culture periods unless you are at extreme values (such as $Da_{Lac-Am} = 0.1$).

LPR measurements made within our lab were significantly higher than those previously reported [154; 155]. However, as with GCR values discussed in Chapter 6 previously reported values were for high purity rodent islet tissue as opposed to the human islet preparations used in this study, which contain a significant amount of exocrine tissue (non-islet tissue in the pancreas). Islet tissue normally has a low level of lactate dehydrogenase (LDH) suggesting a low LPR [119]. Non-islet tissue may have higher LDH expression resulting in higher LPR than islet tissue thereby increasing the overall LPR. Though this suggests a correlation with preparation purity none was observed. APR measurements were also higher than the previously reported value, but of the same order of magnitude suggesting that the method used for determining production rates was not an issue.

Based on data obtained in this study and Chapters 2 and 6 a species balance between oxygen, glucose, and lactate can be performed to see if the values we have found are consistent. The average oxygen consumption rate (OCR), glucose consumption rate (GCR), and LPR of human islets was roughly 3.68 x 10^{-8} mol/s cm^3 (Chapter 2), 5.55 x 10^{-8} mol/s cm^3 (Chapter 6), and 5.3 x 10^{-8} mol/s cm^3, respectively. The breakdown of glucose through glycolysis results in the production of two lactate molecules while that through the TCA cycle requires six oxygen molecules. Thus, assuming that glycolysis and the TCA cycle are the only cellular processes in which glucose is used, the GCR should equal the OCR divided by six plus the LPR divided by two. The GCR calculated using the OCR and LPR production rates is 3.3 x 10^{-8} mol/s cm^3, which is lower than the measured value in Chapter 6, but within its standard deviation, indicating consistency between OCR, GCR, and LPR.

As mentioned in Chapter 6 most islet centers culture at a total tissue volume equivalent to 570 "IE"/cm^2, where "IE" in this case is based on total tissue, not only islet tissue. Like the glucose (Chapter 6) and oxygen models (Chapter 3-5) the pH model accounts for the total tissue surface density. Thus all references to IE in all the figures indicate a total tissue volume, not islet volume specifically. The pH at the islet surface for culture on polystyrene in 3 mm medium is not likely to drop below 7.2 even after 60 hr culture at 500 IE/cm^2 (Figure 7.3). This indicates that drastic pH changes are not present during conventional culture. Further, though pH in the islet does shift below 7 during culture at large medium depths on polystyrene, these changes may be decreased since tissue will be oxygen starved resulting in decreased CO_2 production and decreased viability.

The fractional recovery of viable tissue decreases as surface density increases for culture on a silicone rubber membrane due to limitations independent of oxygen (Chapter 4). Based on the data presented here, changes in pH are also unlikely to cause the empirically observed decrease. Culture on a silicone rubber membrane keeps pH near 7.4 by allowing CO_2 to escape the system at a much faster rate thereby preventing the buildup of CO_2 in medium, which in turn prevents the bicarbonate reaction from shifting to more acidic conditions. Therefore significant changes in pH only occur if LPR is significantly larger than APR or vice versa (Figure 7.7).

In summary, the theoretical predictions indicate that islet tissue can be exposed to pH significantly different than the physiological value of 7.4 during high density culture on polystyrene. Based on data in literature, these pH shifts could cause changes in cellular rates leading to a decrease in viability. However, standard clinical culture and culture on a silicone rubber membrane are unlikely to result in large shifts in pH.

7.7 Nomenclature

APR	Ammonia production rate
CO_2	Carbon dioxide
d	Diameter of islet
Da	Damkohler number, measure of rate of reaction relative to rate of diffusion
Da_{CO_2}	Da for the production of CO_2
Da_{k_f}	Da for the forward reaction producing bicarbonate
Da_{k_r}	Da for the reverse reaction producing bicarbonate
Da_{Lac-Am}	Da for the lactate minus ammonia production rates
F_V	The fraction of original viable tissue after culture
GCR	Glucose production rate
h	Medium depth
H	Non-dimensional medium depth, h/R_{islet}
H^+	Hydrogen ion
HL	Lactic acid
IE	Islet equivalent

K	Ionization constant for carbonic acid
k_{-1}	First-order dehydration reaction rate constant
k_f	First-order hydration reaction rate constant
k_r	Second-order reverse reaction rate constant
Lac^-	Lactate ion
LPR	Lactate production rate
NH_3	Ammonia
NH_4^+	Ammonium ion
OCR	Oxygen consumption rate
R_{islet}	Radius of islet
t	Time
V_{max}	Maximum reaction velocity
w	Center-to-center distance between islets
x	Axis in Cartesian coordinates
X	Non-dimensional axis in Cartesian coordinates, x/R_{islet}
y	Axis in Cartesian coordinates
Y	Non-dimensional axis in Cartesian coordinates, y/R_{islet}
z	Vertical axis in Cartesian coordinates
Z	Non-dimensional vertical axis in Cartesian coordinates, z/R_{islet}
α	Solubility of CO_2 in medium
δ	Thickness of silicone rubber membrane
η	Non-dimensional concentration
τ	Non-dimensional time
χ	Cell surface density (cells/cm^2)

Subscripts for D, α, p, C

CO_2	Carbon dioxide
H^+	Hydrogen ions
HCO_3^-	Bicarbonate ions
i	Islet tissue

j	Reference to any species
Lac^-	Lactate ion
m	Medium
$NH4^+$	Ammonium ion
Si	Silicone rubber

8 Improvements in islet transportation

8.1 Introduction

The quality of shipped islet tissue, which varies widely between islet centers and within some islet centers [26], depends on specific pancreas characteristics, isolation process, culture following isolation, and shipment of the tissue. Isolation and pre-isolation variables cause much of the variation since the success rate for isolation ranges from 25-75% even within expert islet centers [27]. Centralization of islet isolation will attempt to reduce some variation between preparations allowing centers that most frequently produce high quality islet preparations to supply researchers and hospitals thereby making efficient use each pancreas [174]. However, in order for islet transplantation to be applied on a large scale, there needs to be the ability to transport large amounts of high quality tissue without loss in viability and/or function from these centralized islet isolation facilities.

Maintaining islet viability and function during shipment poses significant challenges. The current shipping method involves placing islet tissue in an oxygen-impermeable container (i.e. a flask or centrifuge tube), which is filled with medium, sealed, and placed in a Styrofoam box for shipment at room temperature. Though this is perhaps the easiest method there are several problems with it. First, even though the tissue is in a Styrofoam box, exposure to extreme temperature variations (often reaching below freezing during ground or flight transportation) have been recorded in several shipments originating from the University of Minnesota (K. Papas, personal communication), which could irreversibly damage islets. Another problem with the current shipping method is that the islet tissue is sealed in an oxygen-impermeable flask preventing the replenishment of oxygen (O_2). Depending on the amount of tissue, its respiration rate, and the duration of shipment portions may be exposed to hypoxia, which could result in a decrease in viability and function (Chapter 3 and 4, [16]). A shipment at 25°C in 300-ml culture medium (similar to a T-75 flask), which has an O_2 solubility at 25°C of 1.6×10^{-9} mol/cm^3 mmHg [16], contains 77 μmol O_2, enough O_2 to supply 34,000 islet equivalents (IE) for 24 hr (assuming OCR at 37°C 2.5 fmol/min cell (Chapter 2), 1560 cell/IE [13], OCR at 25°C is 40% of that at 37°C Chapter 4). However, this is likely a gross overestimate since transport limitations, which are significant during culture on polystyrene (Chapter 3), are ignored. Further, for transplantation purposes large numbers of islets

(100-500K) may need to be shipped, which if done using the current method, could expose tissue to severe hypoxia resulting in a large loss in viability.

There is a need for a method that will allow large numbers of islets to be transported for 24 hours with minimal loss of viability and function. In this chapter we discuss a controlled environment container that actively maintains temperature and O_2 level during shipment that was developed and tested in collaboration with Giner, Inc., and the University of Minnesota. An inexpensive alternative shipping method is proposed and feasibility is determined through preliminary experiments and theoretical calculations.

8.2 Giner, Inc., controlled environment container

Giner, Inc., in collaboration with MIT and University of Minnesota, developed a shipping container that controls temperature using thermoelectric heating and cooling, and controls O_2 level using an electrochemical O_2 generator. Oxygen is transferred continuously to the islet tissue throughout shipment through the use of silicone rubber bottom flasks. Similar vessels have been shown to be beneficial for high density culture (Chapter 4 and [60]). We hypothesized that these improvements would maintain a higher tissue quality during shipment than the conventional shipping method. To test this we conducted a shipping experiment comparing islet tissue shipped in the controlled environment container to islet tissue shipped in a Styrofoam box.

8.2.1 Methods

Experimental protocol

Following 48-hour culture human islets isolated at the University of Minnesota were sent to MIT overnight in either a T-25 flask within a Styrofoam box or in the Giner, Inc., controlled environment shipping container set at 72°F with a gas phase 40% O_2. The amount of tissue and CMRL 1066 medium (Miami formulation, Mediatech Inc.) with 10% FBS (Mediatech Inc.) in each vessel is given in Table 8.1. The manual IE counts were performed at the University of Minnesota. The human islet tissue was analyzed at MIT upon receipt.

DNA content

At MIT, DNA was measured by fluorospectrophotometry [55] using the CyQUANT Cell Proliferation Assay Kit (Molecular Probes, C-7026 Eugene, OR), and a λ DNA standard (Invitrogen) and 50-250 IE/sample. Fluorescence was read at 480 nm excitation and 520 nm

emission wavelengths in a plate reader (Spectra MAX Gemini microplate spectrophotometer, Molecular Devices, Sunnyvale CA).

Islet enumeration by nuclei counting

Nuclei were prepared by adding equal 100-µl volumes of sample containing 160 or more IE and of lysis solution (0.1 M citric acid (Sigma) and 1% (v/v) Triton X-100 (Sigma)) to a 1.5 ml microtube [55]. The mixture was incubated at room temperature for 5 min with vortex mixing every 1.5 min, and nuclei were liberated by shearing through a needle. Isolated nuclei were diluted with Dulbecco's phosphate buffered saline (D-PBS, Invitrogen, Carlsbad, CA) to a concentration no higher than 5 x 10^5 nuclei/ml, stained with 7-aminoactinomycin D (7-AAD, Molecular Probes, Eugene, OR), and analyzed using a flow cytometer (Guava Personal Cell Analysis (PCA) system, Guava Technologies, Hayward, CA) to determine the total number of cells with intact nuclei in the sample.

Oxygen consumption rate (OCR)

OCR was measured as previously described [39]. Briefly, suspensions containing about 2500 IE/ml in DMEM containing 4.5 g/l glucose and 0.6 g/l L-glutamine supplemented with 100 U/ml penicillin, 100 µg/ml streptomycin, 10 mM HEPES, and no added serum were sealed in a 200-µl stirred titanium chamber (Micro Oxygen Uptake System, FO/SYSZ- P250, Instech Laboratories, Plymouth Meeting, PA) maintained at 37°C. The time dependent pO_2 within the chamber was recorded with a fluorescence-based oxygen sensor (Ocean Optics, Dunedin, FL), and data at high pO_2 were fit to a straight line. The maximal OCR was evaluated from $OCR=V_{ch}\alpha(\Delta pO_2/\Delta t)$, where V_{ch} is the chamber volume and α = 1.27 nmol/mm·Hg·ml is the Bunsen solubility coefficient for oxygen in medium [16]. OCR measurements were normalized by the measured number of cells (nuclei counting) or DNA content of the sample examined.

Membrane Integrity

7-Aminoactinomycin (7-AAD) sequential staining

Cell membrane integrity was assessed by differential staining with 7-AAD (Molecular Probes, Eugene, OR) [55]. An aliquot of about 300 islets was re-suspended in 100 µl of D-PBS, and 5 µl of 1 mg/ml 7-AAD and incubated for 20 min at 4°C protected from light. After two washes with 1 ml of D-PBS, cells were disrupted by adding equal volume of lysis solution in D-PBS to the islet suspension and sheared as described for islet enumeration. Labeled nuclei

were counted immediately in the flow cytometer or stored on ice for less than 15 min before counting. A portion of the islet suspension was further stained with 7-AAD, thereby labeling all of the previously unlabelled nuclei, and the total number of nuclei was counted. The fraction of cells with compromised membranes was estimated as the ratio of the initially stained nuclei (first measurement) to the total number of nuclei (second measurement).

Fluorescein diacetate (FDA)/propidium iodide (PI)

Immediately after human islet isolation was completed, a 250 µl aliquot was taken from the preparation, re-suspended in 5 ml of PBS solution in a 60 mm Petri dish, and 10 µl of 24 mM fluoroscein diacetate (FDA) and 750 µM propidium iodide (PI) was added [58; 62]. The tissue was examined in a light microscope by focusing through the tissue to visually estimate the volume fraction of cells containing nuclei stained red because of loss of membrane integrity.

Statistics

Measurements were made with three or more replicates and reported as mean ± SD. Statistical significance was determined using a Student t-test for unpaired data for comparing population means, and for paired data when appropriate.

8.2.2 Shipment results

Approximately 24 hours after leaving the University of Minnesota, the containers arrived at MIT. The majority of tissue had collected in a 1-2 mm thick mass along the edge of the silicone rubber bottom flask in the controlled environment (Figure 8.1). Because of the size of the flask the tissue could not be observed under the microscope while in the culture vessel. The islets from the T-25 flask in the Styrofoam box were not piled together, but fragmented and suspended in medium with a significant amount of single cells (Figure 8.2).

The total amount of tissue in each container was estimated through DNA quantification and nuclei counting (Table 8.2). Nuclei and DNA measurements indicated a 40% and 80% higher fraction of original tissue collected after shipment in the controlled environment than observed for a solid flask in a Styrofoam box. DNA content of tissue shipped in the controlled environment was also higher than in the Styrofoam container.

Membrane integrity was measured using two assays: sequential nuclei staining with 7AAD and islet vital staining with FDA/PI. Based on 7AAD nuclei staining the tissue shipped in the Styrofoam box had a fraction of cells with intact membranes of 0.90 ± 0.03 while the tissue

shipped in the controlled environment had 0.93 ± 0.01. Though FDA/PI is not as quantitative, it revealed necrotic cores representing an estimated 10-30% of the tissue in large islets (most cases 200-μm or larger) from both shipment methods (Figure 8.3 and Figure 8.4). Smaller islets showed no necrotic cores.

OCR/cell, OCR/DNA, total OCR, and the relative recovery of original viable tissue from each shipment are reported in Table 8.3. The OCR/cell was statistically higher for tissue shipped in the controlled environment compared to the Styrofoam box, a trend similar to that for OCR/DNA though no significance is observed. The total OCR recovered from the silicone rubber bottom vessel was 20 times that from the solid flask though it had only 10 times more viable tissue prior to shipment. The resulting relative fraction of original viable tissue remaining after shipment, where that collected from the controlled environment is set to 1, was 0.49 for the Styrofoam box (Table 8.3).

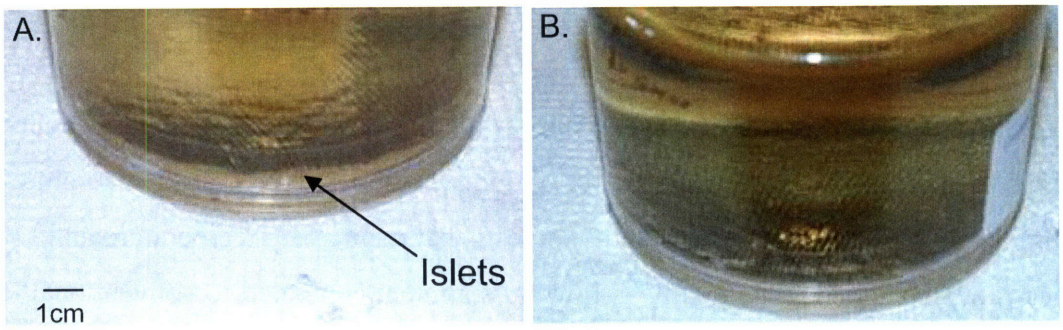

Figure 8.1. (A) Islets piled along the edge in the silicone rubber bottom vessel sent in the controlled environment container. (B) Opposite side of the same culture vessel.

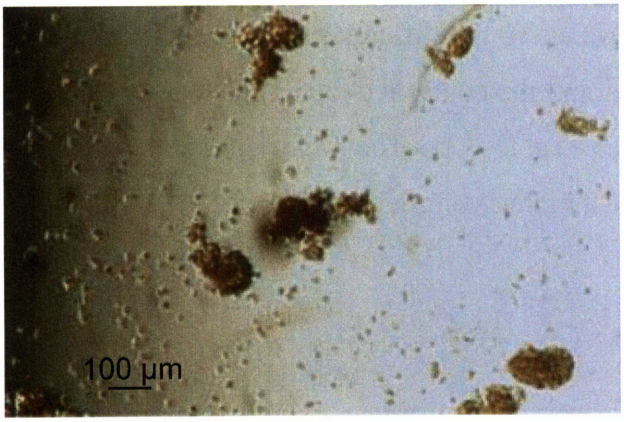

Figure 8.2. Islets following shipment in a solid flask in a Styrofoam box overnight.

Figure 8.3. Staining of islets shipped in solid flask in a Styrofoam box.
From left to right the pictures are with white light, PI staining, and FDA staining.

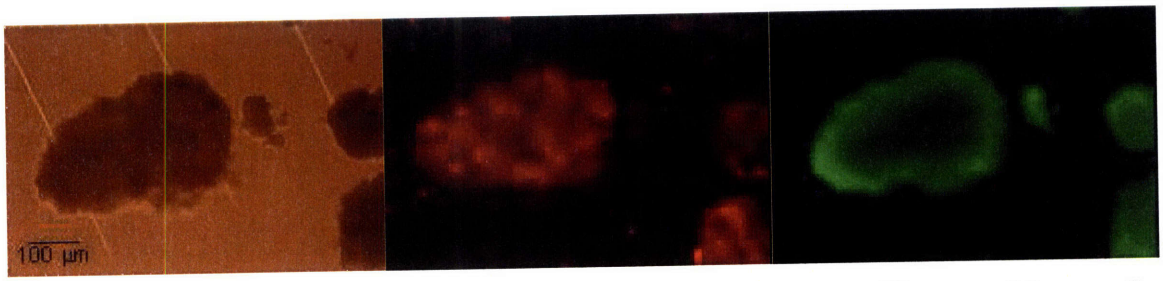

Figure 8.4. Staining of islets shipped in controlled environment on silicone rubber surface.
From left to right the pictures are with white light, PI staining, and FDA staining.

8.2.3 Discussion

In this study we compared islet tissue shipped in a plastic flask within a Styrofoam container to that shipped in a silicone rubber bottom vessel at a controlled temperature and O_2 concentration. This experiment tested the hypothesis that controlling temperature and O_2 during shipment results in higher tissue quality following shipment compared to conventional shipping methods.

Tissue surface density is a key parameter that determines tissue viability following culture (Chapter 3 and 4). Due to the difference in vessels and a miscommunication, the tissue sent in the Styrofoam box and the controlled environment was at different surface densities and different volume densities (Table 8.1). The tissue in the controlled environment had both a higher surface density and a higher volume density.

Table 8.1. Conditions for islets shipped in the silicone rubber bottom vessel within the controlled environment container and in the solid T-25 flask in the Styrofoam box.

Culture vessel	Total IE	Medium volume (ml)	Surface area (cm^2)	Islet concentration (IE/cm^3)	Islet surface area (IE/cm^2)
Silicone rubber bottom vessel	100,000	~500	100	200	1,000
Solid flask	10,000	~100	25	100	400

Table 8.2. Total tissue estimation for islets received from both the silicone rubber bottom vessel and in the solid flask.

Culture vessel	Total IE[a]	Nuclei count (x 10^6 nuclei)	DNA content (x 10^4 ng)	DNA/nuclei (pg/nuclei)	Recovery based on DNA[b]	Recovery based on nuclei[b]
Silicone rubber bottom vessel	100,000	99.3	99.4	10.0	0.98	0.64
Solid flask	10,000	7.07	5.46	7.73	0.54	0.45

[a]**Manual IE counts conducted at the University of Minnesota prior to shipment.**

[b]**Assumes that there are 1560 nuclei/IE [13] and 6.5 pg DNA/cell [68].**

Table 8.3. OCR/cell, OCR/DNA, total OCR, and the relative recovery of original viable tissue collected from both the silicone rubber and solid bottom dishes after transportation.

Culture vessel	Total IE[a]	OCR/nuclei (fmol/min cell)	OCR/DNA (nmol/min mg DNA)	Total OCR received (nmol/min)	Relative recovery of viable tissue[b]
Silicone rubber bottom vessel	100,000	*2.05 ± 0.10	205 ± 17	204 ± 10	1.0
Solid flask	10,000	1.40 ± 0.16	181 ± 20	10 ± 1	0.49

[a] Based on manual IE counts conducted at the University of Minnesota prior to shipment.
[b] Sets original viable tissue collected from the shipment in the controlled environment to 1.
* indicates statistical significance ($p<0.05$) compared to solid flask.

[a] Manual IE counts conducted at the University of Minnesota prior to shipment.

[b] Sets original viable tissue collected from the shipment in the controlled environment to 1.

*** indicates statistical significance ($p<0.05$) compared to solid flask.**

Despite the higher surface and volume densities, shipping in the controlled environment had several beneficial effects. It increased tissue recovery 40 to 80% from that obtained with the traditional method based on nuclei and DNA measurements (Table 8.2), respectively. OCR/cell was higher for tissue shipped in the controlled environment compare to the Styrofoam container indicating an increased viability (Table 8.3). OCR/DNA indicated a similar trend, but the difference was not significant. The reason for this discrepancy is indicated by the difference in DNA content. The DNA content was higher for the islets shipped in the controlled environment (10 pg/cell) as opposed to those shipped in a solid flask (7.7 pg/cell, Table 8.2), which had a DNA content closer to the expected value of 6.5 pg/cell reported in literature [68]. DNA content > 6.5 pg/cell is indicative of cells that have died, broken down the nucleus, and released their DNA, but the DNA has not yet degraded. Though this suggests that the tissue in the controlled environment has been damaged, tissue recovery and viability measurements (membrane integrity, OCR/cell, and OCR/DNA) are at least as good if not higher than that of tissue from the Styrofoam box.

Total OCR, which indicates the total amount of viable tissue, was the most encouraging. When converted to the relative fraction of viable tissue recovered after shipment, it indicated that shipment in the controlled environment resulted in double the amount of viable tissue after shipment compared to the Styrofoam box even though it was shipped at a higher surface density (Table 8.3). Thus controlling temperature and O_2 level throughout shipment results in a 100% increase in the fraction of original viable tissue collected after shipment compared to the conventional shipping method.

Though shipment in the controlled environment resulted in higher tissue recovery, viability, and viable tissue recovery than the Styrofoam container, it still can be improved. As indicated by islet vital staining necrotic cores developed in larger islets in both containers. Necrotic cores usually result from nutrient transport limitations at the center of the islet (Chapter 3 and [16]). In previous studies O_2 has been shown to be the limiting nutrient for islets in culture on polystyrene (Chapter 3). Though O_2 limitations were expected for islets shipped in a Styrofoam container they were not expected for the islets on a silicone rubber membrane since O_2 transport through the membrane allows islets at high surface densities to maintain a higher viability than they otherwise could on a plastic dish (Chapter 4). There are at least three possible explanations that could account for the necrotic cores observed in islets on the silicone rubber

bottom dish. First, the mass of tissue that had accumulated on one side of the flask prior to receipt (Table 8.1) could have increased O_2 limitations to the point where portions were exposed to hypoxia as was indicated in Chapter 5 for stacked islets on a silicone rubber membrane. Second, glucose or some other nutrient could become limiting at high surface densities when O_2 limitations have been removed as shown in Chapter 6.

In summary, despite the significantly higher islet surface density in the controlled environment the fraction of original tissue, OCR/cell, and relative fraction of original viable tissue collected after shipment was significantly higher in the silicone rubber bottom flask within the controlled environment compared to a plastic flask within a Styrofoam box demonstrating that the controlled environment container is a substantial improvement for islet transportation.

However, the controlled environment device is large, weighs about 30lbs, requires battery operation, and would expensive for isolation centers to buy. Thus, even though it improves the quality of tissue following transportation, it is not a feasible option for most islet centers. As a result, an inexpensive alternative to this actively controlled environment is desirable. The alternative container should eliminate large temperature swings and provide sufficient O_2 throughout shipment like the Giner, Inc., device, but it should be less cumbersome, easier to use, and less expensive.

8.3 Passive shipping device

The controlled environment container developed by Giner Inc in collaboration with the MIT and the University of Minnesota prevented large temperature swings, generated O_2, and allowed the generated O_2 to be transported to the tissue throughout shipment. Here we propose a passive shipping container that will perform similar functions, but be much smaller, significantly less expensive, and require no battery for operation. The passive shipping device proposed is illustrated in Figure 8.5. Like the Giner, Inc., controlled environment container it uses a culture vessel with a silicone rubber bottom to allow transport of oxygen from the surrounding environment to the tissue throughout shipment. However, instead of using thermoelectric heating and cooling it utilizes phase change materials (PCMs) to control temperature during shipment. Using theoretical calculations and proof of concept experiments we demonstrate the feasibility of the modified container, which can be used as a basis for future work.

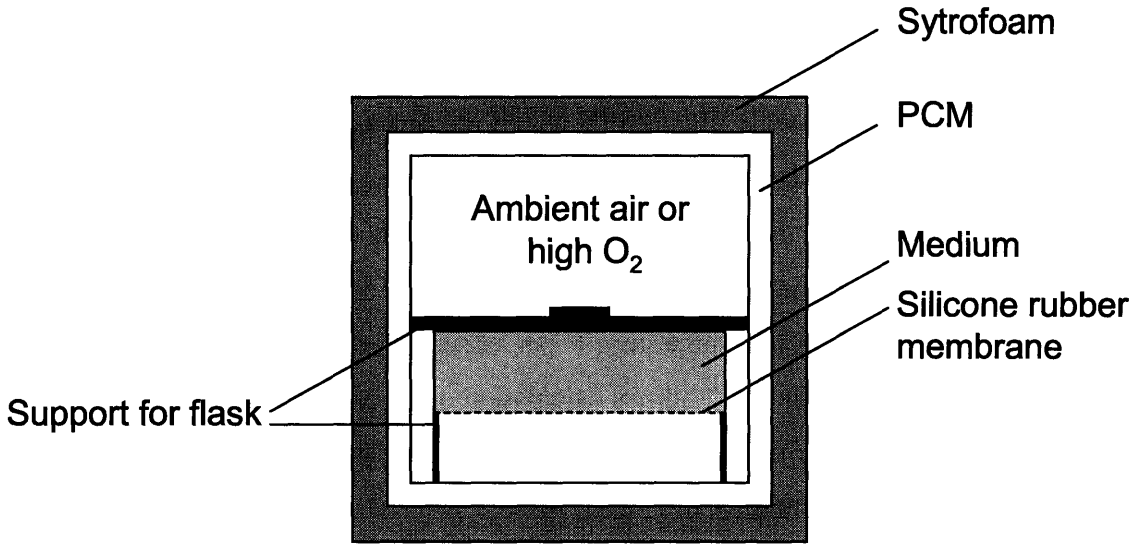

Figure 8.5. Schematic of passive shipping device that will provide sufficient oxygen and maintain temperature during shipment.

8.3.1 Oxygen

The amount of tissue, shipment temperature, and transport limitations within the shipping device determine the O_2 requirements needed to keep tissue viable during shipment. Here we consider several possible shipping conditions to determine what limitations our passive shipping container may have with regards to O_2 supply.

Islet tissue cultured on a 100 to 500-μm thick silicone rubber membrane at 37°C 142 mmHg O_2 maintains viability until an OCR density of 5 nmol/min cm^2 above which the fraction of original viable tissue after culture decreases due to limitations other than O_2 (Chapter 4). Thus by utilizing vessels with silicone rubber membrane bottoms, we can ship at OCR densities $\leq$ 5 nmol/min cm^2 or, assuming that tissue has an OCR of about 2.5 fmol/min cell (Chapter 2), 1280 IE/cm^2. In order to ship islets from an entire isolation containing a tissue volume equivalent to 500,000 IE a surface area of 400 cm^2 is needed.

The OCR of islet tissue decreases exponentially as inverse temperature increases following the equation

$$V_{max} = V_o \cdot e^{-\frac{E}{RT}} \qquad \textbf{8.1}$$

where V_o is 1.86 x 10^3 mol/min cm^3, E is 53 kJ/mol, and R is the gas constant (0.008314 kJ/mol K) (Chapter 4). Assuming the container holds temperature throughout

shipment, the amount of O_2 required for differing amounts if islet tissue over a given shipment period were estimated using Equation 8.1 as indicated in Figure 8.6 for a 36 hr shipment. At 37°C a tissue volume equivalent to 500,000 IE would require 4.2 mmol of O_2 which, if an ideal gas, is 108 cm^3 of pure O_2 at 1 atm or 520 cm^3 of air containing 20.9% O_2. Lower temperatures and shorter times make the requirements for adequate O_2 supply even less.

Additionally, the partial pressure of O_2 (p) in the container should not fall below 142 mmHg thereby ensuring the same results as observed previously with silicone rubber membranes (Chapter 4). Equation 8.2 allows calculation of the volume of the gas phase required in order to have enough O_2 for tissue consumption and that the pO_2 within the container does not drop below 142 mmHg (assuming O_2 is an ideal gas).

$$V = \frac{n_{islet} R_{gas} T}{p_{initial} - p_{end}} \qquad \textbf{8.2}$$

where n_{islet} is the O_2 required by the tissue during shipment (Figure 8.6), R_{gas} is the gas constant, T is the temperature inside the container, V is the gas phase volume in the container, p_{end} is the desired ending pO_2 in the container after shipment (142 mmHg), and $p_{initial}$ is the initial pO_2 in the container. If 500,000 IE were shipped, which requires 4.2 mmol O_2 for consumption over 36 hr, a 4.8 L volume of ambient air (159 mmHg, 20.9% O_2) or 0.6 L of a 40% O_2 mixture is needed within the shipping container to ensure that the pO_2 in the container would not drop below 142 mmHg.

8.3.2 Temperature

Phase change materials (PCMs) are materials that absorb or liberate heat at constant temperature as the material changes from solid to liquid or vice versa. Ice packs are PCMs designed to operate at 0°C. Though several PCMs are available commercially, we will consider PCMs available from TCP Reliable and PCM Energy P. Ltd. that range in phase change temperature from 18-36°C (Table 8.4) [175; 176].

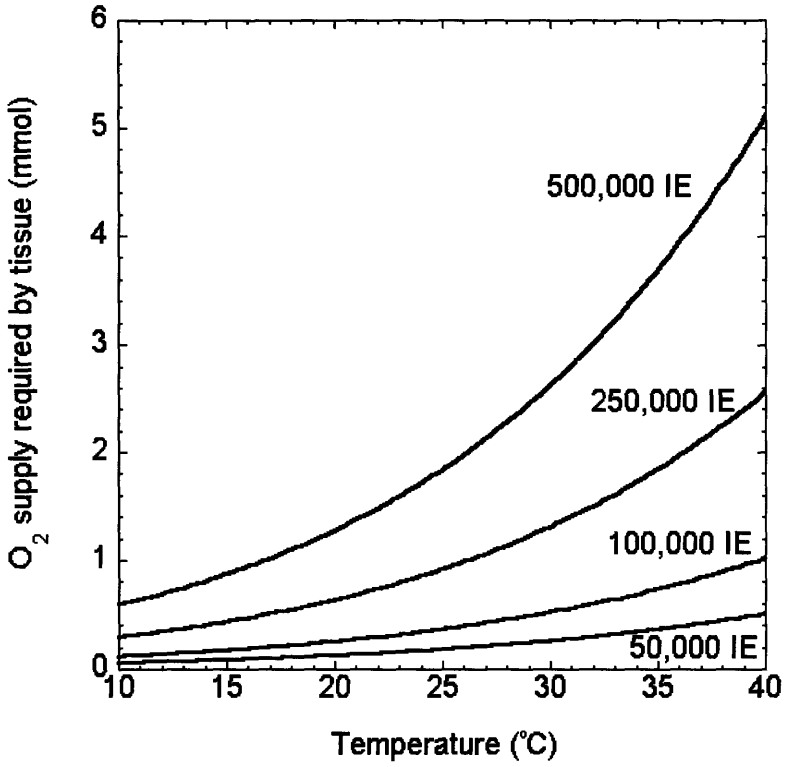

Figure 8.6. The amount of O_2 consumed by 50,000-500,000 IE for 36 hr at temperatures ranging from 10 to 40°C.

Table 8.4. Commercially available phase change materials and their properties.

Product	Phase Change Temperature (°C)	Latent heat (J/g)	Thermal conductivity (Watt/m °C)	Specific Heat (J/g °C)	Specific gravity
PCM Energy P. Ltd.					
Latest™18T	17-19	175	1	2	1.48-1.50
Latest™20T	19-20	175	1	2	1.48-1.50
Latest™25T	24-26	175	1	2	1.48-1.50
Latest™25S	24-26	200	0.6	2	1.45
Latest™29T	28-30	175	1	2	1.48-1.50
Latest™30S	29-31	230	0.6	2	1.45
Latest™36S	34-36	260	0.6	2	1.45
TCP Reliable					
Phase 22	22	-	-	-	-
Exo-Gel	27	-	-	-	-

Information taken from [175; 176].

Simple theoretical calculations can determine whether it is feasible to control the temperature inside our container for 24 hr with PCM. For simplicity assume the temperature

inside (i.e. the phase change temperature) and surrounding the container are constant throughout shipment and that the PCM thermal conductivity is negligible compared to the Styrofoam box, which is 3 inches thick (thermal conductivity of 0.033 W/m K [118]). The heat flux through a one-dimensional solid is calculated using Fourier's law (8.3) [97].

$$q = k\nabla T = k\frac{dT}{dx} \qquad \textbf{8.3}$$

where T is temperature, q is the heat flux, and k is the thermal conductivity.

The volume of the void space in the container needs to be 4.8 L as determined above for 500,000 IE, which also requires a vessel with a silicone rubber bottom surface area of 400 cm^2 and a 2.2 cm medium depth (medium depth used in study with silicone rubber dishes Chapter 4) for a total medium volume of 0.88 L. To be safe assume that 1.5 L is large enough to account for the vessel containing the tissue, the tissue itself, and the medium within the vessel. Thus the cargo space of the container needs to be about 6.3 L (25 cm x 25 cm x 11 cm).

Now assume that for practical reasons no more than about 10 lbs of PCM (3.0-3.2 L) should be used such that the container weight stays manageable. If panels are used to cover all four sides, top, and bottom of the container, then a thickness of 1.2 cm is needed such that a volume of 3.2 L is held in the panels. For simplicity assume 2 cm thick panels to account for the material that contains the PCM. Thus the cargo space of the Styrofoam box is about 12.6 L (29 cm x 29 cm x 15 cm). If the thickness of the Styrofoam is 3 inches, then the dimensions of the box are about 44 cm x 44 cm x 30 cm resulting in a surface area of 9300 cm^2.

If we assume a constant heat flux (8.3) throughout shipment, the amount of PCM required to maintain the phase change temperature inside the container with a constant external temperature for a 24 hr shipment can be determined by 8.4.

$$\Delta H \cdot m = q \cdot \tau \cdot A \qquad \textbf{8.4}$$

where m is the mass of PCM, ΔH is the latent heat, A is the surface area of the container, and τ is the duration of shipment. Figure 8.7 illustrates the volume of PCM required as a function of the ambient temperature. Based on this simple analysis 3.2 L is a feasible amount of PCM for all phase change temperatures considered. The only case where the PCM would be unable to maintain temperature was when the ambient temperature is below 2°C for the entire shipment

and the desired container temperature was 36°C. Even in this case, the passive shipping device would still maintain temperature much better than the traditional Styrofoam box.

Preliminary experiments were conducted at constant temperatures to confirm experimentally that temperature control with PCM is feasible. A 27.5 cm x 23 cm x 20.3 cm Styrofoam box 1.5 inches thick was placed in a 37°C incubator overnight. HOBO 2K Temp Data Loggers were placed inside and outside recording temperature every 2 minutes. The data logger inside was sitting on the bottom of the box. Following incubation at 37°C the box was moved to 12°C. After overnight incubation at reduced temperature the data loggers were collected and the data analyzed. For some experiments a single Phase 22 PCM panel provided by TCP Reliable was added to the Styrofoam box. The panel was 13.2 cm x 13.2 cm x 2.5 cm and is estimated to contain 250-300 ml of Phase 22 PCM. When the PCM panel was added to the box the data logger inside the box was placed on top of the panel.

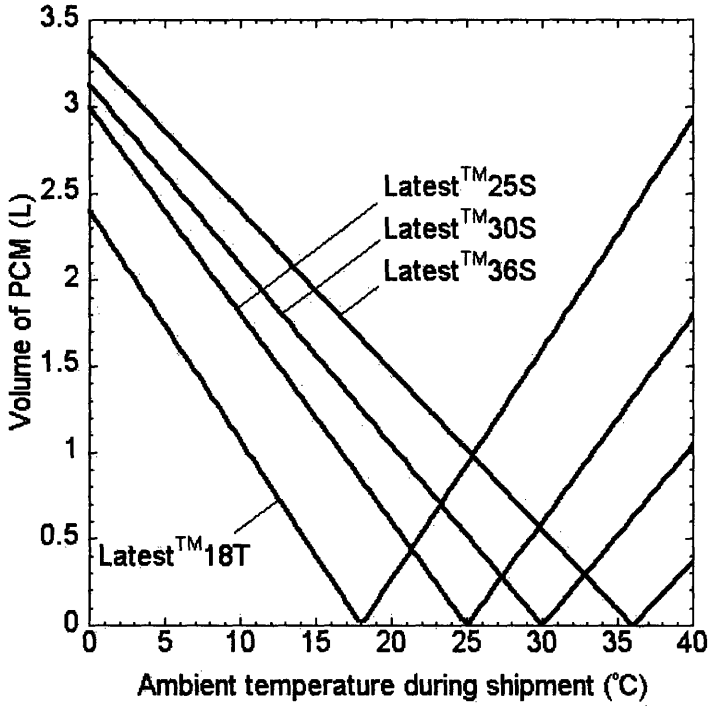

Figure 8.7. Volume of various PCMs required to maintain the phase change temperature of the container (18, 25, 30, or 36°C) for 24 hr during shipment at constant ambient temperature.

A sample temperature profile inside and outside the box when ambient temperature dropped to 12°C is given in Figure 8.8 for experiments with and without PCM. When PCM is used the temperature inside the container is maintained at 18-20°C for an extended period of time. Without PCM the temperature drops continuously until it reaches the ambient temperature. This proof of concept experiment demonstrates how PCM can be beneficial and how Styrofoam alone does not prevent temperature fluctuations.

Using Fourier's law the latent heat of the PCM can be calculated for these experiments. Based on data from three experiments, the Phase 22 PCM has a latent heat of about 900 ± 80 J/ml PCM. If the Phase 22 PCM has a specific gravity similar to the other PCMs in Table 8.4, then the latent heat would be about 600 J/g which is much higher than the latent heat listed for the other PCMs in Table 8.4. This large latent heat probably resulted from the over simplified assumptions of the calculation. For example, we did not account for the heat conduction though the PCM or from the Styrofoam through the air to the PCM.

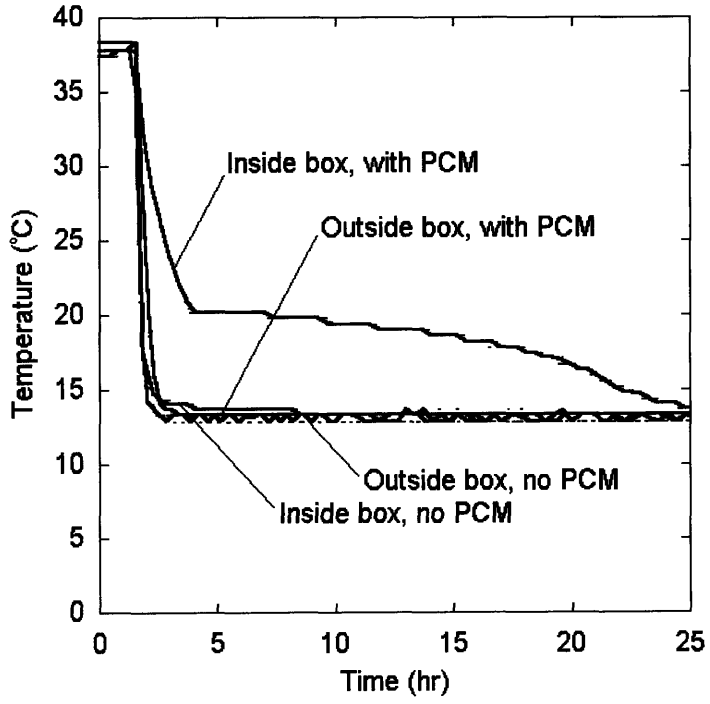

Figure 8.8. Sample profile for controlled PCM experiment.
Containers with and without PCM were equilibrated at 37°C before being transferred to a 12-14°C environment. Temperature inside and outside the container was monitored.

8.4 Conclusions

Temperature and O_2 control has beneficial effects on islet recovery and viability following shipment as demonstrated using the Giner, Inc., controlled environment container. The passive shipping device described has all the benefits of the Giner, Inc., controlled environment container, but is less cumbersome, less expensive, and does not require battery operation. As such further work is warranted to create a passive shipping device that can be used for transporting islet tissue.

8.5 Nomenclature

7-AAD	7-aminoactinomycin D
A	Surface area of the container
C	Concentration of O_2
D	Diffusivity of O_2
D-PBS	Dulbecco's phosphate buffered saline
E	Activation energy
FBS	Fetal bovine serum
FDA	Fluorescent diacetate
F_V	The fraction of original viable tissue after culture
IE	Islet equivalent
k	Thermal conductivity
LDH	Lactate dehydrogenase
m	Mass of PCM
N	O_2 flux
O_2	Oxygen
OCR	O_2 consumption rate
p	O_2 partial pressure
PCM	Phase change material
p_{gas}	Ambient partial pressure of O_2
PI	Propidium iodide
q	Heat flux

R	Gas constant
R_{islet}	Radius of islet
T	Temperature
t	Time
V	Volume
V_{max}	Maximum reaction velocity
V_o	Constant in Arrhenius equation
α	Solubility of O_2 in medium
ΔH	Latent heat
τ	Duration of shipment.

9 Conclusions and outlook

9.1 Maintaining islet quality during culture

This project was based on the hypothesis that islet tissue is exposed to oxygen transport limitations during conventional culture and shipment that result in decreases in viable tissue suggesting that removal of these limitations will improve the tissue quality after culture and/or shipment.

A detailed study investigating how tissue changes during culture in the absence of oxygen limitations was conducted providing a complete understanding of islet and non-islet tissue behavior prior to and during culture at 37°C and 24°C in terms of the recovery of tissue, it viability, and its purity. The portion most relevant to the remainder of the thesis relates to the cultured tissue. The data revealed that a significant amount of tissue adhered to the polystyrene surfaces. The adherent tissue fraction was shown to contain fewer β cells and decrease as tissue surface density increases. Though the data confirms current practice of not collecting adherent tissue for transplantation, it does give additional insight into changes the islet and non-islet tissue go through during culture that has not been shown previously for human islet tissue.

A key conclusion from this study investigating culture in the absence of oxygen limitations that set the stage for the work that followed was that when adherent and non-adherent were combined, nearly 100% of the original viable tissue placed in culture was recovered from preparations that were given time to recover from the harsh isolation process. Though original tissue including β cells was lost, the tissue that was lost was dead (as determined by OCR) when culture was initiated. Increasing tissue surface density resulted in the appearance and amplification of oxygen limitations resulting in drastic decreases in the fractional recovery of viable tissue. The data suggest that current clinical practice likely imposes oxygen limitations during culture that can result in a decrease in the fractional recovery of viable tissue by 0.20.

The oxygen limitations present using conventional methods were reduced through culture in elevated ambient oxygen, at a reduced temperature, or on a silicone rubber membrane allowing tissue to be cultured at higher densities (at least 3 fold higher) without a reduction in viability. However, questions remain about oxygen toxicity and the effects of reduced culture temperature on islet function. Culture on silicone rubber was the most promising resulting in the complete removal of oxygen limitations. Though other limitations became important at very high

densities on silicone rubber membranes, culture at densities 5 fold higher than conventional methods was possible with little loss in viable tissue. In addition to developing new culture techniques, an in-depth theoretical analysis of oxygen transport revealed that tissue size, islet stacking, and clumping, all of which may be present during high density culture and islet shipment, can greatly exacerbate oxygen limitations.

When oxygen transport limitations are removed glucose limitations likely become limiting during both culture on polystyrene and silicone rubber. Conventional culture (3 mm medium, polystyrene surface) may performed at a total tissue volume up to 570 "IE"/cm^2, where "IE" in this case is based on total tissue (400 IE/cm^2, 70% islet tissue by volume), which could result a glucose concentration < 1 mM within 30 hr of culture. Culture in large medium depths prevents glucose depletion from the bulk medium, but because glucose consumption may be high relative to the rate of diffusion, diffusional limitations to the islet may result in exposure to concentrations < 1 mM at densities above 1700 IE/cm^2, which is a similar surface density to that where the empirical fractional recovery of viable tissue began to decrease consistently on silicone rubber membranes.

Changes in local pH can be significant during culture on polystyrene due to the buildup of CO_2 in the medium. However, at low density these changes are small, especially at low medium depths like those used in conventional culture. Changes in pH during culture on a silicone rubber membrane are unlikely because CO_2 can escape the system at a much faster rate thereby preventing a shift to more acidic conditions through the bicarbonate reaction. As a result drastic changes in pH during culture are unlikely though there is much uncertainty in many of the parameters used in the theoretical model.

Using the knowledge gained investigating oxygen transport, a shipping container was developed and tested in collaboration with Giner, Inc., and the University of MN that actively controlled temperature and oxygen resulting in increases in islet recovery and viability following 24 hr shipment as compared to the "state-of-the-art" method using a Styrofoam box. A passive shipping device was outlined that has all the benefits of the actively controlled environment container, but is less cumbersome, less expensive, and does not require battery operation.

The culture techniques examined greatly improve tissue oxygenation compared to conventional culture allowing tissue to be cultured at high densities without a reduction in viability. The methods are easily implemented allowing clinical centers to reduce space and

handling requirements during culture prior to transplantation without the reduction in islet viability that can occur using conventional methods thereby maximizing the use of limited islet resources likely improving transplantation success rates.

9.2 Future work

The concepts presented here revealed many more avenues that could be investigated further. First transplantation studies would provide confirmation that the developed techniques in this thesis improve or at least maintain tissue viability and function compared to the conventional method.

Another beneficial study would involve assessing islet quality as a function of time starting immediately after isolation and follow it through culture. Based on the data in Chapter 2 we hypothesize that the islet isolation process damages tissue thereby initiating the cell death process. The damage incurred by the isolation process was partially quantified in Chapter 2, but measurement earlier in culture may provide insight into the dynamics of the death process initiated by isolation. Additionally, longer culture periods (>2 days) would reveal whether tissue quality is maintained or eventually begins to decrease even in the absence of transport limitations.

The quantification of tissue adherence had not previously been reported in literature. Though we presented data indicating that the adherent tissue contained fewer β cells, the identity of the cells that adhered was not determined. Further insight into which cells adhere to the culture vessel may lead to techniques that remove impure tissue. An initial study could identify the cells that adhere and test whether adherence occurs multiple times with the same preparation when the culture vessel is changed.

Reduced culture temperature was shown to be beneficial for high density culture, but questions remained about whether tissue function was changed since low density culture reduced the OCR of the tissue. Transplantation experiments would be best to determine whether tissue cultured at reduced temperature have the same potency of those cultured at 37°C. Variations in recovery period following reduced temperature culture would show if function is lost and whether it ever recovers. For these studies all cultures should be conducted in the absence of oxygen limitations for culture at 37°C.

Oxygen toxicity in islet tissue could also be investigated further especially if culture in elevated ambient oxygen is applied. The study would be best conducted using silicone rubber membranes allowing for accurate control of oxygen level at the tissue surface. The use of small islets or islet cell-aggregates will reduce internal oxygen gradients resulting in a more uniform exposure to the desired O_2 level. The theoretical oxygen transport model already developed can be used to confirm the uniform oxygen exposure.

Based on the analysis in this thesis the development of a passive shipping device that provides sufficient oxygen and prevents large temperature swings is feasible. The next step in developing such a container is to obtain the materials for a prototype and then fabricate the shipping container. PCMs for multiple temperatures could be tested until an optimal shipment temperature is determined. The container should be tested in controlled environments, during shipment without tissue, and during shipment with tissue. All shipments should be compared to the standard shipping method of a Styrofoam box. One problem that has not been addressed with this passive device is islet pooling during shipment. If the container is slanted, pooling will result exacerbating nutrient transport limitations as was observed with the Giner, Inc., container. A possible solution to this is to combine the technology discussed here with a shipping device developed by the University of Miami that prevents tilting of the culture vessel.

10 Appendices

10.1 Supplemental material for Chapter 2

Purity measurements on day 2 were performed using immunoperoxidase staining for insulin in conjunction with stereological point counting while day 0 measurements were made using morphological analysis. The reason a second method was used to determine purity following culture was because several samples contained single cells following culture that resulted from trypsinization of the adherent tissue. Morphology differences in single cells would be hard to differentiate whereas differences in color based on insulin staining are easier to distinguish resulting in a more accurate reflection of tissue composition. For insulin staining quantification by stereological point counting vascular space was excluded because vascular space in non-adherent tissue will be different than in adherent tissue. These measurements resulted in the β cell volume fraction exclusive of vascular spaces ($\Phi_{\beta XV}$), which is defined as

$$\Phi_{\beta XV} = \frac{P_\beta}{P_I + P_{NI}} = \frac{V_\beta + V_{\beta INT}}{V_I + V_{NI} - V_{VI}} \qquad \textbf{10.1}$$

where P_β is the points counted as insulin positive, P_I is a point counted as islet tissue, P_{NI} is a point counted as non-islet tissue, V_β is the volume of insulin positive cells, $V_{\beta INT}$ is the volume of the interstitial space of insulin positive cells, V_I is the volume of islet tissue, V_{NI} is the volume of non-islet tissue, and V_{VI} is the volume of the vascular void space. If P_β is only counted if insulin staining is present, which should only occur in cells and not interstitial space (i.e. $V_{\beta INT} = 0$), then the following is true.

$$\Phi_{\beta XV} = \frac{V_\beta}{V_I + V_{NI} - V_{VI}} \qquad \textbf{10.2}$$

In order to compare the morphological measurements made on day 0 for the volume fraction islets (Φ_I) with $\Phi_{\beta XV}$ from day 2 samples we needed to perform some data conversions, which are summarized in Figure 10.1. Previously it has been shown that Φ_I can be converted to the islet volume fraction exclusive of vascular spaces (Φ_{IXV}) assuming the vascular void fraction (Φ_{VI}) in the islet tissue is known (equation 6.4 from [13]). Φ_{IXV} can be converted to $\Phi_{\beta XV}$ using

$$1+\frac{\frac{V_{INT}}{V_I}}{\frac{V_{IC}}{V_I}}=\frac{\phi_{\beta IC}\Phi_{IXV}}{\Phi_{\beta XV}} \qquad \textbf{10.3}$$

where V_{IC} is the volume if islet cells, V_{INT} is the volume of interstitial space in islet cells, and $\phi_{\beta IC}$ is the β-cell cell volume fraction. This equation can be obtained by combining Equation 10.2 and the definition of Φ_{IXV}, which is

$$\Phi_{IXV}=\frac{P_I}{P_I+P_{NI}}=\frac{V_{IC}+V_{INT}}{V_I+V_{NI}-V_{VI}} \qquad \textbf{10.4}$$

From previous analysis fresh tissue has an average $\phi_{\beta IC}= 0.867$, $\frac{V_{INT}}{V_I} = 0.15$, and $\frac{V_{IC}}{V_I} = 0.71$ [13] thereby allowing us to estimate $\Phi_{\beta XV}$ of fresh tissue from measurements of Φ_I.

In order to combine nuclei measurements with purity measurement $\Phi_{\beta XV}$ and Φ_I need to be converted from volume fractions to number fractions. In particular we will convert each volume fraction to the number fraction beta cells (f_β). Day 0 measurements of Φ_I were converted to f_β as outlined in Figure 10.2. Φ_I was converted to the volume fraction islets (ϕ_{IC}) which was converted to the number fraction islet cells (f_{IC}) which was converted to f_β using previously defined relationships and assuming the volume fraction of islet extracellular space (Φ_{IEC}), the volume fraction of non-islet extracellular space (Φ_{NIEC}), the average cell volume for islet cells ($\bar{v}_{IC}$),the average cell volume of all cells ($\bar{v}_{TC}$), the β cell volume (v_β), and $\phi_{\beta IC}$ are the same as previously reported [13].

Day 2 measurements of $\Phi_{\beta XV}$ were converted to f_β using the procedure outlined in Figure 10.3. $\Phi_{\beta XV}$ is converted to Φ_{IXV} using Equation 10.3 and equation 6.20 from Colton et al [13]. Values for $\frac{V_{INT}}{V_I}$, $\frac{V_{IC}}{V_I}$, v_β, $f_{\beta IC}$ (f_β/f_{IC}), and $\bar{v}_{IC}$ are estimated as indicated in Table 10.1. Φ_{IXV} is converted to Φ_I which is then converted to ϕ_{IC} using previously defined relationships and assuming values for Φ_{IEC}, Φ_{NIEC}, and Φ_{VI}. ϕ_{IC} is converted to f_{IC} using equation 6.18 from Colton et al [13]. f_β is calculated from f_{IC} by assuming $f_\beta/f_{IC} = 0.739$ (i.e. $f_{\beta IC}$ does not change with culture).

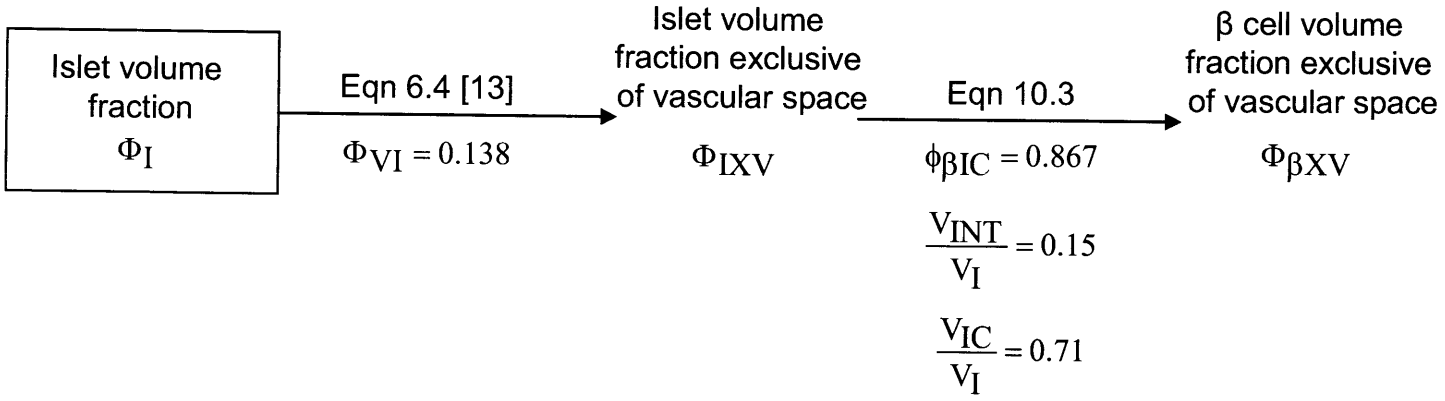

Figure 10.1. Conversion of day 0 islet volume fraction to β cell volume fraction exclusive of vascular spaces.

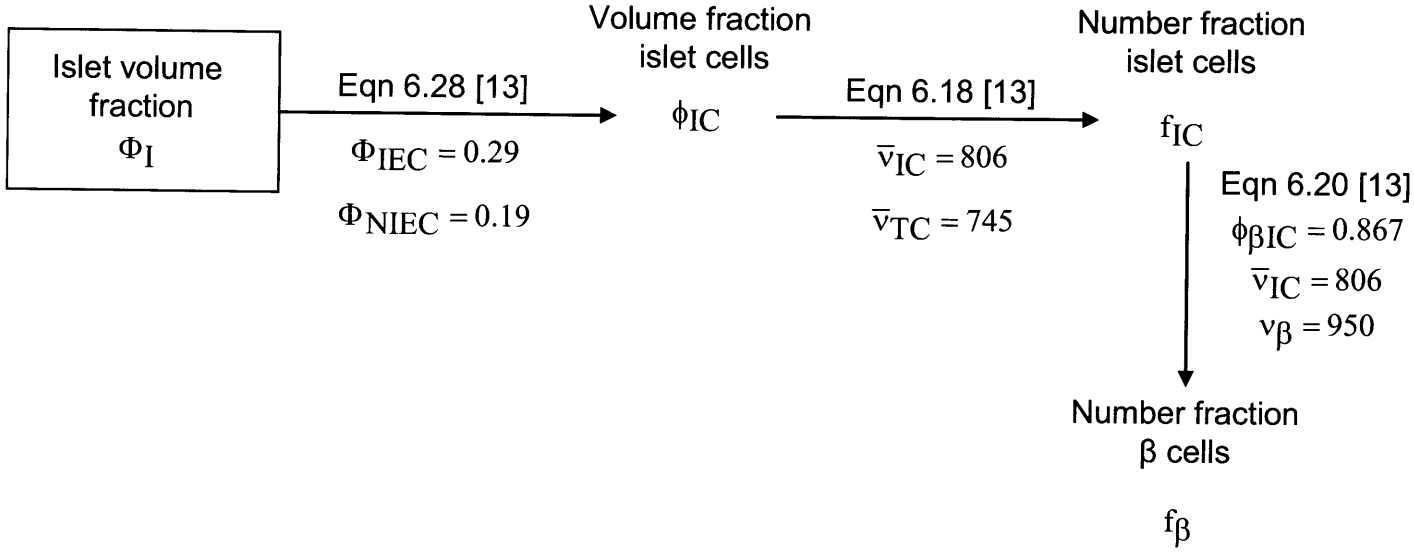

Figure 10.2. Conversion of day 0 islet volume fraction to number fraction β cells.

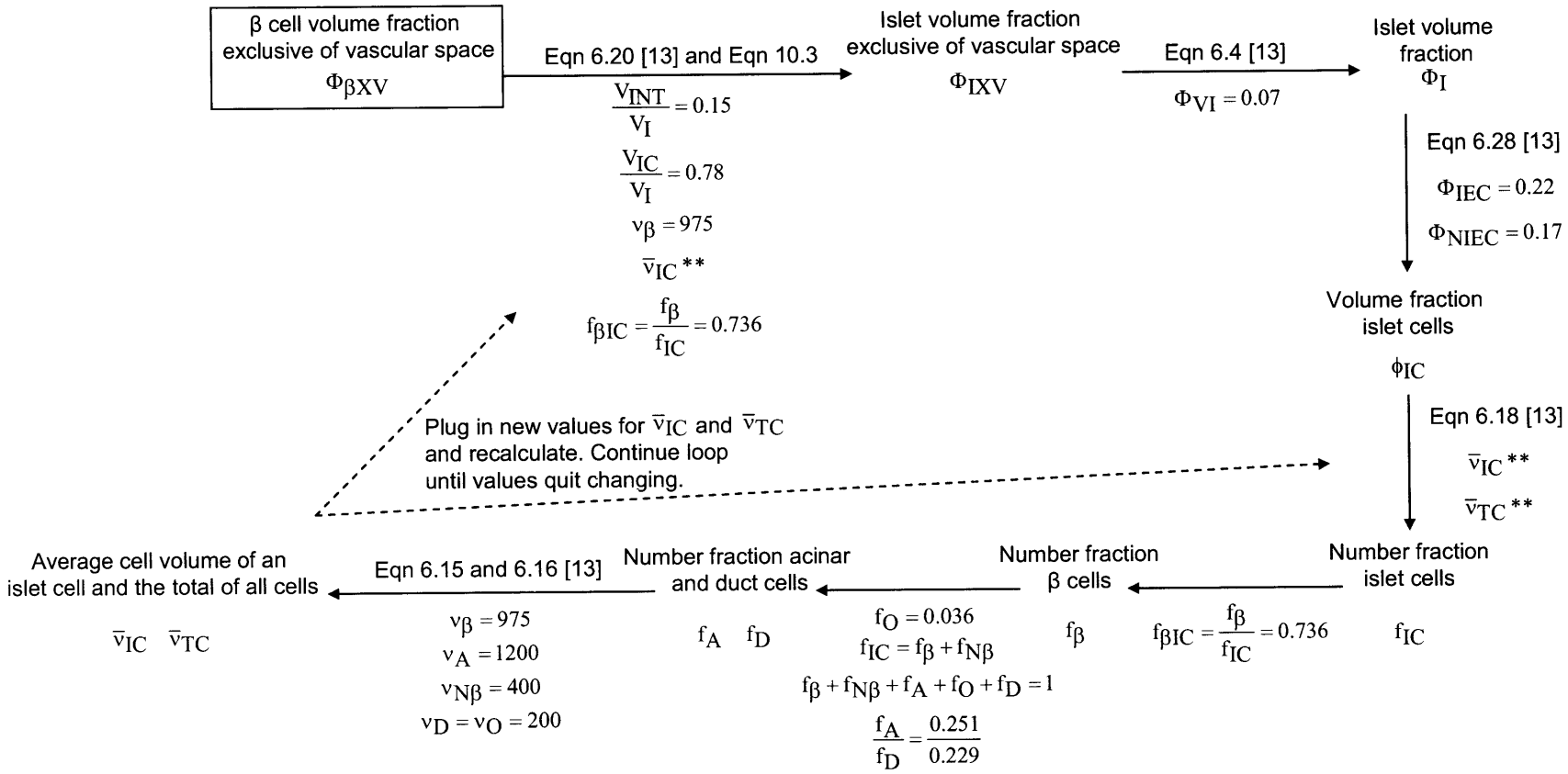

Figure 10.3. Conversion of day 2 β cell volume fraction exclusive of vascular spaces to number fraction β cells.

Table 10.1. Parameter values used to estimate $\Phi_{\beta XV}$ and f_β from day 0 measurements of Φ_I and day 2 measurements of $\Phi_{\beta XV}$.

		Day 2 non-adherent		Day 2 adherent	
	Fresh value	Scenario 1	Scenario 2	Scenario 1	Scenario 2
Assumed					
V_{INT}/V_I	0.15	0.15	0.1	0.1	0.05
V_{IC}/V_I	0.71	0.78	0.9	0.9	0.95
Φ_{VI}	0.138	0.07	0	0	0
Φ_{NIEC}	0.19	0.17	0.1	0.1	0.05
Φ_{IEC}	0.29	0.22	0.1	0.1	0.05
ν_β	950	975	1000	975	1000
$\nu_{N\beta}$	400				
ν_A	1200				
ν_D	200				
ν_O	200				
f_O	0.036				
f_A/f_D	1.1				
$f_{\beta IC}$	0.736				
Calculated averages					
$\bar{\nu}_{IC}$	806	823	841	823	841
$\bar{\nu}_{TC}$	745	763	767	724	726
f_A	0.251	0.20	0.23	0.40	0.41
f_D	0.229	0.18	0.21	0.37	0.37

Though we have a value for f_β we need to make sure all variables are consistent. We assume that the number fraction of other cells (f_O) is the same as fresh tissue thereby suggesting that the change in f_β and f_{IC} (which allows determination of the number fraction non-β islet cells, $f_{N\beta}$) is offset by a change in exocrine tissue, specifically the number fraction of acinar cells (f_A) and duct cells (f_D) such that $f_{N\beta} + f_D + f_O + f_\beta + f_A = 1$. This change in exocrine tissue is assumed to be equally distributed between acinar and duct cells such that f_A/f_D is constant (personal communication from Susan Bonnier-Weir). Using the number fraction of each cell type and the assumed cell volumes of each, $\bar{\nu}_{IC}$ and $\bar{\nu}_{TC}$ can be calculated as previously indicated [13]. These calculated values are compared to those originally assumed in the calculation. If unequal,

the new values replace the old ones and the calculation is performed again. The loop continues until the calculated $\bar{v}_{IC}$ and $\bar{v}_{TC}$ matches those assumed.

The parameters used in the above calculations for fresh tissue and tissue following 2 day culture, both non-adherent and adherent, are shown in Table 10.1. The values of the parameters for fresh tissue (day 0) were determined previously [13]. During culture these parameters are likely to change. Since the degree of change is unknown, we will consider two different scenarios, one that we feel is realistic and one that has more extreme changes in parameter values allowing us to see how sensitive the analysis is to the assumptions.

For non-adherent tissue in scenario 1 we assume that the vascular void space is cut in half during culture for both islet and non-islet tissue, but that the volume fraction of the interstitial space in an islet does not change. In scenario 2 we assume that all the vascular void space is gone and that $\frac{V_{INT}}{V_I}$ decreases from 0.15 to 0.1. These assumptions allow us to calculate $\frac{V_{IC}}{V_I}$, Φ_{IEC}, Φ_{VI}, and Φ_{NIEC}. In scenario 1 and 2 we assume that the v_β increases to 975 and 1000 μm^3, respectively based on observations from our collaborators that show a slight increase in size of β cells during culture (personal communication from Susan Bonner-Weir). For adherent tissue on day 2 we assume that all vascular void space is gone since trypsinization is conducted. We also assume that $\frac{V_{INT}}{V_I}$ decreases to 0.1 and 0.05 for scenarios 1 and 2 allowing $\frac{V_{IC}}{V_I}$, Φ_{IEC}, Φ_{VI}, and Φ_{NIEC} to be calculated. v_β is the same as that for non-adherent tissue (975 and 1000 μm^3 for scenario 1 and 2). The results presented were determined using scenario 1. When performing the calculations with the two scenarios there was at most a 7% change in f_β (absolute change of 0.027).

It should be noted $\frac{V_{INT}}{V_I}$ determined for fresh human islet tissue did not include capillary space, which is normally considered interstitial space. In the original study the pericapillary space was counted as vascular space. This brings into question the use of its value in our data conversions. Despite this the value of $\frac{V_{INT}}{V_I}$ for fresh tissue (0.15) is inline with estimates for the mean interstitial space in the human body [177] and the error associated with it is likely small.

Once f_β was determined the fraction of original β cells collected from culture (F_β) could be calculated using

$$F_\beta = \frac{\left(n_{TC} f_\beta\right)_2}{\left(n_{TC} f_\beta\right)_0} \qquad \textbf{10.5}$$

where n_{TC} is the total number of cells either placed in culture (day 0) or collected from culture (day 2).

10.1.1 Nomenclature

f_A	Number fraction acinar cells
f_D	Number fraction duct cells
$f_{N\beta}$	Number fraction non-beta islet cells
f_O	Number fraction other cells
f_{IC}	Number fraction of all islet cells
f_β	Number fraction of β cells among all cells
$f_{\beta IC}$	Number fraction beta cells in among islet cells
F_β	Fraction of original β cells collected from culture
n_i	Number of cells of type i
n_{TC}	Total number of cells
P_β	Number of points falling within the domain of β cells
P_I	Number of points falling within the domain of islets
P_{NI}	Number of points falling within the domain of non-islets tissue
P_V	Number of points falling within the domain of islet vascular space
$V_{\beta INT}$	Volume of interstitial space of β cells
V_I	Total volume of the islet domain
V_{IC}	Volume of islet cells
V_{INT}	Volume of interstitial space in islet

V_{NI}	Total volume of the non-islet domain
V_{VI}	Volume of vascular voids in islet
V_{β}	Volume of β cells
ϕ_{IC}	Volume fraction of islet cells among all cells
$\phi_{\beta IC}$	Volume fraction of β cells among all islet cells
$\Phi_{\beta XV}$	Volume fraction of β cells exclusive of islet vascular spaces
Φ_{I}	Volume fraction of islets
Φ_{IEC}	Volume fraction of islet extracellular space within the islets
Φ_{IXV}	Volume fraction of islets exclusive of islet vascular spaces
Φ_{NIEC}	Volume fraction of non-islet extracellular space based on the total non-islet volume
Φ_{VI}	Volume fraction of vascular voids within islets
ν_{A}	Cell volume of acinar cells
ν_{D}	Cell volume of duct cells
$\bar{\nu}_{IC}$	Average cell volume for islet cells
$\nu_{N\beta}$	Cell volume of non-β islet cells
ν_{O}	Cell volume of other cells
$\bar{\nu}_{TC}$	Average cell volume for all of the cells
ν_{β}	Cell volume of β cells

10.2 Carbon monoxide (CO) treatment of βTC3 cells exposed to TNF-α or anoxia

10.2.1 Introduction

Successive implants of islets of Langerhans from two or more human pancreas are normally required to treat type 1 diabetes [8] though a small fraction of the islets in the normal human pancreas are required to maintain normoglycemia [9]. Stresses during islet isolation, islet culture, and following transplantation can cause a reduction in tissue viability and function. Cell death can be triggered by a variety of stresses, including hypoxia, oxidative stress, and pro-inflammatory cytokines. A method for protecting islets from these and other stresses would provide more efficient and effective use of this limited resource.

Exposure to carbon monoxide (CO), a product of heme degradation catalyzed by heme oxygenase-1 (HO-1), which itself acts as a cellular defense for many types of cells in vitro [88; 178-190], has been shown to protect a variety of cell types from various stresses. CO provides protection against hyperoxia [191-193], serum deprivation [194], cytokines such as TNF-α [194-196], and hypoxia-reoxygenation [197]. A limited amount of work has been carried out to study the effects of CO on β-cells. In a study by Gunther et al. [194], CO (10,000 ppm) protected βTC3 cells from apoptosis induced by TNF-α, serum starvation, and etoposide, and mouse islets from TNF-α and cyclohexamide-induced apoptosis. A two-hour CO treatment of islets in medium presaturated with CO resulted in a significantly shorter time to reach normoglycemia after transplantation with a marginal islet mass compared to islets not given the CO treatment [194].

No study has examined in depth how the nature of the stress, CO concentration, duration of CO exposure, time between CO treatment and stress exposure, duration of stress exposure, time since cessation of stress, and the temporal relationship of CO and stress exposure (i.e. pre-incubation or co-incubation) affect the protection provided by CO. We hypothesize that CO protection of β-cells and islets from a variety of stresses will be dependent on these variables. However, before investigating various treatments, we needed to replicate the results obtained by Gunther et al. [194] that showed CO provided protection for βTC3 cells from TNF-α.

10.2.2 Methods

Cell culture

βTC3 cells (passages 40-50) were cultured in DMEM supplemented with 10% FBS, 100 U/ml penicillin, and 100 μg/ml streptomycin (Mediatech Inc., Herdon, VA). Cells were cultured in a fully humidified environment at 37°C with 95% air/5% CO_2. For cytokine experiments TNF-α was added to a final concentration of either 50 or 500 U/ml and incubated with cells for 24 hr. Exposure to anoxia was conducted in a 5 L chamber at 37°C for 24 hr. The chambers were purged for 15 min with 95% N_2/5% CO_2 at 3 L/min before reducing the flow rate such that there was a very slight flow through the chamber keeping the gas composition constant throughout the experiment.

CO exposure

Gases were obtained in premixed cylinders. For cytokine experiments flasks were placed in 5 L chambers 0, 2, or 24 hr before TNF-α addition and purged for 15 min with 1% CO/20% O_2/5% CO_2/balance N_2 at 3 L/min before reducing the flow rate. The flasks were removed when adding TNF-α, but returned after addition and immediately purged again. Exposure to CO+anoxia was in a similar fashion but using 1% CO/5% CO_2/balance N_2.

For experiments investigating the effects of CO on tissue OCR 1% CO/20% O_2/5% CO_2/balance N_2 was bubble through serum free DMEM at 37°C for > 5 min. Cells were resuspended in the CO containing medium and immediately added to the OCR chambers and sealed. Control cells were handled similarly, but re-suspended in medium without CO.

Islet enumeration by nuclei counting

Nuclei were prepared by adding equal 100-μl volumes of sample containing 160 or more IE and of lysis solution (0.1 M citric acid (Sigma) and 1% (v/v) Triton X-100 (Sigma)) to a 1.5 ml microtube [55]. The mixture was incubated at room temperature for 5 min with vortex mixing every 1.5 min, and nuclei were liberated by shearing through a needle. Isolated nuclei were diluted with Dulbecco's phosphate buffered saline (D-PBS, Invitrogen, Carlsbad, CA) to a concentration no higher than 5 x 10^5 nuclei/ml, stained with 7-aminoactinomycin D (7-AAD, Molecular Probes, Eugene, OR), and analyzed using a flow cytometer (Guava Personal Cell Analysis (PCA) system, Guava Technologies, Hayward, CA) to determine the total number of cells with intact nuclei in the sample.

Oxygen consumption rate (OCR)

OCR was measured as previously described [39]. Briefly, suspensions containing about 2500 IE/ml in DMEM containing 4.5 g/l glucose and 0.6 g/l L-glutamine supplemented with 100 U/ml penicillin, 100 μg/ml streptomycin, 10 mM HEPES, and no added serum were sealed in a 200-μl stirred titanium chamber (Micro Oxygen Uptake System, FO/SYSZ- P250, Instech Laboratories, Plymouth Meeting, PA) maintained at 37°C. The time dependent pO_2 within the chamber was recorded with a fluorescence-based oxygen sensor (Ocean Optics, Dunedin, FL), and data at high pO_2 were fit to a straight line. The maximal OCR was evaluated from $OCR=V_{ch}\alpha(\Delta pO_2/\Delta t)$, where V_{ch} is the chamber volume and α = 1.27 nmol/mm·Hg·ml is the Bunsen solubility coefficient for oxygen in medium [16]. OCR measurements were normalized by the measured number of cells (nuclei counting) or DNA content of the sample examined.

Membrane Integrity

7-Aminoactinomycin (7-AAD) sequential staining

Cell membrane integrity was assessed by differential staining with 7-AAD (Molecular Probes, Eugene, OR) [55]. An aliquot of about 300 islets was re-suspended in 100 μl of D-PBS, and 5 μl of 1 mg/ml 7-AAD and incubated for 20 min at 4°C protected from light. After two washes with 1 ml of D-PBS, cells were disrupted by adding equal volume of lysis solution in D-PBS to the islet suspension and sheared as described for islet enumeration. Labeled nuclei were counted immediately in the flow cytometer or stored on ice for less than 15 min before counting. A portion of the islet suspension was further stained with 7-AAD, thereby labeling all of the previously unlabelled nuclei, and the total number of nuclei was counted. The fraction of cells with compromised membranes was estimated as the ratio of the initially stained nuclei (first measurement) to the total number of nuclei (second measurement).

Sytox Orange/LDS 751

Cell suspensions were stained with a solution (in D-PBS) containing 0.8 μM LDS 751 (Molecular Probes), a membrane permeable dye and 0.2 μM Sytox Orange (Molecular Probes), a membrane impermeable dye. LDS 751 was dissolved in dimethyl sulfoxide (DMSO). Samples with a cell concentration no higher than $5x10^5$ cells/ml were incubated for 5 min at room temperature and analyzed in a flow cytometer (Guava PCA) using the Guava Viacount software.

The fraction of cells with compromised membranes was the ratio of the number of cells stained with Sytox Orange over the number of cells stained with LDS 751.

Statistics

Measurements were made with three or more replicates and reported as mean ± SD. Statistical significance was determined using a Student t-test for unpaired data for comparing population means, and for paired data when appropriate.

10.2.3 Results

TNF-α caused a dose dependent reduction in the fraction of cells with intact cell membranes in βTC3 cells (Figure 10.4). 500 U/ml TNF-α caused the most reduction in viability as in previous studies with βTC3 cells [194] and therefore was chosen as the stress level when treating cells with CO. By co-incubating βTC3 cells in 500 U/ml TNF-α with 1% CO the fraction of cells with intact cell membranes increased 0.10-0.15 from that with TNF-α without CO (Figure 10.5). This protection decreased slightly when a pre-incubation period in CO (without stress) was performed.

Exposure to anoxia for 24 hr also caused a reduction in the fraction of cells with intact cell membranes in βTC3 cells, but is dependent on the cell density in culture (Figure 10.6). At higher densities there is a larger decrease in viability based on membrane integrity. Though the surface density of each culture vessel in each individual experiment was the same, they were not always the same between experiments. Though unknown initially, this difference caused a lot of variation between experiments. Data from four independent experiments exposing βTC3 cells to anoxia for 24 hr with and without CO are shown in Figure 10.7. Anoxia caused a large reduction in viability in two of the four experiments (Figure 10.7A and D), possibly due to density differences. However, even accounting for the differences in death, the relative effect of CO was different for each experiment. In some cases CO protected βTC3 cells from anoxia (Figure 10.7A) while others either made no difference (Figure 10.7B) or caused a further reduction in membrane integrity than anoxia alone (Figure 10.7C and 4). Even though differences are seen in the damage caused by anoxia, there are still inconsistencies in CO protection making it difficult to determine whether CO is beneficial.

Though the results presented here focus on membrane integrity measurements, some experiments attempted to use mitochondrial function assays such as ATP or MTT (data not

shown). The results from these assays made data even more variable. Eventually it was determined that part of this variability may be due to the impact CO has on cellular respiration. Adding medium with CO to βTC3 cells resulted in a 19% increase in OCR/cell as compared to cells in medium without CO (Table 10.2).

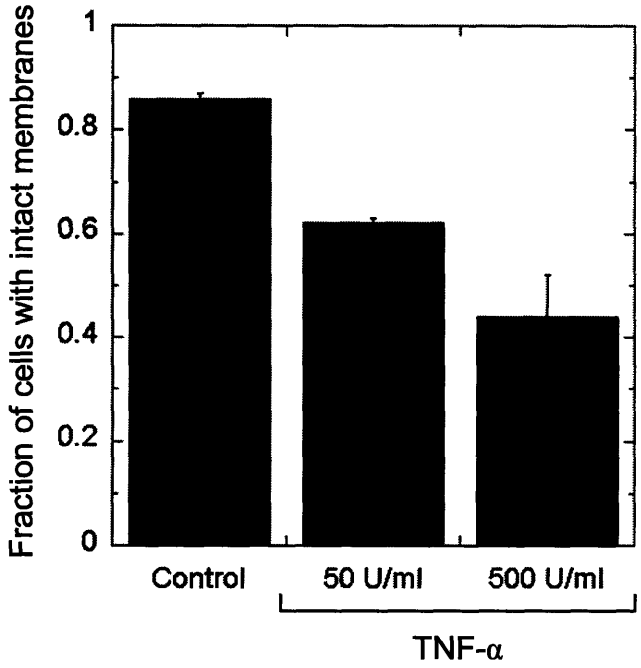

Figure 10.4. The fraction of cells with intact membranes versus TNF-α concentration. Membrane integrity determined by Sytox Orange/LDS 751 staining for 24 hr exposures to βTC3 cells. The error bars are ± the standard deviation for n = 3 measurements. Data are from one representative experiment of 3.

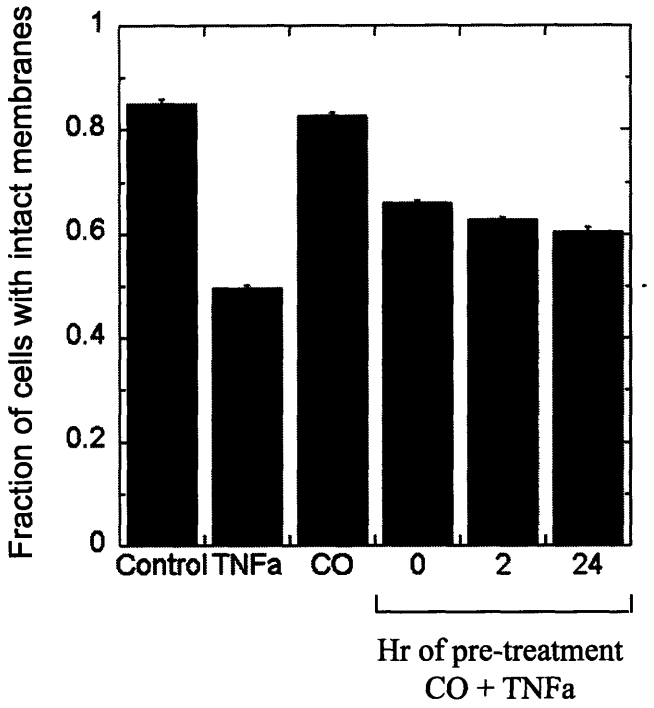

Figure 10.5. The fraction of cells with intact cell membranes with CO and TNF- α treatment.
Membrane integrity determined by Sytox Orange/LDS 751 staining for control cells (no stress), cells exposed to 500 U/ml TNF-α (no CO), cells exposed to CO without stress, and cells exposed to CO for 0, 2, or 24 hr (pretreatment) prior to exposure to CO + 500 U/ml TNF-α for 24 hrs. The error bars are ± the standard deviation for n = 3 measurements. Data are from one representative experiment of 5.

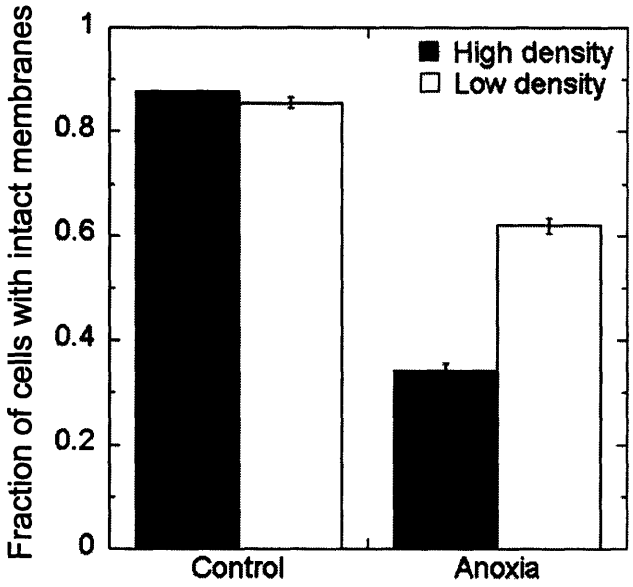

Figure 10.6. The fraction of βTC3 cells with intact cell membranes after exposure to anoxia.
Membrane integrity determined by Sytox Orange/LDS 751 staining for control cells (no stress) and cells exposed to anoxia for 24 hr for a high (> 60,000 cells/cm^2) and low (< 15,000 cells/cm^2) cell density. The error bars are ± the standard deviation for n = 3-5 measurements.

Table 10.2. OCR/cell of βTC3 cells with and without CO present.

	OCR/cell (fmol/min cell)	
Control	3.24 ± 0.35	p < 0.04
CO treated	3.86 ± 0.20	

Data listed as mean ± the standard deviation for n = 3 experiments. Data are significantly different (p < 0.04) based on a Student t-test assuming paired data.

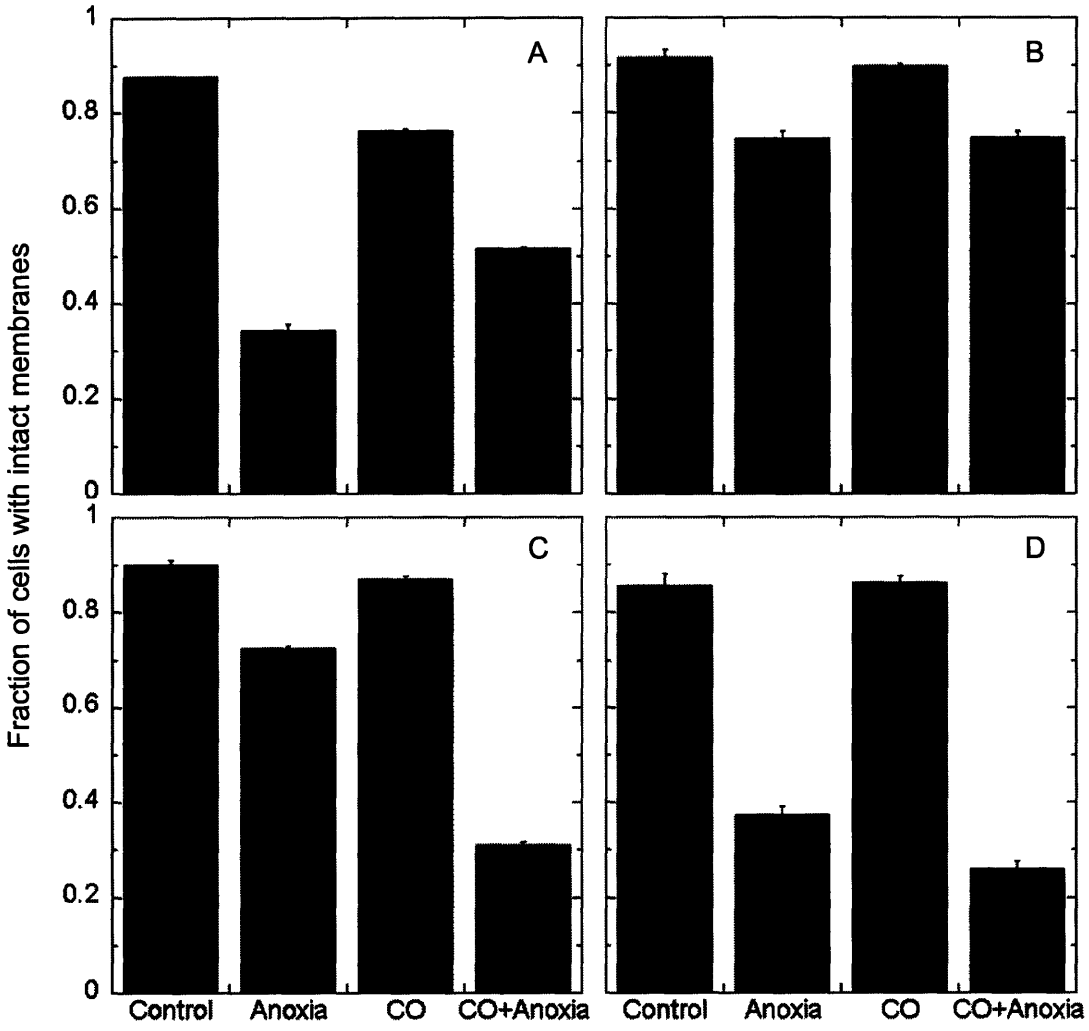

Figure 10.7. CO protection of βTC3 cells from anoxia.
The fraction of cells with intact cell membranes after as determined by Sytox Orange/LDS 751 staining for control cells (no stress), cells exposed to anoxia (no CO), cells exposed to CO without stress, and cells exposed to CO + anoxia for 24 hrs for four different experiments using βTC3 cells. The error bars are ± the standard deviation for n = 3 measurements. Each panel represents a single experiment.

10.2.4 Discussion

In this study we examined whether CO protects βTC3 cells from TNF-α or anoxia to determine whether CO treatment of islet tissue is likely to be beneficial. Unfortunately, several problems were encountered causing inconsistent results preventing the bulk of the initially proposed work from being completed.

Our results indicated that TNF-α caused a dose dependent reduction in βTC3 cell viability resulting in a fraction of cells with intact membranes around 0.45 (Figure 10.4), which is consistent with that observed in other studies [194], though ours varied from 0.35 to 0.50. Treating cells with CO before and during TNF-α exposure resulted in an increase of 0.10-0.15 (Figure 10.5). This increase is significantly less than that observed in previous studies which indicated an increase of roughly 0.70 [194]. The reason our study indicated less protection is unknown, but may be linked to differences in measuring cell viability/survival or slight differences in treatment methods.

A small decrease was observed in the protection CO provided from TNF-α exposure as the pre-incubation period in CO increased (Figure 10.5). A similar diminishing protective effect has been observed when HO-1 is over expressed [198]. HO-1 resulted in cytoprotection when overexpressed less than five fold, but were associated with significant toxicity at higher levels (15 fold expression) [198].

Experiments investigating whether CO provided βTC3 cells with protection from anoxia were far more variable. Cell density had a large impact on the fraction of cells with intact cell membranes (Figure 10.6). Higher density cells may have had lower viability because they will consume oxygen in the medium faster than cells at low density. Though oxygen in the gas phase is removed quickly, it takes a longer period to remove oxygen in the medium. As such, cells at high density are exposed to anoxia sooner than cells at low density. This different in actual exposure time to anoxia is likely to explain the impact density has on membrane integrity.

If we consider the relative effect CO protection has when cells are exposed to anoxia, we still observe variable results. The experimental results indicate that CO could have a protective effect, no effect, or actually damaged tissue further in the presence of anoxia suggesting that the current system used for exposure to CO and/or anoxia is insufficient. A system that includes CO

and O_2 sensors in the culture medium would be beneficial to make sure the cells see the same concentrations for all experiments.

CO treatment increased tissue respiration rate significantly (Table 10.2), which is consistent with experiments that indicated the most damage in CO + anoxia rather than anoxia alone, but contrary to what has been reported previously [199]. D'Amico et al suggest that CO reduces cellular respiration immediately upon exposure [199], which is the exact opposite of what we found. Though it is unknown why the results differ, it could be linked to the concentration of CO to which cells are exposed, the cells used in each study, or the medium in which the respiration rate is measured. In particular, the medium used for OCR analysis in this study included the buffer hepes, which has been shown to decrease nitric oxide (NO) concentration in culture medium [200]. NO can also decrease cellular respiration and has been shown to interact with the HO-1/CO pathway. To confirm this hypothesis OCR measurements using hepes free medium would be needed.

The results presented here indicate that CO may be beneficial in protection of β-cells from cytokine stress, specifically TNF-α. However, more experiments are needed to determine whether CO can protect cells from anoxia. Further, determination of whether CO increases of decreases cellular respiration would be beneficial since an increased respiration could have detrimental effects in hypoxic environments, such as that after transplantation and during conventional culture.

10.2.5 Nomenclature

7-AAD	7-aminoactinomycin D
CO	Carbon monoxide
D-PBS	Dulbecco's phosphate buffered saline
FBS	Fetal bovine serum
HO-1	Heme oxygenase
NO	Nitric oxide
OCR	Oxygen consumption rate
t	Time
V_{ch}	Volume of OCR chamber
α	Solubility of oxygen in medium

10.3 Investigating oxygen consumption rate measurement in static cultures

10.3.1 Introduction

Measurement of cellular oxygen consumption rate (OCR) gives information on the respiratory activity of a tissue sample and is believed to indicate cell viability especially when comparing similar tissue samples. Measurements of islet tissue are of great importance since it has been shown that OCR of human islets can be used to predict transplantation outcome in mice [201]. In addition, OCR is an early indicator of cell death compared to other cell viability assays, such as membrane integrity measurements, allowing for accurate determination of the health of a sample even before the tissue has finished the cell death cycle [55].

The oxygen biosensor system (OBS) was developed for the measurement of OCR of tissue in static culture [146] and has been used for measurement of OCR for different cell lines [146; 202] and islet preparations [75]. The OBS utilizes an oxygen sensitive fluorophor embedded in silicone rubber upon which cells or tissue is placed. As the tissue consumes oxygen, the oxygen partial pressure (p) at the bottom of the plate decreases and is detected by the sensor.

The OBS is much easier to use than other methods that measure OCR allowing for multiple measurements at one time in a single plate. However, the current commercially available device gives inaccurate OCR estimates as compared to perfusion [74] and the stirred chamber [39] methods. In contrast to the perfusion and stirred chamber methods, which measure OCR based on material balances, the OBS relies on the application of a the oxygen species conservation equation with the appropriate initial and boundary conditions for calculation of OCR from the measurement of p. In order to allow easy computation of OCR from the pO_2 measurements several simplifying assumptions are required [146] including (1) the system is at steady state, (2) the well geometry is perfectly cylindrical, (3) the wells are fabricated from oxygen impermeable material, (4) the medium is completely stagnant, (5) there is a uniform and infinitely thin cell layer, at the bottom, overlaying (6) a uniform infinitely thin oxygen sensor material. The validity of these assumptions determines the accuracy of the OCR estimation.

OCR values obtained using the OBS do not agree with measurements made with other methods. Measurements by the OBS for islet tissue resulted in an OCR of approximately 800 fmol/min IE [75] or about 0.5 fmol/min cell (1560 cells per IE [13]), which is much lower

than average values for islets measured in our laboratory using the stirred chamber system (Chapter 2).

In this section we investigate why OCR determined by the OBS is inaccurate. Through the use of a finite element mass transfer model the validity of the assumptions required to estimate OCR from the OBS device is tested by comparing the idealized model with the actual model. We then demonstrate experimentally the impact of two assumptions on the OCR measurement with the OBS including (1) that the wells are fabricated from oxygen impermeable material and (2) that the medium is completely stagnant.

10.3.2 Methods

Fabricating OBS plates

Oxygen sensor particles were made by adsorbing 75 mg 4,7-diphenyl-1,10-phenanthioline ruthenium (Alfa Aesar, CAS#: 36309-88-3) dissolved in 25 ml ethanol onto 11.5 g of silica gel powder (Aldrich, Catalog no: 23,675-6). The mixture was placed in a glass desiccant chamber connected to a vacuum pump and dried after which it was stored at -20°C.

For every 6.5 g of silicone elastomer base (Dow Corning, Sylgard, Catalog no: 3097366-0503) roughly 1.4 g of dried oxygen sensor adsorbed onto silica powder and 0.65 g of the curing agent (Dow Corning, Sylgard, Catalog no: 3097358-0503) were used to make the silicone rubber/sensor mixture. After mixing all three components such that no large clumps of undispersed powder were present, the mixture was added to plates using a 1 ml syringe such that the final sensor thickness was about 0.625 mm. This is more than that in the commercial OBS device plates but results from limitations in the accuracy of the syringe used to measure volume.

After adding the mixture to each well visible clumps of undissolved powder were removed using a 200 µl pipette. The mixture was spread to all edges of the dish and allowed to cure at room temperature for 2 days on a level surface before sterilization with ethanol and UV light.

Culture medium

INS-1 cells (passage 15-30) were cultured in supplemented RPMI (11.1 mM D-glucose, 100 U/ml penicillin, 100 ug/ml streptomycin, 2 mM L-glutamine, 1 mM sodium pyruvate all obtained from Mediatech Inc., Herdon, VA, and 50 µM β-mercaptoethanol obtained from Sigma Aldrich, St. Louis, MO) with 10% FBS (Mediatech Inc.) and either 0 or 0.9% agarose.

One percent agarose medium was made by mixing 2/3 volume of a 1.5% agarose solution (1.5g ultra low melting point agarose powder Sigma, Catalog no: A-5030 in 98.5g DI water) with 1/3 volume of 3X RPMI solution (no FBS). Prior to dilution, the 1.5% agarose solution was heated until boiling to completely dissolve the powder and sterilize the solution. After mixing with the concentrated RPMI, 10% FBS was added to the 1% solution resulting in a 0.9% agarose solution. In order to avoid premature gelling, all components were stored at 37°C in a water bath before mixing.

Experimental protocol

A 2 μg/ml fibronectin solution (made by adding 100μl of 1 mg/ml fibronectin, Sigma, Catalog no: F1141-2MG, to 50ml PBS) was added to each well completely covering the bottom of the vessel. After incubating for four hours at 25°C the fluorescence was measured with 485 nm excitation and 630 nm emission wavelengths in a plate reader and the fibronectin solution was removed. INS-1 cells in liquid and agarose containing medium were added to wells for a targeted surface density of 100,000 cells/cm^2 and a medium depth of 3mm. Petri dishes, 6-well, 12-well, 24-well, and 96-well plates were used in the experiments. In addition one strip of eight glass wells with silica rubber/sensor added were also used in some experiments. Before placing the cells in the humidified 37°C incubator with 5% CO_2, the plates were shaken to make sure there was a uniform distribution of the cells across the bottom of the well.

Four fluorescence intensity readings were obtained for each plate during the course of an experiment all of which were read using the same gain. The first intensity reading was at ambient conditions prior to the removal of the fibronectin solution from the plates. The second reading was obtained after overnight incubation following cell seeding. After the second reading, the agarose plates were gelled for 20 minutes at 4°C before being returned to the 37°C incubator. After incubation for 20 hr in the gelled medium a third reading was taken. Following the third reading, tissue was removed from the plates and a 1M sodium sulfite solution was added to deplete the oxygen in the well. The final reading was taken 4-8 hours after adding sodium sulfite.

Nuclei samples were collected from the plates culturing cells in liquid RPMI after the third fluorescent reading. After removing the liquid medium, lysis solution was to the wells added liberating nuclei. Samples of the lysed cells were quantified using cell enumeration by nuclei counting. In some cases cells from the Petri dishes were trypsinized for 3 min, collected, re-suspended in fresh medium, and analyzed for OCR using the stirred chamber method.

Islet enumeration by nuclei counting

Nuclei were prepared by adding equal 100-µl volumes of sample containing 160 or more IE and of lysis solution (0.1 M citric acid (Sigma) and 1% (v/v) Triton X-100 (Sigma)) to a 1.5 ml microtube [55]. The mixture was incubated at room temperature for 5 min with vortex mixing every 1.5 min, and nuclei were liberated by shearing through a needle. Isolated nuclei were diluted with Dulbecco's phosphate buffered saline (D-PBS, Invitrogen, Carlsbad, CA) to a concentration no higher than 5 x 10^5 nuclei/ml, stained with 7-aminoactinomycin D (7-AAD, Molecular Probes, Eugene, OR), and analyzed using a flow cytometer (Guava Personal Cell Analysis (PCA) system, Guava Technologies, Hayward, CA) to determine the total number of cells with intact nuclei in the sample.

Oxygen consumption rate (OCR)

OCR was measured as previously described [39]. Briefly, suspensions containing about 2500 IE/ml in DMEM containing 4.5 g/l glucose and 0.6 g/l L-glutamine supplemented with 100 U/ml penicillin, 100 µg/ml streptomycin, 10 mM HEPES, and no added serum were sealed in a 200-µl stirred titanium chamber (Micro Oxygen Uptake System, FO/SYSZ- P250, Instech Laboratories, Plymouth Meeting, PA) maintained at 37°C. The time dependent pO_2 within the chamber was recorded with a fluorescence-based oxygen sensor (Ocean Optics, Dunedin, FL), and data at high pO_2 were fit to a straight line. The maximal OCR was evaluated from $OCR=V_{ch}\alpha(\Delta pO_2/\Delta t)$, where V_{ch} is the chamber volume and α = 1.27 nmol/mm·Hg·ml is the Bunsen solubility coefficient for oxygen in medium [16]. OCR measurements were normalized by the measured number of cells (nuclei counting) or DNA content of the sample examined.

Statistics

Measurements were made with three or more replicates and reported as mean ± SD. Statistical significance was determined using a Student t-test for unpaired data for comparing population means, and for paired data when appropriate.

10.3.3 Theoretical model

Previously we utilized a theoretical oxygen transport model to simulate steady state islet culture (Chapter 3 and 4). Here we apply similar model equations to the OBS system. The species conservation equation for O_2 in the absence of convection is given by [16; 97]

$$\frac{\partial C}{\partial t} = D\nabla^2 C + R \qquad \textbf{10.6}$$

where C is the concentration of oxygen, D is the diffusivity of oxygen, and R is the production rate of oxygen. For convenience, the concentration terms in Equation 10.6 are replaced with oxygen partial pressure (p) using

$$C = \alpha p \qquad \textbf{10.7}$$

where α is the solubility of oxygen. We assume that solubility is constant in each phase so that at steady state Equation 10.6 becomes

$$0 = D\alpha\nabla^2 p + R \qquad \textbf{10.8}$$

Oxygen consumption within the tissue is assumed to follow Michaelis-Menten kinetics [16] for which the reaction rate is expressed as

$$R = -\frac{V_{max} p}{K_m + p} \qquad \textbf{10.9}$$

where V_{max} is the maximum reaction velocity, and the Michaelis constant K_m is the pO_2 at which the reaction rate is $V_{max}/2$. V_{max} was determined by multiplying the OCR/cell times the number of cells per well divided by the volume of the cell layer within the geometry. This oxygen consumption reaction only occurs above a critical pO_2 (p_{crit}). Below p_{crit}, the tissue dies and no longer consumes oxygen.

Three theoretical models were developed to explore oxygen transport within the OBS. The first assumed the ideal geometry with infinitely thin cell and sensor layers in an oxygen-impermeable dish (Figure 10.8A). The second geometry was a close representation of the actual well accounting for vessel curvature, oxygen permeability in polystyrene and finite thicknesses of the tissue and sensor (Figure 10.8B). The final geometry was similar to that in Figure 10.8B, but assumed a flat bottom vessel instead of a round bottom vessel (Figure 10.8C). This vessel represents the OBS plates of varying size that were fabricated in our lab. All these geometries assume that the system is axisymmetric around r = 0. The assumptions made in each geometry result in models governed by slight variations of basic mass transport equations.

For the idealized model (Figure 10.8A) the following equation is applied to transport in the medium (m).

$$0 = (D\alpha)_m \nabla^2 p \qquad \textbf{10.10}$$

The boundary conditions for the idealized model include: constant external pO_2 across the gas-liquid interface,

at $z = h$, $$p_{gas} = p_m \qquad \textbf{10.11}$$

no oxygen flux through the oxygen-impermeable dish,

at $r = R_{well}$, $$\frac{\partial p}{\partial r} = 0 \qquad \textbf{10.12}$$

and the oxygen consumption in the infinitely thin cell layer at the bottom of the well is

at $z = 0$, $$N = -\frac{OCR/cell \cdot \chi \cdot p}{K_m + p} \qquad \textbf{10.13}$$

where N is the oxygen flux, χ is the cell surface density (cells/cm^2) and OCR/cell is the normalized OCR measured using the stirred tank reactor.

The non-idealized models (Figure 10.8B and C) require separate equations for each domain: one for the medium (m), one for the polystyrene (ps), one for the silicone rubber/sensor layer (s), and one for the tissue (t). The respective equations are

$$0 = (D\alpha)_m \nabla^2 p \qquad \textbf{10.14}$$

$$0 = (D\alpha)_{ps} \nabla^2 p \qquad \textbf{10.15}$$

$$0 = (D\alpha)_s \nabla^2 p \qquad \textbf{10.16}$$

$$0 = (D\alpha)_t \nabla^2 p - \frac{V_{max} p}{K_m + p} \qquad \textbf{10.17}$$

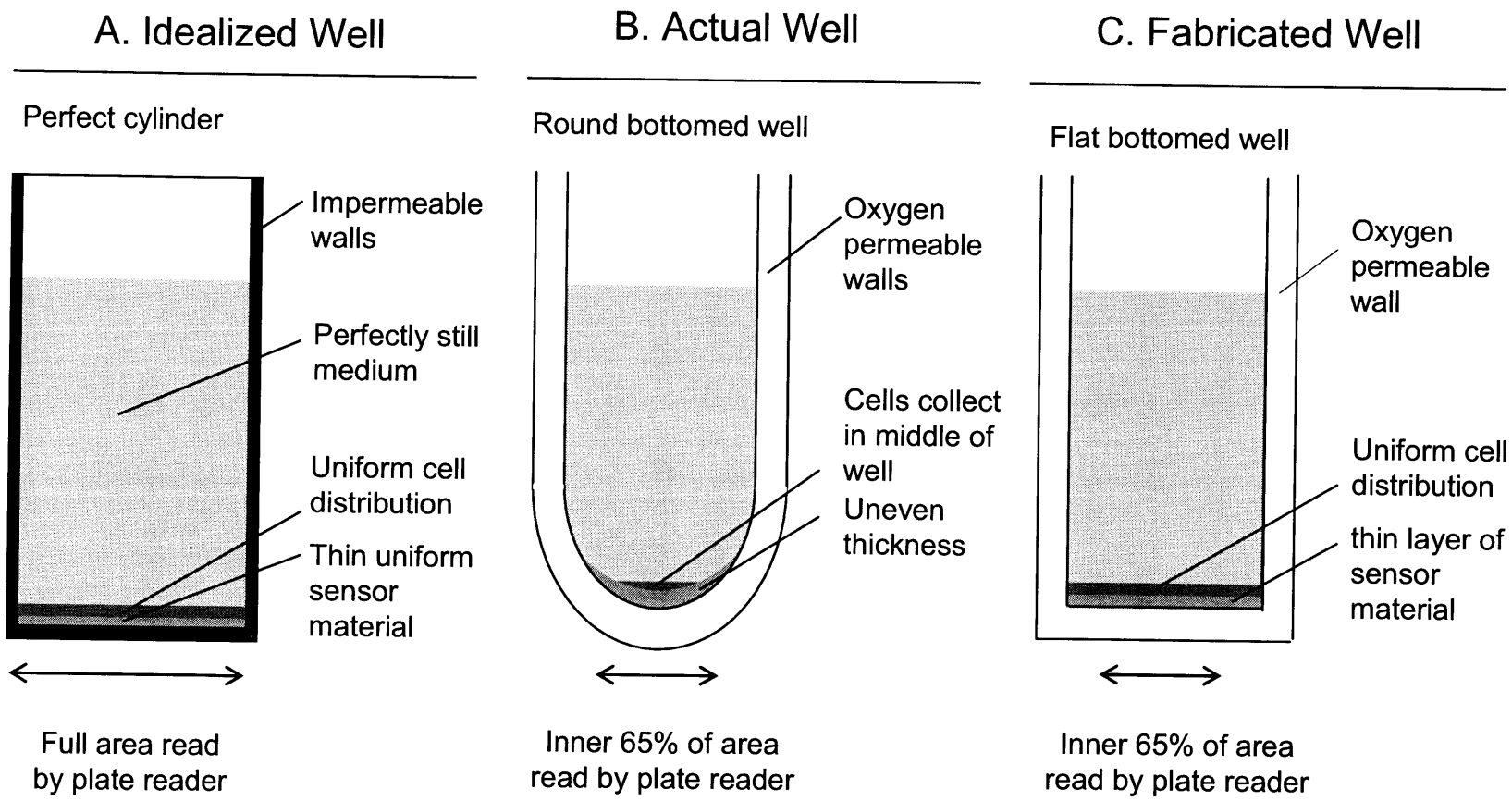

Figure 10.8. Geometry and the associated assumptions used for the three different theoretical models.

The boundary conditions for the non-idealized OBS include constant external pO_2 across the gas-liquid and gas-polystyrene interface,

$$p_{gas} = p_m \quad \textbf{10.18}$$

$$p_{gas} = p_{ps} \quad \textbf{10.19}$$

continuity of pO_2 and the oxygen flux across domain interfaces including polystyrene-medium, polystyrene-tissue, polystyrene-sensor, medium-tissue, and tissue-sensor,

$$n \bullet ((-D\alpha\nabla p)_{domain1} - (-D\alpha\nabla p)_{domain2}) = 0 \quad \textbf{10.20}$$

$$p_{domain1} = p_{domain2} \quad \textbf{10.21}$$

and symmetry boundary conditions for the axisymmetric problem, at r= 0,

$$n \bullet (-D\alpha\nabla p) = 0 \quad \textbf{10.22}$$

Table 10.3 contains the values for the parameters used in the simulations. All parameter values have been discussed previously (Chapter 5) with the exception of oxygen diffusivity and solubility in polystyrene. The oxygen solubility in polystyrene at 25°C ranges from 0.53 – 1.1 x 10^{-8} mol/cm^3 mmHg depending on how it was crystallized [203] while the diffusivity at 25°C ranges from 0.11 – 5.4 x 10^{-7} cm^2/s [203-207]. The oxygen permeability in polystyrene at 25°C ranges from 0.54 – 11.9 x 10^{-15} mol/cm s mmHg [144; 145; 203; 208]. Using the extremes of each parameter from literature we find a wide range of 0.0583 – 11.9 x 10^{-15} mol/cm s mmHg for oxygen permeability in polystyrene at 25°C. Since temperature is at 37°C during culture the permeability should be adjusted to account for the temperature difference. To adjust for the temperature difference we assume that oxygen transport in polystyrene is similar to that in polycarbonate, which has resulted in a 25% increase in oxygen permeability when temperature was increased from 30 to 40°C or about a 2.5% increase every degree [209]. Thus a 30% increase in oxygen permeability in polystyrene is assumed for the 12°C difference between the desired permeability temperature at 37°C and 25°C. The resulting permeability at 37°C is estimated to be between 0.076 – 15.5 x 10^{-15} mol/cm s mmHg with a base case value of 3.5 x 10^{-15} mol/cm s mmHg.

The model was solved with the finite element method using the commercially available software COMSOL Multiphysics (COMCOL Inc., Burlington, MA) in conjunction with Matlab (Mathworks, Natick, MA). We required the mesh to contain more than 2500 nodes and set a convergence criterion such that the relative error estimated by the finite element software in the solution vector for concentration, which takes into account the current and previous solution in the iterative solver, was less than 10^{-6} [99].

After the theoretical model was solved the results were analyzed to determine the pO_2 measured by the OBS. Using COMSOL Multiphysics the pO_2 in the sensor layer was converted to an intensity ratio (I/I_o) using a version of the Stern-Volmer relationship

$$\frac{I}{I_O} = \frac{1}{1 + K_{SV} \cdot p} \qquad \textbf{10.23}$$

where I and I_o are the emission intensities in the presence and absence of oxygen and K_{sv} is a constant characteristic related to the sensor quenching rate and emission lifetime [210]. For the idealized model (Figure 10.8A) the average intensity ratio was determined by integrating the intensity over the area of the plate read by the sensor (from r = 0 cm to r = 0.256 cm) and then dividing by the integrated surface area. For the models that accounted for the sensor thickness the average intensity ratio was determined by integrating over the volume of the sensor read by the plate reader (from r = 0 cm to r = 0.256 cm) and then dividing by the integrated volume. The average intensity was converted to a pO_2 and an OCR/cell using

$$p = \frac{\left(\left(\frac{I_O}{I}\right)_{ave} - 1\right)}{K_{SV}} \qquad \textbf{10.24}$$

$$\frac{OCR}{cell} = \frac{(D\alpha)_m \left(p_{gas} - p\right)}{h \cdot \chi} \qquad \textbf{10.25}$$

Table 10.3. Parameters used in theoretical simulations for oxygen transport in the OBS device.

Parameter	Symbol	Value	Units	Reference
Michaelis constant	K_m	0.44	mmHg	[98]
O_2 diffusivity - medium	D_m	2.78×10^{-5}	cm^2/s	[16]
O_2 diffusivity - tissue	D_i	1.22×10^{-5}	cm^2/s	[16]
O_2 diffusivity - silicone rubber	D_s	2.17×10^{-5}	cm^2/s	[116]
O_2 solubility - medium	α_m	1.27×10^{-9}	mol/cm^3 mmHg	[16]
O_2 solubility - tissue	α_i	1.02×10^{-9}	mol/cm^3 mmHg	[16]
O_2 solubility - silicone rubber	α_s	1.21×10^{-9}	mol/cm^3 mmHg	[116]
O_2 permeability - polystyrene	$(D\alpha)_{ps}$	3.5×10^{-15}	mol/cm s mmHg	Varied - see text
Stern-Volmer constant	K_{sv}	0.03125		Based on experiment
Medium depth		3	mm	Based on medium volume and well area
Tissue thickness		12	μm	Based on average cell diameter
OCR/cell		2.8	fmol/min cell	Experimentally measured
Area analyzed by plate reader		0.256	cm^2	Based on equipment capabilities
Sensor volume - actual OBS		7	μl	Based on commercial device
Sensor thickness - fabricated wells		0.0625	cm	Based on sensor volume and well area
Polystyrene thickness		1.2	mm	Experimentally measured
Minimum pO_2 for viability	p_{crit}	0.1	mmHg	[16]
External p	p_{gas}	142	mmHg	Partial pressure of O_2 in humidified incubator at 37°C with 95% air/5% CO_2

OCR/cell of INS-1 cells was determined using the stirred chamber method. The reading position assumed for the plate reader was equal to 65% of the bottom surface area for a 96 well plate (0.209 cm^2).

10.3.4 Calculating experimental OCR from OBS

This section describes the step-by-step procedure of converting the fluorescent intensity readings of the OBS plate to pO_2 and OCR/cell values. The initial reading of a plate containing 2 μg/ml fibronectin solution equilibrated with ambient air at room temperature is set equivalent to the initial ambient intensity, I_A. Intensity readings at the end of the experiment (3rd reading, after cell addition and gelling) for sample (wells containing cells) and control (wells with only medium) wells corresponded to I_S and I_C, respectively. The final reading 4 to 8 hours after adding 1 M sodium sulfite solution corresponded to the zero pO_2 and is the maximum intensity reading I_0.

To calculate pO_2 multiple manipulations of the intensity readings need to be made. First, I_S for each particular well is adjusted for variations in sensor concentration by dividing by the corresponding I_A for that well resulting in I_S', the adjusted sample intensity.

$$I_S' = \frac{I_S}{I_A} \qquad \textbf{10.26}$$

A similar adjustment is made for the control wells.

$$I_C' = \frac{I_C}{I_A} \qquad \textbf{10.27}$$

Signal drift correction associated with changes in the ambient is performed by dividing I_S' by $\overline{I_C'}$, the averaged adjusted control intensities, to obtain I_S'', the adjusted cell sample intensity normalized for drift.

$$\overline{I_C'} = \frac{1}{n}\sum_n I_{C,n}' \qquad \textbf{10.28}$$

$$I_S'' = \frac{I_S'}{\overline{I_C'}} \qquad \textbf{10.29}$$

The maximum increase in fluorescent signal, R, is found for each individual well.

$$R = \frac{I_O}{I_A} \tag{10.30}$$

Then, the Stern Volmer equation is applied to find corresponding cell surface pO_2 values.

$$p = \frac{\frac{R}{I_S''} - 1}{\frac{R-1}{p_{gas}}} \tag{10.31}$$

where p_{gas} is the O_2 partial pressure at ambient conditions at the end of the experiment when the final measurement is taken. Once the pO_2 for each well is determined OCR/cell can be calculated using 10.25.

10.3.5 Theoretical results

Oxygen profiles for the idealized model, the commercially available device, and the fabricated flat bottom wells for the specific case of 250,000 cells/cm^2 in 3 mm medium are shown in Figure 10.9 with the minimum pO_2 in the tissue and the OCR/cell that would be determined by the OBS listed above each plot. The idealized model indicates uniform diffusion through the medium resulting in an OCR/cell of 2.8 nmol/min cm^2, which is the same as the inputted value based on the stirred chamber measurements (Table 10.3). The model based on the commercially available device and the fabricated devices indicate significant transport through the polystyrene resulting in lower OCR/cell values. In both the commercial and fabricated devices the oxygen flux through the polystyrene accounts for 43-46% of the total oxygen flux into the system (data not shown). The differences in minimum pO_2 and OCR/cell between the fabricated well and the commercially available device result because one is a round-bottom well and one is a flat-bottom well. Though both have transport through the polystyrene, the commercially available device has additional limitations including tissue pooling and a larger medium depth in the center of the well and thus the pO_2 in the sensor layer is lower.

The sensitivity of the fabricated device to changes in the parameter values was explored to provide insight into which parameters have the largest impact on the OBS system. Variations in tissue thickness, sensor layer thickness, polystyrene thickness (side and bottom), reader position, and oxygen permeability in medium, the sensor, and the tissue did not have a large

effect on the steady state OCR determined by the OBS for a realistic range of values (data not shown).

OCR/cell determined by the OBS does not vary with surface density assuming a uniform distribution until the partial pressure in the tissue decreases significantly. The low pO_2 in the tissue at high surface densities causes OCR to decrease because of Michaelis-Menten kinetics (10.9) and in extreme cases, at $pO_2 < 0.1$ mmHg, could result in tissue death from hypoxia (Figure 10.10). This suggests that the cell density used in experiments should $< 400{,}000$ cells/cm^2 for a 96-well plate or $< 300{,}000$ cells/cm^2 for a Petri dish. Note that if the tissue distribution is not uniform predictions could change significantly.

Oxygen permeability in polystyrene varied significantly in literature and has a large effect on the OCR determined by the OBS (Figure 10.11). The more oxygen coming through the polystyrene (i.e. the higher the oxygen permeability in polystyrene), the lower the OCR/cell measured by the OBS. The base case value of 3.5×10^{-15} mol/cm s mmHg, which is in the mid to upper end of values obtained from literature, results in an OCR/cell that is only 60% of that obtained with the stirred chamber method.

Significant amounts of oxygen enter the system through the polystyrene at both the bottom of the well and the sides, which suggests that well size should have an impact on the OCR determined by the OBS. As well radius increases, the OCR/cell obtained from the device increases until it reaches a plateau (Figure 10.12), which occurs when the polystyrene walls no longer affect the central portion of the well. Though this suggests that increasing well size will bring the measurement closer to the benchmark, the plateau can still be well below the stirred chamber value if a significant amount of oxygen is transported through the polystyrene directly below the sensor.

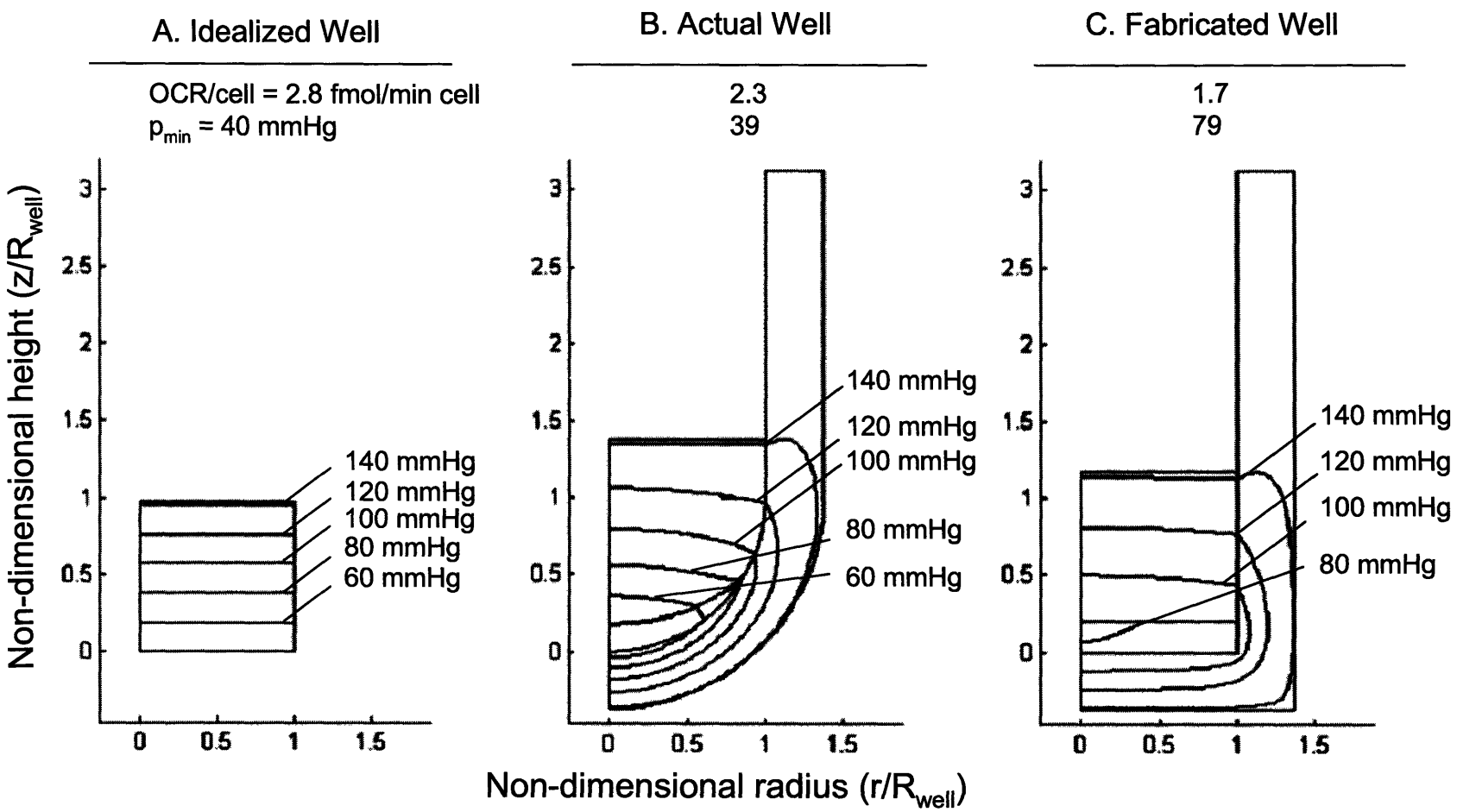

Figure 10.9. Theoretical oxygen profiles in the (A) idealized, (B) actual, and (C) fabricated OBS plates. Predictions assume 250,000 cells/cm^2. The resulting minimum pO_2 in the tissue and the OCR/cell that would be calculated by the OBS for is given above each model.

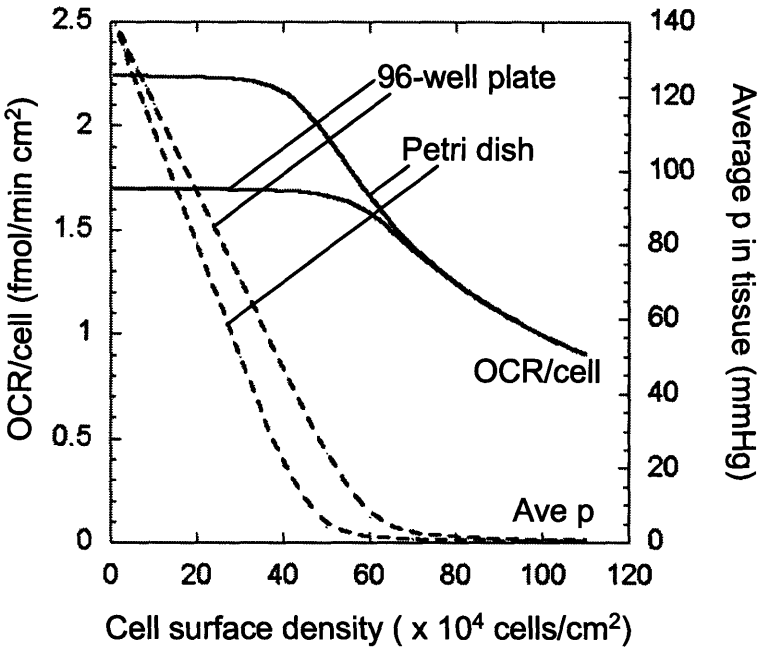

Figure 10.10. Predicted OCR/cell determined by the OBS (solid lines) and the average pO_2 in the tissue (dashed lines) as a function of cell density for a 96-well plate and Petri dish.

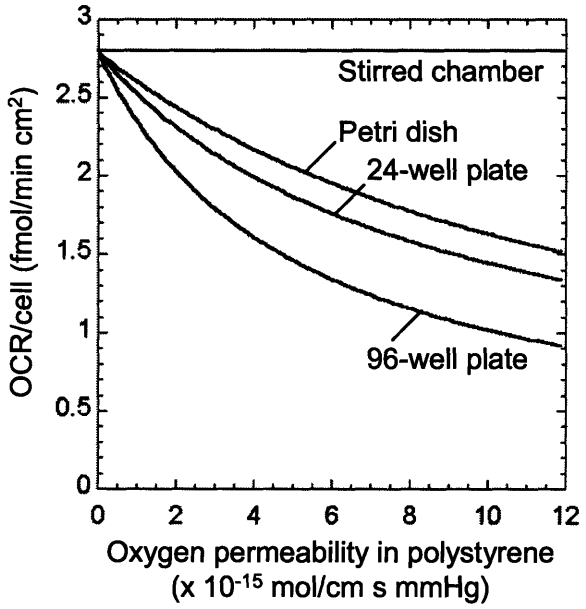

Figure 10.11. Predicted OCR/cell determined by the OBS as a function of oxygen permeability in polystyrene for a Petri dish, 24-well plate, and 96-well plate.

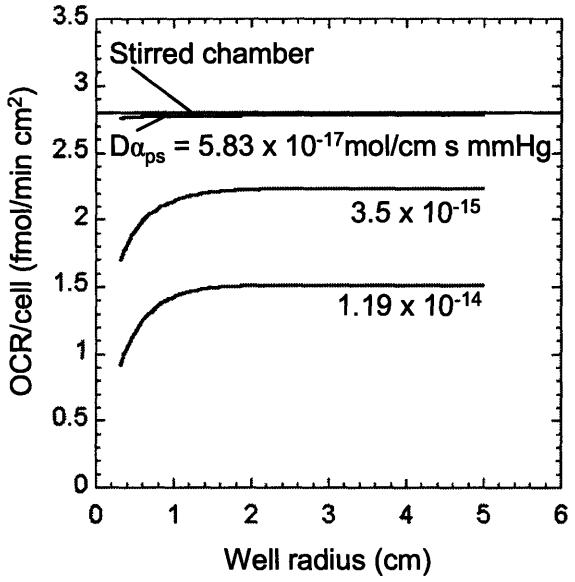

Figure 10.12. Predicted OCR/cell determined by the OBS as a function of well radius and oxygen permeability in polystyrene.

10.3.6 Experimental results

The OCR/cell obtained for INS-1 cells in both the liquid (Figure 10.13A) and gelled medium (Figure 10.13B) from the 96 well plates was below the value of the stirred chamber. As plate size increased the OCR/cell determined by the fabricated OBS dishes increased eventually resulting in OCR/cell similar to the benchmark. The OCR/cell obtained from the 96-well plate is significantly lower than the values obtained from larger wells for cells in gelled medium ($p < 0.05$). On the other hand OCR/cell values of cells cultured in the larger well sizes did not differ significantly. Results were similar for liquid medium.

The experimental data in Figure 10.13 and theoretical results in Figure 10.11 and Figure 10.12 suggest that polystyrene could cause lower OCR values than that obtained by the stirred chamber. However, the OCR/cell obtained from INS-1 cells in gelled medium in polystyrene and glass wells (size of wells in a 96-well plate) were 1.9 ± 0.3 and 1.9 ± 0.2 ($p > 0.6$, n=3), respectively, suggesting that the assumption that polystyrene is oxygen-impermeable is valid.

Difference between OCR obtained from gelled and liquid medium revealed that convective transport was present during normal OBS operation. OCR/cell measured by the OBS for INS-1 cells in gelled medium was statistically higher than that in liquid medium when all the data except for the 24-well plate, which had a high standard deviation, is considered ($p < 0.10$).

Comparisons between individual well sizes varied in differences with $p < 0.10$ for only the glass wells and the 12-well plates (Table 10.4). The lack of significance in other well size comparisons is likely due to the limited number of experiments and variation between them. In addition, the averages of two plates that suggest convection is not important (24-well plate and the Petri dish) each contain a single point that was somewhat different than the other two, but that could not be thrown out because of limited data. Though the effect of convection varies between experiments the results suggest that convection decreased OCR measurements by roughly 15% on average (ignoring data from 24-well plate), but as much as 35%.

10.3.7 Discussion

In this study we examined the use of oxygen sensors embedded in silicone rubber at the bottom static culture dishes for measurement of pO_2 and calculation of OCR. Through theoretical modeling and experimental measurements we investigated two assumptions required for easy calculation of OCR from the static culture devices including (1) oxygen-impermeable dishes and (2) stagnant medium. The results here provide insight into why OCR measurements with the commercially available device are inaccurate and suggest modifications that can be made to get accurate measurements with a static culture device.

Several model parameters were examined, but only a few had a large impact on the model predictions. Cell surface density had a significant impact on the OCR determined by the OBS (Figure 10.10). Very high densities caused a reduction in the apparent OCR/cell because of Michaelis-Menten kinetics indicating the theoretical limitations of the system.

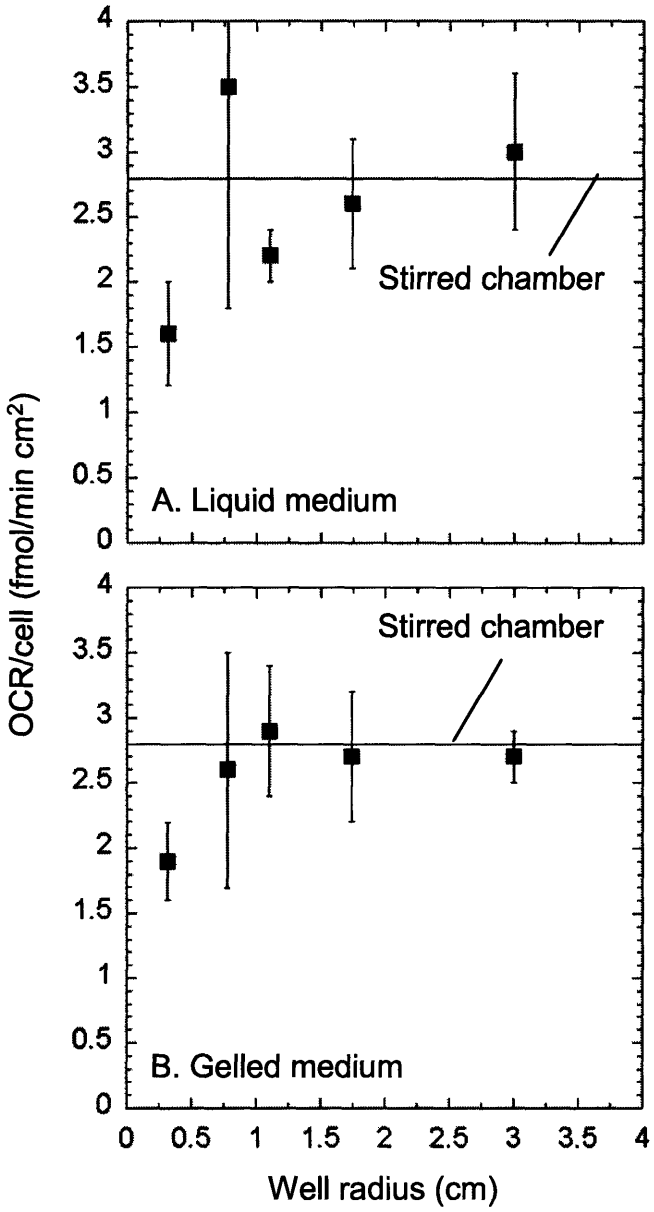

Figure 10.13. OCR/cell determined by fabricated OBS plates as a function of well radius. Predictions for INS-1 cells cultured in (A) liquid and (B) gelled medium. The horizontal line represents the benchmark value obtained from the stirred chamber. The error bars are ± standard deviation for n = 3 experiments.

Table 10.4. Comparison of OCR/cell between cells in liquid and gelled agarose medium.

Well size	Liquid OCR/cell fmol/(min cell)	Agarose OCR/cell fmol/(min cell)	p-value
96 well plate	1.6 ± 0.4	1.9 ± 0.3	0.12
24 well plate	3.5 ± 0.7	2.6 ± 0.9	0.26
12 well plate	2.2 ± 0.2	2.9 ± 0.5	0.07
6 well plate	2.6 ± 0.5	2.7 ± 0.5	0.14
Petri dish	3.0 ± 0.6	2.7 ± 0.2	0.62
Glass plate	1.4 ± 0.1	1.9 ± 0.2	0.03

Data listed as mean ± standard deviation for 3 independent experiments.

The theoretical model suggested that oxygen flux through the polystyrene could be a significant source of error if the oxygen permeability was too high (Figure 10.11). However, experimental comparisons between glass and polystyrene wells demonstrated that oxygen transport through the polystyrene was negligible and thus $D\alpha_{ps}$ is lower than that assumed for most of the simulations. This is consistent with our experimental measurements in large wells that indicate no significant flux through the polystyrene on the bottom of the dish (Figure 10.13B). However, at low rates of oxygen consumption or measurement in low pO_2 environments, the oxygen permeability in polystyrene could become more problematic as suggested previously [210-212].

The assumption of stagnant medium is more problematic. Convective transport decreased the apparent OCR/cell 25% from that of cells cultured in gelled medium (Table 10.4). This convective transport may be due to vibrations and thermal variations within the incubator, but is most likely due to movement in the plate reader and when transferring the plate from the incubator to the plate reader. The substantial motion in the plate reader has been demonstrated by comparing the transient reequilibration with oxygen at the bottom of wells initially purged with nitrogen and filled with either water or an agarose gel that prevents fluid motion (unpublished data). For accurate measurement of OCR using the OBS the use of gelled medium is critical since the convective transport could vary each time the plate is removed from the incubator.

Despite the removal of convection and the confirmation that oxygen flux through polystyrene is negligible, variations still exist between wells of different size which may be related to curvature of the sensor in the plate. Though sensor is added to the plate for a uniform height, capillary forces the edge of the wells draw up the silicone rubber/sensor mixture resulting in a slightly curved bottom. This curvature tends to be larger for smaller wells, especially for the 96 well plate, which gives the lowest OCR/cell. The use of larger wells results in accurate OCR/cell measurements by the fabricated OBS device though additional experiments are needed to confirm.

10.3.8 Nomenclature

C	Concentration of oxygen
D	Diffusivity of oxygen
D-PBS	Dulbecco's phosphate buffered saline
FBS	Fetal bovine serum
h	Medium depth
I	Emission intensity in the presence of oxygen
I_A	Emission intensity for ambient reading
I_C	Emission intensity for control reading
I_C'	Adjusted control intensity
$\overline{I_C'}$	Averaged adjusted control intensities
I_o	Emission intensity in the absence of oxygen, maximum intensity reading
I_S	Emission intensity for sample reading
I_S'	Adjusted sample intensity
I_S''	Adjusted cell sample intensity normalized for drift
K_m	Michaelis constant, the pO_2 at which the reaction rate is $V_{max}/2$
K_{sv}	Characteristic related to the sensor quenching rate and emission lifetime
OBS	Oxygen biosensor system
OCR	Oxygen consumption rate
p	Oxygen partial pressure

p_{crit}	The pO_2 below which a cell dies and no longer consumes oxygen
p_{gas}	Ambient partial pressure of oxygen
R	Production rate of oxygen
R	Maximum increase in fluorescent signal
r	Radial direction in cylindrical coordinates
R_{well}	Radius of well
t	Time
V_{ch}	Volume of OCR chamber
V_{max}	Maximum reaction velocity
α	Solubility of oxygen in medium
χ	Cell surface density (cells/cm^2)

Subscripts for D, α, p, C

m	Medium
s	Sensor/silicone rubber mixture
ps	Polystyrene
t	Tissue

10.4 Matlab code for oxygen transport during static culture on polystyrene

```
% FEMLAB Model M-file
flclear fem
% COMSOL version
clear vrsn
vrsn.name = 'COMSOL 3.2';
vrsn.ext = 'a';
vrsn.major = 0;
vrsn.build = 300;
vrsn.rcs = '$Name:  $';
vrsn.date = '$Date: 2005/12/20 19:02:30 $';
fem.version = vrsn;

% Get input for parameters
po2ext = 142;  % mmHg
V_max = 3.68e-8; % mol/cm3 s
K_m = 0.44;  % mmHg
height = 0.3;  % cm
radius_islet= 0.0075;  % cm
diff_alpha_islet = 1.24e-14; % mol/cm mmHg s
diff_alpha_medium = 3.53e-14; % mol/cm mmHg s
P_crit = 0.1;  % mmHg
islet_density = 100; % islets/cm2
alpha_medium = 1.27e-9; % mol/cm3 mmHg
alpha_islets = 1.02e-9; % mol/cm3 mmHg
% Place constant into fem
fem.const={'alpham',alpha_medium,'alphai',alpha_islets,'Pext',po2ext,'Dai',diff_alpha_islet','Vmax',V_max,'Dam',dif
f_alpha_medium,'Km',K_m,'Rislet',radius_islet,'Pcrit',P_crit};
% Specifies dimensions
fem.sdim=3;

% GEOMETRY
%%%%%%%%%%%%%%%%%%%%%%%%%%%%%%%%%%%%%%%%%%%
% Function to create geometry for islet array (equally spaced islets in a
% square array. Only an eighth of an islet will be modeled because of
% symmetry.
% Set length of sides of block
% scaling parameter for height of medium, radius of islet=1
scale_height = height/radius_islet; % scaling parameter for height of box
scale_space = ((1/islet_density)^(1/2))/radius_islet; % calculating length of sides for given density
Lx = scale_space; % center to center distance between islets
Ly = scale_space;
Lz = (scale_height);
% Create block for medium
B3_1=block3(Lx,Ly,Lz,'base','corner','pos',{'0','0','0'},'axis',{'0','0','1'},'rot','0');
B3_2=block3(Lx,Ly,Lz,'base','corner','pos',{'0','0','0'},'axis',{'0','0','1'},'rot','45');
B3_3=block3(Lx/2,Ly/2,Lz,'base','corner','pos',{'0','0','0'},'axis',{'0','0','1'},'rot','0');
B3_4=B3_1*B3_2;
B3_triangle1=B3_3-B3_4;
% Now we will add in the sphere for islet of a given radius set to 1
S3a = sphere3(1,[0 0 1]);
% make sphere into one eighth of islet
S3_eighth=S3a*B3_triangle1;
```

```
% remove corner from lower block
B3_triangle2=B3_triangle1-S3a;
% Combine into a single geometry
clear s
s.objs={S3_eighth,B3_triangle2};
s.name={'CO1','Blk1'};
s.tags={'S3_eighth','B3_triangle2'};
fem.draw = struct('s',s);
fem.geom = geomcsg(fem);
%%%%%%%%%%%%%%%%%%%%%%%%%%%%%%%%%%%%%% Initialize mesh
fem.mesh=meshinit(fem);
mesh_test = size(fem.mesh.t,2);
while mesh_test<2500
fem.mesh=meshrefine(fem);
mesh_test = size(fem.mesh.t,2);
end

% (Default values are not included)
% Application mode 1
clear appl
appl.mode.class = 'FlDiffusion';
appl.shape = {'shlag(2,"lm1")','shlag(2,"c")'};
appl.assignsuffix = '_di';
clear prop
clear weakconstr
weakconstr.value = 'non-ideal';
weakconstr.dim = {'lm1'};
prop.weakconstr = weakconstr;
appl.prop = prop;
clear bnd
bnd.type = {'N0','cont','C'};
bnd.weakconstr = {0,0,1};
bnd.c0 = {0,0,1};
bnd.wcshape = 1;
bnd.ind = [1,1,2,1,1,1,2,3,1];
appl.bnd = bnd;
clear equ
equ.D = {1,'Dam/Dai'};
equ.init = 1;
equ.R = {'-Vmax*Rislet^2/(Dai*Pext)*c/(c+Km/Pext)*(c>Pcrit/Pext)',0};
equ.shape = 2;
equ.ind = [1,2];
appl.equ = equ;
fem.appl{1} = appl;
fem.border = 1;
fem.outform = 'general';

% Multiphysics
fem=multiphysics(fem);
% Extend mesh
fem.xmesh=meshextend(fem);
% Solve problem
[fem.sol, fem.stop]=femnlin(fem, ...
            'solcomp',{'c','lm1'}, ...
            'outcomp',{'c','lm1'}, ...
            'out',{'sol','stop'},...
```

```
        'hnlin','on','maxiter',100);
% Save current fem structure for restart purposes
fem0=fem;
% Post processing
max_PO2 = postmax(fem,'c','solnum',1,'Dl',[1]); % Maximum node in islet
min_PO2 = postmin(fem,'c','solnum',1,'Dl',[1]); % Minimum node in islet
convergence1=fem.stop;
% Integrate islet without O2
frac_no_O2 = postint(fem,'1*c<=Pcrit/Pext','solnum',1,'phase',0*pi/180,'edim',3,'intorder',4,'geomnum',1,'dl',[1]);
% Integrate whole islet
islet_int = postint(fem,'1','solnum',1,'phase',0*pi/180,'edim',3,'intorder',4,'geomnum',1,'dl',[1]);
frac_dead=frac_no_O2/islet_int;
OCR = postint(fem,'lm1', ...
        'solnum',1, ...
        'phase',0*pi/180, ...
        'edim',2, ...
        'intorder',4, ...
        'geomnum',1, ...
        'dl',[8]); % Total oxygen flux into system
min_quality_mesh = min(meshqual(fem.mesh));
element_num = size(fem.mesh.t,2);
```

10.5 Matlab code for oxygen transport during static culture on silicone rubber

```
% FEMLAB Model M-file
flclear fem
% COMSOL version
clear vrsn
vrsn.name = 'COMSOL 3.2';
vrsn.ext = 'a';
vrsn.major = 0;
vrsn.build = 300;
vrsn.rcs = '$Name:  $';
vrsn.date = '$Date: 2005/12/20 19:02:30 $';
fem.version = vrsn;

% Get input for parameters
po2ext = 142;  % mmHg
V_max = 5.33e-8; % mol/cm3 s
K_m = 0.44;  % mmHg
height = 2.2;  % cm
radius_islet= 0.0075;  % cm
diff_alpha_islet = 1.24e-14; % mol/cm mmHg s
diff_alpha_medium = 3.53e-14; % mol/cm mmHg s
P_crit = 0.1;  % mmHg
islet_density = 100; % IEQ/cm2
diff_alpha_simembrane = 2.17e-5*1.21e-8; % mol/cm mmHg s
thickness = 0.05; % cm
% Place constant into fem
fem.const={'Pext',po2ext,'Dai',diff_alpha_islet','Vmax',V_max,'Dam',diff_alpha_medium,'Km',K_m,'Rislet',radius_i
slet,'Dasi',diff_alpha_simembrane,'Pcrit',P_crit};
% Specifies dimensions
fem.sdim=3;

%%%%%%%%%%%% GEOMETRY%%%%%%%%%%%%%%%%%%
% Function to create geometry for islet array (equally spaced spheres in a
% square array. Only one quarter of an islet will be modeled because of
% symmetry.
pt = [0 0 0]; % base point of 3D block
vec = [0 0 1]; % specifies direction of block
% Set length of sides of block
% scaling parameter for height of medium, radius of islet=1
scale_height = height/radius_islet; % scaling parameter for height of box
scale_space = ((1/islet_density)^(1/2))/radius_islet; % calculating length of sides for given density
Lx = scale_space; % center to center distance between islets
Ly = scale_space;
Lz = (scale_height-2);
% Create block for medium
B3top=block3(Lx/2,Ly/2,Lz,'corner',[0 0 2],vec);
% Now we will add in the spheres for islets of a given radius
% Spheres at vertices of block B3
S3a = sphere3(1,[0 0 1]);
% Create composite objects.
B3bottom=block3(Lx/2,Ly/2,2,'corner',pt,vec);
% First make sphere into quarters.
COa = S3a*B3bottom;
```

```
B3med=B3bottom+B3top;
B3meda=B3med-S3a; % remove corner from block
% Create block for membrane
Lzmem=thickness/radius_islet;
B3mem=block3(Lx/2,Ly/2,Lzmem,'corner',[0,0,-Lzmem],vec);
B3medb=B3meda+COa;
B3medc=B3medb+B3mem;
clear s
s.objs={B3medc};
s.name={'CO1'};
s.tags={'B3medc'};
fem.draw = struct('s',s);
fem.geom = geomcsg(fem);
%%%%%%%%%%%% END GEOMETRY %%%%%%%%%%%%%%%%%%%%
% Initialize mesh
fem.mesh=meshinit(fem, ...
                  'hmaxfact',5, ...
                  'hcutoff',0.07, ...
                  'hgrad',2, ...
                  'hcurve',1, ...
                  'hnarrow',0.1);
mesh_test = size(fem.mesh.t,2);
while mesh_test<2500
fem.mesh=meshrefine(fem);
mesh_test = size(fem.mesh.t,2);
end

%%%%%%%%%%%%%%%% Application mode no necrotic core %%%%%%%%%%%%%%%%
% Application mode 1
clear appl
appl.mode.class = 'FlDiffusion';
appl.shape = {'shlag(2,"lm1")','shlag(2,"c")'};
appl.assignsuffix = '_di';
clear prop
clear weakconstr
weakconstr.value = 'non-ideal';
weakconstr.dim = {'lm1'};
prop.weakconstr = weakconstr;
appl.prop = prop;
clear bnd
bnd.c0 = {0,1,0};
bnd.type = {'N0','C','cont'};
bnd.weakconstr = {0,1,1};
bnd.wcshape = 1;
bnd.ind = [1,1,2,1,1,1,3,3,1,1,1,3,3,2,3,1,1,1,1,1,1];
appl.bnd = bnd;
clear equ
equ.shape = 2;
equ.init = 1;
equ.D = {'Dasi/Dai',1,'Dam/Dai'};
equ.R = {0,'-Vmax*Rislet^2/(Dai*Pext)*c/(c+Km/Pext)*(c>Pcrit/Pext)',0};
equ.ind = [1,2,3,3];
appl.equ = equ;
fem.appl{1} = appl;
fem.border = 1;
fem.outform = 'general';
```

```
%%%%%%%%%%%%%%% End application mode no necrotic %%%%%%%%%%%%%
  % Multiphysics
  fem=multiphysics(fem);
  % Extend mesh
  fem.xmesh=meshextend(fem);
% Solve problem
[fem.sol, fem.stop]=femnlin(fem, ...
          'solcomp',{'c','lm1'}, ...
          'outcomp',{'c','lm1'}, ...
          'out',{'sol','stop'},...
          'hnlin','on','maxiter',100,...
          'ntol', 1e-006);
% Save current fem structure for restart purposes
fem0=fem;
convergence=fem.stop;
max_PO2 = postmax(fem,'c','solnum',1,'Dl',[2]); % Maximum node in islet
min_PO2 = postmin(fem,'c','solnum',1,'Dl',[2]); % Minimum node in islet
% Integrate islet without O2
frac_no_O2 = postint(fem,'1*c<=Pcrit/Pext','solnum',1,'phase',0*pi/180,'edim',3,'intorder',4,'geomnum',1,'dl',[2]);
% Integrate whole islet
islet_int = postint(fem,'1','solnum',1,'phase',0*pi/180,'edim',3,'intorder',4,'geomnum',1,'dl',[2]);
frac_dead=(frac_no_O2)/(islet_int);
OCRtop = postint(fem,'lm1', ...
       'solnum',1, ...
       'phase',0*pi/180, ...
       'edim',2, ...
       'intorder',4, ...
       'geomnum',1, ...
       'dl',[14]); % Total oxygen flux into system from top
OCRbottom = postint(fem,'lm1', ...
       'solnum',1, ...
       'phase',0*pi/180, ...
       'edim',2, ...
       'intorder',4, ...
       'geomnum',1, ...
       'dl',[3]); % Total oxygen flux into system from bottom
OCR = OCRtop+OCRbottom;
min_quality_mesh = min(meshqual(fem.mesh));
element_num = size(fem.mesh.t,2);
```

10.6 Matlab code for oxygen transport model with 2 sphere sizes

```
% FEMLAB Model M-file
% Set up vectors to store specific numbers of solutions
n=6;
max_PO2_1=linspace(1,n,n);
min_PO2_1=linspace(1,n,n);
frac_dead_1=linspace(1,n,n);
max_PO2_2=linspace(1,n,n);
min_PO2_2=linspace(1,n,n);
frac_dead_2=linspace(1,n,n);
OCR=linspace(1,n,n);
min_quality_mesh=linspace(1,n,n);
element_num=linspace(1,n,n);
convergence1=linspace(1,n,n);
i_density = [100 500 750 1000 1100 1110];

for i=1:n
flclear fem
% COMSOL version
clear vrsn
vrsn.name = 'COMSOL 3.2';
vrsn.ext = 'a';
vrsn.major = 0;
vrsn.build = 300;
vrsn.rcs = '$Name:  $';
vrsn.date = '$Date: 2005/12/20 19:02:30 $';
fem.version = vrsn;
% Get input for parameters
po2ext = 142;  % mmHg
V_max = 5.33e-8; % mol/cm3 s
K_m = 0.44;  % mmHg
height = 0.3;  % cm
radius_islet1= 0.0075;  % cm
radius_islet2= 0.0125;  % cm
diff_alpha_islet = 1.24e-14; % mol/cm mmHg s
diff_alpha_medium = 3.53e-14; % mol/cm mmHg s
P_crit = 0.1;  % mmHg
islet_density = i_density(i); % islets/cm2
alpha_medium = 1.27e-9; % mol/cm3 mmHg
alpha_islets = 1.02e-9; % mol/cm3 mmHg
V1 = 4/3*3.14*(radius_islet1)^3; %cm3
V2 = 4/3*3.14*(radius_islet2)^3; %cm3
V_IEQ = 4/3*3.14*0.0075^3; %cm3
R2R1 = radius_islet2/radius_islet1;
% Place constant into fem
fem.const={'alpham',alpha_medium,'alphai',alpha_islets,'Pext',po2ext,'Dai',diff_alpha_islet','Vmax',V_max,'Dam',dif
f_alpha_medium,'Km',K_m,'Rislet',radius_islet1,'Pcrit',P_crit};
% Specifies dimensions
fem.sdim=3;

% GEOMETRY
%%%%%%%%%%%%%%%%%%%%%%%%%%%%%%%%%%%%%%%%%%%%%%%%%%%%
% Function to create geometry for islet array (equally spaced islets in a
```

```
% square array. Only an eighth of an islet will be modeled because of
% symmetry.
% Set length of sides of block
% scaling parameter for height of medium, radius of islet=1
scale_height = height/radius_islet1; % scaling parameter for height of box
scale_space = (1/islet_density)^(1/2)/radius_islet1; % calculating length of sides for given density
Lx = scale_space; % center to center distance between islets
Ly = scale_space;
Lz = (scale_height);
% Create block for medium
B3_1=block3(Lx,Ly,Lz,'base','corner','pos',{'0','0','0'},'axis',{'0','0','1'},'rot','0');
B3_2=block3(2*Lx,2*Ly,Lz,'base','corner','pos',{'0','0','0'},'axis',{'0','0','1'},'rot','45');
B3_3=block3(2*Lx,2*Ly,Lz,'base','corner','pos',{Lx,'0','0'},'axis',{'0','0','1'},'rot','45');
B3_4=B3_1-B3_2;
B3_triangle1=B3_4-B3_3;
% Now we will add in the sphere for islet of a given radius set to 1
S3a = sphere3(1,[0 0 1]);
S3b = sphere3(R2R1,[Lx 0 R2R1]);
% make sphere into one eighth of islet
S3_eighth1=S3a*B3_triangle1;
S3_eighth2=S3b*B3_triangle1;
% remove corner from lower block
B3_triangle2=B3_triangle1-S3a;
B3_triangle3=B3_triangle2-S3b;
% Combine into a single geometry
B3_triangle4=B3_triangle3+S3_eighth1;
B3_triangle5=B3_triangle4+S3_eighth2;
clear s
s.objs={B3_triangle5};
s.name={'CO1'};
s.tags={'B3_triangle5'};
fem.draw = struct('s',s);
fem.geom = geomcsg(fem);
%%%%%%%%%%%%%%%%%%%%%%%%%%%%%%%%%%%%%%%%%%%%%%%%%%%%%%%%%%%%%%%%%%%%%%%%%%%%%%%

mesh_test = 0;
% Initialize mesh
fem.mesh=meshinit(fem);
mesh_test = size(fem.mesh.t,2);
while mesh_test<1100
  fem.mesh=meshrefine(fem);
  mesh_test = size(fem.mesh.t,2);
end

% Application mode 1
clear appl
appl.mode.class = 'FlDiffusion';
appl.shape = {'shlag(2,"lm1")','shlag(2,"c")'};
appl.assignsuffix = '_di';
clear prop
prop.weakconstr=struct('value',{'non-ideal'},'dim',{{'lm1'}});
appl.prop = prop;
clear bnd
bnd.c0 = {0,1,0};
bnd.type = {'cont','C','N0'};
bnd.weakconstr = {0,1,0};
```

```
bnd.wcshape = 1;
bnd.ind = [3,3,1,3,3,3,1,2,3,1,1,3,3];
appl.bnd = bnd;
clear equ
equ.shape = 2;
equ.init = 1;
equ.D = {1,'Dam/Dai'};
equ.R = {'-Vmax*Rislet^2/(Dai*Pext)*c/(c+Km/Pext)*(c>Pcrit/Pext)',0};
equ.ind = [1,2,1];
appl.equ = equ;
fem.appl{1} = appl;
fem.border = 1;
fem.outform = 'general';
% Multiphysics
fem=multiphysics(fem);
% Extend mesh
fem.xmesh=meshextend(fem);
% Solve problem
[fem.sol, fem.stop]=femnlin(fem, ...
        'solcomp',{'c','lm1'}, ...
        'outcomp',{'c','lm1'}, ...
        'out',{'sol','stop'},...
        'hnlin','on','maxiter',100);
% Save current fem structure for restart purposes
fem0=fem;
% Post processing
[max_PO2_1(i)] = postmax(fem,'c','solnum',1,'Dl',[1]); % Maximum node in islet
[min_PO2_1(i)] = postmin(fem,'c','solnum',1,'Dl',[1]); % Minimum node in islet
[max_PO2_2(i)] = postmax(fem,'c','solnum',1,'Dl',[3]); % Maximum node in islet
[min_PO2_2(i)] = postmin(fem,'c','solnum',1,'Dl',[3]); % Minimum node in islet
convergence1(i)=fem.stop;
% Integrate islet without O2
frac_no_O2_1 = postint(fem,'1*c<=Pcrit/Pext','solnum',1,'phase',0*pi/180,'edim',3,'intorder',4,'geomnum',1,'dl',[1]);
% Integrate whole islet
islet_int_1 = postint(fem,'1','solnum',1,'phase',0*pi/180,'edim',3,'intorder',4,'geomnum',1,'dl',[1]);
frac_dead_1(i)=frac_no_O2_1/islet_int_1;
% Integrate islet without O2
frac_no_O2_2 = postint(fem,'1*c<=Pcrit/Pext','solnum',1,'phase',0*pi/180,'edim',3,'intorder',4,'geomnum',1,'dl',[3]);
% Integrate whole islet
islet_int_2 = postint(fem,'1','solnum',1,'phase',0*pi/180,'edim',3,'intorder',4,'geomnum',1,'dl',[3]);
frac_dead_2(i)=frac_no_O2_2/islet_int_2;

OCR(i) = postint(fem,'lm1', ...
        'solnum',1, ...
        'phase',0*pi/180, ...
        'edim',2, ...
        'intorder',4, ...
        'geomnum',1, ...
        'dl',[8]); % Total oxygen flux into system

min_quality_mesh(i) = min(meshqual(fem.mesh));
element_num(i) = size(fem.mesh.t,2);
end
```

10.7 Matlab code for glucose transport

```
% FEMLAB Model M-file
% Set up vectors to store specific numbers of solutions
n=6;
max_gluc=linspace(1,n,n);
min_gluc=linspace(1,n,n);
min_quality_mesh=linspace(1,n,n);
element_num=linspace(1,n,n);
Data = zeros(61,n);
% Beginning of for loops
A1 = [0.1 0.5 1 1.5 2 3];

for i=1:n
flclear fem
% COMSOL version
clear vrsn
vrsn.name = 'COMSOL 3.3';
vrsn.ext = '';
vrsn.major = 0;
vrsn.build = 405;
vrsn.rcs = '$Name:  $';
vrsn.date = '$Date: 2006/08/31 18:03:47 $';
fem.version = vrsn;

% Get input for parameters
Conc_bulk = 10e-6;  % mol/cm3  10mM
V_max = 1e-7; % mol/cm3 s
Km = 8e-6; % mol/cm3 8mM
height = 2.2;  % cm
radius_islet= 0.0075;  % cm
islet_density = 4440; %IE/cm2
diff_islet = 3.8e-7; % cm2/s
diff_medium = 6.7e-6; % cm2/s
B1 = diff_medium/diff_islet;
A = A1(i); % IEQ/cm2
end_time = 60; % hours
% Place constant into fem
fem.const={'Cbulk',Conc_bulk,'A',A,'Km',Km,'B1',B1,'Rislet',radius_islet};
% Specifies dimensions
fem.sdim=3;

%%%%%%%%%% GEOMETRY %%%%%%%%%%%%%%%%%%%%%%%%%%%%%%%%%%%%
   % Function to create geometry for islet array (equally spaced spheres in a
   % square array. Only one quarter of an islet will be modeled because of
   % symmetry.
pt = [0 0 0]; % base point of 3D block
vec = [0 0 1]; % specifies direction of block
% Set length of sides of block
% scaling parameter for height of medium, radius of islet=1
scale_height = height/radius_islet; % scaling parameter for height of box
scale_space = (((radius_islet^3)/(0.0075^3)/islet_density)^(1/2))/radius_islet; % calculating length of sides for given
density
Lx = scale_space; % center to center distance between islets
```

```
Ly = scale_space;
Lz = (scale_height-2);
% Create block for medium
B3top=block3(Lx/2,Ly/2,Lz,'corner',[0 0 2],vec);
% Now we will add in the spheres for islets of a given radius
% Spheres at vertices of block B3
S3a = sphere3(1,[0 0 1]);
% Create composite objects.
B3bottom=block3(Lx/2,Ly/2,2,'corner',pt,vec);
% First make spheres into quarters.
COa = S3a*B3bottom;
B3med=B3bottom+B3top;
B3meda=B3med-S3a;
clear s
s.objs={COa,B3meda};
s.name={'CO1','Blk1'};
s.tags={'COa','B3meda'};
fem.draw = struct('s',s);
fem.geom = geomcsg(fem);
%%%%%%%%%%%% END GEOMETRY %%%%%%%%%%%%%%%%%%
% Initialize mesh
fem.mesh=meshinit(fem, ...
            'hmaxfact',1.5, ...
            'hcurve',0.7, ...
            'hgrad',1.6, ...
            'hcutoff',0.04, ...
            'hnarrow',0.4);
mesh_test = size(fem.mesh.t,2);
while mesh_test<2500
fem.mesh=meshrefine(fem);
mesh_test = size(fem.mesh.t,2);
end

%%%%%%%%%%%%%%%% Application mode no necrotic core %%%%%%%%%%%%%%%%%%
% Application mode 1
clear appl
appl.mode.class = 'FlDiffusion';
appl.shape = {'shlag(2,"lm1")','shlag(2,"c")'};
appl.assignsuffix = '_di';
clear prop
prop.weakconstr=struct('value',{'non-ideal'},'dim',{{'lm1'}});
appl.prop = prop;
clear bnd
bnd.c0 = {0,0,1};
bnd.type = {'N0','cont','N'};
bnd.weakconstr = {0,1,1};
bnd.wcshape = 1;
bnd.ind = [1,1,1,2,1,1,1,1,2,2,3,2,1,1,1,1];
appl.bnd = bnd;
clear equ
equ.shape = 2;
equ.init = 1;
equ.D = {1,'B1'};
equ.R = {'-A*c/(c+Km/Cbulk)*(c>0)',0};
equ.ind = [1,2,2];
appl.equ = equ;
```

```
fem.appl{1} = appl;
fem.border = 1;
fem.outform = 'general';

% Multiphysics
fem=multiphysics(fem);
% Extend mesh
fem.xmesh=meshextend(fem);
% Solve problem
final=end_time*60*60*diff_islet/radius_islet^2;
[fem.sol]=femtime(fem, ...
            'solcomp',{'c'}, ...
            'outcomp',{'c'}, ...
            'tlist',[0:final/60:final], ...
            'tout','tlist');
   % Save current fem structure for restart purposes
   fem0=fem;
max_gluc(i) = postmax(fem,'c','solnum',61,'Dl',[1]); % Maximum node in islet
min_gluc(i) = postmin(fem,'c','solnum',61,'Dl',[1]); % Minimum node in islet
min_quality_mesh(i) = min(meshqual(fem.mesh));
element_num(i) = size(fem.mesh.t,2);
%save data at top of islet
Data(:,i)= postint(fem,'c', ...
        'dl',[2], ...
        'edim',0, ...
        'solnum','all');
end
```

10.8 Matlab code for changes in local pH during culture on polystyrene

```
% FEMLAB Model M-file
% Set up vectors to store specific numbers of solutions
m = 1801; %time broken into m-1 intervals
n=5;
min_quality_mesh1=linspace(1,n,n);
element_num1=linspace(1,n,n);
pH_Data1 = zeros(m,n);
H_Data1 = zeros(m,n);
HCO3_Data1 = zeros(m,n);
CO2_Data1 = zeros(m,n);
L_Data1 = zeros(m,n);
A_Data1 = zeros(m,n);
Diff_H1 = zeros(m,n);
X = [100 500 1000 2000 4400] ;

for i=1:n
flclear fem
% COMSOL version
clear vrsn
vrsn.name = 'COMSOL 3.3';
vrsn.ext = 'a';
vrsn.major = 0;
vrsn.build = 511;
vrsn.rcs = '$Name:  $';
vrsn.date = '$Date: 2007/02/02 19:05:58 $';
fem.version = vrsn;
% Get input for parameters
D_CO2_islet = 1.0e-5; %cm2/s
D_CO2_medium = 2.55e-5; %cm2/s
D_lac_islet = 5.3e-6; %cm2/s
D_lac_medium = 1.1e-5; %cm2/s
D_amm_islet = 2.0e-6; %cm2/s
D_amm_medium = 2.7e-5; %cm2/s
D_HCO3_islet = 8.6e-7; %cm2/s
D_HCO3_medium = 11.9e-6; %cm2/s
D_H_islet = 6.0e-6; %cm2/s
D_H_medium = 11.2e-5; %cm2/s
Rxn_CO2 = 3.68e-8; %mol/s cm3
Rxn_lac = 5.3e-8; %mol/s cm3
Rxn_amm = 5.0e-8; %mol/s cm3
kf_HCO3 = 0.145; %1/s
kr_HCO3 = 17.2e4*1000.0; %cm3/mol s
Ext_CO2 = 760.0*0.05; %mmHg
radius_islet = 0.0075; %cm
islet_density = X(i); % islets/cm2
initial_pH = 7.4;
initial_H_medium = 10^(-initial_pH)/1000; %mol/cm3
initial_H_islet = initial_H_medium; %mol/cm3
initial_amm = 0.0/1000.0; %mol/cm3
initial_lac = 0.0/1000.0; %mol/cm3
A_CO2_islet = 3.21e-5/1000.0; % mol/cm3 mmHg
A_CO2_medium = 3.18e-5/1000.0; % mol/cm3 mmHg
```

```
initial_CO2_islet = A_CO2_islet*Ext_CO2; %mol/cm3
initial_CO2_medium = A_CO2_medium*Ext_CO2; %mol/cm3
M = 1.0e6;
initial_HCO3_medium = kf_HCO3/kr_HCO3*initial_CO2_medium/initial_H_medium; %mol/cm3
initial_HCO3_islet = kf_HCO3/kr_HCO3*initial_CO2_islet/initial_H_islet; %mol/cm3
height = 0.3; %cm
end_time = 60.0; % hours
final=end_time*60*60*D_CO2_medium/radius_islet^2;
Da_CO2 = radius_islet^2/D_CO2_medium*Rxn_CO2/initial_CO2_medium;
Da_kfb = radius_islet^2/D_CO2_medium*kf_HCO3;
Da_krb = radius_islet^2/D_CO2_medium*kr_HCO3*initial_CO2_medium;
Da_am = radius_islet^2/initial_CO2_medium*Rxn_amm/D_CO2_medium;
Da_lac = radius_islet^2/D_CO2_medium*Rxn_lac/initial_CO2_medium;
Da_am_lac = Da_lac-Da_am;
% Place constant into fem
% Constants
fem.const = {'D_CO2_islet',D_CO2_islet, ...
 'A_CO2_islet',A_CO2_islet, ...
 'Ext_CO2',Ext_CO2, ...
 'Da_CO2',Da_CO2, ...
 'D_lac_islet',D_lac_islet, ...
 'D_lac_medium',D_lac_medium, ...
 'Rislet',radius_islet, ...
 'D_CO2_medium',D_CO2_medium, ...
 'A_CO2_medium',A_CO2_medium, ...
 'D_amm_islet',D_amm_islet, ...
 'D_amm_medium',D_amm_medium, ...
 'Da_am_lac',Da_am_lac, ...
 'Da_am',Da_am, ...
 'Da_lac',Da_lac, ...
 'Da_krb',Da_krb, ...
 'Da_kfb',Da_kfb, ...
 'D_HCO3_islet',D_HCO3_islet, ...
 'D_HCO3_medium',D_HCO3_medium, ...
 'D_H_islet',D_H_islet, ...
 'D_H_medium',D_H_medium, ...
 'HCO3_init_medium',initial_HCO3_medium, ...
 'HCO3_init_islet',initial_HCO3_islet, ...
 'H_init_medium',initial_H_medium, ...
 'H_init_islet',initial_H_islet, ...
 'lac_init',initial_lac, ...
 'amm_init',initial_amm, ...
 'CO2_init_medium',initial_CO2_medium, ...
 'CO2_init_islet',initial_CO2_islet, ...
 'tau_end',final,...
 'M',M};
% Specifies dimensions
fem.sdim=3;

% GEOMETRY
%%%%%%%%%%%%%%%%%%%%%%%%%%%%%%%%%%%%%%%%%%%%%%%%%%%%%%%%%%
% Function to create geometry for islet array (equally spaced islets in a
% square array. Only an eighth of an islet will be modeled because of
% symmetry.
% Set length of sides of block
% scaling parameter for height of medium, radius of islet=1
```

```
scale_height = height/radius_islet; % scaling parameter for height of box
scale_space = ((1/islet_density)^(1/2))/radius_islet; % calculating length of sides for given density
Lx = scale_space; % center to center distance between islets
Ly = scale_space;
Lz = (scale_height);
% Create block for medium
B3_1=block3(Lx,Ly,Lz,'base','corner','pos',{'0','0','0'},'axis',{'0','0','1'},'rot','0');
B3_2=block3(Lx,Ly,Lz,'base','corner','pos',{'0','0','0'},'axis',{'0','0','1'},'rot','45');
B3_3=block3(Lx/2,Ly/2,Lz,'base','corner','pos',{'0','0','0'},'axis',{'0','0','1'},'rot','0');
B3_4=B3_1*B3_2;
B3_triangle1=B3_3-B3_4;
% Now we will add in the sphere for islet of a given radius set to 1
S3a = sphere3(1,[0 0 1]);
% make sphere into one eighth of islet
S3_eighth=S3a*B3_triangle1;
% remove corner from lower block
B3_triangle2=B3_triangle1-S3a;
B3_triangle3=B3_triangle2+S3_eighth;
% Combine into a single geometry
clear s
s.objs={B3_triangle3};
s.name={'CO1'};
s.tags={'B3_triangle3'};
fem.draw = struct('s',s);
fem.geom = geomcsg(fem);
%%%%%%%%%%%%%%%%%%%%%%%%%%%%%%%%%%%%%%%%%%%%%%%%%%%%%%%%
%%%%%%%%%%%%%%%%%%%%%%%%%%%%%%%%%%%%%%%%%%%%%%%%%%%%%%%%
% Initialize mesh
fem.mesh=meshinit(fem, ...
           'hauto',6);
mesh_test = size(fem.mesh.t,2);
while mesh_test<1000
fem.mesh=meshrefine(fem);
mesh_test = size(fem.mesh.t,2);
end

% (Default values are not included)
% Application mode 1
clear appl
appl.mode.class = 'Diffusion';
appl.dim = {'c7'};
appl.module = 'CHEM';
appl.shape = {'shlag(2,''lm8'')','shlag(2,''c7'')'};
appl.gporder = {10,4};
appl.assignsuffix = '_chdi';
clear prop
clear weakconstr
weakconstr.value = 'non-ideal';
weakconstr.dim = {'lm8'};
prop.weakconstr = weakconstr;
appl.prop = prop;
clear bnd
bnd.type = {'N0','N','cont'};
bnd.weakconstr = {0,0,1};
bnd.wcshape = 1;
bnd.N = {0,'M*(c8-c7/A_CO2_islet*A_CO2_medium)',0};
```

```
bnd.ind = [1,1,2,3,3,3,2,3,3];
appl.bnd = bnd;
clear equ
equ.D = {'D_CO2_islet/D_CO2_medium',1};
equ.init = {'CO2_init_islet/CO2_init_medium',0};
equ.R = {'Da_CO2-Da_kfb*c7+Da_krb*c6*c2', ...
 0};
equ.shape = 2;
equ.gporder = 2;
equ.usage = {1,0};
equ.ind = [1,2];
appl.equ = equ;
fem.appl{1} = appl;

% Application mode 2
clear appl
appl.mode.class = 'Diffusion';
appl.dim = {'c8'};
appl.name = 'chdi2';
appl.module = 'CHEM';
appl.shape = {'shlag(2,"lm9")','shlag(2,"c8")'};
appl.gporder = {10,4};
appl.assignsuffix = '_chdi2';
clear prop
clear weakconstr
weakconstr.value = 'non-ideal';
weakconstr.dim = {'lm9'};
prop.weakconstr = weakconstr;
appl.prop = prop;
clear bnd
bnd.type = {'cont','N','N0','C'};
bnd.c0 = {0,0,0,1};
bnd.weakconstr = {1,0,0,1};
bnd.wcshape = 1;
bnd.N = {0,'M*(c7*A_CO2_medium/A_CO2_islet-c8)',0,0};
bnd.ind = [1,1,2,3,3,3,2,4,3];
appl.bnd = bnd;
clear equ
equ.init = {0,1};
equ.R = {0,'-Da_kfb*c8+Da_krb*c6*c2'};
equ.shape = 2;
equ.gporder = 2;
equ.usage = {0,1};
equ.ind = [1,2];
appl.equ = equ;
fem.appl{2} = appl;

% Application mode 3
clear appl
appl.mode.class = 'Diffusion';
appl.dim = {'c2','c3','c4','c6'};
appl.name = 'chdi3';
appl.module = 'CHEM';
appl.gporder = 4;
appl.cporder = 2;
appl.assignsuffix = '_chdi3';
```

```
clear bnd
bnd.type = {{'N0';'N0';'N0';'N0'},{'cont';'cont';'cont';'cont'}};
bnd.ind = [1,1,2,1,1,1,2,1,1];
appl.bnd = bnd;
clear equ
equ.D = {{'D_HCO3_islet/D_CO2_medium';'D_lac_islet/D_CO2_medium';'D_amm_islet/D_CO2_medium'; ...
 'D_H_islet/D_CO2_medium'},{'D_HCO3_medium/D_CO2_medium';'D_lac_medium/D_CO2_medium'; ...
 'D_amm_medium/D_CO2_medium';'D_H_medium/D_CO2_medium'}};
equ.init = {{'HCO3_init_islet/CO2_init_medium';'lac_init/CO2_init_medium'; ...
 'amm_init/CO2_init_medium';'H_init_islet/CO2_init_medium'},{'HCO3_init_medium/CO2_init_medium'; ...
 'lac_init/CO2_init_medium';'amm_init/CO2_init_medium';'H_init_medium/CO2_init_medium'}};
equ.R = {{'Da_kfb*c7-Da_krb*c6*c2';'Da_lac'; ...
 'Da_am';'Da_am_lac+Da_kfb*c7-Da_krb*c6*c2'}, ...
 {'Da_kfb*c8-Da_krb*c6*c2';0;0;'Da_kfb*c8-Da_krb*c6*c2'}};
equ.ind = [1,2];
appl.equ = equ;
fem.appl{3} = appl;
fem.border = 1;
fem.outform = 'general';
% Subdomain settings
clear equ
equ.ind = [1,2];
equ.dim = {'c7','c8','c2','c3','c4','c6'};
% Subdomain expressions
equ.expr = {'c_all',{'c7','c8'}};
fem.equ = equ;
% Multiphysics
fem=multiphysics(fem);
% Extend mesh
fem.xmesh=meshextend(fem);
% Solve problem
fem.sol=femtime(fem, ...
            'solcomp',{'c2','lm9','c7','c8','c4','c3','c6'}, ...
            'outcomp',{'c2','lm9','c7','c8','c4','c3','c6'}, ...
            'tlist',[0:final/(m-1):final], ...
            'atol',{'c2','1e-6','c3','1e-6','c4','1e-6','c6','1e-8','c7','1e-6','c8','1e-6','lm9','1e-6'}, ...
            'tout','tlist');
min_quality_mesh1(i) = min(meshqual(fem.mesh));
element_num1(i) = size(fem.mesh.t,2);
%save data at top of islet
pH_Data1(:,i)= postint(fem,'-log10(c6*CO2_init_medium*1000)', ...
        'dl',[2], ...
        'edim',0, ...
        'solnum','all');
L_Data1(:,i)=  postint(fem,'c3*CO2_init_medium*1000*1000', ...
        'dl',[2], ...
        'edim',0, ...
        'solnum','all');
A_Data1(:,i)=  postint(fem,'c4*CO2_init_medium*1000*1000', ...
        'dl',[2], ...
        'edim',0, ...
        'solnum','all');
HCO3_Data1(:,i)=  postint(fem,'c2*CO2_init_medium*1000*1000', ...
        'dl',[2], ...
        'edim',0, ...
        'solnum','all');
```

```
CO2_Data1(:,i)=  postint(fem,'c_all*CO2_init_medium*1000*1000', ...
        'dl',[2], ...
        'edim',0, ...
        'solnum','all');
H_Data1(:,i)=  postint(fem,'c6*CO2_init_medium*1000*1000', ...
        'dl',[2], ...
        'edim',0, ...
        'solnum','all');
Diff_H1(:,i)=postint(fem,'ndflux_c6_chdi3', ...
        'unit','', ...
        'dl',[3,7], ...
        'edim',2, ...
        'solnum','all');
end
```

10.9 *Matlab code for changes in local pH during culture on silicone rubber*

```
% FEMLAB Model M-file
% Set up vectors to store specific numbers of solutions
%%%%%%% Stored values for solution to simulated culture
m = 1801; %time broken into m-1 intervals
n=2;
min_quality_mesh1=linspace(1,n,n);
element_num1=linspace(1,n,n);
pH_Data1 = zeros(m,n);
H_Data1 = zeros(m,n);
X = [100 4400] ;
%%%%%%%%%%%%%%%%%%%%%%%%%%%%%%%%%%%%%%
%%%%            Si exp
%%%%%%%%%%%%%%%%%%%%%%%%%%%%%%%%%%%%%%
for i=1:n
flclear fem
% COMSOL version
clear vrsn
vrsn.name = 'COMSOL 3.3';
vrsn.ext = 'a';
vrsn.major = 0;
vrsn.build = 511;
vrsn.rcs = '$Name:  $';
vrsn.date = '$Date: 2007/02/02 19:05:58 $';
fem.version = vrsn;
% Get input for parameters
D_CO2_islet = 1.0e-5; %cm2/s
D_CO2_medium = 2.55e-5; %cm2/s
D_CO2_Si = 2.9e-5; %cm2/s
D_lac_islet = 5.3e-6; %cm2/s
D_lac_medium = 1.1e-5; %cm2/s
D_amm_islet = 2.0e-6; %cm2/s
D_amm_medium = 2.7e-5; %cm2/s
D_HCO3_islet = 8.6e-7; %cm2/s
D_HCO3_medium = 11.9e-6; %cm2/s
D_H_islet = 6.0e-6; %cm2/s
D_H_medium = 11.2e-5; %cm2/s
Rxn_CO2 = 3.68e-8; %mol/s cm3
Rxn_lac = 5.3e-8; %mol/s cm3
Rxn_amm = 5.0e-8; %mol/s cm3
kf_HCO3 = 0.145; %1/s
kr_HCO3 = 17.2e4*1000.0; %cm3/mol s
Ext_CO2 = 760.0*0.05; %mmHg
radius_islet = 0.0075; %cm
islet_density = X(i); % islets/cm2
initial_pH = 7.4;
initial_H_medium = 10^(-initial_pH)/1000; %mol/cm3
initial_H_islet = initial_H_medium; %mol/cm3
initial_amm = 0.0/1000.0; %mol/cm3
initial_lac = 0.0/1000.0; %mol/cm3
A_CO2_islet = 3.21e-5/1000.0; % mol/cm3 mmHg
A_CO2_medium = 3.18e-5/1000.0; % mol/cm3 mmHg
A_CO2_Si = 7.7e-5/1000.0; % mol/cm3 mmHg
```

```
initial_CO2_islet = A_CO2_islet*Ext_CO2; %mol/cm3
initial_CO2_medium = A_CO2_medium*Ext_CO2; %mol/cm3
initial_CO2_Si = A_CO2_Si*Ext_CO2; %mol/cm3
M = 1.0e6;
initial_HCO3_medium = kf_HCO3/kr_HCO3*initial_CO2_medium/initial_H_medium; %mol/cm3
initial_HCO3_islet = kf_HCO3/kr_HCO3*initial_CO2_islet/initial_H_islet; %mol/cm3
height = 2.2; %cm
thickness = 0.05; %cm
end_time = 60.0; % hours
final=end_time*60*60*D_CO2_medium/radius_islet^2;
Da_CO2 = radius_islet^2/D_CO2_medium*Rxn_CO2/initial_CO2_medium;
Da_kfb = radius_islet^2/D_CO2_medium*kf_HCO3;
Da_krb = radius_islet^2/D_CO2_medium*kr_HCO3*initial_CO2_medium;
Da_am = radius_islet^2/initial_CO2_medium*Rxn_amm/D_CO2_medium;
Da_lac = radius_islet^2/D_CO2_medium*Rxn_lac/initial_CO2_medium;
Da_am_lac = Da_lac-Da_am;
% Place constant into fem
% Constants
fem.const = {'D_CO2_islet',D_CO2_islet, ...
 'A_CO2_islet',A_CO2_islet, ...
 'D_CO2_Si',D_CO2_Si, ...
 'A_CO2_Si',A_CO2_Si, ...
 'Ext_CO2',Ext_CO2, ...
 'Da_CO2',Da_CO2, ...
 'D_lac_islet',D_lac_islet, ...
 'D_lac_medium',D_lac_medium, ...
 'Rislet',radius_islet, ...
 'D_CO2_medium',D_CO2_medium, ...
 'A_CO2_medium',A_CO2_medium, ...
 'D_amm_islet',D_amm_islet, ...
 'D_amm_medium',D_amm_medium, ...
 'Da_am_lac',Da_am_lac, ...
 'Da_am',Da_am, ...
 'Da_lac',Da_lac, ...
 'Da_krb',Da_krb, ...
 'Da_kfb',Da_kfb, ...
 'D_HCO3_islet',D_HCO3_islet, ...
 'D_HCO3_medium',D_HCO3_medium, ...
 'D_H_islet',D_H_islet, ...
 'D_H_medium',D_H_medium, ...
 'HCO3_init_medium',initial_HCO3_medium, ...
 'HCO3_init_islet',initial_HCO3_islet, ...
 'H_init_medium',initial_H_medium, ...
 'H_init_islet',initial_H_islet, ...
 'lac_init',initial_lac, ...
 'amm_init',initial_amm, ...
 'CO2_init_medium',initial_CO2_medium, ...
 'CO2_init_islet',initial_CO2_islet, ...
 'tau_end',final,...
 'thickness',thickness,...
 'initial_CO2_Si',initial_CO2_Si,...
 'M',M};
% Specifies dimensions
fem.sdim=3;

% GEOMETRY
```

```
%%%%%%%%%%%%%%%%%%%%%%%%%%%%%%%%%%%%%%%%%%%%%%%%%%%
% Function to create geometry for islet array (equally spaced islets in a
% square array. Only an eighth of an islet will be modeled because of
% symmetry.
% Set length of sides of block
% scaling parameter for height of medium, radius of islet=1
scale_height = height/radius_islet; % scaling parameter for height of box
scale_space = ((1/islet_density)^(1/2))/radius_islet; % calculating length of sides for given density
Lx = scale_space; % center to center distance between islets
Ly = scale_space;
Lz = (scale_height-2);
pt = [0 0 0]; % base point of 3D block
vec = [0 0 1]; % specifies direction of block
Lzmem=thickness/radius_islet;
Lztot = Lzmem+2+Lz;
% Create block for medium
B3top=block3(Lx/2,Ly/2,Lz,'corner',[0 0 2],vec);
% Now we will add in the spheres for islets of a given radius
% Spheres at vertices of block B3
S3a = sphere3(1,[0 0 1]);
% Create composite objects.
B3bottom=block3(Lx/2,Ly/2,2,'corner',pt,vec);
% First make sphere into quarters.
COa = S3a*B3bottom;
B3_2=block3(Lx,Ly,Lztot,'base','corner','pos',{'0','0',-Lzmem},'axis',{'0','0','1'},'rot','45');
B3mem=block3(Lx/2,Ly/2,Lzmem,'corner',[0,0,-Lzmem],vec);
COb = COa-B3_2;
B3med=B3bottom+B3top;
B3meda = B3med+B3mem;
B3medb=B3meda-B3_2;
B3medc=B3medb-S3a; % remove corner from block
B3medd=B3medc+COb;
clear s
s.objs={B3medd};
s.name={'CO1'};
s.tags={'B3medd'};
fem.draw = struct('s',s);
fem.geom = geomcsg(fem);
%%%%%%%%%%%%%%%%%%%%%%%%%%%%%%%%
% Initialize mesh
fem.mesh=meshinit(fem, ...
              'hauto',4, ...
              'hmaxsub',[2,1]);
fem.mesh=meshrefine(fem, ...
               'mcase',0, ...
               'rmethod','longest', ...
               'subdomain',[2,3]);
mesh_test = size(fem.mesh.t,2);
while mesh_test<1000
fem.mesh=meshrefine(fem);
mesh_test = size(fem.mesh.t,2);
end
% Application mode 1
clear appl
appl.mode.class = 'Diffusion';
appl.dim = {'c7'};
```

```
appl.module = 'CHEM';
appl.shape = {'shlag(2,"lm8")','shlag(2,"c7")'};
appl.gporder = {10,4};
appl.assignsuffix = '_chdi';
clear prop
clear weakconstr
weakconstr.value = 'non-ideal';
weakconstr.dim = {'lm8'};
prop.weakconstr = weakconstr;
appl.prop = prop;
clear bnd
bnd.type = {'cont','cont','N','N0','N','C'};
bnd.c0 = {0,0,0,0,0,1};
bnd.weakconstr = {0,1,0,0,0,1};
bnd.wcshape = 1;
bnd.N = {0,0,'M*(c8-c7/A_CO2_medium*A_CO2_islet)',0,'M*(c7/A_CO2_medium*A_CO2_Si-c9)', ...
 0};
bnd.ind = [1,1,1,2,2,3,4,4,5,4,4,3,1,6,1,4,4];
appl.bnd = bnd;
clear equ
equ.D = {'D_CO2_islet/D_CO2_medium',1,1};
equ.init = {'CO2_init_islet/CO2_init_medium',0,1};
equ.R = {0,0,'-Da_kfb*c7+Da_krb*c6*c2'};
equ.shape = 2;
equ.gporder = 2;
equ.usage = {0,0,1};
equ.ind = [1,2,3,3];
appl.equ = equ;
fem.appl{1} = appl;

% Application mode 2
clear appl
appl.mode.class = 'Diffusion';
appl.dim = {'c8'};
appl.name = 'chdi2';
appl.module = 'CHEM';
appl.shape = {'shlag(2,"lm9")','shlag(2,"c8")'};
appl.gporder = {10,4};
appl.assignsuffix = '_chdi2';
clear prop
clear weakconstr
weakconstr.value = 'non-ideal';
weakconstr.dim = {'lm9'};
prop.weakconstr = weakconstr;
appl.prop = prop;
clear bnd
bnd.type = {'cont','cont','N0','N','C'};
bnd.c0 = {0,0,0,0,1};
bnd.weakconstr = {1,0,0,0,1};
bnd.wcshape = 1;
bnd.N = {0,0,0,'M*(c7*A_CO2_islet/A_CO2_medium-c8)',0};
bnd.ind = [1,1,2,3,3,4,2,5,2,1,1,4,1,1,1,1,1];
appl.bnd = bnd;
clear equ
equ.D = {1,'D_CO2_islet/D_CO2_medium'};
equ.init = {0,'CO2_init_islet/CO2_init_medium'};
```

```
equ.R = {0,'Da_CO2-Da_kfb*c8+Da_krb*c6*c2'};
equ.shape = 2;
equ.gporder = 2;
equ.usage = {0,1};
equ.ind = [1,2,1,1];
appl.equ = equ;
fem.appl{2} = appl;

% Application mode 3
clear appl
appl.mode.class = 'Diffusion';
appl.dim = {'c2','c3','c4','c6'};
appl.name = 'chdi3';
appl.module = 'CHEM';
appl.gporder = 4;
appl.cporder = 2;
appl.assignsuffix = '_chdi3';
clear bnd
bnd.type = {{'cont';'cont';'cont';'cont'},{'N0';'N0';'N0';'N0'}};
bnd.ind = [1,1,1,2,2,1,2,2,2,2,2,1,1,2,1,2,2];
appl.bnd = bnd;
clear equ
equ.D = {{'D_HCO3_islet/D_CO2_medium';'D_lac_islet/D_CO2_medium';'D_amm_islet/D_CO2_medium'; ...
 'D_H_islet/D_CO2_medium'},{'D_HCO3_islet/D_CO2_medium';'D_lac_islet/D_CO2_medium'; ...
 'D_amm_islet/D_CO2_medium';'D_H_islet/D_CO2_medium'},{'D_HCO3_medium/D_CO2_medium'; ...
 'D_lac_medium/D_CO2_medium';'D_amm_medium/D_CO2_medium';'D_H_medium/D_CO2_medium'}};
equ.init = {{'HCO3_init_islet/CO2_init_medium';'lac_init/CO2_init_medium'; ...
 'amm_init/CO2_init_medium';'H_init_islet/CO2_init_medium'},{'HCO3_init_islet/CO2_init_medium'; ...
 'lac_init/CO2_init_medium';'amm_init/CO2_init_medium';'H_init_islet/CO2_init_medium'}, ...
 {'HCO3_init_medium/CO2_init_medium';'lac_init/CO2_init_medium';'amm_init/CO2_init_medium'; ...
 'H_init_medium/CO2_init_medium'}};
equ.R = {{'Da_kfb*c7-Da_krb*c6*c2';'Da_lac';'Da_am';'Da_am_lac+Da_kfb*c7-Da_krb*c6*c2'}, ...
 {'Da_kfb*c8-Da_krb*c6*c2';'Da_lac';'Da_am';'Da_am_lac+Da_kfb*c8-Da_krb*c6*c2'}, ...
 {'Da_kfb*c7-Da_krb*c6*c2';0;0;'Da_kfb*c7-Da_krb*c6*c2'}};
equ.usage = {0,1,1};
equ.ind = [1,2,3,3];
appl.equ = equ;
fem.appl{3} = appl;

% Application mode 4
clear appl
appl.mode.class = 'Diffusion';
appl.dim = {'c9'};
appl.name = 'chdi4';
appl.module = 'CHEM';
appl.shape = {'shlag(2,"lm5")','shlag(2,"c9")'};
appl.gporder = {10,4};
appl.assignsuffix = '_chdi4';
clear prop
prop.analysis='static';
clear weakconstr
weakconstr.value = 'non-ideal';
weakconstr.dim = {'lm5'};
prop.weakconstr = weakconstr;
appl.prop = prop;
clear bnd
```

```
bnd.type = {'N0','C','cont','N'};
bnd.c0 = {0,'Ext_CO2*A_CO2_Si/CO2_init_medium',0,0};
bnd.weakconstr = {0,1,1,0};
bnd.wcshape = 1;
bnd.N = {0,0,0,'M*(c9/A_CO2_Si*A_CO2_medium-c7)'};
bnd.ind = [1,1,2,3,3,3,3,3,4,3,3,3,3,3,1,3,3];
appl.bnd = bnd;
clear equ
equ.D = {'D_CO2_Si/D_CO2_medium',1};
equ.init = {'CO2_init_Si/CO2_init_medium',0};
equ.shape = 2;
equ.gporder = 2;
equ.usage = {1,0};
equ.ind = [1,2,2,2];
appl.equ = equ;
fem.appl{4} = appl;
fem.border = 1;
fem.outform = 'general';
% Subdomain settings
clear equ
equ.ind = [1,2,3,3];
equ.dim = {'c7','c8','c2','c3','c4','c6','c9'};
% Subdomain expressions
equ.expr = {'c_all',{'c9','c8','c7'}};
fem.equ = equ;
% Multiphysics
fem=multiphysics(fem);
% Extend mesh
fem.xmesh=meshextend(fem);
% Solve problem
fem.sol=femtime(fem, ...
            'solcomp',{'lm5','c9','c2','c7','c8','c3','c4','c6'}, ...
            'outcomp',{'lm5','c9','c2','c7','c8','c3','c4','c6'}, ...
            'tlist',[0:final/(m-1):final], ...
            'atol',{'c2','1e-6','c3','1e-6','c4','1e-6','c6','1e-8','c7','1e-6','c8','1e-6','c9','1e-6','lm5','1e-6'}, ...
            'tout','tlist');
min_quality_mesh1(i) = min(meshqual(fem.mesh));
element_num1(i) = size(fem.mesh.t,2);
%save data at top of islet
pH_Data1(:,i)= postint(fem,'-log10(c6*CO2_init_medium*1000)', ...
        'dl',[3], ...
        'edim',0, ...
        'solnum','all');
H_Data1(:,i)=  postint(fem,'c6*CO2_init_medium*1000*1000', ...
        'dl',[3], ...
        'edim',0, ...
        'solnum','all');
end
```

10.10 Matlab code for oxygen transport in OBS – base case

```
% FEMLAB Model M-file
flclear fem
% COMSOL version
clear vrsn
vrsn.name = 'COMSOL 3.3';
vrsn.ext = '';
vrsn.major = 0;
vrsn.build = 405;
vrsn.rcs = '$Name:  $';
vrsn.date = '$Date: 2006/08/31 18:03:47 $';
fem.version = vrsn;
% Constants
Da_medium = 3.53e-14; % mol/s/mmHg/cm
Radius_well = 0.32; % cm   radius of well
Cell_density = 250000; % cells/cm2
h_medium = 0.1/(pi*Radius_well^2); % cm    medium depth
P_ext = 142; % mmHg     External pO2
Km = 0.44; % mmHg      Km for oxygen consumption
P_critical = 0.1; % mmHg    Critical pO2 of cells
Reader_position = 0.8*0.32/Radius_well; % non-dimensional length that plate reader sees
OCR_cell = 2.8; % fmol/min cell
V_max = OCR_cell/60*Cell_density*10^-15; %mol/cm2 s  OCR of cells
fem.const={'Rwell',Radius_well,'h_medium',h_medium,'Pext',P_ext,'Km',Km,'Da',Da_medium,'Vmax',V_max,...
   'Pcrit',P_critical};
% Geometry
Media=rect2('1','h_medium/Rwell','base','corner','pos',{'0','0'},'rot','0','const',fem.const);
parr={point2(0.8,0)};
Pt=geomcoerce('point',parr);
clear p s
p.objs={Pt};
p.name={'PT1'};
p.tags={'Pt'};
s.objs={Media};
s.name={'R1'};
s.tags={'Media'};
fem.draw=struct('p',p,'s',s);
fem.geom = geomcsg(fem);
% Initialize mesh
fem.mesh=meshinit(fem, ...
            'hmaxfact',0.55, ...
            'hcutoff',0.01, ...
            'hgrad',1.4, ...
            'hcurve',0.4, ...
            'hnarrow',0.7);
mesh_test = size(fem.mesh.t,2);
if mesh_test<2500
fem.mesh=meshrefine(fem);
mesh_test = size(fem.mesh.t,2);
end
% (Default values are not included)
% Application mode 1
clear appl
```

```
appl.mode.class = 'FlDiffusion';
appl.mode.type = 'axi';
appl.shape = {'shlag(2,"lm1")','shlag(2,"c")'};
appl.assignsuffix = '_di';
clear prop
prop.weakconstr=struct('value',{'non-ideal'},'dim',{{'lm1'}});
appl.prop = prop;
% Bnd 1 = Center of well, Bnd 2 = Bottom of well where plate reader reads, Bnd 3 = top, Bnd 4 = Bottom of the
well where plate reader doesn't read, Bnd 5 = the inner side of the wall
clear bnd
bnd.N = {0,'-Vmax*Rwell/(Da*Pext)*c/(c+Km/Pext)*(c>0)',0,'-Vmax*Rwell/(Da*Pext)*c/(c+Km/Pext)*(c>0)',0};
bnd.c0 = {0,0,1,0,0};
bnd.type = {'N0','N','C','N','N0'};
bnd.weakconstr = {0,0,1,0,0};
bnd.wcshape = 1;
bnd.ind = [1,2,3,4,5];
appl.bnd = bnd;
% Subdomain 1 = media
clear equ
equ.shape = 2;
equ.init = 1; % initial pO2
equ.ind = [1];
appl.equ = equ;
fem.appl{1} = appl;
fem.sdim = {'r','z'};
fem.border = 1;
fem.outform = 'general';
% Multiphysics
fem=multiphysics(fem);
% Extend mesh
fem.xmesh=meshextend(fem);
% Solve problem
[fem.sol, fem.stop]=femnlin(fem, ...
            'solcomp',{'c','lm1'}, ...
            'outcomp',{'c','lm1'}, ...
            'out',{'sol','stop'},...
            'maxiter',100,...
            'ntol', 1e-006);
% Save current fem structure for restart purposes
fem0=fem;
convergence=fem.stop;
%%%%%%%%%%%%%%%%%%%%%%%%%%%%Integrate
Total_I =postint(fem,'2*pi*r*(1/(1+.03125*c*Pext))', ...
        'dl',[2],'edim',1);
Total_PO2_bottom =postint(fem,'2*pi*r*c', ...
        'dl',[2],'edim',1);
min_PO2 = postmin(fem,'c','solnum',1,'Dl',[2 4],'edim',1);
min_quality_mesh = min(meshqual(fem.mesh));
element_num = size(fem.mesh.t,2);
Top_flux =postint(fem,'2*pi*lm1', ...
        'dl',[3], ...
        'edim',1);
```

10.11 Matlab code for oxygen transport in OBS – full model

```
% FEMLAB Model M-file
flclear fem
% COMSOL version
clear vrsn
vrsn.name = 'COMSOL 3.3';
vrsn.ext = '';
vrsn.major = 0;
vrsn.build = 405;
vrsn.rcs = '$Name:  $';
vrsn.date = '$Date: 2006/08/31 18:03:47 $';
fem.version = vrsn;
%%%%%%%%%%%%%%%%%%%%%%%%%%%%%%%%stants
%Diffusivities of oxygen
Diff_silicone_fl = 2.17e-5; % cm2/s
Diff_polystyrene = 1; % cm2/s
Diff_medium = 2.78e-5; % cm2/s
Diff_tissue = 1.22e-5; % cm2/s
%Solubilities of oxygen
Alpha_silicone_fl = 1.21e-8; % mol/cm3 mmHg
Alpha_polystyrene = 3.5e-15; % mol/cm3 mmHg
Alpha_medium = 1.27e-9; % mol/cm3 mmHg
Alpha_tissue = 1.02e-9; % mol/cm3 mmHg
Radius_well = 0.32; % cm   radius of well
Cell_density = 250000; % cells/cm2
h_medium = 0.3; % cm    medium depth
P_ext = 142; % mmHg    External pO2
Km = 0.44; % mmHg      Km for oxygen consumption
P_critical = 0.1; % mmHg   Critical pO2 of cells
Poly_thickness_bot = 0.12; % cm polystyrene thickness for bottom
Poly_thickness_side = 0.12; % cm polystyrene thickness for side
Dish_height = 1; % cm height of well
Tissue_volume = 0.008015*Radius_well^3; % cm3
Silicone_fl_thickness = 0.0625; % cm thickness of silicone with fl
Reader_position = 0.8*0.32/Radius_well; % non-dimensional length that plate reader sees
OCR_cell = 2.8; % fmol/min cell
V_max = OCR_cell/60*Cell_density*10^-15*(pi*Radius_well^2)/Tissue_volume; %mol/cm3 s  OCR of cells

fem.const={'Rwell',Radius_well,'h_medium',h_medium,'Pext',P_ext,'Km',Km,
'D_medium',Diff_medium,'D_silicone_fl',Diff_silicone_fl,...
D_poly',Diff_polystyrene,'D_tissue',Diff_tissue,'A_silicone_fl',
Alpha_silicone_fl,...
A_poly',Alpha_polystyrene,'A_medium',Alpha_medium,'A_tissue',Alpha_tissue,
'Vmax',V_max,... 'Pcrit',P_critical,'poly_bot',Poly_thickness_bot,'poly_side',
Poly_thickness_side,... 'tissue_V',Tissue_volume,'Si_fl_t',Silicone_fl_thickness,'h_dish',
Dish_height,'Read_plate',Reader_position};
%%%%%%%%%%%%%%%%%%%%%%%%%%%%%%%%%% Geometry
g2=circ2('1','base','center','pos',{'0','1'},'rot','0');
g3=rect2('1','1','base','corner','pos',{'0','0'},'rot','0');
% this is curved portion of media
g4=geomcomp({g2,g3},'ns',{'g2','g3'},'sf','g2*g3','edge','none');
% this is top of media
g5=rect2('1',((0.1 - 1.848844*Radius_well^3)/(pi*Radius_well^2)/Radius_well),'base','corner','pos',{'0','1'},'rot','0');
```

```
g7=circ2(1+Poly_thickness_side/Radius_well,'base','center','pos',{'0','1'},'rot','0');
g8=square2(1+Poly_thickness_side/Radius_well,'base','corner','pos',{'0',-Poly_thickness_side/Radius_well},'rot','0');
% this is round part of polystyrene
g9=geomcomp({g7,g8},'ns',{'g7','g8'},'sf','g7*g8','edge','none');
% this is rectangular part of polystyrene
g10=rect2(Poly_thickness_side/Radius_well,(Dish_height/Radius_well-1),'base','corner','pos',{'1','1'},'rot','0');%
height of 1 cm for well
%%%% At this point we have the round bottom with polystyrene
% Layer of Si
g20=ellip2('1.08','0.83','base','center','pos',{'0','1'},'rot','0');
g29=geomcomp({g4,g20},'ns',{'CO1','E2'},'sf','CO1-E2','edge','none');
g30=geomcomp({g29},'ns',{'CO4'},'sf','CO4','edge','none');
% Layer of tissue
g41=ellip2('1.1','0.82','base','center','pos',{'0','1'},'rot','0');
g43=geomcomp({g4,g41},'ns',{'CO1','E3'},'sf','CO1-E3','edge','none');
g44=geomcomp({g43},'ns',{'CO5'},'sf','CO5','edge','none');
% making the point of the plate-reader
parr={point2(0.8,0.4)};
g12=geomcoerce('point',parr);
G1 = g4 + g5;
G2 = G1 + g9;
G3 = G2 + g10;
G4 = G3 + g30;
G5 = G4 + g44;
final = G5 + g12;

clear s
s.objs={final};
s.name={'CO1'};
s.tags={'final'};
fem.draw=struct('s',s);
fem.geom=geomcsg(fem);
fem.sdim = {'r','z'};
fem.border = 1;
% Multiphysics
fem=multiphysics(fem);
% Mesh
fem.mesh = meshinit(fem);
fem.mesh = meshrefine(fem);
% Application mode 1
clear appl
appl.mode.class = 'FlDiffusion';
appl.mode.type = 'axi';
appl.shape = {'shlag(2,"lm1")','shlag(2,"c")'};
appl.border = 'on';
appl.assignsuffix = '_di';
clear prop
clear weakconstr
weakconstr.value = 'non-ideal';
weakconstr.dim = {'lm1'};
prop.weakconstr = weakconstr;
appl.prop = prop;
clear bnd
bnd.type = {'N0','cont','C'};
bnd.c0 = {0,0,1};
bnd.weakconstr = {0,0,1};
```

```
bnd.wcshape = 1;
bnd.ind = [1,1,1,1,1,2,3,2,2,3,3,3,3,2,2,2,2,2,2,2,2];
appl.bnd = bnd;
clear equ
equ.D = {'D_poly*A_poly/(D_medium*A_medium)',
'D_silicone_fl*A_silicone_fl/(D_medium*A_medium)',
 'D_tissue*A_tissue/(D_medium*A_medium)',1};
equ.init = 1;
equ.R = {0,0,
'-Vmax*Rwell^2/(D_medium*A_medium*Pext)*c/(c+Km/Pext)*(c>Pcrit/Pext)',0};
equ.shape = 2;
equ.ind = [1,2,3,4,4,1,2];
appl.equ = equ;
fem.appl{1} = appl;
fem.sdim = {'r','z'};
fem.border = 1;
fem.outform = 'general';

% Multiphysics
fem=multiphysics(fem);
% Extend mesh
fem.xmesh=meshextend(fem);
%%%%%%%%%%%%%%%%%%%%%%%%%%%%%%%%%% Solve problem
[fem.sol, fem.stop]=femnlin(fem, ...
            'solcomp',{'c','lm1'}, ...
            'outcomp',{'c','lm1'}, ...
            'out',{'sol','stop'},...
            'maxiter',100,...
            'ntol', 1e-006);
% Save current fem structure for restart purposes
fem0=fem;
convergence=fem.stop;
%%%%%%%%%%%%%%%%%%%%%%%%%%%%%%%%%%%%%%%%%%%%%%%%%% Analysis
% Integrate
Total_I =postint(fem,'2*pi*r*(1/(1+.03125*c*Pext))', ...
        'dl',[2 7]);
Total_PO2_fl =postint(fem,'2*pi*r*c', ...
        'dl',[2 7]);
Total_PO2_cell =postint(fem,'2*pi*r*c', ...
        'dl',[3]);
min_PO2 = postmin(fem,'c','solnum',1,'Dl',[3]);
min_quality_mesh = min(meshqual(fem.mesh));
element_num = size(fem.mesh.t,2);
Top_flux =postint(fem,'2*pi*lm1', ...
        'dl',[7], ...
        'edim',1);
Poly_flux = postint(fem,'2*pi*lm1', ...
        'dl',[10 11 12 13], ...
        'edim',1);
Total_flux =Poly_flux+Top_flux;
```

10.12 Matlab code for oxygen transport in OBS – flat bottom

```
% FEMLAB Model M-file

flclear fem
% COMSOL version
clear vrsn
vrsn.name = 'COMSOL 3.3';
vrsn.ext = '';
vrsn.major = 0;
vrsn.build = 405;
vrsn.rcs = '$Name:  $';
vrsn.date = '$Date: 2006/08/31 18:03:47 $';
fem.version = vrsn;
%%%%%%%%%%%%%%%%%%%%%%%%%%%%%%%%%%%%%%%% Constants
%Diffusivities of oxygen
Diff_silicone_fl = 2.17e-5; % cm2/s
Diff_polystyrene = 1; % cm2/s
Diff_medium = 2.78e-5; % cm2/s
Diff_tissue = 1.22e-5; % cm2/s
%Solubilities of oxygen
Alpha_silicone_fl = 1.21e-8; % mol/cm3 mmHg
Alpha_polystyrene = 3.5e-15; % mol/cm3 mmHg
Alpha_medium = 1.27e-9; % mol/cm3 mmHg
Alpha_tissue = 1.02e-9; % mol/cm3 mmHg
Radius_well = 0.32; % cm   radius of well
Cell_density = 250000; % cells/cm2
h_medium = 0.1/(pi*Radius_well^2); % cm    medium depth
P_ext = 142; % mmHg     External pO2
Km = 0.44; % mmHg      Km for oxygen consumption
P_critical = 0.1; % mmHg    Critical pO2 of cells
Poly_thickness_bot = 0.12; % cm polystyrene thickness for bottom
Poly_thickness_side = 0.12; % cm polystyrene thickness for side
Dish_height = 1; % cm height of well
Tissue_thickness = 0.0012; % cm thickness of tissue layer
Silicone_fl_thickness = 0.0625; % cm thickness of silicone with fl
Reader_position = 0.8*0.32/Radius_well; % non-dimensional length that plate reader sees
OCR_cell = 2.8; % fmol/min cell
V_max = OCR_cell/60*Cell_density*10^-15/Tissue_thickness; %mol/cm3 s  OCR of cells

fem.const={'Rwell',Radius_well,'h_medium',h_medium,'Pext',P_ext,'Km',Km,
'D_medium',Diff_medium,'D_silicone_fl',Diff_silicone_fl,...
'D_poly',Diff_polystyrene,'D_tissue',Diff_tissue,'A_silicone_fl',
Alpha_silicone_fl,...
'A_poly',Alpha_polystyrene,'A_medium',Alpha_medium,'A_tissue',
Alpha_tissue,'Vmax',V_max,...
'Pcrit',P_critical,'poly_bot',Poly_thickness_bot,'poly_side',
Poly_thickness_side,...
'tissue_t',Tissue_thickness,'Si_fl_t',Silicone_fl_thickness,'h_dish',
Dish_height,'Read_plate',Reader_position};
%%%%%%%%%%%%%%%%%%%%%%%%%%%%%%%%%%%%%%%%
%%%%%%%%%%%%%%%%%%%%%%%%%%%%%%%%%%%%%%%% Geometry
Medium=rect2('1',h_medium/Radius_well+Tissue_thickness/Radius_well+Silicone_fl_thickness/Radius_well,'base',
'corner','pos',{'0','0'},'rot','0');
```

```
Bottom_dish=rect2(1+Poly_thickness_side/Radius_well,Poly_thickness_bot/Radius_well,'base','corner','pos',{'0',-
Poly_thickness_bot/Radius_well},'rot','0');
Side_dish=rect2(Poly_thickness_side/Radius_well,Dish_height/Radius_well,'base','corner','pos',{'1','0'},'rot','0');
Si_fl_layer=rect2('1',Silicone_fl_thickness/Radius_well,'base','corner','pos',{'0','0'},'rot','0');
Tissue_layer=rect2('1',Tissue_thickness/Radius_well,'base','corner','pos',{'0',Silicone_fl_thickness/Radius_well},'rot'
,'0');
Plate_reader=rect2(Reader_position,Silicone_fl_thickness/Radius_well,'base','corner','pos',{'0','0'},'rot','0');

G1 = Medium + Bottom_dish;
G2 = G1 + Side_dish;
G3 = G2 + Si_fl_layer;
G4 = G3 + Tissue_layer;
final = G4 + Plate_reader;
clear s
s.objs={final};
s.name={'CO1'};
s.tags={'final'};
fem.draw=struct('s',s);
fem.geom=geomcsg(fem);
fem.sdim = {'r','z'};
fem.border = 1;
%%%%%%%%%%%%%%%%%%%%%%%%%%%%%%%%%%%%%%%%%%%%%%%%%%%%%%%%%%%%%
%%%%%%%%%%%%%%%%%%%%%%%%%%%%%%%%%%%%%%%%%%%%%%%%%%% Mesh
% Multiphysics
fem=multiphysics(fem);

% Initialize mesh
fem.mesh=meshinit(fem, ...
              'hmaxfact',0.55, ...
              'hcutoff',0.01, ...
              'hgrad',1.4, ...
              'hcurve',0.4, ...
              'hnarrow',0.7);
mesh_test = size(fem.mesh.t,2);
while mesh_test<2500
fem.mesh=meshrefine(fem);
mesh_test = size(fem.mesh.t,2);
end
%%%%%%%%%%%%%%%%%%%%%%%%%%%%%%%%%%%%%%%%%%%%%%%%%%%%%%%%%%%%%%%%
%%%%%%%%%%%%%%%%%%%%%%%%%%%%%% Application mode 1
clear appl
appl.mode.class = 'FlDiffusion';
appl.mode.type = 'axi';
appl.sdim = {'r','z1','z'};
appl.shape = {'shlag(2,''lm1'')','shlag(2,''c'')'};
appl.gporder = {40,4};
appl.assignsuffix = '_di';
clear prop
clear weakconstr
weakconstr.value = 'non-ideal';
weakconstr.dim = {'lm1'};
prop.weakconstr = weakconstr;
appl.prop = prop;
clear bnd
bnd.type = {'ax','C','cont'};
bnd.c0 = {0,1,0};
```

```
bnd.weakconstr = {0,1,0};
bnd.wcshape = 1;
bnd.ind = [1,2,1,3,1,3,1,3,2,3,3,3,3,3,3,3,2,2,2,2];
appl.bnd = bnd;
clear equ
equ.gporder = 2;
equ.D = {'D_poly*A_poly/(D_medium*A_medium)',
'D_silicone_fl*A_silicone_fl/(D_medium*A_medium)', ...
  'D_tissue*A_tissue/(D_medium*A_medium)',1};
equ.init = 1;
equ.R = {0,0,'-Vmax*Rwell^2/(D_medium*A_medium*Pext)*c/(c+Km/Pext)*(c>Pcrit/Pext)',0};
equ.shape = 2;
equ.ind = [1,2,3,4,2,1];
appl.equ = equ;
fem.appl{1} = appl;
fem.sdim = {'r','z'};
fem.border = 1;
fem.outform = 'general';
%%%%%%%%%%%%%%%%%%%%%%%%%%%%%%%%%%%%%%%%%%%%%%%%%%%%%%%%%%%%
% Multiphysics
fem=multiphysics(fem);
% Extend mesh
fem.xmesh=meshextend(fem);
%%%%%%%%%%%%%%%%%%%%%%%%%%%%%%%%%%%%%%%%%%%%%%%%%%%%%%%% Solve problem
[fem.sol, fem.stop]=femnlin(fem, ...
            'solcomp',{'c','lm1'}, ...
            'outcomp',{'c','lm1'}, ...
            'out',{'sol','stop'},...
            'maxiter',100,...
            'ntol', 1e-006);
% Save current fem structure for restart purposes
fem0=fem;
convergence=fem.stop;
%%%%%%%%%%%%%%%%%%%%%%%%%%%%%%%%%%%%%%%%%%%%%%%%%%%%%%%%%%%%%% Analysis
% Integrate
Total_I =postint(fem,'2*pi*r*(1/(1+.03125*c*Pext))', ...
        'dl',[2]);
Total_PO2_fl =postint(fem,'2*pi*r*c', ...
        'dl',[2]);
Total_PO2_cell =postint(fem,'2*pi*r*c', ...
        'dl',[3]);
min_PO2 = postmin(fem,'c','solnum',1,'Dl',[3]);
min_quality_mesh = min(meshqual(fem.mesh));
element_num = size(fem.mesh.t,2);
Top_flux =postint(fem,'2*pi*lm1', ...
        'dl',[9], ...
        'edim',1);
Poly_flux = postint(fem,'2*pi*lm1', ...
        'dl',[2 17 18 19 20], ...
        'edim',1);
Total_flux =Poly_flux+Top_flux;
```

References

1. 2007. American Diabetes Association. http://www.diabetes.org/home.jsp.
2. Colton CK, Avgoustiniatos ES. 1991. Bioengineering in development of the hybrid artificial pancreas. Journal of Biomechanical Engineering-Transactions of the Asme 113(2):152-170.
3. Silva AI, de Matos AN, Brons IG, Mateus M. 2006. An overview on the development of a bio-artificial pancreas as a treatment of insulin-dependent diabetes mellitus. Med Res Rev 26(2).
4. Meier JJ, Bhushan A, Butler PC. 2006. The potential for stem cell therapy in diabetes. Pediatric Research 59(4, Part 2):65R-73R.
5. Madsen OD. 2005. Stem cells and diabetes treatment. Apmis 113(11-12):858-875.
6. Ren JQ, Jin P, Wang E, Liu E, Harlan DM, Li X, Stroncek DF. 2007. Pancreatic islet cell therapy for type I diabetes: understanding the effects of glucose stimulation on islets in order to produce better islets for transplantation. Journal of Translational Medicine 5.
7. Shapiro AMJ, Lakey JRT, Ryan EA, Korbutt GS, Toth E, Warnock GL, Kneteman NM, Rajotte RV. 2000. Islet transplantation in seven patients with type 1 diabetes mellitus using a glucocorticoid-free immunosuppressive regimen. New England Journal of Medicine 343(4):230-238.
8. Ryan EA, Paty BW, Senior PA, Bigam D, Alfadhli E, Kneteman NM, Lakey JRT, Shapir AMJ. 2005. Five-year follow-up after clinical islet transplantation. Diabetes 54(7):2060-2069.
9. Pyzdrowski KL, Kendall DM, Halter JB, Nakhleh RE, Sutherland DER, Robertson RP. 1992. Preserved insulin-secretion and insulin independence in recipients of islet autografts. New England Journal of Medicine 327(4):220-226.
10. Korc M. 1993. Normal function of the endocrine pancreas. In: Go V, Dimango E, Gardner J, Lebenthal E, Reber H, Scheele G, editors. The Pancreas. New York: Raven Press. p 751-758.
11. Volk B, Wellmann K. 1985. Quantitative studies of the islets of nondiabetic patients. In: Volk B, Wellmann E, editors. The Diabetic Pancreas. New York: Plenum Medical. p 117-125.
12. Ryan EA, Lakey JRT, Rajotte RV, Korbutt GS, Kin T, Imes S, Rabinovitch A, Elliott JF, Bigam D, Kneteman NM and others. 2001. Clinical outcomes and insulin secretion after islet transplantation with the edmonton protocol. Diabetes 50(4):710-719.
13. Colton CK, Papas KK, Pisania A, Rappel MJ, Powers D, O'Neil JJ, Omer A, Weir GC, Bonner-weir S. 2007. Characterization of Islet Preparations. In: Halberstadt C, Emerich DF, editors. Cellular Transplantation: From Laboratory to Clinic. New York: Elsevier Inc.
14. Balamurugan AN, Bottino R, Giannoukakis N, Smetanka C. 2006. Prospective and challenges of islet transplantation for the therapy of autoimmune diabetes. Pancreas 32(3):231-43.
15. Ricordi C, Lacy PE, Finke EH, Olack BJ, Scharp DW. 1988. Automated-method for isolation of human pancreatic-islets. Diabetes 37(4):413-420.

16. Avgoustiniatos ES. 2001. Oxygen diffusion limitations in pancreatic islet culture and immunoisolation. Cambridge: MIT.
17. Hering BJ, Kandaswamy R, Harmon JV, Ansite J, Clemmings SM, Sakai T, Paraskevas S, Eckman PM, Sageshima J, Nakano M and others. 2004. Bluestone JA 2003 Transplantation of cultured islets from two-layer preserved pancreases in type 1 diabetes with anit-CD3 antibody. Am J Transplant 4:390-401.
18. Hering BJ. 2005. Achieving and maintaining insulin independence in human islet transplant recipients. Transplantation 79(10):1296-1298.
19. Kaufman DB, Lowe WLJ. 2003. Clinical islet transplantation. Curr Diab Rep 3(4):344-350.
20. Lakey JRT, Burridge PW, Shapiro AMJ. 2003. Technical aspects of islet preparation and transplantation. Transplant Int 16(9):613-632.
21. Ricordi C, Inverardi L, Kenyon NS, Goss J, Bertuzzi F, Alejandro R. 2005. Requirements for success in clinical islet transplantation. Transplantation 79(10):1298-1300.
22. Sutherland DER. 2003. Current status of beta-cell replacement therapy (pancreas and islet transplantation) for treatment of diabetes mellitus. Transplant Proc 35(5):1625-1627.
23. Knazek RA. 2002. The human pancreatic islet cell resource consortium. Diab Technol Ther 4(4):551-552.
24. Weber DJ, McFarland RD, Irony I. 2002. Selected Food an Drug Administration review issues for regulation of allogeneic islets of Langerhans as somatic cell therapy. Transplantation 74:1816-1820.
25. Eckhard E, Brandhorst D, Winter D, Jaeger C, Jahr H, Bretzel RG, Brendel MD. 2004. The role of current product release criteria for identification of human islet preparations suitable for clinical transplantation. Transplant Proc 36:1528-1531.
26. Brissova M, Poffenberger G, Jewel M, Dai CH, Powers AC. 2006. Human islet preparations have major variations in islet function within and between islet isolation facilities. Diabetes 55:A443-A444.
27. Shapiro AMJ, Nanji SA, Lakey JRT. 2003. Clinical islet transplant: current and future directions towards tolerance. Immunological Reviews 196(1):219-236.
28. Ricordi C, Scharp DW, Lacy PE. 1988. Reversal in nude mice after transplantation of fresh and 7 days culutred (24 °C) human pancreatic islets. Transplantation 45:994-996.
29. Gaber AO, Fraga DW, Kotb M, Lo A, Sabek O, Latif K. 2004. Human islet graft function in NOD-SCID mice predicts clinical response in islet transplant recipients. Transplant Proc 36:1108-1110.
30. Hering BJ, Kandaswamy R, Harmon JV, Ansite JD, Clemmings SM, Sakai T, S. P, M. EP, Sageshima J, Nakano M and others. 2004. Transplantation of cultured islets from two-layer preserved pancreases in type 1 diabetes with anti-CD3 antibody. Am J Transplant 4:390-401.
31. Bretzel RG, Alejandro R, Hering BJ, van Suylichem PT, Ricordi C. 1994. Clinical islet transplantation: guidelines for islet quality control. Transplant Proc. 26:388-392.
32. Latif ZA, Noel J, Alejandro R. 1988. A simple method of staining fresh and cultured islets. Transplantation 45(4):827-830.
33. London NJ, Contractor H, Lake SP, Aucott GC, Bell PR, James RF. 1989. A microfluorometric viability assay for isolated human and rat islets of Langerhans. Diabetes Res 12(3):141-149.

34. 2000. FDA Biological Response Modifier Advisory Committee summary minutes Meeting no. 26, March 20-21. http://www.fda.gov/ohrms/dockets/ac/00minutes/3604m1minutes.pdf.
35. 2003. FDA Biological Response Modifier Advisory Committee summary minutes Meeting no. 36, Oct. 9-10. http://www.fda.gov/ohrms/dockets/ac/cber03.html#BiologicalRepsonseModofiers.
36. Ricordi C, Lakey JRT, Hering BJ. 2001. Challenges toward standardization of islet isolation technology. Transplant Proc 33(1-2):1709.
37. Ichii H, Inverardi L, Pileggi A, Damaris Molano R, Cabrera O, Caicedo A, Mesinger S, Kuroda Y, Berggren PO, Ricordi C. 2005. A novel method for the assessment of cellular composition and beta-cell viability in human islet preparations. Am J Transplant 5:1635-1645.
38. Goto M, Holgersson J, Kumagai-Braesch M, Korsgren O. 2006. The ADP/ATP ratio: a novel predictive assay of quality assessment of isolated pancreatic islets. Am J Transplant 6:2483-2487.
39. Papas KK, Pisania A, Wu H, Weir GC, Colton CK. 2007. A stirred microchamber for oxygen consumption rate measurements with pancreatic islets. Submitted.
40. Murdoch TB, McGhee-Wilson D, Shapiro AMJ, Lakey JRT. 2004. Methods of human islet culture for transplantation. Cell Transplantation 13(6):605-617.
41. Kuttler B, Hartmann A, Wanka H. 2002. Long-term culture of islets abrogates cytokine-induced or lymphocyte-induced increase of antigen expression on beta cells. Transplantation 74(4):440-445.
42. Ricordi C, Lacy PE, Sterbenz K, Davie JM. 1987. Low-temperature culture of cuman islets or in vivo treatment with L3t4 antibody produces a marked prolongation of islet human-to-mouse xenograft survival. Proceedings of the National Academy of Sciences of the United States of America 84(22):8080-8084.
43. Stein E, Mullen Y, Benhamou PY, Watt PC, Hober C, Watanabe Y, Nomura Y, Brunicardi FC. 1994. Reduction in immunogenicity of human islets by 24-degrees-C culture. Transplantation Proceedings 26(2):755.
44. Lacy PE, Davie JM, Finke EH. 1979. Prolongation of islet allograft survival following in vitro culture (24-Degrees-C) and a single injection of ALS. Science 204(4390):312-313.
45. Lafferty KJ, Prowse SJ, Simeonovic CJ, Warren HS. 1983. Immunobiology of tissue-transplantation - a return to the passenger leukocyte concept. Annual Review of Immunology 1:143-173.
46. Kim SC, Han DJ, Kim IH, Woo KO, We YM, Kang SY, Back JH, Kim YH, Kim JH, Lim DG. 2005. Comparative study on biologic and immunologic characteristics of the pancreas islet cell between 24 degrees C and 37 degrees C culture in the rat. Transplantation Proceedings 37(8):3472-3475.
47. Matsumoto S, Goel S, Qualley S, Strong DM, Reems JA. 2003. A comparative evaluation of culture conditions for short-term maintenance (<24 h) of human islets isolated using the Edmonton protocol. Cell and Tissue Banking 4(2-4):85-93.
48. Clayton HA, London NJM. 1996. Survival and function of islets during culture. Cell Transplantation 5(1):1-12.
49. Brandhorst D, Brandhorst H, Hering BJ, Bretzel RG. 1999. Long-term survival, morphology and in vitro function of isolated pig islets under different culture conditions. Transplantation 67(12):1533-1541.

50. Degraaff MPA, Wolters GHJ, Vanschilfgaarde R. 1994. Endothelial-cells in pancreatic-islets and the effect of culture. Transplantation Proceedings 26(3):1171-1171.
51. Cui Y-F, Ma M, Wang G-Y, Han D-E, Vollmar B, Menger MD. 2005. Prevention of core cell damage in isolated islets of Langerhans by low temperature preconditioning. World J Gastroenterol 11(4).
52. Ono J, Lacy PE, Michael HEB, Greider MH. 1979. Studies of the functional and morphologic status of islets maintained at 24-C for 4 weeks in vitro. American Journal of Pathology 97(3):489-&.
53. Ilieva A, Yuan S, Wang R, Duguid W, Rosenberg L. 1999. The structural integrity of the islet in vitro: the effect of incubation temperature. Pancreas 19(3):297-303.
54. Lakey JRT, Warnock GL, Kneteman NM, Ao Z, Rajotte RV. 1994. Effects of pre-cryopreservation culture on human islet recovery and in vitro function. Transplant Proc 26(2):820.
55. Pisania A. 2007. Development of quantitative assays for quality assessment of islets of Langerhans. Cambridge: Massachusetts Institute of Technology.
56. Lacy PE, Kostianovsky M. 1967. Method for the isolation of intact islets of Langerhans from the rat pancreas. Diabetes 16(1):35.
57. Gotoh M, Maki T, Kiyoizumi T, Satomi S, Monaco AP. 1985. An improved method for isolation of mouse pancreatic islets. Transplantation 40:437-438.
58. O'Neil JJ, Omer A, Tchipashvili T, Lei J, Pisania A, Colton CK, Weir GC, Bonner-Weir S. 2007. Quantitative analysis of cell composition of human pancreatic islet preparations. Lab Invest submitted.
59. O'Neil JJ, Stegemann JP, Nicholson DT, Gagnon KA, Solomon BA, Mullon CJ. 2001. The isolation and function of porcine islets from market weight pigs. Cell Transplant 10(3):235-246.
60. Papas KK, Avgoustiniatos ES, Tempelman LA, Weir GC, Colton CK, Pisania A, Rappel MJ, Friberg AS, Bauer AC, Hering BJ. 2005. High-density culture of human islets on top of silicone rubber membranes. Transplantation Proceedings 37(8):3412-3414.
61. Papas KK, Colton CK, Nelson RA, Rosack PR, Avgoustiniatos ES, Scott II WE, Pisania A, Weir GC, Hering BJ. 2007. Human islet oxygen consumption rate and DNA measurements predict diabetes reversal in nude mice. Am J Transplant 7(3):707-713.
62. Bank HL. 1987. Assessment of islet cell viability using fluorescent dyes. Diabetologia 30(10):812-816.
63. Weibel ER. 1979. Practical methods for biological morphometry. London: Academic Press.
64. Bonner-Weir S, Trent DF, Weir GC. 1983. Partial pancreatectomy in the rat and subsequent defect in glucose-induced insulin release. Journal of Clinical Investigation 71(6):1544-1553.
65. Erlandsen SL, Parsons JA, Burke JP, Redick JA, Van Orden DE, Van Orden LS. 1975. A modification of the unlabeled antibody enzyme method using heterologous antisera for the light microscopy and ultrastructural localization of insulin, glucagon, and growth hormone. J Histochem Cytochem 23(9):666-677.
66. Polak JM, Noorden SV. 2003. Visualizing the end-product reaction. Introduction to immunocytochemistry. Oxford, UK: BIOS Scientific Publishers Ltd. p 50.

67. Pipeleers DG, Int' Veld PA, Van De Winkel M, Maes E, Schuit FC, Gepts W. 1985. A new in vitro model fro the study of pancreatic A and B cells. Endocrinology 117:806-816.
68. Dolezel J, Bartos J, Voglmayr H, Greilhuber J. 2003. Nuclear DNA content and genome size of trout and human. Cytometry Part A 51A(2):127-128.
69. Hellerstrom C. 1967. Effects of carbohydrates on the oxygen consumption of isolated pancreatic islets of mice. Endocrinology 81(1):105-112.
70. Lundgren G, Andersson A, Borg H, Buschard K, Groth CG, Gunnarsson R, Hellerstrom C, Petersson B, Ostman J. 1977. Structural and functional integrity of isolated human islets of Langerhans maintained in tissue culture for 1-3 weeks. Transplant Proc 9:237-240.
71. Sweet IR, Gilbert M, Jensen R, Sabek O, Fraga DW, Gaber AO, Reems JA. 2005. Glucose stimulation of cytochrome C reduction and oxygen consumption as assessment of human islet quality. Transplantation 80(8):1003-1011.
72. Andersson A, Gunnarsson R, Hellerstrom C. 1976. Long-Term Effects of a Low Extracellular Glucose Concentration on Glucose-Metabolism and Insulin-Biosynthesis and Release of Mouse Pancreatic-Islets Maintained in Tissue-Culture. Acta Endocrinologica 82(2):318-329.
73. Dionne KE. 1990. Effect of hypoxia on insulin secretion and viability of pancreatic islet tissue. Cambridge: MIT.
74. Sweet IR, Khalil G, Wallen AR, Steedman M, Schenkman KA, Reems JA, Kahn SE, Callis JB. 2002. Continuous measurement of oxygen consumption by pancreatic islets. Diabetes Technol Ther 4(5).
75. Wang WJ, Upshaw L, Strong DM, Robertson RP, Reems JA. 2005. Increased oxygen consumption rates in response to high glucose detected by a novel oxygen biosensor system in non-human primate and human islets. Journal of Endocrinology 185(3):445-455.
76. Schwartzman RA, Cidlowski JA. 1993. Apoptosis: the biochemistry and molecular biology of programmed cell death. Endocrine Rev 14(2):133-151.
77. Gershengorn MC, Hardikar AA, Wei CJ, Geras-Raaka E, Marcus-Samuels B, Raaka BM. 2004. Epithelial-to-mesenchymal transition generates proliferative human islet precursor cells. Science 306(5705):2261-2264.
78. Weir GC, Halban PA, Meda P, Wollheim CB, Orci L, Renold AE. 1984. Dispersed adult rat pancreatic islet cells in culture: A, B, and D cell function. Metabolism 33:447-453.
79. Ghosh A, Ronner P, Cheong E, Khalid P, Matchinsky FM. 1991. The role of ATP and free ADP in metabolic coupling during fuel stimulated insulin release from islet β-cells in the isolated perfused rat pancreas. J Biol Chem 286(34):22887-22892.
80. Fraker C, Guarino R, Timmins M, Presnell S, Molano D, Pileggi A, Ricordi C. The BD oxygen biosensor as a potential predictive tool for islet function in-vivo; 2004; Boston, MA.
81. Korsgren O, Nilsson B, Berne C, Felldin M, Foss A, Kallen R, Lundgren T, Salmela K, Tibell A, Tufveson G. 2005. Current status of clinical islet transplantation. Transplantation 79(10):1289-1293.
82. Ryan EA, Lakey JRT, Paty BW, Imes S, Korbutt GS, Kneteman NM, Bigam D, Rajotte RV, Shapiro AMJ. 2002. Successful islet transplantation: Continued insulin reserve provides long-term glycemic control. Diabetes 51(7):2148-2157.

83. Gaglia JL, Shapiro AMJ, Weir GC. 2005. Islet transplantation: Progress and challenge. Archives of Medical Research 36(3):273-280.
84. Moriscot C, Candel S, Sauret V, Kerr-Conte J, Richard MJ, Favrot MC, Benhamou PY. 2007. MnTMPyP, a metalloporphyrin-based superoxide dismutase/catalase mimetic, protects INS-1 cells and human pancreatic islets from an in vitro oxidative challenge. Diabetes Metab 33(1).
85. Hara Y, Fujino M, Li XK. 2006. The reduction of hypoxia-induced and reoxygenation-induced apoptosis in rat islets by epigallocatechin gallate. Transplantation Proceedings 38(8):2722-2725.
86. Pileggi A, Molano RD, Berney T, Cattan P, Vizzardelli C, Oliver R, Fraker C, Ricordi C, Pastori RL, Bach FH and others. 2001. Heme oxygenase-1 induction in islet cells results in protection from apoptosis and improved in vivo function after transplantation. Diabetes 50(9):1983-1991.
87. Contreras JL, Bilbao G, Smyth CA, Eckhoff DE, Jiang XL, Jenkins S, Thomas FT, Curiel DT, Thomas JM. 2002. Cytoprotection of pancreatic islets before and early after transplantation using gene therapy. Kidney Int 61(1 Suppl).
88. Li YX, Ge L, Dong WP, Lu DR, Tan JM. 2006. Protection of human islets from induction of apoptosis and improved islet function with HO-1 gene transduction. Chinese Medical Journal 119(19):1639-1645.
89. Fenjves ES, Ochoa MS, Gay-Rabinstein C, Ricordi C, Curran MA. 2004. Retrovirally transferred genes inhibit apoptosis in an insulin-secreting cell line: Implications for islet transplantation. Cell Transplantation 13(5):489-496.
90. McCabe C, Samali A, O'Brien T. 2006. beta cell cytoprotective strategies: Establishing the relative roles for iNOS and ROS. Biochemical and Biophysical Research Communications 342(4):1240-1248.
91. Gaber AO, Fraga DW, Callicutt CS, Gerling IC, Sabek OM, Kotb MY. 2001. Improved in vivo pancreatic islet function after prolonged in vitro islet culture. Transplantation 72(11):1730-1736.
92. Dionne KE, Colton CK, Yarmush ML. 1993. Effect of hypoxia on insulin-secretion by isolated rat and canine islets of Langerhans. Diabetes 42(1):12-21.
93. Nyqvist D, Kohler M, Wahlstedt H, Berggren PO. 2005. Donor islet endothelial cells participate in formation of functional vessels within pancreatic islet grafts. Diabetes 54(8):2287-2293.
94. Parr EL, Bowen KM, Lafferty KJ. 1980. Cellular-changes in cultured mouse thyroid-glands and islets of Langerhans. Transplantation 30(2):135-141.
95. Mendola JF, Goity C, Fernandezalvarez J, Saenz A, Benarroch G, Fernandezcruz L, Gomis R. 1994. Immunocytochemical study of pancreatic-islet revascularization in islet isograft - effect of hyperglycemia of the recipient and of in-vitro culture of islets. Transplantation 57(5):725-730.
96. Olsson R, Carlsson P-O. 2006. Oxygenation of cultured pancreatic islets. Advances in Experimental Medicine and Biology. p 263-268.
97. Deen WM. 1998. Analysis of Transport Phenomena. New York: Oxford University Press, Inc.
98. Wilson DF, Rumsey WL, Green TJ, Vanderkooi JM. 1988. The oxygen dependence of mitochondrial oxidative-phosphorylation measured by a new optical method for measuring oxygen concentration. Journal of Biological Chemistry 263(6):2712-2718.

99. 2005. COMSOL Documentaion - Users Guide. COMSOL.
100. Bonner-Weir S, Taneja M, Weir GC, Tatarkiewicz K, Song KH, Sharma A, O'Neil JJ. 2000. In vitro cultivation of human islets from expanded ductal tissue. Proceedings of the National Academy of Sciences of the United States of America 97(14):7999-8004.
101. Gschwind M, Huber G. 1997. Detection of apoptotic or necrotic death in neuronal cells by morphological, biochemical, and molecular analysis. In: Poirier J, editor. Apoptosis Techniques and Protocols. Totowa, New Jersey: Humana Press.
102. Rudolf E, Cervinka M. 2006. Cytoskeletal changes in non-apoptotic cell death. Acta Medica (Hradec Kralove) 49(2).
103. Kaneto H, Fujii J, Seo HG, Suzuki K, Matsuoka T, Nakamura M, Tatsumi H, Yamasaki Y, Kamada T, Taniguchi N. 1995. Apoptotic Cell-Death Triggered by Nitric-Oxide in Pancreatic Beta-Cells. Diabetes 44(7):733-738.
104. Hoorens A, Stange G, Pavlovic D, Pipeleers D. 2001. Distinction between interleukin-1-induced necrosis and apoptosis of islet cells. Diabetes 50(3):551-557.
105. Dive C, Gregory CD, Phipps DJ, Evans DL, Milner AE, Wyllie AH. 1992. Analysis and discrimination of necrosis and apoptosis (programmed cell-death) by multiparameter flow-cytometry. Biochimica Et Biophysica Acta 1133(3):275-285.
106. Papas KK. 2007. personal communication noting islet surface density employed in clinical preparations.
107. Omer A. 2007. personal communication noting islet surface density employed in clinical preparations.
108. Freshney RI. 1983. Culture of animal cells a manual of basic technique. Freshney, R. I. Culture of Animal Cells: A Manual of Basic Technique. Xiv+295p. Alan R. Liss, Inc.: New York, N.Y., USA. Illus.
109. Bergert H, Knoch KP, Meisterfeld R, Jager M, Ouwendijk J, Kersting S, Saeger HD, Solimena M. 2005. Effect of oxygenated perfluorocarbons on isolated rat pancreatic islets in culture. Cell Transplantation 14(7):441-448.
110. Rutzky LP, Bilinski S, Kloc M, Phan T, Zhang HM, Katz SM, Stepkowski SM. 2002. Microgravity culture condition reduces immunogenicity and improves function of pancreatic islets. Transplantation 74(1):13-21.
111. Murray HE, Paget MB, Downing R. 2005. Preservation of glucose responsiveness in human. islets maintained in a rotational cell culture system. Molecular and Cellular Endocrinology 238(1-2):39-49.
112. Sardonini CA, Wu YJ. 1993. Expansion and differentiation of human hematopoietic-cells from static cultures through small-scale bioreactors. Biotechnology Progress 9(2):131-137.
113. Collins PC, Nielsen LK, Patel SD, Papoutsakis ET, Miller WM. 1998. Characterization of hematopoietic cell expansion, oxygen uptake, and glycolysis in a controlled, stirred-tank bioreactor system. Biotechnology Progress 14(3):466-472.
114. Collins PC, Miller WM, Papoutsakis ET. 1998. Stirred culture of peripheral and cord blood hematopoietic cells offers advantages over traditional static systems for clinically relevant applications. Biotechnology and Bioengineering 59(5):534-543.
115. Jorjani P, Ozturk SS. 1999. Effects of cell density and temperature on oxygen consumption rate for different mammalian cell lines. Biotechnology and Bioengineering 64(3):349-356.

116. Colton CK, Drake RF. 1971. Effect of boundary conditions on oxygen transport to blood flowing in a tube. Chemical Engineering Progress Symposium Series 67(114):88-95.
117. Perry RH, Green DW. 1997. Perry's Chemical Engineers' Handbook: McGraw-Hill.
118. 2007. CRC Handbook of Chemistry and Physics. Boca Ranton, FL: Taylor and Francis.
119. Sekine N, Cirulli V, Regazzi R, Brown LJ, Gine E, Tamaritrodriguez J, Girotti M, Marie S, Macdonald MJ, Wollheim CB and others. 1994. Low lactate-dehydrogenase and high mitochondrial glycerol phosphate dehydrogenase in pancreatic beta-cells - potential role in nutrient sensing. Journal of Biological Chemistry 269(7):4895-4902.
120. Hummerich H, Degroot H, Noll T, Soboll S. 1988. Dependence of mitochondrial and cytosolic adenine-nucleotides on oxygen partial-pressure in isolated hepatocytes - application of a new rapid high-pressure filtration technique for fractionation. Biochemical Journal 250(3):641-645.
121. Noll T, de Groot H, Wissemann P. 1986. A computer-supported oxystat system maintaining steady-state O2 partial pressures and simultaneously monitoring O2 uptake in biological systems. Biochem J 236(3).
122. Casey TM, Arthur PG. 2000. Hibernation in noncontracting mammalian cardiomyocytes. Circulation 102(25):3124-3129.
123. Venkatasubramanian R, Henson MA, Forbes NS. 2006. Incorporating energy metabolism into a growth model of multicellular tumor spheroids. Journal of Theoretical Biology 242(2):440-453.
124. Patton JN, Palmer AF. 2006. Numerical simulation of oxygen delivery to muscle tissue in the presence of hemoglobin-based oxygen carriers. Biotechnology Progress 22(4):1025-1049.
125. Dash RK, Bassingthwaighte JB. 2006. Simultaneous blood-tissue exchange of oxygen, carbon dioxide, bicarbonate, and hydrogen ion. Annals of Biomedical Engineering 34(7):1129-1148.
126. Littbrand B, Revesz L. 1969. The effect of oxygen on cellular survival and recovery after radiation. Br J Radiol 42(504).
127. Buerk DG, Goldstick TK. 1992. Spatial variation of aortic wall oxygen diffusion coefficient from transiet polarographic measurements. Annals of Biomedical Engineering 20:629-646.
128. Bentley TB, Meng H, Pittman RN. 1993. Temperature-dependence of oxygen diffusion and consumption in mammalian striated-muscle. American Journal of Physiology 264(6):H1825-H1830.
129. Mahler M, Louy C, Homsher E, Peskoff A. 1985. Reappraisal of diffusion, solubility, and consumption of oxygen in frog skeletal-muscle, with applications to muscle energy-balance. Journal of General Physiology 86(1):105-134.
130. Weind KL, Ellis CG, Boughner DR. 2002. Aortic valve cusp vessel density: Relationship with tissue thickness. Journal of Thoracic and Cardiovascular Surgery 123(2):333-340.
131. Filion RJ, Ellis CG. 2003. A finite difference model of O2 transport in aortic valve cusps: importance of intrinsic microcirculation. American Journal of Physiology-Heart and Circulatory Physiology 285(5):H2099-H2104.
132. Groebe K. 1990. A versatile model of steady-state O2 supply to tissue - application to skeletal-muscle. Biophysical Journal 57(3):485-498.
133. Radisic M, Deen W, Langer R, Vunjak-Novakovic G. 2005. Mathematical model of oxygen distribution in engineered cardiac tissue with parallel channel array perfused with

culture medium containing oxygen carriers. American Journal of Physiology-Heart and Circulatory Physiology 288(3):H1278-H1289.
134. Vadapalli A, Goldman D, Popel AS. 2002. Calculations of oxygen transport by red blood cells and hemoglobin solutions in capillaries. Artificial Cells Blood Substitutes and Immobilization Biotechnology 30(3):157-188.
135. Evans NTS, Naylor PFD, Quinton TH. 1981. The diffusion-coefficient of oxygen in respiring kidney and tumor-tissue. Respiration Physiology 43(3):179-188.
136. Groebe K, Thews G. 1990. Calculated intracellular and extracellular pO2 gradients in heavily working red muscle. American Journal of Physiology 259(1):H84-H92.
137. Clark A, Clark PAA, Connett RJ, Gayeski TEJ, Honig CR. 1987. How large is the drop in pO2 between cytosol and mitochondrion. American Journal of Physiology 252(6):C583-C587.
138. Kawashiro T, Nusse W, Scheid P. 1975. Determination of diffusivity of oxygen and carbon-dioxide in respiring tissue - results in rat skeletal-muscle. Pflugers Archiv-European Journal of Physiology 359(3):231-251.
139. Han P, Bartels DM. 1996. Temperature dependence of oxygen diffusion in H2O and D2O. Journal of Physical Chemistry 100(13):5597-5602.
140. Wichterlova J, Wichterle K, Michalek J. 2005. Determination of permeability and diffusivity of oxygen in polymers by polarographic method with inert gas. Polymer 46(23):9974-9986.
141. Stern SA, Shah VM, Hardy BJ. 1987. Structure-permeability relationships in silicone polymers. Journal of Polymer Science Part B-Polymer Physics 25(6):1263-1298.
142. McDonagh C, Bowe P, Mongey K, MacCraith BD. 2002. Characterisation of porosity and sensor response times of sol-gel-derived thin films for oxygen sensor applications. Journal of Non-Crystalline Solids 306(2):138-148.
143. Lu X, Manners I, Winnik MA. 2001. Polymer/silica composite films as luminescent oxygen sensors. Macromolecules 34(6):1917-1927.
144. Mark JE. 1999. Polymer data handbook. New York: Oxford University Press.
145. 1999. Polymer Handbook. Bloch DR, editor: John Wiley & Sons.
146. Guarino RD, Dike LE, Haq TA, Rowley JA, Pitner JB, Timmins MR. 2004. Method for determining oxygen consumption rates of static cultures from microplate measurements of pericellular dissolved oxygen concentration. Biotechnology and Bioengineering 86(7):775-787.
147. Hoorens A, VandeCasteele M, Kloppel G, Pipeleers D. 1996. Glucose promotes survival of rat pancreatic beta cells by activating synthesis of proteins which suppress a constitutive apoptotic program. Journal of Clinical Investigation 98(7):1568-1574.
148. Ling Z, Hannaert JC, Pipeleers D. 1994. Effect of Nutrients, Hormones and Serum on Survival of Rat Islet Beta-Cells in Culture. Diabetologia 37(1):15-21.
149. Van de Casteele M, Kefas BA, Cai Y, Heimberg H, Scott DK, Henquin JC, Pipeleers D, Jonas JC. 2003. Prolonged culture in low glucose induces apoptosis of rat pancreatic beta-cells through induction of c-myc. Biochemical and Biophysical Research Communications 312(4):937-944.
150. Deeney JT, Prentki M, Corkey BE. 2000. Metabolic control of beta-cell function. Seminars in Cell & Developmental Biology 11(4):267-275.

151. Li CH, Najafi H, Daikhin Y, Nissim IB, Collins HW, Yudkoff M, Matschinsky FM, Stanley CA. 2003. Regulation of leucine-stimulated insulin secretion and glutamine metabolism in isolated rat islets. Journal of Biological Chemistry 278(5):2853-2858.
152. Casciari JJ, Sotirchos SV, Sutherland RM. 1988. Glucose Diffusivity in Multicellular Tumor Spheroids. Cancer Research 48(14):3905-3909.
153. Kauri LM, Jung SK, Kennedy RT. 2003. Direct measurement of glucose gradients and mass transport within islets of Langerhans. Biochemical and Biophysical Research Communications 304(2):371-377.
154. Tamarit-Rodriguez J, Idahl LA, Gine E, Alcazar O, Sehlin J. 1998. Lactate production in pancreatic islets. Diabetes 47(8):1219-1223.
155. Erecinska M, Bryla J, Michalik M, Meglasson MD, Nelson D. 1992. Energy-Metabolism in Islets of Langerhans. Biochimica Et Biophysica Acta 1101(3):273-295.
156. Zong-Chao L, Efendic S, Wibom R, Abdel-Halim SM, Ostenson C-G, Landau BR, Khan A. 1998. Glucose metabolism in Goto-Kakizaki rat islets. Endocrinology 139(6):2670-2675.
157. Borelli MI, Francini F, Gagliardino JJ. 2004. Autocrine regulation of glucose metabolism in pancreatic islets. American Journal of Physiology-Endocrinology and Metabolism 286(1):E111-E115.
158. Matschinsky FM. 2002. Regulation of pancreatic beta-cell glucokinase - From basics to therapeutics. Diabetes 51:S394-S404.
159. Haber EP, Ximenes HMA, Procopio J, Carvalho CRO, Curi R, Carpinelli AR. 2003. Pleiotropic effects of fatty acids on pancreatic beta-cells. Journal of Cellular Physiology 194(1):1-12.
160. Holmes MA, Clayton HA, Chadwick DR, Bell PRF, London NJM, James RFL. 1995. Functional-studies of rat, porcine, and human pancreatic-islets cultured in 10 commercially available media. Transplantation 60(8):854-860.
161. Lindstrom P, Sehlin J. 1986. Effect of intracellular alkalinization on pancreatic-islet calcium-uptake and insulin-secretion. Biochemical Journal 239(1):199-204.
162. Roos A, Boron WF. 1981. Intracellular pH. Physiological Reviews 61(2):296-434.
163. Ohta M, Nelson D, Nelson J, Meglasson MD, Erecinska M. 1991. Relationships between energy-level and insulin-secretion in isolated rat islets of Langerhans - a study at various pH values. Biochemical Pharmacology 42(3):593-598.
164. Simpson NE, Bennett LK, Papas KK, Sambanis A, Constantinidis I. 2000. Effects of pH on murine insulinoma beta TC3 cells. Biochemical and Biophysical Research Communications 273(3):937-941.
165. Fraker C, Montelongo J, Szust J, Khan A, Ricordi C. 2004. The use of multiparametric monitoring during islet cell isolation and culture: A potential tool for in-process corrections of critical physiological factors. Cell Transplantation 13(5):497-502.
166. Tai J, Tsang A, Tze WJ. 1994. Effects of serum and medium supplements, pH, and temperature on the viability of cultured porcine islets. Transplantation Proceedings 26(2):818-819.
167. Garg LC, Maren TH. 1972. The rates of hydration of carbon dioxide and dehydration of carbonic acid at 37 degrees. Biochim Biophys Acta 261(1).
168. Soukane DM, Shirazi-Adl A, Urban JPG. 2005. Analysis of nonlinear coupled diffusion of oxygen and lactic acid in intervertebral discs. Journal of Biomechanical Engineering-Transactions of the Asme 127(7):1121-1126.

169. Patel AA, Gawlinski ET, Lemieux SK, Gatenby RA. 2001. A cellular automaton model of early tumor growth and invasion: The effects of native tissue vascularity and increased anaerobic tumor metabolism. Journal of Theoretical Biology 213(3):315-331.
170. Sarangapani R, Wexler AS. 1996. Growth and neutralization of sulfate aerosols in human airways. Journal of Applied Physiology 81(1):480-490.
171. Fatt I, Giasson CJ, Mueller TD. 1998. Non-steady-state diffusion in a multilayered tissue initiated by manipulation of chemical activity at the boundaries. Biophysical Journal 74(1):475-486.
172. Geers C, Gros G. 2000. Carbon dioxide transport and carbonic anhydrase in blood and muscle. Physiological Reviews 80(2):681-715.
173. Shah VM, Hardy BJ, Stern SA. 1986. Solubility of carbon-dioxide, methane, and propane in silicone polymers - effect of polymer side-chains. Journal of Polymer Science Part B-Polymer Physics 24(9):2033-2047.
174. Goss JA, Schock AP, Brunicardi FC, Goodpastor SE, Garber AJ, Soltes G, Barth M, Froud T, Alejandro R, Ricordi C. 2002. Achievement of insulin independence in three consecutive type-1 diabetic patients via pancreatic islet transplantation using islets isolated at a remote islet isolation center. Transplantation 74(12):1761-1766.
175. 2007. TCP Reliable. http://www.tcpreliable.com.
176. 2007. PCM Energy P. Ltd.
177. Guyton AC, Hall J. 2005. Textbook of Medical Physiology: Saunders.
178. Aburaya M, Tanaka KI, Hoshino T, Tsutsumi S, Suzuki K, Makise M, Akagi R, Mizushima T. 2006. Heme oxygenase-1 protects gastric mucosal cells against non-steroidal anti-inflammatory drugs. Journal of Biological Chemistry 281(44):33422-33432.
179. Kruger AL, Peterson SJ, Schwartzman M, Fusco H, McClung JA, Weiss M, Shnouda S, Goodman AI, Goligorsky MS, Kappas A and others. 2006. Upregulation of heme oxygenase provides vascular protection in an animal model of diabetes through its anti-oxidant and anti-apoptotic effects. Circulation 114(18):106-106.
180. Min KS, Hwang YH, Ju HJ, Chang HS, Kang KH, Pi SH, Lee SK, Kim EC. 2006. Heme oxygenase-1 mediates cytoprotection against nitric oxide-induced cytotoxicity via the cGMP pathway in human pulp cells. Oral Surgery Oral Medicine Oral Pathology Oral Radiology and Endodontics 102(6):803-808.
181. Otterbein LE, Kolls JK, Mantell LL, Cook JL, Alam J, Choi AMK. 1999. Exogenous administration of heme oxygenase-1 by gene transfer provides protection against hyperoxia-induced lung injury. Journal of Clinical Investigation 103(7):1047-1054.
182. Otterbein LE, Soares MP, Yamashita K, Bach FH. 2003. Heme oxygenase-1: unleashing the protective properties of heme. Trends in Immunology 24(8):449-455.
183. Petrache I, Otterbein LE, Alam J, Wiegand GW, Choi AMK. 2000. Heme oxygenase-1 inhibits TNF-alpha-induced apoptosis in cultured fibroblasts. American Journal of Physiology-Lung Cellular and Molecular Physiology 278(2):L312-L319.
184. Tsuchihashi SI, Livhits M, Zhai Y, Busuttil RW, Araujo JA, Kupiec-Weglinski JW. 2006. Basal rather than induced heme oxygenase-1 levels are crucial in the antioxidant cytoprotection. Journal of Immunology 177(7):4749-4757.
185. Lee PJ, Alam J, Wiegand GW, Choi AMK. 1996. Overexpression of heme oxygenase-1 in human pulmonary epithelial cells results in cell growth arrest and increased resistance

to hyperoxia. Proceedings of the National Academy of Sciences of the United States of America 93(19):10393-10398.
186. Brouard S, Otterbein LE, Anrather J, Tobiasch E, Bach FH, Choi AMK, Soares MP. 2000. Carbon monoxide generated by heme oxygenase 1 suppresses endothelial cell apoptosis. Journal of Experimental Medicine 192(7):1015-1025.
187. Chen K, Gunter K, Maines MD. 2000. Neurons overexpressing heme oxygenase-1 resist oxidative stress-mediated cell death. Journal of Neurochemistry 75(1):304-313.
188. Shiraishi F, Curtis LM, Truong L, Poss K, Visner GA, Madsen K, Nick HS, Agarwal A. 2000. Heme oxygenase-1 gene ablation or expression modulates cisplatin-induced renal tubular apoptosis. American Journal of Physiology-Renal Physiology 278(5):F726-F736.
189. Suttner DM, Sridhar K, Lee CS, Tomura T, Hansen TN, Dennery PA. 1999. Protective effects of transient HO-1 overexpression on susceptibility to oxygen toxicity in lung cells. American Journal of Physiology-Lung Cellular and Molecular Physiology 276(3):L443-L451.
190. Abraham NG, Lavrovsky Y, Schwartzman ML, Stoltz RA, Levere RD, Gerritsen ME, Shibahara S, Kappas A. 1995. Transfection of the human heme oxygenase gene into rabbit coronary microvessel endothelial-cells-protective effect against heme and hemoglobin toxicity. Proceedings of the National Academy of Sciences of the United States of America 92(15):6798-6802.
191. Wang X, Wang Y, Kim HP, Nakahira K, Ryter SW, Choi AMK. 2007. Carbon monoxide protects against hyperoxia-induced endothelial cell apoptosis by inhibiting reactive oxygen species formation. Journal of Biological Chemistry 282(3):1718-1726.
192. Otterbein LE, Mantell LL, Choi AMK. 1999. Carbon monoxide provides protection against hyperoxic lung injury in rats. American Journal of Respiratory and Critical Care Medicine 159(3):A218-A218.
193. Ryter SW, Otterbein LE, Morse D, Choi AMK. 2002. Heme oxygenase/carbon monoxide signaling pathways: Regulation and functional significance. Molecular and Cellular Biochemistry 234(1):249-263.
194. Gunther L, Berberat PO, Haga M, Brouard S, Smith RN, Soares MP, Bach FH, Tobiasch E. 2002. Carbon monoxide protects pancreatic beta-cells from apoptosis and improves islet function/survival after transplantation. Diabetes 51(4):994-999.
195. Kim HS, Loughran PA, Kim PK, Billiar TR, Zuckerbraun BS. 2006. Carbon monoxide protects hepatocytes from TNF-alpha/Actinomycin D by inhibition of the caspase-8-mediated apoptotic pathway. Biochemical and Biophysical Research Communications 344(4):1172-1178.
196. Chae HJ, Chin HY, Lee GY, Park HR, Yang SK, Chung HT, Pae HO, Kim HM, Chae SW, Kim HR. 2006. Carbon monoxide and nitric oxide protect against tumor necrosis factor-alpha-induced apoptosis in osteoblasts: HO-1 is necessary to mediate the protection. Clinica Chimica Acta 365(1-2):270-278.
197. Bainbridge SA, Belkacemi L, Dickinson M, Graham CH, Smith GN. 2006. Carbon monoxide inhibits hypoxia/reoxygenation-induced apoptosis and secondary necrosis in syncytiotrophoblast. American Journal of Pathology 169(3):774-783.
198. Suttner DM, Dennery PA. 1999. Reversal of HO-1 related cytoprotection with increased expression is due to reactive iron. Faseb Journal 13(13):1800-1809.
199. D'Amico G, Lam F, Hagen T, Moncada S. 2006. Inhibition of cellular respiration by endogenously produced carbon monoxide. Journal of Cell Science 119(11):2291-2298.

200. Keynes RG, Griffiths C, Garthwaite J. 2003. Superoxide-dependent consumption of nitric oxide in biological media may confound in vitro experiments. Biochemical Journal 369:399-406.
201. Papas KK, Colton CK, Nelson RA, Rozak PR, Avgoustiniatos ES, Scott WE, Wildey GM, Pisania A, Weir GC, Hering BJ. 2007. Human islet oxygen consumption rate and DNA measurements predict diabetes reversal in nude mice. American Journal of Transplantation 7(3):707-713.
202. Dike LE, Xia HY, Guarino RD, Presnell SC, Timmins MR. 2005. Rapid method for assessing oxygen consumption rate of cells from transient-state measurements of pericellular dissolved oxygen concentration. Cytotechnology 49(2-3):133-141.
203. Hodge K, Prodpran T, Shenogina NB, Nazarenko S. 2001. Diffusion of oxygen and carbon dioxide in thermally crystallized syndiotactic polystyrene. Journal of Polymer Science Part B-Polymer Physics 39(20):2519-2538.
204. Bowyer WJ, Xu WY, Demas JN. 2004. Determining oxygen diffusion coefficients in polymer films by lifetimes of luminescent complexes measured in the frequency domain. Analytical Chemistry 76(15):4374-4378.
205. Gao YP, Ogilby PR. 1992. A New Technique to Quantify Oxygen Diffusion in Polymer-Films. Macromolecules 25(19):4962-4966.
206. Kneas KA, Demas JN, Nguyen B, Lockhart A, Xu WY, DeGraff BA. 2002. Method for measuring oxygen diffusion coefficients of polymer films by luminescence quenching. Analytical Chemistry 74(5):1111-+.
207. Schappacher G, Hartmann P. 2003. Partial analytical solution of a model used for measuring oxygen diffusion coefficients of polymer films by luminescence quenching. Analytical Chemistry 75(16):4319-4324.
208. Boersma A, Cangialosi D, Picken SJ. 2003. Mobility and solubility of antioxidants and oxygen in glassy polymers - II. Influence of physical ageing on antioxidant and oxygen mobility. Polymer Degradation and Stability 79(3):427-438.
209. Bae SY, Cho DH, Kim HT, Kumazawa H. 1994. Transport of oxygen and carbon-dioxide through polycarbonate membrane. Korean Journal of Chemical Engineering 11(2):127-130.
210. Papkovsky DB. 2004. Methods in optical oxygen sensing: Protocols and critical analyses. Oxygen Sensing. p 715-735.
211. Arain S, Weiss S, Heinzle E, John GT, Krause C, Klimant I. 2005. Gas sensing in microplates with optodes: Influence of oxygen exchange between sample, air, and plate material. Biotechnology and Bioengineering 90(3):271-280.
212. Chapman JD, Sturrock J, Boag JW, Crookall JO. 1970. Factors affecting the oxygen tension around cells growing in plastic Petri dishes. Int J Radiat Biol Relat Stud Phys Chem Med 17(4).